From gut to brain: novel therapeutic strategies to combat obesity-associated cardiometabolic diseases

Li, Z.

From Gut to Brain: Novel Therapeutic Strategies to Combat Obesity-Associated Cardiometabolic Diseases

Zhuang Li

From Gut to Brain: Novel Therapeutic Strategies to Combat Obesity-Associated Cardiometabolic Diseases

ZHUANG LI

From Gut to Brain: Novel Therapeutic Strategies to Combat Obesity-Associated Cardiometabolic Diseases

ISBN: 978-94-92597-71-7

Cover design: Zhuang Li & Jiaxin Du & Zeyuan Li
Layout: Zhuang Li
Printing: PRINTSUPPORT4U

From Gut to Brain: Novel Therapeutic Strategies to Combat Obesity-Associated Cardiometabolic Diseases

Proefschrift

ter verkrijging van
de graad van doctor aan de Universiteit Leiden,
op gezag van rector magnificus Prof. dr. ir. H. Bijl,
volgens besluit van het college voor promoties
te verdedigen op woensdag 28 april 2021
klokke 15.00 uur

door

Zhuang Li
geboren te Changchun, China
in 1988

PROMOTORES

Prof. dr. P.C.N. Rensen
Prof. dr. Y. Wang (Xi'an Jiaotong University, Xi'an, Shaanxi Province, China)

PROMOTIECOMMISSIE

Prof. dr. J.A.P. Willems van Dijk
Prof. dr. A.K. Groen (AMC, Amsterdam)
Prof. dr. E.E. Blaak (MUMC, Maastricht)

The work described in this thesis was performed at the Department of Medicine, Division of Endocrinology of the Leiden University Medical Center, Leiden, the Netherlands.

The research described in this thesis was supported by a personal grant of the China Scholarship Council to Zhuang Li (No. 201506170051).

Financial support by the Netherlands Association for the Study of Obesity (NASO) for the publication of this thesis is gratefully acknowledged.

TABLE OF CONTENTS

CHAPTER 1

GENERAL INTRODUCTION AND OUTLINE

Obesity is a medical condition that is characterized by excessive accumulation of body fat mass, which is the result of a chronic imbalance of energy homeostasis, with energy intake exceeding energy expenditure [1]. Obesity is related to various cardiometabolic diseases including type 2 diabetes (T2D), cardiovascular diseases (CVD) and non-alcoholic fatty liver disease (NAFLD) [2], and is becoming a global health concern [3]. Therefore, understanding how we can modulate energy expenditure to outweigh energy intake is of great importance and will be useful for developing strategies to combat obesity and associated cardiometabolic diseases. Lifestyle modulation, including restricting caloric intake and increasing physical activity, continues to be the first choice and a critical method of combating obesity. However, lifestyle intervention is difficult to adhere to and often not adequate for achieving sustained weight loss. Likewise, pharmacotherapy aimed to restrict caloric intake can effectively induce weight loss [4], but the cessation of treatment generally leads to weight regain. Therefore, novel intervention strategies to regulate energy metabolism, thereby attaining persistent weight loss, are required to combat obesity and associated cardiometabolic diseases.

1. Energy metabolism and its regulation

Energy metabolism can be defined as the processes involved in digestion and uptake of nutrients from the diet (energy intake), catabolism of those nutrients to produce the energy-rich compound adenosine triphosphate (ATP), the release of that energy to allow organisms to grow, reproduce and maintain their physical activities (energy expenditure), and preservation of excess energy in the body (energy storage). Energy metabolism is complex and includes a series of precise chemical and biological reactions throughout the body, and therefore requires strict central and peripheral regulation. The coordinated regulation of energy intake, expenditure and storage contributes to the homeostatic control of energy metabolism, thereby maintaining a healthy weight.

1.1 Energy intake and storage

Energy intake is defined as the total oral intake of calories (unit of energy) within macronutrients including carbohydrates (4 kilocalories (kcal)/gram), proteins (4 kcal/gram), and fats (9 kcal/gram). In the intestine, carbohydrates are broken down into a few simple monomers, including glucose, an essential energy source in almost every organism. After intestinal digestion of carbohydrates, liberated glucose is absorbed into the circulation, where it boosts insulin secretion from the pancreas and is taken up by mainly the liver (hepatocytes), skeletal muscle (myocytes) and white adipose tissue (WAT; adipocytes). Under coordinated actions of several enzymes, in the liver and muscle glucose can be stored as glycogen (i.e., glucose polymers), providing the body with a readily available energy source when the

blood glucose level decreases. Especially the brain should be continuously fed with glucose, as it cannot use fatty acids (FAs) as an energy source. Both in the liver and WAT, glucose can also be converted into lipids and be stored. Dietary proteins are broken down in the intestine into various amino acids, di- and tripeptides, which are absorbed by enterocytes, and released into the bloodstream as amino acids that are transported throughout the body and used to build functional proteins to maintain bones, muscles, and skin. Alternatively, they can also be used as an energy source by muscle cells, and be converted into lipids at persistent high intake. Ingested triglycerides (TG) are broken down in the stomach and small intestine by gastric and pancreatic lipases into 2-monoacylglycerol and FAs, which are then imported across the intestinal mucosa. Within enterocytes, 2-monoacylglycerol and long-chain FAs are converted back in TG, then loaded into the core of chylomicron particles, which via the lymphatics reach the circulation. In contrast, medium-chain fatty acids are directly secreted by enterocytes into the circulation via the portal vein. In the circulation, chylomicrons interact with lipoprotein lipase (LPL) on metabolic tissues including WAT, BAT, skeletal muscle and heart, to liberate FAs, which are then taken up by these tissues. After a meal, the majority of FAs are transported to WAT for storage as TG. Lipolysis by LPL results in generation of chylomicron remnants, which become enriched with apolipoprotein E (apoE) that is subsequently recognized by the LDL receptor and LDL receptor-related protein (LRP) on hepatocytes, after which these receptors take up the remnants by endocytosis.

While amino acids are thus mainly used for anabolic processes, glucose and FAs are mainly used in catabolic processes as a fuel. Glucose undergoes glycolysis and FAs undergo beta-oxidation, both yielding acetyl-CoA, which is the primary input metabolite of the mitochondrial tricarboxylic acid cycle (TCA cycle). In the TCA cycle, acetyl-CoA is further oxidized to generate carbon dioxide, water, but also reducing equivalents (NADH). These reducing equivalents are fed into the mitochondrial electron transfer chain to generate a proton gradient over the mitochondrial inner membrane, which drives ATP synthase to convert ADP into ATP that provides energy for e.g., contraction in skeletal muscle and heart. In BAT, the unique presence of the uncoupling protein-1 (UCP-1) within the mitochondrial inner membrane results in dissipation of the protein gradient to produce heat instead of ATP. Given its incredibly small energy density, ATP cannot be stored in large quantities. Therefore, energy is mostly stored in the liver (glycogen), skeletal muscle (glycogen) and WAT (TG).

Generally, the daily energy intake is around 2,000 kcal for women and 2,500 kcal for men. A balanced daily caloric intake is crucial to fortify the body against the risk of various health problems. Undernutrition, referred to as the status of insufficient caloric intake, may induce symptoms including short height and thin body [5]. On the other hand, overnutrition, defined as caloric intake exceeding that required for maintaining normal energy metabolism, results in storage of excess glucose and lipids in WAT, which can lead to overweight (defined as Body Mass Index (BMI) between 25-30 kg/m^2) and ultimately obesity (BMI > 30 kg/m^2). In obesity,

the lipid-storing capacity of WAT may become insufficient, resulting in cell death and chronic metabolic inflammation, which via induction of insulin resistance of adipose tissue may result in overflow of lipids to other organs, resulting in ectopic lipid deposition in metabolic tissues such as the liver, skeletal muscles and pancreas. In the short term, ectopic lipid deposition results in insulin resistance of those organs, which in the long term may result in failure of the pancreas to produce insulin, resulting in T2D. Restriction of energy intake seems to be the most direct way to combat obesity and its complications. For example, 40% energy restriction of adult mice has been demonstrated to result in 15% bodyweight reduction [6]. Similarly, a pioneering trial in humans showed that restricting caloric intake by 25% per day for 2 years resulted in 10% loss of body weight [7]. Of note, this study also demonstrated that energy restriction reduces risk factors for obesity-related diseases, including T2D and heart disease [8], indicating that caloric restriction is an effective strategy to combat obesity and its associated cardiometabolic diseases.

1.2 Energy expenditure

Energy expenditure is defined as a sum of calories utilized to carry out physical functions, such as breathing, exercising, and digesting food. Based on these different functions, energy expenditure can be divided into three components: basal energy expenditure (BEE, ~70% of total energy expenditure), physical activity-induced energy expenditure (AEE, ~20% of total energy expenditure), and diet-induced energy expenditure (DEE, ~10% of total energy expenditure), the relative contributions being variable between individuals. BEE is the energy needed to maintain fundamental metabolic functions, including respiration, ion transport, and body temperature maintenance. Differences in BEE exist between genders and across ages, which is however mainly caused by differences in organs contributing to lean mass, mostly skeletal muscles [9]. AEE is the energy expenditure resulting from any bodily movement produced by skeletal muscles. DEE refers to the energy expenditure related to the energy required to digest, absorb and store food. An average adult of 70 kg with a sedentary lifestyle expends around 2,000 kcal/day, which can increase up to around 3,000 kcal/day in a physically active person [10]. Calculating an individual's energy expenditure is therefore crucial to understand how to attain a neutral energy balance. Energy expenditure can be assessed by different technologies including indirect calorimetry, electrical bioimpedance, doubly marked water, and predictive equations.

Lower energy expenditure at unchanged caloric intake may ultimately result in weight gain. Indeed, a fairly strong inverse correlation has been demonstrated between a relatively low total energy expenditure and the rate of weight gain (r=-0.39) [11]. Consistently, a meta-analysis of factors affecting exercise-induced changes in body mass revealed that exercise results in at least a moderate decrease in body fat at approximately 0.1 kg/week [12]. Thus, strategies to increase energy

expenditure might provide therapeutic potential in combating obesity and its complications.

Collectively, as depicted in **Figure 1**, energy metabolism can be defined as the processes of energy intake, energy expenditure, and energy storage. Macronutrients including carbohydrates, proteins and fats, are taken via diet and utilized for anabolic processes (skeletal muscle), to produce ATP (skeletal muscle, heart) or heat (BAT) or for storage (WAT). These complex metabolic processes are tightly regulated via central and peripheral pathways.

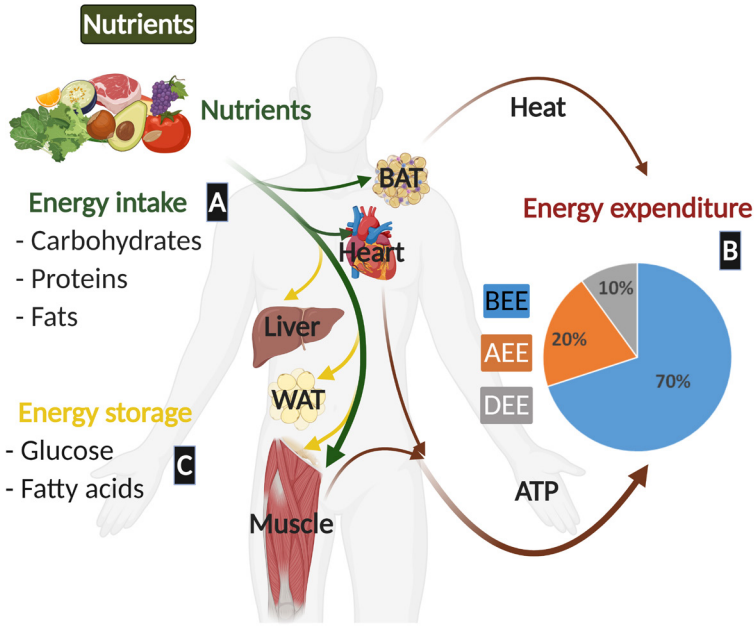

Figure 1. Systemic overview of energy metabolism. Energy metabolism can be defined as the processes of energy intake (green arrows, A), energy expenditure (red arrows, B), and energy storage (yellow arrows, C). See text for more detailed explanation. AEE, physical activity-induced energy expenditure; ATP, adenosine triphosphate; BAT, brown adipose tissue; BEE, basal energy expenditure; DEE, diet-induced energy expenditure; WAT, white adipose tissue.

1.3 Regulation of energy metabolism

1.3.1 Regulation of energy intake

The brain plays a central role in the regulation of energy intake. Specifically, the hypothalamus within the brain controls energy intake due to the presence of two different neurons expressing either the neuropeptide Y (NPY) and agouti-related peptide (AgRP), or the pro-opiomelanocortin (POMC) and cocaine and amphetamine-regulated transcript (CART), with opposite regulatory effects on energy intake. In animal studies, it has been demonstrated that both NPY and other agonists of the NPY receptor increase food intake [13, 14]. In line with these findings, an NPY receptor antagonist has been evaluated in a clinical trial and was found to cause lower energy intake and induce modest weight loss [15]. Together, these findings demonstrate that NPY-expressing neurons play the main role in the central upregulation of energy intake. On the other hand, activation of POMC-expressing neurons suppresses appetite. POMC is a complex polypeptide precursor that can be cleaved into smaller biologically active peptides including melanocortin, which inhibits appetite via binding to G-protein coupled melanocortin receptors (MCRs). Rodent studies demonstrated that deficiency of MCRs (either MC3R or MC4R) results in higher energy intake and obesity [16, 17]. Consistently, mutations in human MCR genes are associated with obesity [18, 19]. Recently, MC4R agonism has indeed been described to cause marked weight loss in obese leptin-deficient individuals, caused by substantial and durable reduction in caloric intake [20]. Collectively, these studies indicate a well-established function of POMC-expressing neurons in inhibiting energy intake and inducing weight loss. Based on these findings, novel strategies that focus on regulating the activity of neurons expressing NPY or POMC aimed to reduce energy intake are likely promising treatment modalities for obesity.

In addition to the brain, the gastrointestinal (GI) tract, which includes the mouth, esophagus, stomach, small intestine and large intestine, is also closely involved in peripheral regulation of energy intake. The GI tract senses the entry of nutrients and in response releases gut hormones, e.g., glucagon-like peptide-1 (GLP-1), peptide YY (PYY) [21] and cholecystokinin (CCK) [22], all of which can transmit signals from the gut to the brain and as a consequence regulate energy intake centrally. In particular, GLP-1, mainly secreted by enteroendocrine L-cells in the GI tract, is well recognized to attenuate energy intake in addition to increasing insulin secretion by the pancreas. Peripheral administration of GLP-1 was demonstrated to inhibit food intake in both rodents [23] and humans [24]. However, the mechanisms underlying the release of GLP-1 by intestinal L-cells and the specific targets of GLP-1 involved in reducing food intake are not fully understood.

In addition to multiple peripheral organs, such as pancreas and stomach, the GLP-1 receptor is also expressed in hypothalamus of the brain [25], and can be stimulated by GLP-1 and its analogues that cross the blood-brain barrier [26], suggesting that the effect of GLP-1 on regulating energy intake might, at least

in part, depend on the central GLP-1 receptor system. This is confirmed by a rodent study showing that central intracerebroventricular administration of GLP-1 reduces appetite [27], which can be reversed by central administration of the GLP-1 receptor antagonist Exendin (9-39) [28]. However, not all endogenously secreted GLP-1 reach the hypothalamus since GLP-1 has a very short half-life as it is rapidly degraded by dipeptidyl peptidase-4 (DPP4) within 2 minutes, resulting in about only 15% of active GLP-1 in the systemic circulation. Of note, the GLP-1 receptor has also been found in the afferent vagal nerve [29, 30], one of the essential neural circuits between the GI tract and brain, suggesting a potential role of the vagal nerve in the induction of satiety effects by GLP-1. This is confirmed by a human study demonstrating that the effect of GLP-1 on reducing food intake is lost in vagotomised males [31]. Taken together, these findings indicate that GLP-1 can attenuate energy intake via central mechanisms, either directly in the brain or indirectly through activation of peripheral vagal nerves, suggesting the concerted action of both central and peripheral targets to control energy intake (**Figure 2**).

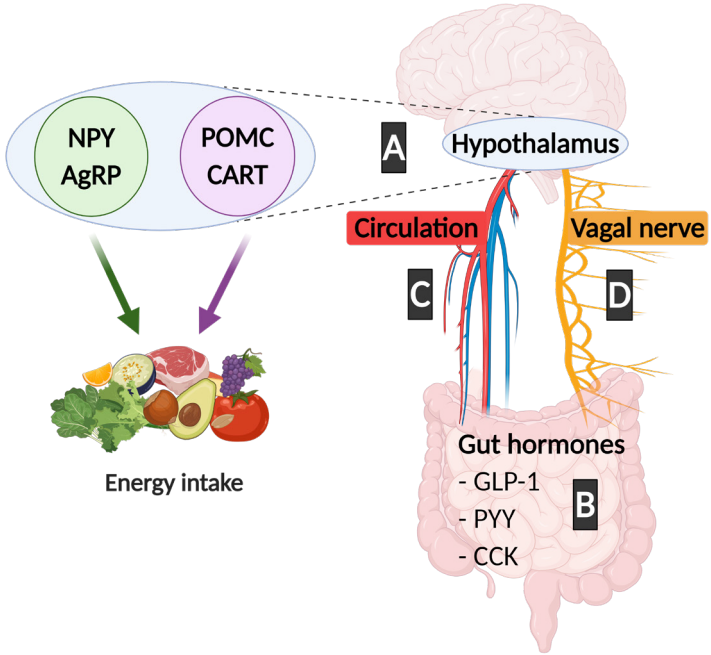

Figure 2. Overview of energy intake regulation. Energy intake is mainly and oppositely regulated by neurons expressing either NPY/AgRP (increasing food intake) or POMC/CART (decreasing food intake) in the hypothalamus (A), and by peripheral gut hormones secreted from the gastrointestinal tract (B), either directly via the circulation (C) and indirectly via activation of peripheral vagal nerves (D). See text for more detailed explanation. AgRP, agouti-related peptide; CART, cocaine and amphetamine-regulated transcript; CCK, cholecystokinin; GLP-1, glucagon-like peptide-1; NPY, neuropeptide Y; POMC, pro-opiomelanocortin; PYY, peptide YY.

1.3.2 Regulation of energy expenditure

As described in section *1.2*, total energy expenditure is determined by AEE, BEE and DEE. Given that AEE is the most variable component that may raise total energy expenditure by as much as 50%, the most effective way to increase energy expenditure is to exercise more. This is confirmed by a systematic review of human studies demonstrating that exercise training is an effective strategy to increase total energy expenditure [32]. Mechanistically, processes associated with working muscle contractions result in burning more calories. In detail, muscle contraction occurs as myosin heads bind to actin and pull the actin inward, requiring energy provided by ATP. The amount of energy consumption varies widely depending on the type of exercise, intensity level, and individual characteristics such as body weight. For example, walking at 3.5 miles per hour (mph) of a person who weighs 75 kg for an hour will consume around 300 kcal, and running at 5 mph for an hour will burn around 600 kcal. Accordingly, physical training consisting of 20 minutes cycling or running, 20 minutes swimming, followed by 20 minutes of warm-up/cool-down during 4 weeks, resulted in a significant reduction in body weight and fat mass percentage and improved whole-body glucose uptake [33]. Taken together, these data confirm that exercise is a valid strategy for treating obesity, which can act in concert reducing caloric intake.

BAT is another player involved in energy expenditure. BAT has long been known to play an essential role in thermogenesis in small rodents and infants, and has been revealed just over a decade ago to be also present and metabolically active in human adults [34]. Cold exposure is the most potent and physiological activator of BAT [34, 90], and prolonged cold acclimation has been identified to induce a moderate decrease in fat mass in humans [91]. Mechanistically, upon cold exposure, increased sympathetic outflow from the hypothalamus to BAT increases norepinephrine production and release in nerve endings in the vicinity of brown adipocytes, which activates β-adrenergic receptors (β-ARs) on brown adipocytes. This sequence of events promotes an intracellular signaling cascade via the production of cyclic AMP (cAMP) and activation of protein kinase A (PKA). PKA stimulates phosphorylation of transcription factors that enhance expression and synthesis of UCP-1. Furthermore, PKA stimulates intracellular hydrolysis of triglycerides stored in lipid droplets, resulting in increased flux of liberated FAs towards mitochondria for subsequent combustion. FAs also allosterically bind to UCP-1, resulting in uncoupling between the respiratory chain and ATP synthase by inducing leakage of protons from the mitochondrial intermembrane space into the mitochondrial matrix leading to heat production instead of synthesis of ATP [35]. To replenish lipid stores, brown adipocytes take up large amounts of glucose as well as TG-rich lipoprotein (TRL)-derived FAs from the circulation thereby accelerating TRL remnant clearance by the liver [36]. At the same time, TRL surface remnants are used to generate HDL precursors that increase reverse cholesterol transport [37]. A clinical study showed that healthy adults with an active BAT have a lower BMI [38], indicating that active BAT may be a potential therapeutic target for combating obesity.

2. Obesity-associated cardiometabolic diseases

2.1 Type 2 diabetes

Diabetes is a chronic metabolic condition characterized by increased plasma glucose. To date, diabetes is becoming one of the most significant public health problems as it affects nearly 450 million patients globally and is set to escalate to around 650 million by the year 2040 [39]. There are two main types of diabetes: type 1 and type 2. Type 1 diabetes is an auto-immune disease that is not linked to obesity and usually occurs when the immune system attacks pancreatic beta-cells, so that they can no longer produce enough insulin. As explained in section *1.1*, T2D can result from obesity as a consequence of the development of insulin resistance of the expanding adipose tissue and of other metabolic tissues due to ectopic lipid deposition resulting from lipid overflow. Once insulin resistance develops, the pancreas will initially secrete more insulin to maintain normal blood glucose. This chronically elevated insulin production, however, will eventually lead to a failure of the beta-cell function, which will cease to produce insulin and finally result in the state of T2D. In fact, epidemiological studies showed that obesity is one of the major risk factors of T2D [40-42].

2.2 Cardiovascular disease

In addition to T2D, obesity is also a well-known independent risk factor for CVD [43]. CVD is the leading cause of mortality globally, taking an estimated 17.9 million lives each year [44]. One of the major underlying causes of CVD is atherosclerosis, a lipid-driven, systemic inflammatory disease in which plaques, made up of lipids, connective tissue and immune cells, build up in and progressively narrow the lumen of the blood vessel. The most important causal risk factor of atherosclerosis is (V)LDL-C [45], which can extravasate to induce inflammation in the intima of arteries that attracts monocytes from the circulation. In the intima, these monocytes differentiate into macrophages that engulf modified (V)LDL to become cholesterol-rich foam cells. Therefore, hypercholesterolemia is the priority target for treating atherosclerosis. Statin therapy, supported by a broad evidence base, has demonstrated its superior efficacy in reducing (V)LDL-C and subsequent cardiovascular risk. Although this strategy targets those most at risk, it merely addresses those most susceptible and does not account for the fact that most cardiovascular events occur in those at moderate to low risk [46]. Therefore, new therapeutic strategies to treat atherosclerosis by further lowering cholesterol or targeting other pathways are needed.

Obesity can lead to and worsen the development of atherosclerosis by various mechanisms such as hypertension, hyperglycemia, dyslipidemia, endothelial dysfunction and systemic inflammation [47]. Thus, therapeutic strategies aiming at inducing weight loss may also ameliorate atherosclerotic CVD. Indeed, a clinical

trial reported that weight loss ranging between 7-20% improves atherosclerosis-associated parameters, including ejection fraction and systolic output [48]. Consistently, a four-year clinical study of obese subjects confirmed that weight loss of 19% by surgery improves blood pressure, lipids, and insulin [49]. Collectively, these studies indicate the therapeutic potential of weight loss in treatment of atherosclerotic CVD and indicate the urgency of developing novel strategies to manage body weight.

2.3 Non-alcoholic fatty liver disease

NAFLD is a metabolic disease that is characterized by excessive lipid accumulation in the liver (>5%) without excessive alcohol use [50]. NAFLD comprises a spectrum of simple steatosis or non-alcoholic fatty liver (NAFL) to non-alcoholic steatohepatitis (NASH), which is defined histologically as hepatic inflammation in addition to hepatic steatosis [51]. Although the exact sequence of events in NAFLD development is not entirely clear yet, obesity is a well-established factor leading to the accumulation of excessive lipids in hepatocytes (i.e., steatosis), one of the most important hallmarks of NALFD. The increased hepatic lipid accumulation might be caused by 1) excess flux of dietary TG to the liver as constituent of intestinally derived chylomicron particles; 2) increased TG synthesis in the liver from FAs formed from de novo lipogenesis; 3) excess FAs influx into the liver from lipolysis of adipose tissue in obese with subsequent conversion to TG (i.e., lipid overflow hypothesis, as explained in section 1.1); 4) diminished export of lipids from the liver as VLDL; and/or 5) reduced hepatic oxidation of FAs.

A systematic review and meta-analysis recently showed evidence of the association between weight loss interventions and improved biomarkers of NAFLD [52]. Consistently, a population-based study in the US suggested that the prevalence rate of NAFLD increases with increased BMI [53]. Although NAFLD is rapidly becoming one of the most common chronic liver diseases, there are no approved pharmacological agents for NAFLD treatment so far. Given the close relationship between obesity and NAFLD, lifestyle modulation, including energy restriction and exercise, is still the primary NALFD intervention strategy, indicating the therapeutic potential of weight loss in NAFLD management.

3. Novel therapeutic strategies to combat obesity and associated cardiometabolic diseases

3.1 Gut microbiota

In humans, the gut harbors trillions of microbes that are essential for host development and physiology. The gut microbiota interact with each other and also with the host to modulate host metabolic health. Over the past 20 years, the gut microbiota has received increasing attention in cardiometabolic health, because of their participation in regulating fat storage [54], influencing thermogenesis in BAT [55], and modulating host energy intake [56]. Individuals with anorexia nervosa or higher body fat were demonstrated to have a low diversity of gut microbiota [57, 58], indicating the role of the ecology of gut microbiota in maintaining host energy homeostasis. In addition, microbiota reconstitution in germ-free C57BL/6J mice (i.e., having no microorganisms living in or on them) increased their body fat content by 60% [54]. In line, another study found that transplantation of gut microbiota from obese humans is able to transmit high total body weight and fat mass, as well as associated metabolic phenotypes in germ-free mice [59]. However, mechanisms of how gut microbiota induce metabolic benefits in the host are still debated.

It has been demonstrated that gut microbiota might exert its functions on host physiology in different ways, including via their genes, direct interactions of the bacteria with the host, or through their metabolites. Obesity and its associated co-morbidities in fact result from a complex interaction of host genetics, environment, and gut microbiome [60]. Interestingly, a rodent study found that gut microbiota can modulate intestinal endocannabinoids to increase gut permeability, which results in leakage of gut microbial lipopolysaccharides (LPS) through the gut barrier into blood, inducing metabolic endotoxemia and obesity [61], consistent with a role of LPS as a bacterial modulator in host metabolic health. Of note, almost 10% of all circulating metabolites in the human organism are derived from bacteria, including short-chain fatty acids (SCFAs), branched-chain amino acids, secondary bile acids, and trimethylamine, all of which are involved in the host metabolic pathways [62]. Collectively, these findings implicate the attractive therapeutic possibility of manipulating gut microbiota to improve host metabolic health. Most relevant, a clinical study demonstrated that gut microbiota fermentation of prebiotics decreases hunger via increasing plasma GLP-1 and PYY, the gut hormones known to regulate energy intake [63]. Taken together, these findings indicate that gut microbiota play a vital role in regulating host energy intake that might be attributed to the release of gut hormones. However, the specific gut microbe(s) that may contribute to regulating energy intake and the underlying mechanisms remain to be discovered.

The composition of gut microbiota is relatively stable within healthy adult individuals over time [64]. However, this temporal consistency is dependent on the diet. A systemic review evaluating the effects of several standard dietary

components on gut microbiota showed that consuming particular food types, such as protein, fats, and carbohydrates, produces predictable shifts in gut microbiota [65]. In particular, non-digestible fiber, classified as fiber and resistant starch which cannot be degraded by human cells, undergo fermentation in the large intestine by gut microbiota, thereby altering the niche environment in the gut by providing substrates for microbial growth, allowing microbial species that are able to utilize these substrates to expand their populations [66]. This property of fibers shows their potential as prebiotics, which are defined as dietary components that benefit host health via selective stimulation of the growth and/or activity of 'good' gut microbes [67]. A study with 49 obese subjects showed that higher fiber consumption resulted in increased gut microbiota diversity and improved metabolic phenotypes [68]. Food containing 'good' gut microbes, referred to as probiotics, represents a source of ingestible gut microbiota that can also beneficially regulate host health. Although it has been proven that some probiotics, such as *Lactobacillus Rhamnosus **GG*** and *VSL#3*, used alone or in symbiotic mixtures, are able to exert anti-obese effects in animal and human studies [69, 70], the precise actions of those probiotics in combating obesity are still not fully elucidated. With the increasing evidence that gut microbiota are involved in host cardiometabolic health, several techniques to manipulate gut microbiota populations have been developed, e.g., use of germ-free mice, depletion of gut microbiota by antibiotics, cohousing of mice, and fecal microbiota transplantation (FMT). In particular, FMT has been widely used as an effective method to manipulate gut microbiota, in order to investigate the causal relationship between gut microbiota and host cardiometabolic health [71, 72]. Notably, a recent proof-of-concept study demonstrated the feasibility of administering *Akkermansia muciniphila* to improve insulin resistance in overweight humans, providing a promising start for the development of future clinical interventions aimed at manipulating gut microbiota [73].

3.2 Short-chain fatty acids

As human cells cannot degrade dietary fiber, they are digested by the gut microbiota into SCFAs including acetate, propionate and butyrate, all of which are critical mediators between gut microbiota and host metabolic health. A ground-breaking human intervention study showed that adding fiber to a hypocaloric, isoenergetic diet beneficially alters the gut microbiota and further alleviates T2D, accompanied by an increased abundance of SCFA-producing microbes [74]. Interestingly, SCFAs not only are an energy source for intestinal cells but also have many beneficial metabolic properties. For example, acetate has been demonstrated to have a direct role in central appetite regulation in mice receiving high-fat diet (HFD) [75] and to promote fat oxidation and improve glucose homeostasis in overweight/obese men [76]. Besides, a human study found that direct delivery of propionate to the colon acutely increases the release of PYY and GLP-1, resulting in a reduction of energy intake, and chronically prevents body weight gain [77]. Oral propionate administration has also been shown to raise basal energy expenditure and fat

oxidation in humans [78]. Furthermore, oral butyrate was previously found to prevent diet induced-obesity by improving glucose homeostasis, increasing energy expenditure, and alleviating insulin resistance in rodents [79, 80], as well as to beneficially affect glucose metabolism in lean humans [81]. However, the causality between SCFAs and host energy metabolism and the mechanisms how SCFAs beneficially improve cardiometabolic health still need further elucidation.

Mechanistically, SCFAs are able to bind to G protein-coupled receptors (GPRs) including GPR41 and GPR43 [82], which are mammalian GPRs expressed in adipocytes, colon epithelial cells, and peripheral blood mononuclear cells. Supplementation of SCFAs prevents HFD-induced obesity in mice, accompanied by changes in the expression of GPR41 and GPR43, i.e., increased in adipose tissue and decreased in the colon [83]. In addition, mice lacking GPR41 or GPR43 exhibit reduced SCFAs-triggered GLP-1 secretion and a parallel impairment of glucose tolerance [84]. Accordingly, a study using *in situ* isolated perfused rat colon demonstrated that SCFAs are an energy source of colonic cells, subsequently triggering GLP-1 secretion independent of the GPR41 and GPR43 [85], inferring other potential pathways involving in the beneficial effects of SCFAs on metabolic health, which are to be further elucidated.

3.3 Brown adipose tissue

BAT is a metabolically active tissue contributing to energy expenditure as described above in *1.3.2*, indicating the therapeutic potential of BAT in treating adiposity. Early evidence for the role of BAT in combating adiposity was provided in mice, in which vagotomy or excision of BAT led to increased fat mass [86]. Also, deficiency of UCP-1 in mice results in a 60-70% reduction in BAT mass and the development of HFD-induced obesity [87]. On the other hand, transgenic mice overexpressing UCP-1 are resistant to genetic and HFD-induced obesity [88, 89]. In humans, an inverse correlation of BAT activity and BMI has been shown [38, 90]. Although correlation does not mean causation, this encouraged research into human BAT as a target to improve energy metabolism.

Preclinical studies also demonstrated beneficial metabolic effects of BAT activation on obesity-associated complications. A complete reversal of HFD-induced insulin resistance was observed in a study with BAT transplantation from donor mice into the visceral cavity of age- and sex-matched recipient mice, indicating that BAT regulates glucose homeostasis and insulin sensitivity [91]. Moreover, cold-activated BAT accelerates plasma clearance of TG in mice [92], which appears to mainly result from enhanced selective LPL-mediated uptake of TRL-derived FAs by BAT [93], collectively suggesting that activation of BAT might be a powerful therapeutic approach to protect from atherosclerosis.

As described in 1.3.2, cold acclimation is the most potent and physiological

stimulator for BAT activation. In addition to cold exposure, BAT is also demonstrated to be activated by selective sympathetic activation. In rodents, β3-AR agonists, such as *CL-316243* and *L-796568*, were found to increase energy expenditure [94, 95]. Of note, a very recent human study demonstrated that chronic treatment with the β3-AR agonist mirabegron increases human brown fat activity, HDL cholesterol levels and insulin sensitivity [96]. Collectively, these findings indicate that developing new methods targeting the sympathetic outflow to activate BAT might provide potential therapeutic handles to combat obesity and its associated cardiometabolic disorders. In fact, previous studies demonstrated that electrical stimulation of specific hypothalamic nuclei is able to promote sympathetic outflow and increase BAT thermogenesis [97, 98]. Others have also used local optogenetics to selectively promote the activity of neurons innervating BAT, indicating that stimulation of the sympathetic nerves is sufficient to elicit thermogenesis in BAT [99]. However, these techniques are difficult to translate to the clinic, and the development of more feasible approaches to increase sympathetic outflow to BAT are thus warranted.

4. Outline of this thesis

This thesis aims to gain insights into novel therapeutic strategies to prevent and treat obesity and its associated cardiometabolic diseases. An introductory overview of energy metabolism and its regulation, how the unbalanced energy metabolism leads to obesity and its associated cardiometabolic diseases, and novel therapeutic strategies to combat obesity and its associated cardiometabolic diseases is presented in **Chapter 1**.

Although the beneficial effects of butyrate on cardiometabolic health are clear, the underlying mechanisms had yet to be further elucidated. In **Chapter 2**, we used our unique APOE*3-Leiden.CETP mouse model, a well-established model for human-like cardiometabolic diseases, to evaluate the mechanisms underlying the effects of dietary butyrate to improve energy metabolism. Interestingly, we revealed that the gut-brain neural circuit plays a crucial role in inducing satiety and activating BAT by dietary butyrate, and we found these effects to be related to alteration of the gut microbiota composition. Therefore, we next explored whether gut microbiota play a causal role in the metabolic benefits of dietary butyrate. To this end, we manipulated microbiota within the gut of the same mouse model by using antibiotics-induced microbiota depletion (AIMD) and FMT in **Chapter 3**, and concluded the causal involvement of a selective proliferation of *Lachnospiraceae bacterium 28-4* in the dietary butyrate induced satiety and ameliorated metabolic health. Previous studies have suggested that SCFAs play a role in metabolic health not only via modulating gut microbiota but possibly also by affecting the production of gut hormones. Therefore, in **Chapter 4** we determined the role of GLP-1 in the beneficial metabolic effects of dietary butyrate, by performing an in-depth mechanistic study to evaluate the contribution of central GLP-1 receptor signaling to the metabolic benefits of dietary butyrate.

In addition to strategies focusing on restricting energy intake, an innovative approach to increase energy expenditure by way of electrical stimulation of BAT was evaluated in **Chapter 5**.

Gut microbial LPS is considered to be another crucial mediator underlying the effects of gut microbiota on metabolic health. In fact, LPS affects lipid metabolism, as evidenced by decreasing hepatic cholesteryl ester transfer protein (CETP) expression. Therefore, in **Chapter 6**, we investigated the mechanisms by which LPS reduces CETP expression and lipid metabolism, again using our APOE*3-Leiden.CETP mouse model.

In **Chapter 7**, the results of these novel therapeutic strategies to combat obesity and its cardiometabolic diseases by restriction of energy intake and promotion of energy expenditure, and their clinical implications are discussed in context of the present scientific literature.

References

1. Hill, J.O., H.R. Wyatt, and J.C. Peters, *Energy balance and obesity.* Circulation, 2012. **126**(1): p. 126-32.
2. Must, A., et al., *The disease burden associated with overweight and obesity.* JAMA, 1999. **282**(16): p. 1523-9.
3. Collaborators, G.B.D.O., et al., *Health Effects of Overweight and Obesity in 195 Countries over 25 Years.* N Engl J Med, 2017. **377**(1): p. 13-27.
4. Kumar, R.B. and L.J. Aronne, *Efficacy comparison of medications approved for chronic weight management.* Obesity (Silver Spring), 2015. **23 Suppl 1**: p. S4-7.
5. Wells, J.C., et al., *The double burden of malnutrition: aetiological pathways and consequences for health.* Lancet, 2020. **395**(10217): p. 75-88.
6. Mahoney, L.B., C.A. Denny, and T.N. Seyfried, *Caloric restriction in C57BL/6J mice mimics therapeutic fasting in humans.* Lipids Health Dis, 2006. **5**: p. 13.
7. Dorling, J.L., et al., *Changes in body weight, adherence, and appetite during 2 years of calorie restriction: the CALERIE 2 randomized clinical trial.* Eur J Clin Nutr, 2020. **74**(8): p. 1210-1220.
8. Most, J., et al., *Significant improvement in cardiometabolic health in healthy nonobese individuals during caloric restriction-induced weight loss and weight loss maintenance.* Am J Physiol Endocrinol Metab, 2018. **314**(4): p. E396-E405.
9. Manini, T.M., *Energy expenditure and aging.* Ageing Res Rev, 2010. **9**(1): p. 1-11.
10. Benton, D. and H.A. Young, *Reducing Calorie Intake May Not Help You Lose Body Weight.* Perspect Psychol Sci, 2017. **12**(5): p. 703-714.
11. Ravussin, E., et al., *Reduced rate of energy expenditure as a risk factor for body-weight gain.* N Engl J Med, 1988. **318**(8): p. 467-72.
12. Ballor, D.L. and R.E. Keesey, *A meta-analysis of the factors affecting exercise-induced changes in body mass, fat mass and fat-free mass in males and females.* Int J Obes, 1991. **15**(11): p. 717-26.
13. Clark, J.T., P.S. Kalra, and S.P. Kalra, *Neuropeptide Y stimulates feeding but inhibits sexual behavior in rats.* Endocrinology, 1985. **117**(6): p. 2435-42.
14. Lecklin, A., et al., *Agonists for neuropeptide Y receptors Y1 and Y5 stimulate different phases of feeding in guinea pigs.* Br J Pharmacol, 2003. **139**(8): p. 1433-40.
15. MacNeil, D.J., *NPY Y1 and Y5 receptor selective antagonists as anti-obesity drugs.* Curr Top Med Chem, 2007. **7**(17): p. 1721-33.
16. Butler, A.A., et al., *A unique metabolic syndrome causes obesity in the melanocortin-3 receptor-deficient mouse.* Endocrinology, 2000. **141**(9): p. 3518-21.
17. Sutton, G.M., et al., *Diet-genotype interactions in the development of the obese, insulin-resistant phenotype of C57BL/6J mice lacking melanocortin-3 or -4 receptors.* Endocrinology, 2006. **147**(5): p. 2183-96.
18. Vaisse, C., et al., *A frameshift mutation in human MC4R is associated with a dominant form of obesity.* Nat Genet, 1998. **20**(2): p. 113-4.
19. Lee, Y.S., L.K. Poh, and K.Y. Loke, *A novel melanocortin 3 receptor gene (MC3R) mutation associated with severe obesity.* J Clin Endocrinol Metab, 2002. **87**(3): p. 1423-6.

20. Clement, K., et al., *MC4R agonism promotes durable weight loss in patients with leptin receptor deficiency.* Nat Med, 2018. **24**(5): p. 551-555.

21. Karra, E., K. Chandarana, and R.L. Batterham, *The role of peptide YY in appetite regulation and obesity.* J Physiol, 2009. **587**(1): p. 19-25.

22. Little, T.J., M. Horowitz, and C. Feinle-Bisset, *Role of cholecystokinin in appetite control and body weight regulation.* Obes Rev, 2005. **6**(4): p. 297-306.

23. Chelikani, P.K., A.C. Haver, and R.D. Reidelberger, *Intravenous infusion of glucagon-like peptide-1 potently inhibits food intake, sham feeding, and gastric emptying in rats.* Am J Physiol Regul Integr Comp Physiol, 2005. **288**(6): p. R1695-706.

24. Gutzwiller, J.P., et al., *Glucagon-like peptide-1: a potent regulator of food intake in humans.* Gut, 1999. **44**(1): p. 81-6.

25. Baggio, L.L. and D.J. Drucker, *Glucagon-like peptide-1 receptors in the brain: controlling food intake and body weight.* J Clin Invest, 2014. **124**(10): p. 4223-6.

26. Hunter, K. and C. Holscher, *Drugs developed to treat diabetes, liraglutide and lixisenatide, cross the blood brain barrier and enhance neurogenesis.* BMC Neurosci, 2012. **13**: p. 33.

27. Meeran, K., et al., *Repeated intracerebroventricular administration of glucagon-like peptide-1-(7-36) amide or exendin-(9-39) alters body weight in the rat.* Endocrinology, 1999. **140**(1): p. 244-50.

28. Turton, M.D., et al., *A role for glucagon-like peptide-1 in the central regulation of feeding.* Nature, 1996. **379**(6560): p. 69-72.

29. Nakagawa, A., et al., *Receptor gene expression of glucagon-like peptide-1, but not glucose-dependent insulinotropic polypeptide, in rat nodose ganglion cells.* Auton Neurosci, 2004. **110**(1): p. 36-43.

30. Bucinskaite, V., et al., *Receptor-mediated activation of gastric vagal afferents by glucagon-like peptide-1 in the rat.* Neurogastroenterol Motil, 2009. **21**(9): p. 978-e78.

31. Plamboeck, A., et al., *The effect of exogenous GLP-1 on food intake is lost in male truncally vagotomized subjects with pyloroplasty.* Am J Physiol Gastrointest Liver Physiol, 2013. **304**(12): p. G1117-27.

32. Washburn, R.A., et al., *Does increased prescribed exercise alter non-exercise physical activity/energy expenditure in healthy adults? A systematic review.* Clin Obes, 2014. **4**(1): p. 1-20.

33. Aoi, W., Y. Naito, and T. Yoshikawa, *Dietary exercise as a novel strategy for the prevention and treatment of metabolic syndrome: effects on skeletal muscle function.* J Nutr Metab, 2011. **2011**: p. 676208.

34. Cypess, A.M., et al., *Identification and importance of brown adipose tissue in adult humans.* N Engl J Med, 2009. **360**(15): p. 1509-17.

35. Cannon, B. and J. Nedergaard, *Brown adipose tissue: function and physiological significance.* Physiol Rev, 2004. **84**(1): p. 277-359.

36. Khedoe, P.P., et al., *Brown adipose tissue takes up plasma triglycerides mostly after lipolysis.* J Lipid Res, 2015. **56**(1): p. 51-9.

37. Bartelt, A., et al., *Thermogenic adipocytes promote HDL turnover and reverse cholesterol transport.* Nat Commun, 2017. **8**: p. 15010.

38. van Marken Lichtenbelt, W.D., et al., *Cold-activated brown adipose tissue in healthy men.* N Engl J Med, 2009. **360**(15): p. 1500-8.

39. International Diabetes Federation, 2017; Available from: http://www.diabetesatlas.org/.

40. Wang, Y. and B.R. Luo, *The association of body composition with the risk of gestational diabetes mellitus in Chinese pregnant women: A case-control study.* Medicine (Baltimore), 2019. **98**(42): p. e17576.

41. Colditz, G.A., et al., *Weight gain as a risk factor for clinical diabetes mellitus in women.* Ann Intern Med, 1995. **122**(7): p. 481-6.

42. Schnurr, T.M., et al., *Obesity, unfavourable lifestyle and genetic risk of type 2 diabetes: a case-cohort study.* Diabetologia, 2020. **63**(7): p. 1324-1332.

43. Hubert, H.B., et al., *Obesity as an independent risk factor for cardiovascular disease: a 26-year follow-up of participants in the Framingham Heart Study.* Circulation, 1983. **67**(5): p. 968-77.

44. World Health Organization, 2017; Available from: https://www.who.int/en/news-room/fact-sheets/detail/cardiovascular-diseases-(cvds).

45. Boren, J., et al., *Low-density lipoproteins cause atherosclerotic cardiovascular disease: pathophysiological, genetic, and therapeutic insights: a consensus statement from the European Atherosclerosis Society Consensus Panel.* Eur Heart J, 2020. **41**(24): p. 2313-2330.

46. Hadjiphilippou, S. and K.K. Ray, *Cholesterol-Lowering Agents.* Circ Res, 2019. **124**(3): p. 354-363.

47. Lovren, F., H. Teoh, and S. Verma, *Obesity and atherosclerosis: mechanistic insights.* Can J Cardiol, 2015. **31**(2): p. 177-83.

48. Oshakbayev, K., et al., *Weight loss therapy for clinical management of patients with some atherosclerotic diseases: a randomized clinical trial.* Nutr J, 2015. **14**: p. 120.

49. Karason, K., et al., *Weight loss and progression of early atherosclerosis in the carotid artery: a four-year controlled study of obese subjects.* Int J Obes Relat Metab Disord, 1999. **23**(9): p. 948-56.

50. Chalasani, N., et al., *The diagnosis and management of nonalcoholic fatty liver disease: Practice guidance from the American Association for the Study of Liver Diseases.* Hepatology, 2018. **67**(1): p. 328-357.

51. Carr, R.M., A. Oranu, and V. Khungar, *Nonalcoholic Fatty Liver Disease: Pathophysiology and Management.* Gastroenterol Clin North Am, 2016. **45**(4): p. 639-652.

52. Koutoukidis, D.A., et al., *Association of Weight Loss Interventions With Changes in Biomarkers of Nonalcoholic Fatty Liver Disease: A Systematic Review and Meta-analysis.* JAMA Intern Med, 2019.

53. Ruhl, C.E. and J.E. Everhart, *Determinants of the association of overweight with elevated serum alanine aminotransferase activity in the United States.* Gastroenterology, 2003. **124**(1): p. 71-9.

54. Backhed, F., et al., *The gut microbiota as an environmental factor that regulates fat storage.* Proc Natl Acad Sci U S A, 2004. **101**(44): p. 15718-23.

55. Li, B., et al., *Microbiota Depletion Impairs Thermogenesis of Brown Adipose Tissue and Browning of White Adipose Tissue.* Cell Rep, 2019. **26**(10): p. 2720-2737 e5.

56. Fetissov, S.O., *Role of the gut microbiota in host appetite control: bacterial growth to animal feeding behaviour.* Nat Rev Endocrinol, 2017. **13**(1): p. 11-25.

57. Fang, S. and R.M. Evans, *Microbiology: Wealth management in the gut.* Nature, 2013. **500**(7464): p. 538-9.

58. Kleiman, S.C., et al., *The Intestinal Microbiota in Acute Anorexia Nervosa and During Renourishment: Relationship to Depression, Anxiety, and Eating Disorder Psychopathology.* Psychosom Med, 2015. **77**(9): p. 969-81.

59. Ridaura, V.K., et al., *Gut microbiota from twins discordant for obesity modulate metabolism in mice.* Science, 2013. **341**(6150): p. 1241214.

60. Ussar, S., S. Fujisaka, and C.R. Kahn, *Interactions between host genetics and gut microbiome in diabetes and metabolic syndrome.* Mol Metab, 2016. **5**(9): p. 795-803.

61. Muccioli, G.G., et al., *The endocannabinoid system links gut microbiota to adipogenesis.* Mol Syst Biol, 2010. **6**: p. 392.

62. Moran-Ramos, S., B.E. Lopez-Contreras, and S. Canizales-Quinteros, *Gut Microbiota in Obesity and Metabolic Abnormalities: A Matter of Composition or Functionality?* Arch Med Res, 2017. **48**(8): p. 735-753.

63. Cani, P.D., et al., *Gut microbiota fermentation of prebiotics increases satietogenic and incretin gut peptide production with consequences for appetite sensation and glucose response after a meal.* Am J Clin Nutr, 2009. **90**(5): p. 1236-43.

64. Costello, E.K., et al., *Bacterial community variation in human body habitats across space and time.* Science, 2009. **326**(5960): p. 1694-7.

65. Singh, R.K., et al., *Influence of diet on the gut microbiome and implications for human health.* J Transl Med, 2017. **15**(1): p. 73.

66. Deehan, E.C., et al., *Modulation of the Gastrointestinal Microbiome with Nondigestible Fermentable Carbohydrates To Improve Human Health.* Microbiol Spectr, 2017. **5**(5).

67. de Vrese, M. and J. Schrezenmeir, *Probiotics, prebiotics, and synbiotics.* Adv Biochem Eng Biotechnol, 2008. **111**: p. 1-66.

68. Cotillard, A., et al., *Dietary intervention impact on gut microbial gene richness.* Nature, 2013. **500**(7464): p. 585-8.

69. Luoto, R., et al., *The impact of perinatal probiotic intervention on the development of overweight and obesity: follow-up study from birth to 10 years.* Int J Obes (Lond), 2010. **34**(10): p. 1531-7.

70. Alisi, A., et al., *Randomised clinical trial: The beneficial effects of VSL#3 in obese children with non-alcoholic steatohepatitis.* Aliment Pharmacol Ther, 2014. **39**(11): p. 1276-85.

71. Smits, L.P., et al., *Therapeutic potential of fecal microbiota transplantation.* Gastroenterology, 2013. **145**(5): p. 946-53.

72. Sung, M.M., et al., *Improved Glucose Homeostasis in Obese Mice Treated With Resveratrol Is Associated With Alterations in the Gut Microbiome.* Diabetes, 2017. **66**(2): p. 418-425.

73. Depommier, C., et al., *Supplementation with Akkermansia muciniphila in overweight and obese human volunteers: a proof-of-concept exploratory study.* Nat Med, 2019. **25**(7): p. 1096-1103.

74. Zhao, L., et al., *Gut bacteria selectively promoted by dietary fibers alleviate type 2 diabetes.* Science, 2018. **359**(6380): p. 1151-1156.

75. Frost, G., et al., *The short-chain fatty acid acetate reduces appetite via a central homeostatic mechanism.* Nat Commun, 2014. **5**: p. 3611.

76. van der Beek, C.M., et al., *Distal, not proximal, colonic acetate infusions promote fat oxidation and improve metabolic markers in overweight/obese men.* Clin Sci (Lond), 2016. **130**(22): p. 2073-2082.

77. Chambers, E.S., et al., *Effects of targeted delivery of propionate to the human colon on appetite regulation, body weight maintenance and adiposity in overweight adults.* Gut, 2015. **64**(11): p. 1744-54.

78. Chambers, E.S., et al., *Acute oral sodium propionate supplementation raises resting energy expenditure and lipid oxidation in fasted humans.* Diabetes Obes Metab, 2018. **20**(4): p. 1034-1039.

79. Gao, Z., et al., *Butyrate improves insulin sensitivity and increases energy expenditure in mice.* Diabetes, 2009. **58**(7): p. 1509-17.

80. Hong, J., et al., *Butyrate alleviates high fat diet-induced obesity through activation of adiponectin-mediated pathway and stimulation of mitochondrial function in the skeletal muscle of mice.* Oncotarget, 2016. **7**(35): p. 56071-56082.

81. Bouter, K., et al., *Differential metabolic effects of oral butyrate treatment in lean versus metabolic syndrome subjects.* Clin Transl Gastroenterol, 2018. **9**(5): p. 155.

82. Ang, Z., et al., *FFAR2-FFAR3 receptor heteromerization modulates short-chain fatty acid sensing.* FASEB J, 2018. **32**(1): p. 289-303.

83. Lu, Y., et al., *Short Chain Fatty Acids Prevent High-fat-diet-induced Obesity in Mice by Regulating G Protein-coupled Receptors and Gut Microbiota.* Sci Rep, 2016. **6**: p. 37589.

84. Tolhurst, G., et al., *Short-chain fatty acids stimulate glucagon-like peptide-1 secretion via the G-protein-coupled receptor FFAR2.* Diabetes, 2012. **61**(2): p. 364-71.

85. Christiansen, C.B., et al., *The impact of short-chain fatty acids on GLP-1 and PYY secretion from the isolated perfused rat colon.* Am J Physiol Gastrointest Liver Physiol, 2018. **315**(1): p. G53-G65.

86. Dulloo, A.G. and D.S. Miller, *Energy balance following sympathetic denervation of brown adipose tissue.* Can J Physiol Pharmacol, 1984. **62**(2): p. 235-40.

87. Hamann, A., J.S. Flier, and B.B. Lowell, *Decreased brown fat markedly enhances susceptibility to diet-induced obesity, diabetes, and hyperlipidemia.* Endocrinology, 1996. **137**(1): p. 21-9.

88. Kopecky, J., et al., *Reduction of dietary obesity in aP2-Ucp transgenic mice: physiology and adipose tissue distribution.* Am J Physiol, 1996. **270**(5 Pt 1): p. E768-75.

89. Kopecky, J., et al., *Expression of the mitochondrial uncoupling protein gene from the aP2 gene promoter prevents genetic obesity.* J Clin Invest, 1995. **96**(6): p. 2914-23.

90. Saito, M., et al., *High incidence of metabolically active brown adipose tissue in healthy adult humans: effects of cold exposure and adiposity.* Diabetes, 2009. **58**(7): p. 1526-31.

91. Stanford, K.I., et al., *Brown adipose tissue regulates glucose homeostasis and insulin sensitivity.* J Clin Invest, 2013. **123**(1): p. 215-23.

92. Bartelt, A., et al., *Brown adipose tissue activity controls triglyceride clearance.* Nat Med, 2011. **17**(2): p. 200-5.

93. Berbee, J.F., et al., *Brown fat activation reduces hypercholesterolaemia and protects from atherosclerosis development.* Nat Commun, 2015. **6**: p. 6356.

94. Atgie, C., et al., *Effects of chronic treatment with noradrenaline or a specific beta3-adrenergic agonist, CL 316 243, on energy expenditure and epididymal adipocyte lipolytic activity in rat.* Comp Biochem Physiol A Mol Integr Physiol, 1998. **119**(2): p. 629-36.

95. van Baak, M.A., et al., *Acute effect of L-796568, a novel beta 3-adrenergic receptor agonist, on energy expenditure in obese men.* Clin Pharmacol Ther, 2002. **71**(4): p. 272-9.

96. O'Mara, A.E., et al., *Chronic mirabegron treatment increases human brown fat, HDL cholesterol, and insulin sensitivity.* J Clin Invest, 2020. **130**(5): p. 2209-2219.

97. Freeman, P.H. and P.J. Wellman, *Brown adipose tissue thermogenesis induced by low level electrical stimulation of hypothalamus in rats.* Brain Res Bull, 1987. **18**(1): p. 7-11.

98. Halvorson, I., L. Gregor, and J.A. Thornhill, *Brown adipose tissue thermogenesis is activated by electrical and chemical (L-glutamate) stimulation of the ventromedial hypothalamic nucleus in cold-acclimated rats.* Brain Res, 1990. **522**(1): p. 76-82.

99. Lyons, C.E., et al., *Optogenetic-induced sympathetic neuromodulation of brown adipose tissue thermogenesis.* FASEB J, 2020. **34**(2): p. 2765-2773.

CHAPTER 2

BUTYRATE REDUCES APPETITE AND ACTIVATES BROWN ADIPOSE TISSUE VIA THE GUT-BRAIN NEURAL CIRCUIT

Li Z, Yi CX, Katiraei S, Kooijman S, Zhou E, Chung CK, Gao Y, Van den Heuvel JK, Meijer OC, Berbée JFP, Heijink M, Giera M, Willems van Dijk K, Groen AK, Rensen PCN, Wang Y

***Gut 2018**, 67: 1269-1279*

Abstract

Objective: Butyrate exerts metabolic benefits in mice and humans, the underlying mechanisms being still unclear. We aimed to investigate the effect of butyrate on appetite and energy expenditure, and to what extent these two components contribute to the beneficial metabolic effects of butyrate.

Design: A cute effects of butyrate on appetite and its method of action were investigated in mice following an intragastric gavage or intravenous injection of butyrate. To study the contribution of satiety to the metabolic benefits of butyrate, mice were fed a high-fat diet with butyrate, and an additional pair-fed group was included. Mechanistic involvement of the gut-brain neural circuit was investigated in vagotomised mice.

Results: A cute oral, but not intravenous, butyrate administration decreased food intake, suppressed the activity of orexigenic neurons that express neuropeptide Y in the hypothalamus, and decreased neuronal activity within the nucleus tractus solitarius and dorsal vagal complex in the brainstem. Chronic butyrate supplementation prevented diet-induced obesity, hyperinsulinemia, hypertriglyceridemie and hepatic steatosis, largely attributed to a reduction in food intake. Butyrate also modestly promoted fat oxidation and activated brown adipose tissue (BAT), evident from increased utilization of plasma triglyceride-derived fatty acids. This effect was not due to the reduced food intake, but explained by an increased sympathetic outflow to BAT. Subdiaphragmatic vagotomy abolished the effects of butyrate on food intake as well as the stimulation of metabolic activity in BAT.

Conclusion: Butyrate acts on the gut-brain neural circuit to improve energy metabolism via reducing energy intake and enhancing fat oxidation by activating BAT.

Introduction

A positive energy balance, which occurs when energy intake exceeds energy expenditure, leads to the development of obesity. The prevalence of obesity has been increasing steadily over the past two decades, and obesity is becoming a global health concern. Obesity and obesity-initiated diseases are associated with high mortality and morbidity, mainly related to diabetes mellitus and cardiovascular disease [1]. Obese individuals have enhanced appetite [2] and/or reduced energy expenditure, mainly due to insufficient physical activity and impaired brown adipose tissue (BAT) activity [3, 4]. BAT contributes substantially to energy expenditure by combusting large amounts of triglycerides (TG) and glucose in humans (reviewed in refs) [5, 6], and its activity is mainly regulated through the sympathetic nervous system (SNS) under the control of the hypothalamus [7, 8]. The hypothalamus is also the central key regulator of food intake [9] and energy intake, receiving hormonal and neural signals emanating from the GI tract, adipose tissue and other peripheral organs. Although several pharmaceutical agents have been approved for the treatment of obesity, the clinical application of these agents for long-term body weight management is hampered due to the high incidence of adverse events [10]. The fundamental approach for combating against obesity is still lifestyle intervention, including diet adjustment.

Dietary fiber is deemed to be a key component in the healthy eating, mainly because dietary fiber is the main resource for production of endogenous short-chain fatty acids (SCFA) during bacterial fermentation in the colon. Interestingly, dietary supplementation of SCFAs has been shown to protect from obesity [11], making SCFAs promising candidates for the prevention of metabolic disorders. Of the SCFAs, in particular butyrate supplementation was found to have profound multiple metabolic benefits, including prevention of high-fat diet (HFD)-induced obesity, insulin resistance and hepatic steatosis [12-15]. A reasonable speculation is that butyrate acts on components of the energy balance, that is, stimulating energy expenditure, and/or reducing energy intake, thereby reducing obesity and obesity-associated disorders. A previous study indeed showed that butyrate induced peroxisome proliferator-activated receptor-γ coactivator-1α activity, thereby enhancing mitochondrial function in BAT and substantially promoting energy expenditure [13]. On the other hand, the effect of butyrate consumption on appetite is rather obscure. Whereas at least one study showed a clear reduction in food intake upon butyrate intervention [11], other studies reported that dietary supplementation of butyrate did not alter food intake [13, 15, 16] in diet-induced obese mice. Interestingly, clinical studies showed that dietary fiber, that is, oligofructose, increases endogenous butyrate production, accompanied by a reduction in energy intake [17, 18].

By using APOE*3-Leiden.CETP mice, a well-established translational model for developing human-like diet-induced obesity, dyslipidemia and metabolic syndrome [19, 20], we now aimed to evaluate the effect of butyrate on energy

intake and energy expenditure with respect to BAT activity, and to dissect the contribution of these two components of the energy balance to the metabolic benefits of butyrate. Here we provide first evidence that oral butyrate via the gut-brain neural circuit reduces appetite and activates BAT.

Materials and methods

Please see online supplementary materials and methods for an expanded version of this section.

Animals

APOE*3-Leiden.CETP (E3L.CETP) mice were obtained as previously described [21] and housed under standard conditions in conventional cages with free access to chow diet and water unless indicated otherwise. At the age of 10-12 weeks, male mice were used for experiments in accordance with the regulations of Dutch law on animal welfare.

Chronic intervention experiment

Mice received an HFD (60% kcal derived from lard fat and 0.25% cholesterol (w/w), Research Diets, New Brunswick, NJ) without (control group) or with 5% (w/w) sodium butyrate (Sigma Aldrich; butyrate group) for 9 weeks. Since butyrate was expected to reduce food intake, a third group of mice received the same amount of HFD as that of the butyrate group (pair-fed group).

Subdiaphragmatic vagotomy surgery

Mice received subdiaphragmatic vagotomy surgery [22] or sham surgery as controls. After a recovery period of 1 week after the surgery, mice received an HFD alone or supplemented with 5% (w/w) sodium butyrate for 7 weeks.

Statistical analysis

All data are expressed as mean ± SEM. For studies including three groups, differences between groups were determined using one-way analysis of variance test. When significant differences were found, Fisher's least significant difference test was used as a post hoc test to determine the differences between two independent groups. For studies including two groups, statistical differences between groups were calculated using a two-tail unpaired Student's t-test. A P value less than 0.05 was considered statistically significant.

Results

Oral rather than intravenous butyrate decreases food intake and inhibits orexigenic neuron activity in hypothalamus

We first evaluated the effect of butyrate on appetite. In overnight fasted mice, butyrate administration via intragastric gavage significantly prevented food intake within 1 hour after refeeding, and led to a 21% reduction in cumulative food intake over 24 hours (figure 1A). This acute reduction in food intake was accompanied with a large decrease in number of FOS-positive neurons within the arcuate nucleus in the hypothalamus (-73%, figure 1B). Furthermore, oral butyrate markedly decreased the portion of neuropeptide Y (NPY)-positive neurons that also express c-FOS (-49%, figure 1C), while did not influence the portion of pro-opiomelanocortin-positive neurons coexpressing c-FOS (figure 1D). In addition, oral butyrate clearly decreased the number of FOS-positive neurons within nucleus tractus solitarius (NTS) and dorsal vagal complex (DVC) in brainstem (-37%, figure 1E), without affecting the neuronal activity in either cortical region or hippocampal region (data not shown). Notably, 1 hour after gavage, oral butyrate supplementation raised the portal vein and peripheral circulating butyrate concentration as compared with the control group. To elucidate whether the increased circulating butyrate evoked the reduced appetite, we also administered butyrate directly into the circulation by intravenous injection. As a result, the circulating butyrate concentration markedly increased (online supplementary figure S1), however without influencing either acute refeeding or food intake within 24 hours (figure 1F). Collectively, these data imply that oral administration of butyrate reduces food intake and hypothalamic neuronal signaling independent of increased circulating butyrate levels, indicating a mechanism involving the gut-brain neural circuit.

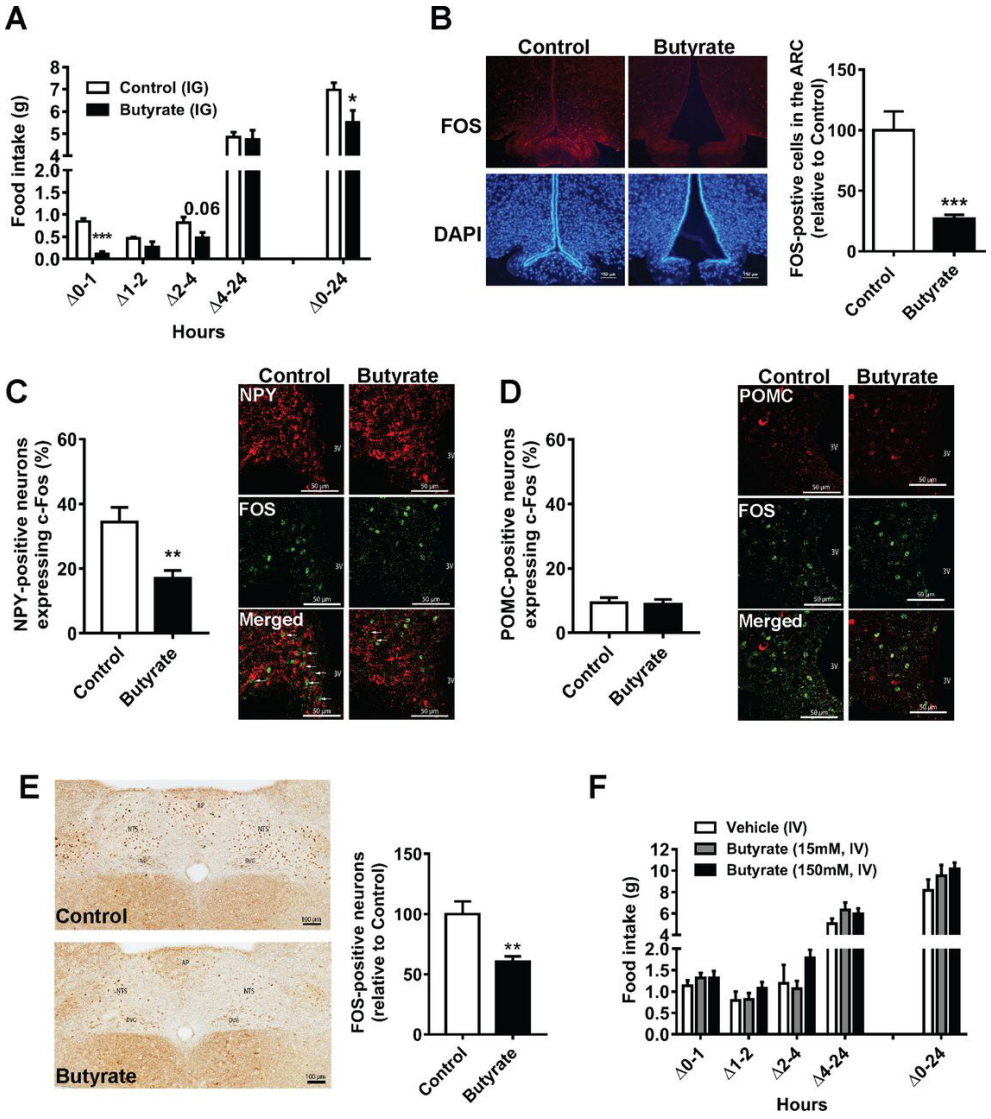

Figure 1. Oral but not intravenous butyrate decreases appetite and suppresses the activity of orexigenic neurons expressing NPY in the hypothalamus. After overnight fasting and randomization based on body weight, mice received vehicle or butyrate via the intragastric gavage (IG, A) or intravenous injection (IV, F). Food intake was measured during 24 hours. One hour after receiving butyrate IG, mice were anaesthetized and brains were collected immediately. FOS staining was performed in cryostat sections of frozen brains. The number of c-FOS-positive neurons within the arcuate nucleus in the hypothalamus (B) and nucleus tractus solitarius (NTS) and dorsal vagal complex (DVC) in the brainstem (E) was quantified. The colocalization percentages of NPY/c-FOS-positive neurons (C) and POMC/c-FOS-positive neurons (D) were quantified, with representative pictures as shown. Data are means ± SEM (n=8–9); *P<0.05, ***P<0.001 compared with control group. NPY, neuropeptide Y; POMC, pro-opiomelanocortin.

Butyrate consumption prevents HFD-induced obesity and hepatic steatosis, mainly via reducing food intake

To evaluate the contribution of reduced food intake to the metabolic benefits of chronic butyrate treatment, we fed E3L.CETP mice an HFD without or with sodium butyrate for 9 weeks, and included an additional group that was pair-fed to the butyrate group while receiving HFD. In line with the acute reduced appetite effect of a single oral butyrate administration, chronic dietary butyrate supplementation also caused a sustained reduction in food intake during the 9-week intervention period (figure 2A), resulting in 22% less food intake as compared with that of the control group (figure 2B).

We observed that butyrate completely prevented HFD-induced body weight gain (figure 2C), accompanied by decreased fat mass gain (figure 2D) without affecting lean mass as compared with the control group. Of note, during the first 7 weeks, food restriction per se by pair feeding diminished diet-induced obesity to a similar extent as observed by butyrate supplementation (figure 2C). After 9 weeks of intervention, as compared with control group, butyrate supplementation decreased body weight by -27% (figure 2E) and the weight of the gonadal (g) white adipose tissue (WAT) pad by -69% (figure 2F); while pair feeding decreased body weight by -18% (figure 2E) and the weight of the gWAT pad by -42% (figure 2F). This suggests that the antiobesity action of butyrate is largely dependent on reduction of food intake.

Butyrate also decreased liver weight (-25%, figure 2G), hepatic TG and phospholipid content (figure 2H) as compared with the HFD control group. Chronic butyrate consumption did not alter the levels of acetate, propionate and butyrate in peripheral blood, nor in portal vein blood (online supplementary figure S2). Pair-fed mice showed the same reduction in liver weight and lipid content as that of butyrate-treated mice (figure 2G, H). Representative pictures of liver sections confirmed that butyrate prevents HFD-induced hepatic steatosis through lowering of food intake (figure 2I).

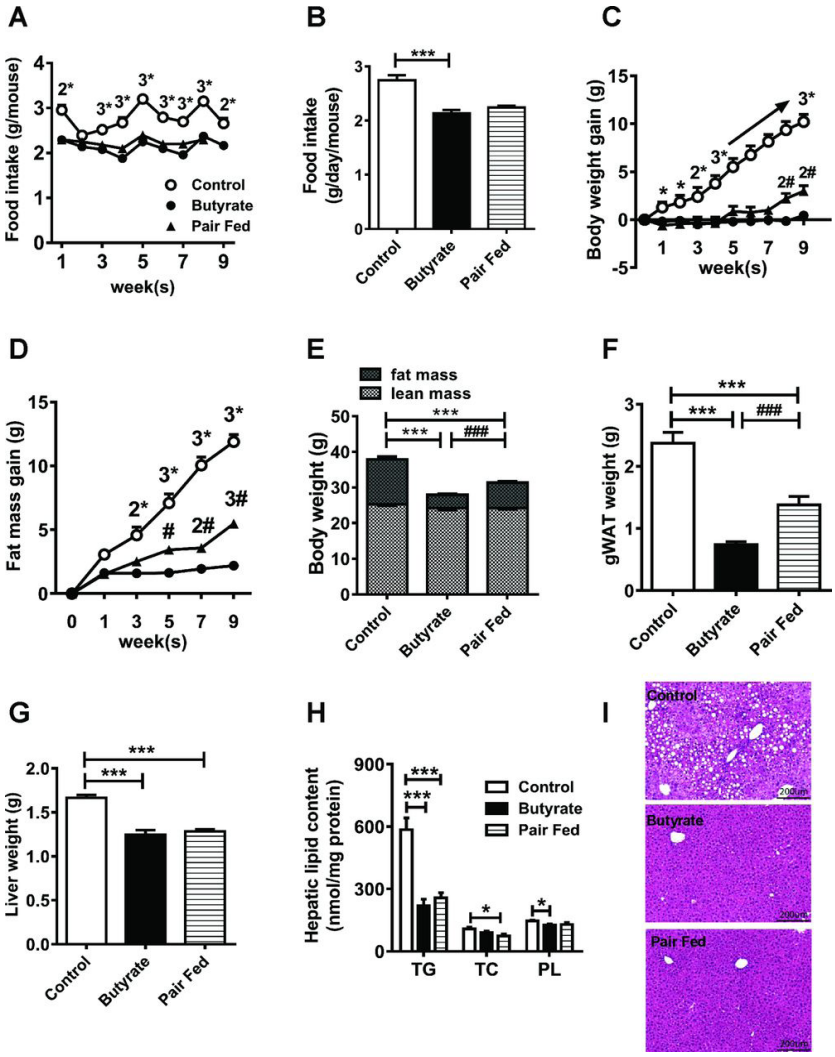

Figure 2. Butyrate consumption prevents high-fat diet (HFD)-induced obesity and hepatic steatosis, mainly via reducing food intake. Mice were individually housed and receive an HFD without (control group), or with 5% (w/w) sodium butyrate (butyrate group) for 9 weeks. A third group of mice received the same amount of HFD as consumed by the butyrate group (pair-fed group). Food intake was measured weekly (A), and average food intake per group through the whole intervention period was calculated (B). Body weight was measured weekly, and fat mass and lean mass were measured every other week by EchoMRI to calculate the body weight gain (C) and fat mass gain (D). At the end of this study, body composition (E), gonadal white fat pad weight (F), liver weight (G) and liver triglycerides (TG), total cholesterol (TC) and phospholipid (PL) content (H) were measured. Representative pictures of liver sections in H&E staining are shown (I). Data are means ± SEM (n=9–10); *P<0.05, **P<0.01, ***P<0.001 as control group compared with butyrate group; #P<0.05, ##P<0.01, ###P<0.001 as pair-fed group compared with butyrate group. gWAT, gonadal white adipose tissue.

Butyrate consumption improves lipid and glucose metabolism, in part by reduced food intake

Butyrate supplementation significantly decreased plasma TG levels (figure 3A), tended to decrease plasma glucose levels (P=0.05; figure 3B) and markedly decreased fasting insulin levels (figure 3C) and homeostatic model assessment of insulin resistance (figure 3D) as compared with controls, indicating that butyrate improves plasma lipid metabolism and insulin sensitivity. The beneficial effects of butyrate on plasma TG and glucose metabolism could be only partially attributed to the reduced food intake by butyrate, as pair feeding only reduced the plasma glucose level, and had no effects on plasma levels of TG and insulin (figure 3B).

To determine the organs involved in the TG and glucose lowering effects of butyrate, we injected mice with [^{3}H]TO-labelled TRL-like particles [23] and [^{14}C]DG. In parallel with a decreased plasma TG level, butyrate accelerated the clearance of [^{3}H]TO from the circulation as evidenced by reduced half-life of [^{3}H]TO (figure 3E). The accelerated [^{3}H]TO clearance was caused by a large increase in the uptake of [^{3}H]TO-derived activity by BAT depots (+174% for interscapular BAT (iBAT) and +123% for subscapular BAT; figure 3F), and to some extent by muscle and WAT (figure 3F). In contrast, food restriction *per se* by pair feeding did not increase the uptake of [^{3}H]TO-derived activity by BAT, muscle and WAT as compared with the control group. As may be expected, both butyrate treatment and pair feeding reduced the half-life of [^{14}C]DG (figure 3G) as compared with control group, indicating that butyrate accelerates the clearance of circulating [^{14}C]DG and could be explained by the reduction of food intake. Indeed, pair feeding increased the uptake of [^{14}C]DG by muscle and WAT to the same extent as that of butyrate treatment.

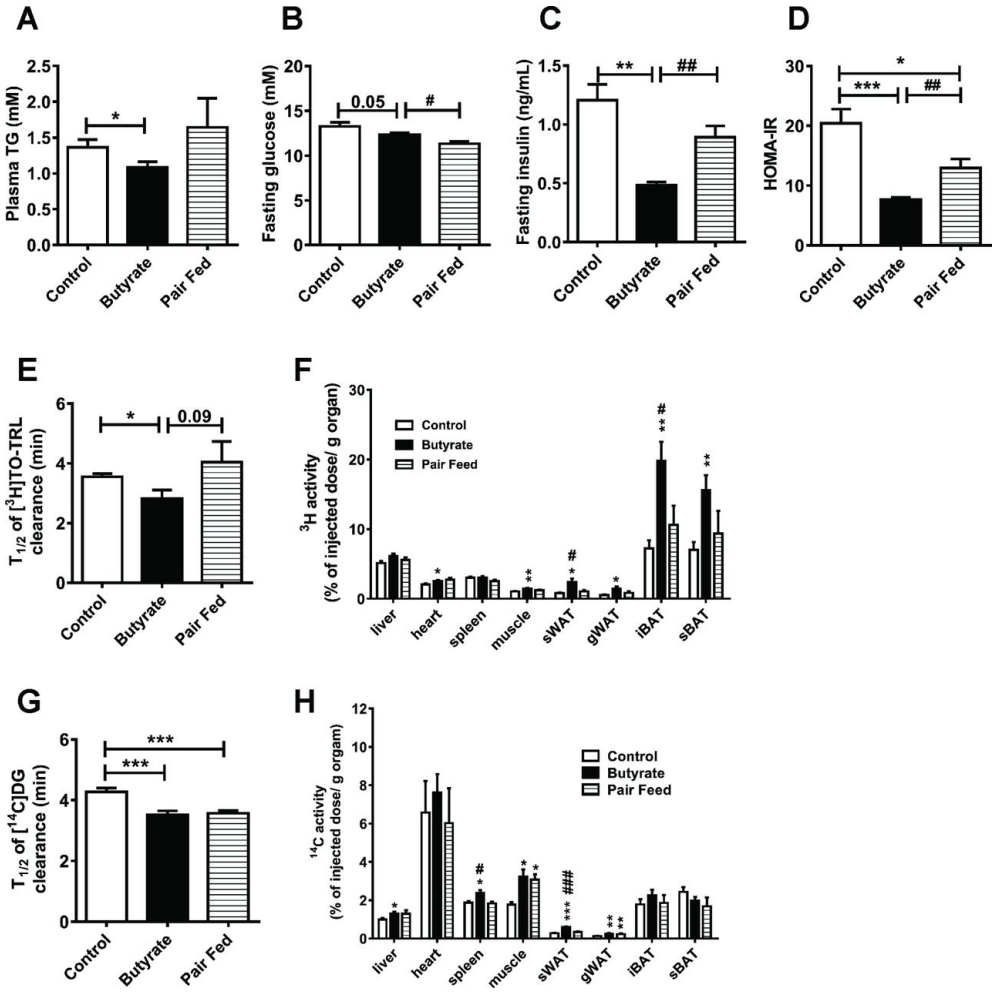

Figure 3. Butyrate consumption improves lipid and glucose metabolism, partially by reducing food intake. After 9 weeks of treatment with butyrate, plasma was assayed for TG (A), glucose (B) and insulin (C), and homeostatic model assessment of insulin resistance (HOMA-IR) (D) was calculated. At the end of this study, a combined TG and glucose clearance test was performed. Conscious mice were intravenously injected with [^{3}H]TO-labelled TRL-like particles and [^{14}C]DG. Subsequently, the plasma half-life of [^{3}H]TO (E) and [^{14}C]DG (G) was calculated, and 15 min after injection, the uptake of ^{3}H (F) and ^{14}C (H) by various tissues was assessed. Data are means±SEM (n=8–9); *P<0.05, **P<0.01, ***P<0.001 as control group compared with butyrate group; #P<0.05, ##P<0.01, ###P<0.001 as pair-fed group compared with butyrate group. gWAT, gonadal white adipose tissue; iBAT, interscapular brown adipose tissue; sBAT, subscapular brown adipose tissue; sWAT, subcutaneous white adipose tissue; TG, triglyceride.

Butyrate consumption promotes fat oxidation at the expense of carbohydrate oxidation

Since the effects of butyrate on body fat and lipid metabolism could only be partly attributed to reduction of food intake, indirect calorimetry was performed to determine the effects of butyrate on energy expenditure. In the first week of the intervention, when body weight of the mice was still comparable between the butyrate and control groups, mice were housed in fully automated metabolic cages. Butyrate treatment did not affect the spontaneous physical activity of the mice (figure 4A). Although no effect on total energy metabolism was detected (figure 4B), butyrate significantly decreased the respiratory exchange ratio during daytime (figure 4C). This was reflected by an increase in fat oxidation (figure 4D), mostly at the expense of carbohydrate oxidation (figure 4E) during daytime.

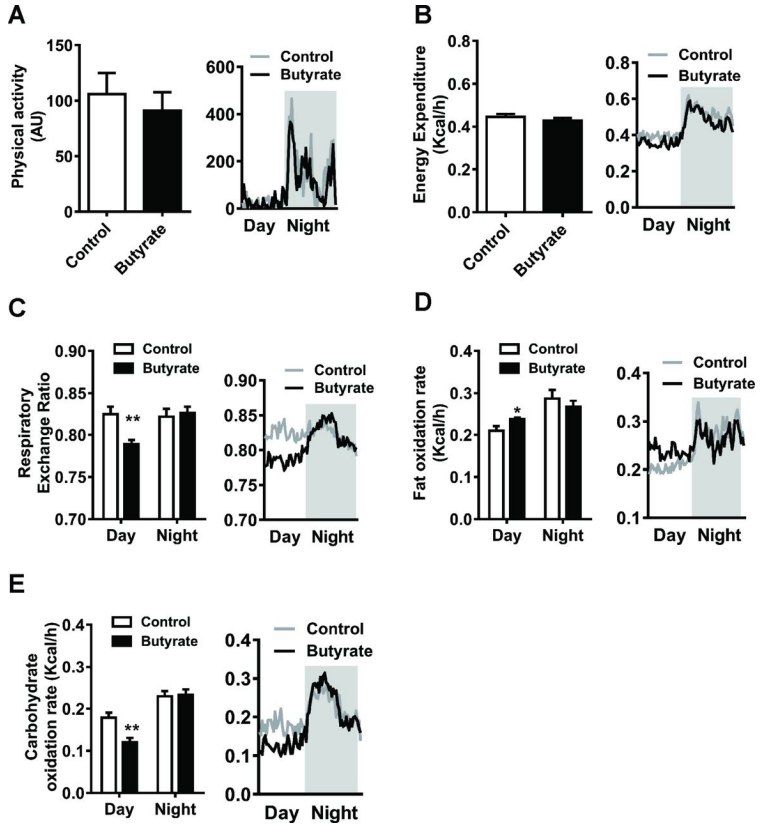

Figure 4. Butyrate promotes fat oxidation at the expense of carbohydrate oxidation. In the first week of the intervention, mice were housed in fully automated metabolic cages, and physical activity (A), energy expenditure (B) and respiratory exchange ratio (C) were monitored. Fat oxidation rate (D) and carbohydrate oxidation rate (E) were calculated. For bar graphs, data are shown as means ± SEM (n=7-8); for line graphs, data are shown as the mean for each group (n=7-8) during a 24-hour cycle (07:00–07:00).

Butyrate consumption increases BAT thermogenic capacity and sympathetic outflow towards BAT

Next we followed up on the stimulating effect of butyrate on [^{3}H]TO uptake by BAT and fat oxidation by studying BAT in more detail. Butyrate markedly decreased the weight of the iBAT pad (figure 5A), accompanied by a decrease in intracellular lipid vacuole content as compared with the control mice (figure 5B, E). The protein content of uncoupling protein (UCP)-1 per area of BAT was increased (figure 5C, E), suggesting increased thermogenic capacity of BAT. Furthermore, butyrate increased sympathetic outflow towards BAT, as evidenced by increased protein expression of tyrosine hydroxylase (TH), a marker of sympathetic nerve activity (figure 5D, E). As compared with the pair-fed group, butyrate-treated mice still showed reduced iBAT pad weight (figure 5A), intracellular lipid content (figure 5B) and increased UCP-1 protein content (figure 5C), suggesting butyrate consumption improves BAT thermogenic capacity only partly via a reduction in food intake.

In both subcutaneous WAT and gWAT, butyrate did not induce mRNA expression of the beige adipocyte markers Ucp-1 and Cidea (online supplementary figure S3A, B). Furthermore, we could not detect any UCP-1 protein expression in either WAT depot, suggesting that butyrate treatment does not induce browning of WAT.

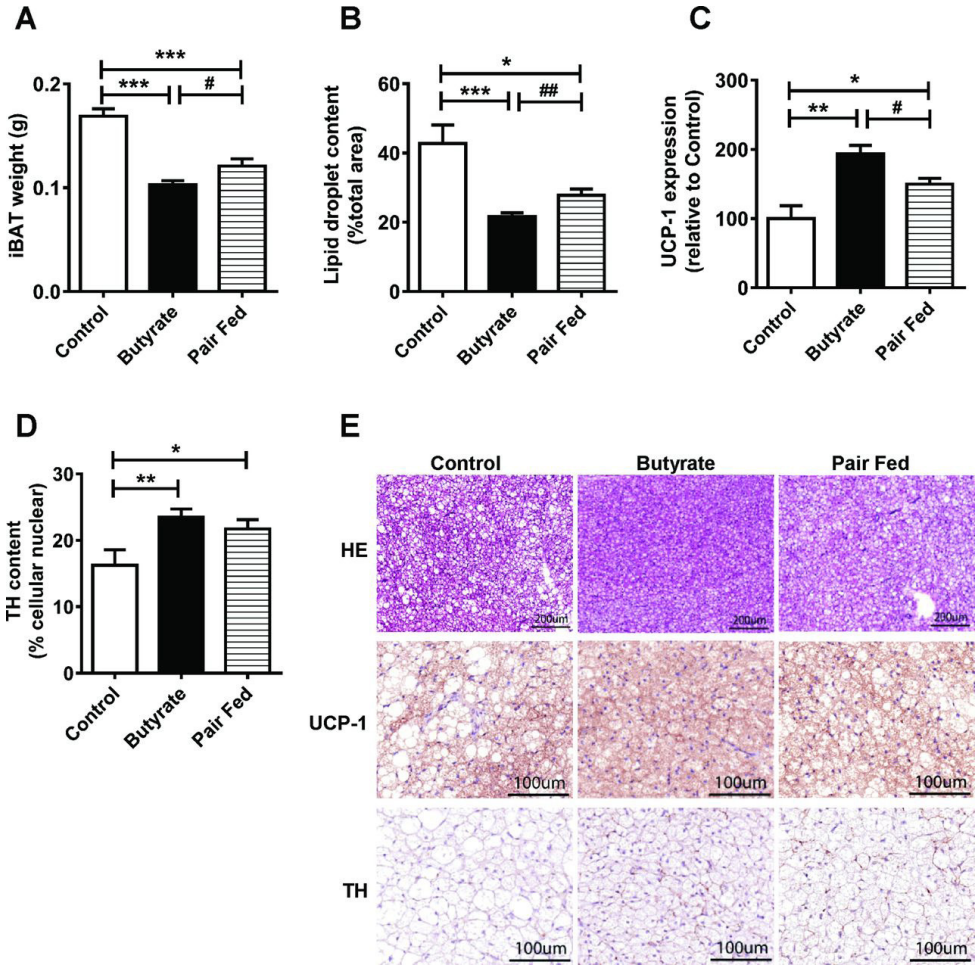

Figure 5. Butyrate increases brown adipose tissue (BAT) thermogenic capacity and sympathetic outflow towards BAT. After 9 weeks of intervention, the interscapular BAT (iBAT) pad was weighed (A) and sectioned. The lipid content within the iBAT was quantified after H&E staining (B). After immunostaining, the expression of UCP-1 (C) and TH (D) in iBAT was quantified with representative pictures shown (E). Data are means ± SEM (n=8–9); *P<0.05, **P<0.01, ***P<0.001 as control group compared with butyrate group; #P<0.05, ##P<0.01 as pair-fed group compared with butyrate group. TH, tyrosine hydroxylase; UCP, uncoupling protein.

The gut-brain neural circuit is necessary for the butyrate-induced satiety and BAT activation

To further investigate the mechanistic involvement of the gut-brain neural circuit in the beneficial effects of butyrate on energy metabolism, we performed the subdiaphragmatic vagotomy and sham surgery, followed by a dietary butyrate intervention for 7 weeks. Again, in the sham-operated group, butyrate reduced cumulative food intake (online supplementary figure S2A) as well as average food intake per se (online supplementary figure S2B) during the 7-week intervention period, and accelerated the clearance of [^{3}H]TO from the circulation (online supplementary figure S2C) as well as increased the uptake of [^{3}H]TO-derived activity by BAT (online supplementary figure S2D). Also, in mice receiving sham surgery, butyrate reduced iBAT pad weight (online supplementary figure S2E) most likely due to a decrease in intracellular lipid vacuole content (online supplementary figure S2F) and enhanced BAT thermogenic capacity as shown by an increased UCP-1 protein content (online supplementary figure S2G). However, after the subdiaphragmatic vagotomy, butyrate failed to reduce the cumulative food intake (figure 6A), and the average food intake *per se* between the control group and butyrate-treated group was equal (figure 6B). In vagotomised mice, butyrate treatment also did not influence the clearance of [^{3}H]TO from the circulation (figure 6C), nor the tissue uptake of [^{3}H]TO-derived activity (figure 6D). The weight of iBAT (figure 6E), the intracellular lipid vacuole content of iBAT (figure 6F) and UCP-1 protein content in iBAT (figure 6G) in the vagotomised mice received butyrate treatment that was comparable to that of control group. Taken together, these data indicate that the gut-brain neural circuit is necessary for the beneficial effects of butyrate on both satiety and BAT activation.

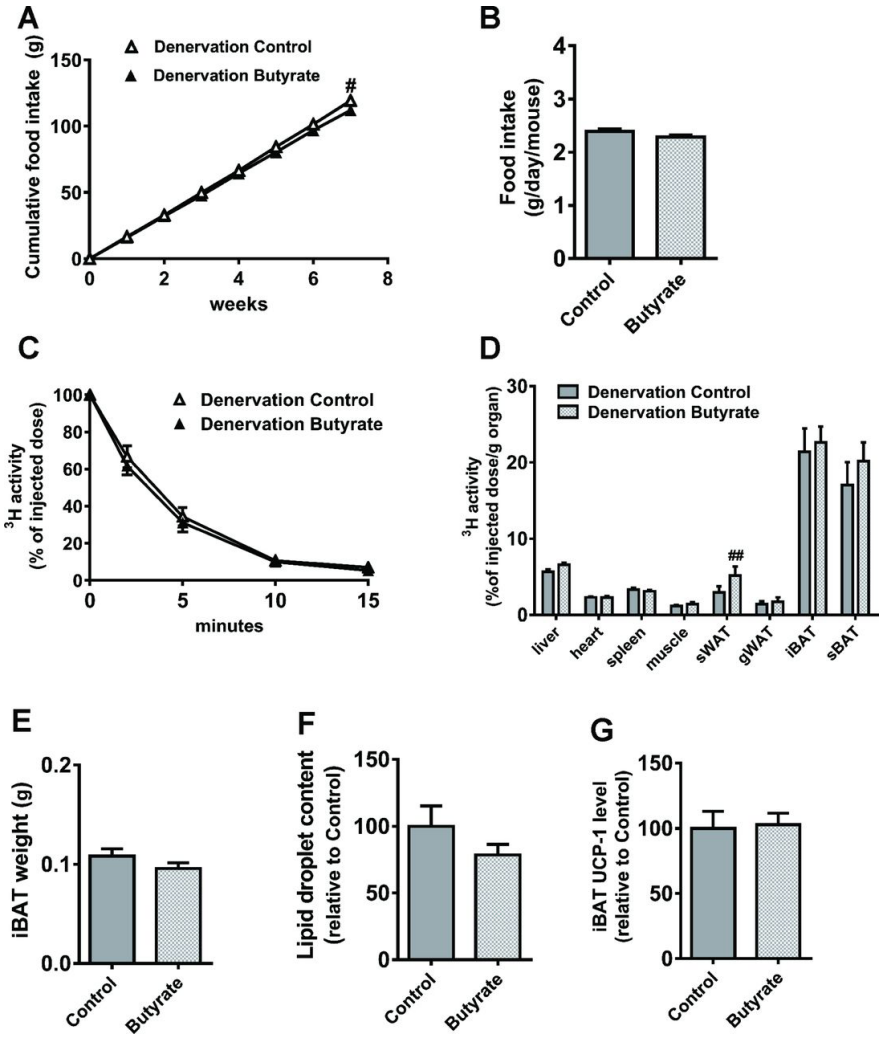

Figure 6. The gut-brain neural circuit is necessary for the butyrate-induced satiety and brown adipose tissue (BAT) activation. Mice were individually housed and received the subdiaphragmatic vagotomy surgery. One week after the surgery, mice were fed a high-fat diet (HFD) without (denervation control) or with 5% (w/w) sodium butyrate (denervation butyrate) for 7 weeks. Food intake was measured weekly and cumulative food intake (A) and average food intake *per se* (B) were calculated. At the end of this study, a triglyceride (TG) clearance test by intravenous injection of [^{3}H]TO-labelled TRL-like particles was performed. The clearance of [^{3}H]TO from the circulation (C) and uptake of ^{3}H by various tissue (D) was assessed. The weight of iBAT pad (E) was measured and the lipid content within the iBAT was quantified after the H&E staining (F). The protein expression of UCP-1 in iBAT was quantified after immunohistochemistry (IHC) of UCP-1 (G). Data are means ± SEM (n=8-9); #P<0.05 compared with denervation control. gWAT, gonadal white adipose tissue; iBAT, interscapular BAT; sBAT, subscapular BAT; sWAT, subcutaneous white adipose tissue; UCP, uncoupling protein.

Butyrate consumption alters gut microbiota composition

To investigate whether dietary butyrate affects the composition of gut microbiota, total bacterial DNA was isolated from the cecum content of sham-operated mice and vagotomised mice, after 7 weeks of butyrate treatment. The 16S rRNA gene was sequenced using the MiSeq platform. In sham-operated mice, dietary butyrate did not influence the number of observed species and the Shannon diversity index of the gut microbiota (figure 7A). However, unweighted UniFrac distance analysis showed a clear separation between control mice and butyrate-treated mice (figure 7B). As compared with control mice, butyrate-treated mice had a relative increased abundance of the phylum *Firmicutes* at the expense of *Bacteroidetes* (figure 7C). Linear discriminant analysis effect size indicated that genera belonging to the phylum *Firmicutes*, class *Erysipelotrichi* were significantly increased in butyrate-treated mice (figure 7D, E). Interestingly, in vagotomised mice, dietary butyrate significantly increased the number of observed species and the Shannon diversity index of the gut microbiota (online supplementary figure S5A). Unweighted UniFrac distance analysis showed a moderate separation between control mice and butyrate-treated vagotomised mice (online supplementary figure S5B). Similar to the effect in non-vagotomised mice, butyrate also increased the relative abundance of the phylum *Firmicutes* (online supplementary figure S5C), with even more classes affected, including *Erysipelotrichi*, *Clostridia* and *Bacilli* (online supplementary figure S5D, E). Collectively, our data clearly indicate that dietary butyrate alters the caecal microbiota composition, and in particular increasing the abundance of the phylum *Firmicutes*, independent of the presence of an intact gut-brain neural circuit.

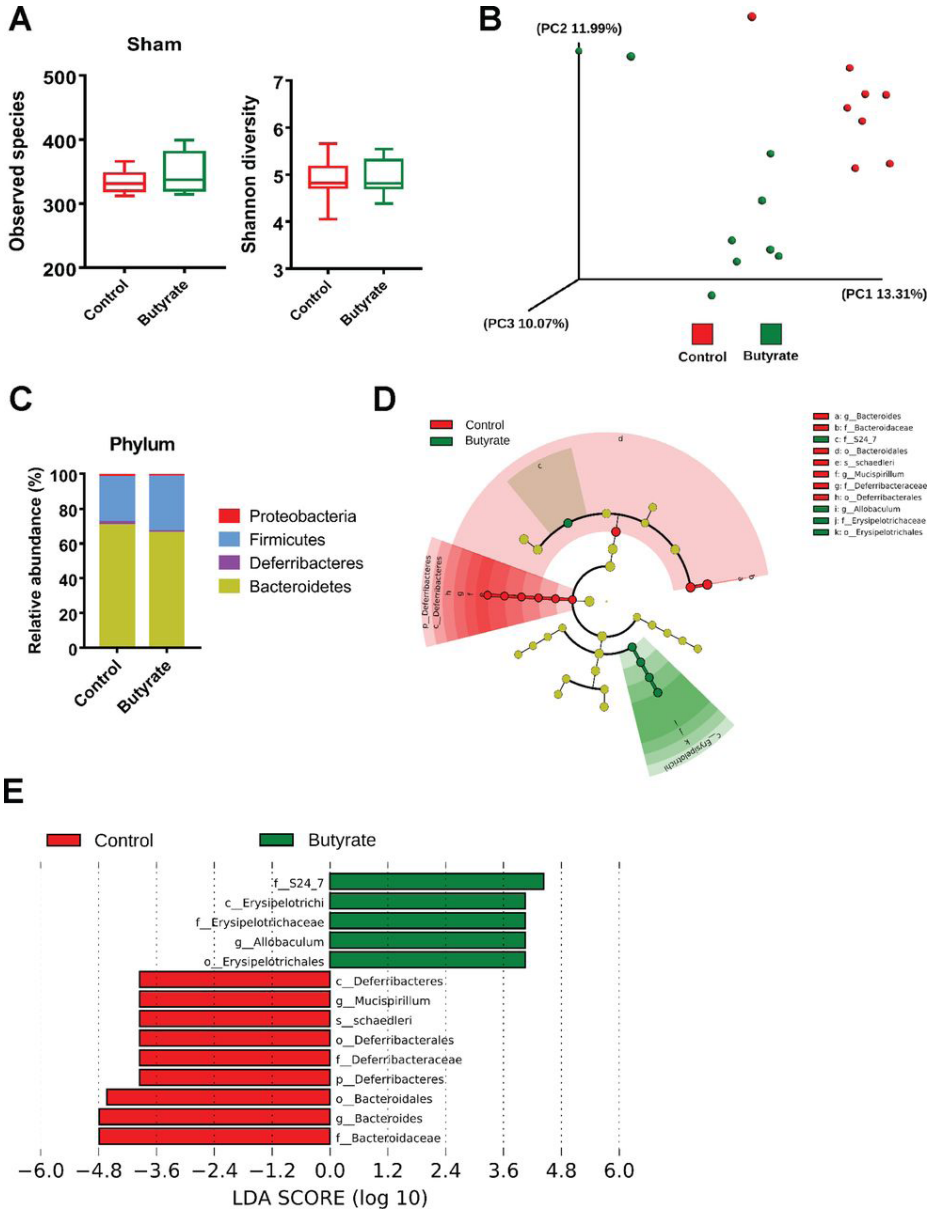

Figure 7. Butyrate consumption alters gut microbiota composition. After 7 weeks of intervention, total bacterial DNA was isolated from the caecum content and 16S rRNA genes were sequenced. (A) The number of observed species and the Shannon diversity of the gut microbiota. (B) Principal coordinates analysis plot of unweighted UniFrac distances. Composition of abundant bacterial phyla (C), cladogram generated from linear discriminant analysis (LDA) effect size (LEfSe) (D) and the LDA score (E) showing the most differentially significant abundant taxa enriched in microbiota from the control (red, n=8) and butyrate (green, n=9) group.

Discussion

Previous findings showed that both dietary administration of butyrate [13, 24] and stimulation of intestinal butyrate production via probiotics [25, 26] exert multiple beneficial effects on non-alcoholic fatty liver disease and energy metabolism. However, the mechanisms underlying the regulation of energy homeostasis by butyrate are still under debate. In this study, we showed that butyrate reduces food intake. This effect contributes dominantly to the various metabolic benefits of butyrate, including preventing HFD-induced obesity, fat mass gain and hepatic steatosis, and improving hyperglycemia and insulin resistance. In addition, butyrate also modestly promotes the oxidation of TG, likely by enhancing TG uptake by BAT activation during daytime.

In the search for mechanisms underlying the beneficial effects of butyrate on metabolism, we first demonstrated that both acute and chronic butyrate administration reduce food intake. Previous preclinical studies [27, 28] and clinical studies [17, 18] have demonstrated that administration of dietary fiber, a main resource for intestinal SCFA production by the gut microbiota, increases satiety and decreases energy intake, accompanied by increased endogenous butyrate production. However, the effect of butyrate per se on satiety was still under debate. den Besten *et al* [16] showed that 5% butyrate (w/w) incorporated into an HFD, in which 45% of calories were from palm oil fat, did not alter food intake in mice. In contrast, Lin *et al* [11] reported that 5% butyrate incorporated into another type of HFD in which 60% of calories were derived from lard and soybean oil, led to a 22% reduction in cumulative food intake over 9 days. We confirmed this finding by using the same lard fat in the diet, showing that 5% butyrate supplementation reduces cumulative food intake by 22% over a 9-week intervention period, without influencing spontaneous physical activity of the mice. These data suggest that butyrate unlikely induces systemic toxicity and abnormal motor and behavior at this dose. Further behavioral assays, including the conditional aversion assay, would be needed to firmly establish whether mice have aversion to butyrate due to its odor and/or taste. The discrepancy between studies may be attributed to the fact that the different dietary fat and carbohydrates distinctly impact the composition of the gut microbiota as well as the production of endogenous SCFAs, especially butyrate [29], therefore interfering with the satiety effect induced by exogenous butyrate. Of note, in chow-fed mice, butyrate administration via intragastric gavage rapidly induces satiety and prevented refeeding after an overnight fast. This finding suggests that independent of dietary composition and intestinal SCFAs, butyrate *per se* induces satiety and reduces cumulative food intake.

The GI tract is intimately connected to the central nervous system (CNS) mainly via hormonal and neuronal pathways, with the vagal nerve as the key neural connection between the GI tract and the CNS [30]. Our findings that reduced food intake coincided with reduced orexigenic NPY neuron activity in the hypothalamus, and decreased neuron activity within the NTS and DVC in the brainstem, indicate that

the effect of butyrate on satiety is likely mediated via vagal inputs to NPY neurons. Indeed, we observed that subdiaphragmatic vagotomy completely abolished the butyrate-induced satiety. It is known that the central terminals of vagal nerve innervate the brainstem, where vagal nerve transmission such as energy status signal projects to the hypothalamus, thereby forming a circuit to regulate satiety [31]. Due to our finding that direct intravenous infusion of butyrate did not affect food intake, hypothalamic neuronal sensing of energy status might be a primary target for butyrate supplementation.

On the other hand, the GI tract releases a number of gut hormones, including glucagon-like peptide 1 (GLP-1), which primarily acts on the vagal nerve and also travels through the circulation to directly act on the hypothalamus to regulate satiety signaling. In fact, several studies showed that oral butyrate has the capacity to stimulate GLP-1 secretion [11, 32]. Convincing evidence shows that GLP-1 receptor activation in vagal afferents [33] regulates food intake and energy metabolism. Collectively, it is tempting to speculate that butyrate consumption stimulates GLP-1 secretion from L cells of the GI tract, which activates GLP-1 receptor signaling in the vagal nerve and consequently induces hypothalamic satiety signaling. In addition, another important function of the gut-brain neural circuit is to regulate the intestinal transit [34], which plays an important role in nutrient harvest, thereby directly influencing host energy metabolism. A previous study has shown that butyrate increases colonic motility [35]. This may contribute to the metabolic benefits of butyrate by reducing nutrient absorption. Furthermore, Wichmann *et al* demonstrated that gut microbiota regulate intestinal transit via modulating GLP-1 production [36]. In the present study, it remains to be determined to what extent intestinal transit time and motility play a role in the beneficial effects of butyrate. By adding a pair-fed group, we could show that the reduced food intake is the dominant mechanism responsible for multiple distal beneficial effects of butyrate, including preventing diet-induced hepatic steatosis and hyperglycemia. The effects of butyrate on body weight and fat mass gain, plasma TG and insulin sensitivity were only partly (60%–70%) explained by reduction of food intake.

In addition to inducing satiety, butyrate also promoted the oxidation of fatty acids at the expense of carbohydrates, in particular during conditions of reduced feeding at daytime. An increase in fatty acid oxidation is characteristic for BAT activation [37] and we have previously reported a similar metabolic shift from glucose to lipid oxidation after central administration of the GLP-1 receptor agonist exendin-4 [38]. Therefore, it was not unexpected to find that butyrate accelerates the clearance of plasma TG by activated BAT. BAT functionality is primarily driven by hypothalamus via the action of the SNS [8]. We speculate that dietary butyrate reaching the GI tract most likely activates the gut-brain neural circuit, thereby stimulating hypothalamic control of the SNS outflow towards BAT. Consequently, butyrate activates BAT and increases oxidation of intracellular fatty acids resulting in a compensatory influx of TG-derived fatty acids. In fact, butyrate increased in BAT the protein level of TH, which is a marker of SNS activity [39]. In vagotomised

mice, butyrate failed to increase the uptake of TG-derived fatty acids by BAT, the utilization of lipid in BAT as well as the protein level of UCP-1, a positive marker for BAT activation. Butyrate also increased the flux of TG-derived fatty acids and glucose into WAT, at least per gram tissue, but did not induce browning of WAT. Since butyrate markedly decreased the size of adipocyte in WAT (online supplementary figure S3C, D), thereby increasing the number of adipocytes per gram tissue, butyrate probably does not affect the uptake capacity of white adipocytes *per se*. Although the relative volume of BAT in humans may be limited compared with skeletal muscle, the uptake of fatty acids per gram tissue by BAT exceeds that by skeletal muscle by >10-fold (figure 3F). Also, a recent paper redefined whole-body BAT distribution in humans and concluded that its metabolic capacity is substantially higher than usually reported [40]. The effects of butyrate on fatty acid uptake and oxidation by BAT we observe in mice may thus well be relevant for humans.

In addition to butyrate, administration of other SCFAs has been reported to induce satiety [41, 42]. Like butyrate, propionate induces satiety in ruminants probably also via the action of the vagal nerve [43], while acetate may directly regulate hypothalamic satiety signaling after crossing the blood–brain barrier [42]. Notably, a recent study showed that an increased production of intestinal acetate due to a high fat-diet feeding led to the development of obesity and insulin resistance through activation of the vagal nerve [44]. This suggests that dietary acetate acts differently on energy metabolism compared with acetate derived from intestinal bacteria fermentation. In this study, dietary butyrate clearly altered the caecal microbiota composition and increased the abundance of the phylum *Firmicutes*. Previously, increased abundance of the phylum *Firmicutes* has been associated with a less beneficial metabolic profile [45]. However, the specific species amplified within this phylum by butyrate may beneficially affect host energy metabolism. Future studies are needed to investigate the specific contribution of the altered gut microbiota to the beneficial effects of butyrate on host energy metabolism, for example, via fecal microbiota transplantation.

Undoubtedly, weight loss-enhancing strategies are among the most effective interventions for obesity-related diseases, that is, diabetes and cardiovascular disease. Body weight loss can be achieved by decreasing energy intake, that is, decreasing the consumption or absorption of food, and/or by increasing energy expenditure. Although bariatric surgery results in clinically significant weight loss and other beneficial effects, it suffers from a number of adverse events, including surgical complications, perioperative technical outcomes and mortality [46, 47]. Several antiobesity agents have been developed and are clinically applied with significant benefits, but do have a high probability of developing adverse effects, in particular in the application for long-term weight management [10]. Butyrate is currently widely emerging as a potential strategy for treatment of cancer, IBD, inherited disorders and neurodegeneration [48]. Our collective data now show that butyrate also induces sustained satiety and enhances fat oxidation, thereby effectively preventing diet-induced obesity, insulin resistance, hypertriglyceridemie

and hepatic steatosis, without inducing any apparent unfavorable effects. Therefore, we propose oral butyrate administration as a promising strategy to combat obesity and related cardiometabolic diseases.

References

1. Grundy, S.M., *Metabolic syndrome update.* Trends Cardiovasc Med, 2016. **26**(4): p. 364-73.
2. Schoeller, D.A., *Insights into energy balance from doubly labeled water.* Int J Obes (Lond), 2008. **32 Suppl 7**: p. S72-5.
3. Cypess, A.M., et al., *Identification and importance of brown adipose tissue in adult humans.* N Engl J Med, 2009. **360**(15): p. 1509-17.
4. van Marken Lichtenbelt, W.D., et al., *Cold-activated brown adipose tissue in healthy men.* N Engl J Med, 2009. **360**(15): p. 1500-8.
5. Cypess, A.M. and C.R. Kahn, *Brown fat as a therapy for obesity and diabetes.* Curr Opin Endocrinol Diabetes Obes, 2010. **17**(2): p. 143-9.
6. Schilperoort, M., et al., *Relevance of lipid metabolism for brown fat visualization and quantification.* Curr Opin Lipidol, 2016. **27**(3): p. 242-8.
7. Labbe, S.M., et al., *Hypothalamic control of brown adipose tissue thermogenesis.* Front Syst Neurosci, 2015. **9**: p. 150.
8. Kooijman, S., J.K. van den Heuvel, and P.C.N. Rensen, *Neuronal Control of Brown Fat Activity.* Trends Endocrinol Metab, 2015. **26**(11): p. 657-668.
9. Ahima, R.S. and D.A. Antwi, *Brain regulation of appetite and satiety.* Endocrinol Metab Clin North Am, 2008. **37**(4): p. 811-23.
10. Apovian, C.M., W.T. Garvey, and D.H. Ryan, *Challenging obesity: Patient, provider, and expert perspectives on the roles of available and emerging nonsurgical therapies.* Obesity (Silver Spring), 2015. **23 Suppl 2**: p. S1-S26.
11. Lin, H.V., et al., *Butyrate and propionate protect against diet-induced obesity and regulate gut hormones via free fatty acid receptor 3-independent mechanisms.* PLoS One, 2012. **7**(4): p. e35240.
12. Khan, S. and G. Jena, *Sodium butyrate reduces insulin-resistance, fat accumulation and dyslipidemia in type-2 diabetic rat: A comparative study with metformin.* Chem Biol Interact, 2016. **254**: p. 124-34.
13. Gao, Z., et al., *Butyrate improves insulin sensitivity and increases energy expenditure in mice.* Diabetes, 2009. **58**(7): p. 1509-17.
14. Mattace Raso, G., et al., *Effects of sodium butyrate and its synthetic amide derivative on liver inflammation and glucose tolerance in an animal model of steatosis induced by high fat diet.* PLoS One, 2013. **8**(7): p. e68626.
15. Henagan, T.M., et al., *Sodium butyrate epigenetically modulates high-fat diet-induced skeletal muscle mitochondrial adaptation, obesity and insulin resistance through nucleosome positioning.* Br J Pharmacol, 2015. **172**(11): p. 2782-98.
16. den Besten, G., et al., *Short-Chain Fatty Acids Protect Against High-Fat Diet-Induced Obesity via a PPARgamma-Dependent Switch From Lipogenesis to Fat Oxidation.* Diabetes, 2015. **64**(7): p. 2398-408.

17. Cani, P.D., et al., *Oligofructose promotes satiety in healthy human: a pilot study.* Eur J Clin Nutr, 2006. **60**(5): p. 567-72.

18. Daud, N.M., et al., *The impact of oligofructose on stimulation of gut hormones, appetite regulation and adiposity.* Obesity (Silver Spring), 2014. **22**(6): p. 1430-8.

19. van den Hoek, A.M., et al., *APOE*3Leiden.CETP transgenic mice as model for pharmaceutical treatment of the metabolic syndrome.* Diabetes Obes Metab, 2014. **16**(6): p. 537-44.

20. van den Maagdenberg, A.M., et al., *Transgenic mice carrying the apolipoprotein E3-Leiden gene exhibit hyperlipoproteinemia.* J Biol Chem, 1993. **268**(14): p. 10540-5.

21. Wang, Y., et al., *Plasma cholesteryl ester transfer protein is predominantly derived from Kupffer cells.* Hepatology, 2015. **62**(6): p. 1710-22.

22. Wieczorek, M., et al., *Physiological and behavioral responses to interleukin-1beta and LPS in vagotomized mice.* Physiol Behav, 2005. **85**(4): p. 500-11.

23. Rensen, P.C., et al., *Selective liver targeting of antivirals by recombinant chylomicrons--a new therapeutic approach to hepatitis B.* Nat Med, 1995. **1**(3): p. 221-5.

24. Jin, C.J., et al., *Supplementation of sodium butyrate protects mice from the development of non-alcoholic steatohepatitis (NASH).* Br J Nutr, 2015. **114**(11): p. 1745-55.

25. Yadav, H., et al., *Beneficial metabolic effects of a probiotic via butyrate-induced GLP-1 hormone secretion.* J Biol Chem, 2013. **288**(35): p. 25088-97.

26. Endo, H., et al., *Butyrate-producing probiotics reduce nonalcoholic fatty liver disease progression in rats: new insight into the probiotics for the gut-liver axis.* PLoS One, 2013. **8**(5): p. e63388.

27. Cani, P.D., et al., *Oligofructose promotes satiety in rats fed a high-fat diet: involvement of glucagon-like Peptide-1.* Obes Res, 2005. **13**(6): p. 1000-7.

28. Kleessen, B., L. Hartmann, and M. Blaut, *Oligofructose and long-chain inulin: influence on the gut microbial ecology of rats associated with a human faecal flora.* Br J Nutr, 2001. **86**(2): p. 291-300.

29. Jurgonski, A., J. Juskiewicz, and Z. Zdunczyk, *A high-fat diet differentially affects the gut metabolism and blood lipids of rats depending on the type of dietary fat and carbohydrate.* Nutrients, 2014. **6**(2): p. 616-26.

30. Chaudhri, O.B., et al., *Gastrointestinal satiety signals.* Annu Rev Physiol, 2008. **70**: p. 239-55.

31. Schneeberger, M., R. Gomis, and M. Claret, *Hypothalamic and brainstem neuronal circuits controlling homeostatic energy balance.* J Endocrinol, 2014. **220**(2): p. T25-46.

32. Tolhurst, G., et al., *Short-chain fatty acids stimulate glucagon-like peptide-1 secretion via the G-protein-coupled receptor FFAR2.* Diabetes, 2012. **61**(2): p. 364-71.

33. Krieger, J.P., et al., *Knockdown of GLP-1 Receptors in Vagal Afferents Affects Normal Food Intake and Glycemia.* Diabetes, 2016. **65**(1): p. 34-43.

34. Ciesielczyk, K., et al., *Altered sympathovagal balance and pain hypersensitivity in TNBS-induced colitis.* Arch Med Sci, 2017. **13**(1): p. 246-255.

35. Soret, R., et al., *Short-chain fatty acids regulate the enteric neurons and control gastrointestinal motility in rats.* Gastroenterology, 2010. **138**(5): p. 1772-82.

36. Wichmann, A., et al., *Microbial modulation of energy availability in the colon regulates intestinal transit.* Cell Host Microbe, 2013. **14**(5): p. 582-90.

37. Berbee, J.F., et al., *Brown fat activation reduces hypercholesterolaemia and protects from atherosclerosis development.* Nat Commun, 2015. **6**: p. 6356.

38. Kooijman, S., et al., *Central GLP-1 receptor signalling accelerates plasma clearance of triacylglycerol and glucose by activating brown adipose tissue in mice.* Diabetologia, 2015. **58**(11): p. 2637-46.

39. Schmidt, R.E. and B.E. Cogswell, *Tyrosine hydroxylase activity in sympathetic nervous system of rats with streptozocin-induced diabetes.* Diabetes, 1989. **38**(8): p. 959-68.

40. Leitner, B.P., et al., *Mapping of human brown adipose tissue in lean and obese young men.* Proc Natl Acad Sci U S A, 2017. **114**(32): p. 8649-8654.

41. Farningham, D.A. and C.C. Whyte, *The role of propionate and acetate in the control of food intake in sheep.* Br J Nutr, 1993. **70**(1): p. 37-46.

42. Frost, G., et al., *The short-chain fatty acid acetate reduces appetite via a central homeostatic mechanism.* Nat Commun, 2014. **5**: p. 3611.

43. Anil, M.H. and J.M. Forbes, *The roles of hepatic nerves in the reduction of food intake as a consequence of intraportal sodium propionate administration in sheep.* Q J Exp Physiol, 1988. **73**(4): p. 539-46.

44. Perry, R.J., et al., *Acetate mediates a microbiome-brain-beta-cell axis to promote metabolic syndrome.* Nature, 2016. **534**(7606): p. 213-7.

45. Turnbaugh, P.J., et al., *An obesity-associated gut microbiome with increased capacity for energy harvest.* Nature, 2006. **444**(7122): p. 1027-31.

46. Maggard-Gibbons, M., et al., *Bariatric surgery for weight loss and glycemic control in nonmorbidly obese adults with diabetes: a systematic review.* JAMA, 2013. **309**(21): p. 2250-61.

47. Hopkins, J.C., et al., *Outcome reporting in bariatric surgery: an in-depth analysis to inform the development of a core outcome set, the BARIACT Study.* Obes Rev, 2015. **16**(1): p. 88-106.

48. Berni Canani, R., M. Di Costanzo, and L. Leone, *The epigenetic effects of butyrate: potential therapeutic implications for clinical practice.* Clin Epigenetics, 2012. **4**(1): p. 4.

Supplementary materials and methods

Appetite test and brain histology

After overnight fasting (7pm-8am), mice were randomized based on body weight and received sodium butyrate or vehicle by intra-gastric gavage (6 M, 0.15 mL per mouse) or intravenous injection (15 mM or 150 mM, 0.1 mL per mouse). Food intake per se was measured during the next 24 hours. In a second experiment, 1 hour after intra-gastric gavage of sodium butyrate or vehicle, mouse brains were collected for histological analysis.

Hypothalamic histology

- C-FOS immunohistochemistry in hypothalamus

One hour after intra-gastric gavage of sodium butyrate or vehicle, mice were anesthetized and perfused transcardially with ice-cold saline followed by freshly prepared 4% paraformaldehyde solution. The brains were collected, postfixed in 4% paraformaldehyde for 48 hours, cryoprotected in 30% sucrose and subsequently frozen on dry ice and stored at −80°C. Thirty-five µm-cryostat sections of frozen brains were cut and stored in cryoprotectant at -20°C.

c-FOS immunohistochemistry was performed on serial hypothalamic sections cut from -1.22 mm to -1.70 mm relative to the bregma according to The Mouse Brain in Stereotaxic Coordinates. Brain sections were blocked by 2% normal goat serum (NGS) and incubated with anti-c-Fos primary antibody (1:1000, Abcam), Alexa 594 secondary goat anti-rabbit antibody (1:500, Abcam) and diaminobenzidine (DAB) and DAPI as chromogen (SK-4100, Vector laboratories). The quantification of c-FOS-positive cells within the arcuate nucleus (3-4 sections per mouse) were determined using Image J software system.

- Double immunofluorescent staining

Double immunofluorescent staining of c-Fos with POMC or NPY were performed on the same serial hypothalamic sections as described above. Brain sections were incubated with primary antibodies: goat anti-c-Fos (1:500, Santa Cruz), and rabbit anti-POMC (1:800, Phoenix Pharmaceuticals), or rabbit anti-NPY (1:500, Abcam), respectively, at 4 °C overnight. Sections were rinsed and incubated with biotinylated secondary anti-goat or anti-rabbit IgG for 1 h, and then rinsed and incubated with streptavidin-conjugated Alexa Fluor® 594 or 647 (Jackson ImmunoResearch, USA) for 1 h. All sections were then rinsed and mounted on gelatin-coated glass slides, dried, covered with polyvinyl alcohol mounting medium containing DABCO® (Sigma, USA), observed and imaged by confocal microscopy (Leica SP8, Germany). The quantification of colocalization percentage of NPY-positive neurons or POMC-positive neurons that coexpress c-FOS within the arcuate nucleus were determined using Image J software system.

Neuron activity in brain regions of cortex, hippocampus, brainstem

c-FOS immunohistochemistry was performed on serial hypothalamic sections cut from -1.22 mm to −1.70 mm, and brainstem sections cut from -7.32 mm to -7.76 mm relative to the bregma according to The Mouse Brain in Stereotaxic Coordinates. Sections were incubated with anti-c-Fos primary antibody (1:1000, Abcam), biotinylated secondary anti-rabbit IgG, avidin-biotin complex (ABC method, Vector Laboratories, Inc., Burlingame, CA), and the reaction product was visualized by incubation in 1% diaminobenzidine with 0.01% hydrogen peroxide. The quantification of c-FOS-positive cells in cortical regions (primary somatosensory cortex and primary and secondary motor cortex), hippocampal regions, nucleus tractus solitarius (NTS) and dorsal vagal complex (DVC) within brainstem were determined using Image J software system.

Short chain fatty acid measurement by the gas chromatography–mass spectrometry (GC-MS)

Plasma short chain fatty acids were analyzed by GC-MS using previously published approach with some modifications [1]. Briefly, 10 µL of plasma was transferred to a glass vial containing 250 µL acetone (Sigma-Aldrich), 10 µL 1 ppm internal standards solution containing acetic acid-d4, propionic acid-6 and butyric acid-d8 (Sigma Aldrich) and 10 µL ethanol. Thereafter, samples were derivatized with pentafluorobenzyl bromide (PFBBr), as follows: 100 µL 172 mM PFBBr (Thermo) in acetone was added, samples were mixed and heated to 60 ˚C for 30 min. After the samples had cooled down to room temperature a liquid-liquid extraction was performed using 500 µL n-hexane (Sigma-Aldrich) and 250 µL GC-MS grade water. The upper n-hexane layer was transferred to a fresh glass vial and subsequently used for GC-MS analysis. Calibration standards were prepared analogous. For calibration standards no plasma was added and 10 µL of EtOH was replaced by 10 µL standards solution (Sigma-Aldrich) in EtOH.

Samples were analyzed on a Bruker Scion 436 GC fitted with an Agilent VF-5ms capillary column (25m × 0.25mm i.d.,0.25 µm film thickness) coupled to a Bruker Scion TQ MS. Injection was performed using a CTC PAL autosampler (G6501-CTC): 1 µL sample was injected splitless at 280˚C. Helium 99.9990% was used as carrier gas at a constant flow of 1.20 mL/min. The GC temperature program was set as follows: 1 min. constant at 50˚C, then linear increase at 40˚C/min to 60˚C, kept constant for 3 min, followed by a linear increase at 25˚C/min to 200˚C, linearly increased at 40˚C/min to 315˚C, kept constant for 2 min. The transfer line and ionization source temperature were 280˚C. The pressure of the chemical ionization gas, methane (99.9990%), was set at 15 psi. Negatively charged ions were detected in the selected ion monitoring mode, and acetic acid, acetic acid-d4, propionic acid, propionic acid-d6, butyric acid and butyric acid-d8 were monitored at m/z 59, 62, 73, 78, 87 and 94 respectively.

Body weight and body composition

Body weight was measured with a scale, and body composition was measured in conscious mice using an EchoMRI-100 analyzer (EchoMRI, Houston, TX).

Hepatic lipid content

Liver lipids were extracted according to a modified protocol from Bligh and Dyer [2]. Small liver pieces (approx. 30 mg) were homogenized in ice-cold methanol. By addition of CH_3OH:$CHCl_3$ (1:3 v/v) to the homogenate, followed by vigorous vortexing and phase separation by centrifugation, lipids were extracted into the $CHCl_3$ phase. Subsequently, the lipid phase was dried and dissolved in 2% Triton X-100. TG, total cholesterol (TC) and phospholipid (PL) concentrations were measured using the commercial kits 11488872, 236691 (Roche Molecular Biochemicals) and phospholipids B (Wako Chemicals), respectively. Hepatic lipid content was expressed as nmol lipid per mg protein, which was determined using the BCA protein assay kit (Pierce).

Plasma parameters

After a 5-h fasting period (8am-1pm), blood was obtained via tail vein bleeding into heparin-coated capillary tubes just before the sodium butyrate supplementation and at the end of the intervention. The capillary tubes were placed on ice and centrifuged, and obtained plasma was snap-frozen in liquid nitrogen and stored at -80°C until further measurements. Plasma was assayed for TG, glucose and insulin using commercially available kits as described previously [3]. The homeostasis model index of insulin (HOMA-IR) as an index for insulin resistance was calculated by multiplying fasting insulin (mU/L) with fasting glucose (nmol/L), and dividing by 22.5 [4].

***In vivo* lipid and glucose clearance**

Triacylglycerol-rich lipoprotein (TRL)-like particles (average size of 80 nm) labeled with glycerol tri[^{3}H]oleate (triolein, [^{3}H]TO) were prepared and mixed with 2-[1-^{14}C] deoxy-D-glucose ([^{14}C]DG) in a 3:1 ratio based on radioactive counts. Particles were stored at 4°C under argon and used for in vivo kinetic experiments.

At 9.00 am, mice were injected with 200 µL of emulsion particles (1 mg TG) and [^{14}C]DG via the tail vein at the end of the intervention period. Blood samples were taken at 2, 5, 10 and 15 min after injection, and lipid and glucose clearance kinetics were determined by measuring plasma ^{3}H and ^{14}C activities. After 15 min, mice were sacrificed by cervical dislocation and perfused with ice-cold saline via the heart. Thereafter, organs were harvested and weighed and dissolved overnight at 60°C in a Tissue Solubilizer (Amersham Biosciences, Roosendaal, the Netherlands). The uptake of [^{3}H]TO- and [^{14}C]DG-derived radioactivity by the organs was calculated

from the ^{3}H and ^{14}C activities in each organ and expressed as percentage of injected dose per gram wet tissue weight.

Indirect calorimetry

Indirect calorimetry was performed in fully automatic metabolic cages (LabMaster System, TSE Systems, Bad Homburg, Germany) in the first week of the intervention. After 2 days of acclimatization, O_2 consumption, CO_2 production and physical activity were measured for 3 consecutive days. The 5 average respiratory exchange ratio, energy expenditure, fat and carbohydrate oxidation rates were calculated as described previously [5].

BAT histology and TG content

Formalin-fixed paraffin-embedded interscapular BAT (iBAT) tissue sections (5 μm) were prepared for hematoxylin and eosin (H&E) staining using standard protocols, and stained for uncoupling protein-1 (UCP-1, 1/4000; Ab10983; Abcam) and tyrosine hydroxylase (TH, 1/2000; Ab112; Abcam) as described previously [6]. The areas occupied by intracellular lipid vacuoles, nuclear, UCP-1 and TH were quantified using Image J software (National Institutes of Health). The protein content of UCP-1 was expressed as positive area per total iBAT area, and the protein content of TH was expressed as positive area per cell nuclear area, which was represented the cell number.

WAT histology and adipocyte size

Formalin-fixed paraffin-embedded subcutaneous WAT (sWAT) and gonadal WAT (gWAT) sections (5 μm) were prepared for hematoxylin and eosin (H&E) staining using standard protocols, and stained for uncoupling protein-1 (UCP-1, 1/4000; Ab10983; Abcam). The average adipocyte size (μm2) was quantified per mouse using Image J software (National Institutes of Health), and normalized to Control group.

Microbiota analysis

After 7 weeks of butyrate treatment, total caecal bacterial DNA was isolated from cecum content in mice received subdiaphragmatic vagotomy surgery or sham surgery as described previously [7]. Microbial 16S rRNA gene was amplified targeting the hyper-variable region V4. Sequencing was performed using the Illumina MiSeq platform (BGI Genomics, Hong Kong) generating paired-end reads of 250 bp in length in each direction. Overlapping paired-end reads were subsequently aligned. Reads quality was checked with Sickle, version:1.33 (https://github.com/najoshi/sickle) and low quality reads were removed. For visualizing the taxonomic composition of the fecal microbiota and further beta diversity analysis, QIIME version: 1.9.1 was used [8]. In brief, closed reference operational taxonomic

unit (OTU) picking with 97% sequence similarity against GreenGenes 13.8 reference database was done. Jackknifed beta-diversity of unweighted UniFrac distances with 10 jackknife replicates was measured at rarefaction depth of 20000 reads / sample. For statistical significance, biological relevance and visualization we used linear discriminant analysis (LDA) effect size (LEfSe) method which uses standard parameters ($P<0.05$ and LDA score 2.0) as described in (https://bitbucket.org/biobakery/biobakery/wiki/lefse).

Supplemental figures

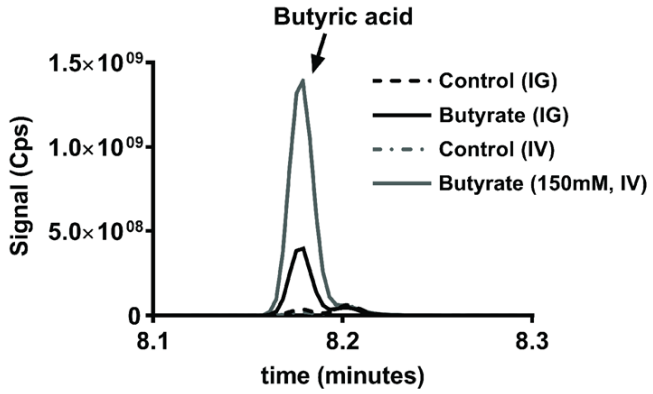

Figure S1. Oral and intravenous butyrate supplementation increases plasma butyrate concentration. After overnight fasting and randomization based on bodyweight, mice received vehicle or butyrate via the intra-gastric gavage (IG) or intravenous injection (IV). 1 hour after receiving butyrate, plasma were pooled for the measurement of butyrate level by GC-MS.

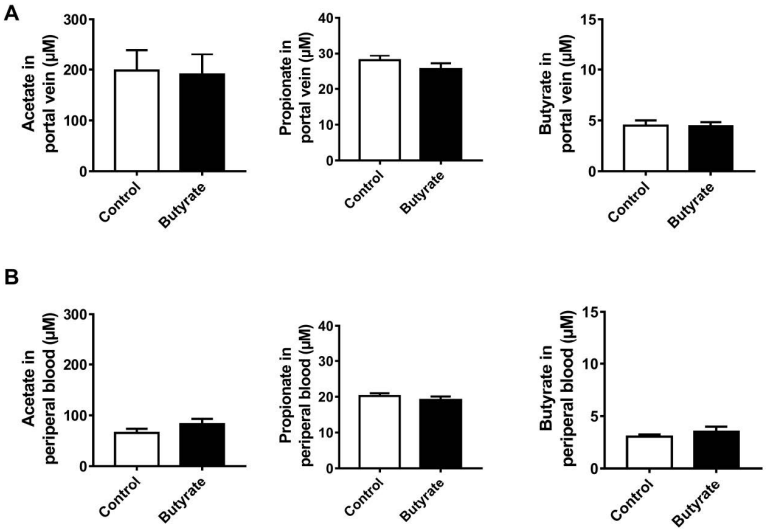

Figure S2. Chronic dietary butyrate consumption does not alter the levels of acetate, propionate and butyrate in portal vein or peripheral blood. Mice were individually housed and receive a HFD without (Control group), or with 5% (w/w) sodium butyrate (Butyrate group) for 9 weeks. At the end of this study, portal vein blood and peripheral blood were collected, the levels of acetate, propionate and butyrate were determined by GC-MS. Data are means ± SEM (n=6-7).

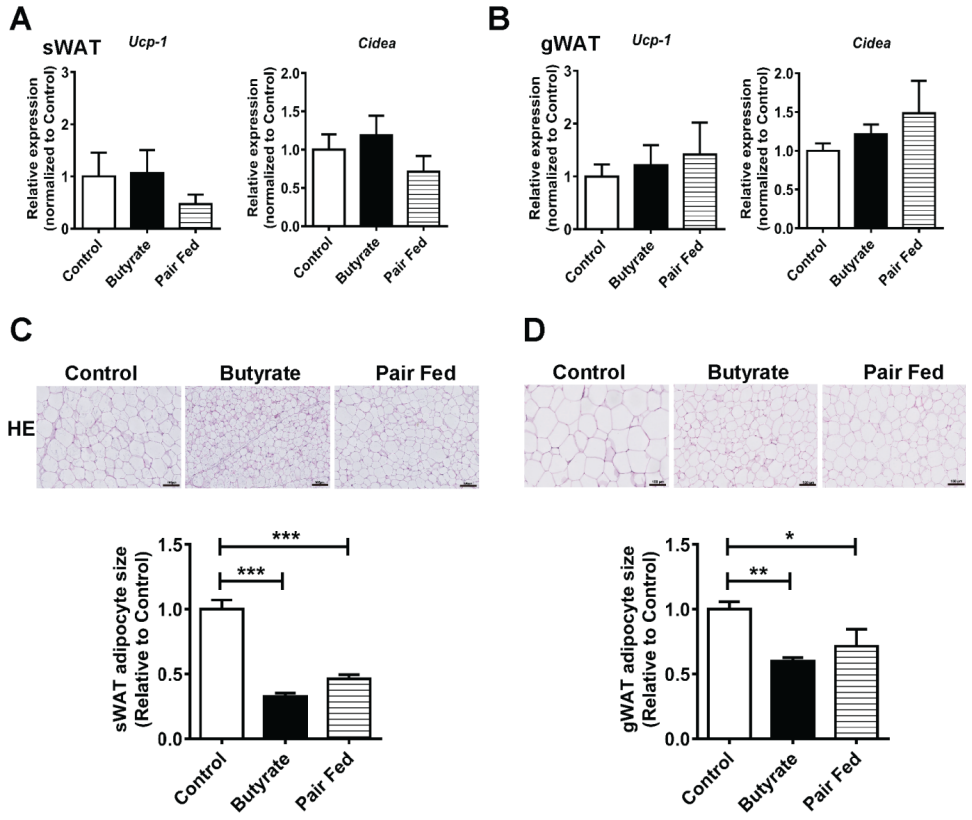

Figure S3. Butyrate treatment does not induce browning of white adipose tissue. After 9 weeks of intervention, the subcutaneous white adipose tissue (sWAT, A, C) and gonadal white adipose tissue (gWAT, B, D) were collected. mRNA expression of *Ucp-1* and *Cidea* were determined (A, B). Slides were stained for H&E, and the adipocyte size was quantified (C, D). Data are means ± SEM (n=8-9). *P<0.05, **P<0.01, ***P<0.001 as compared to control group.

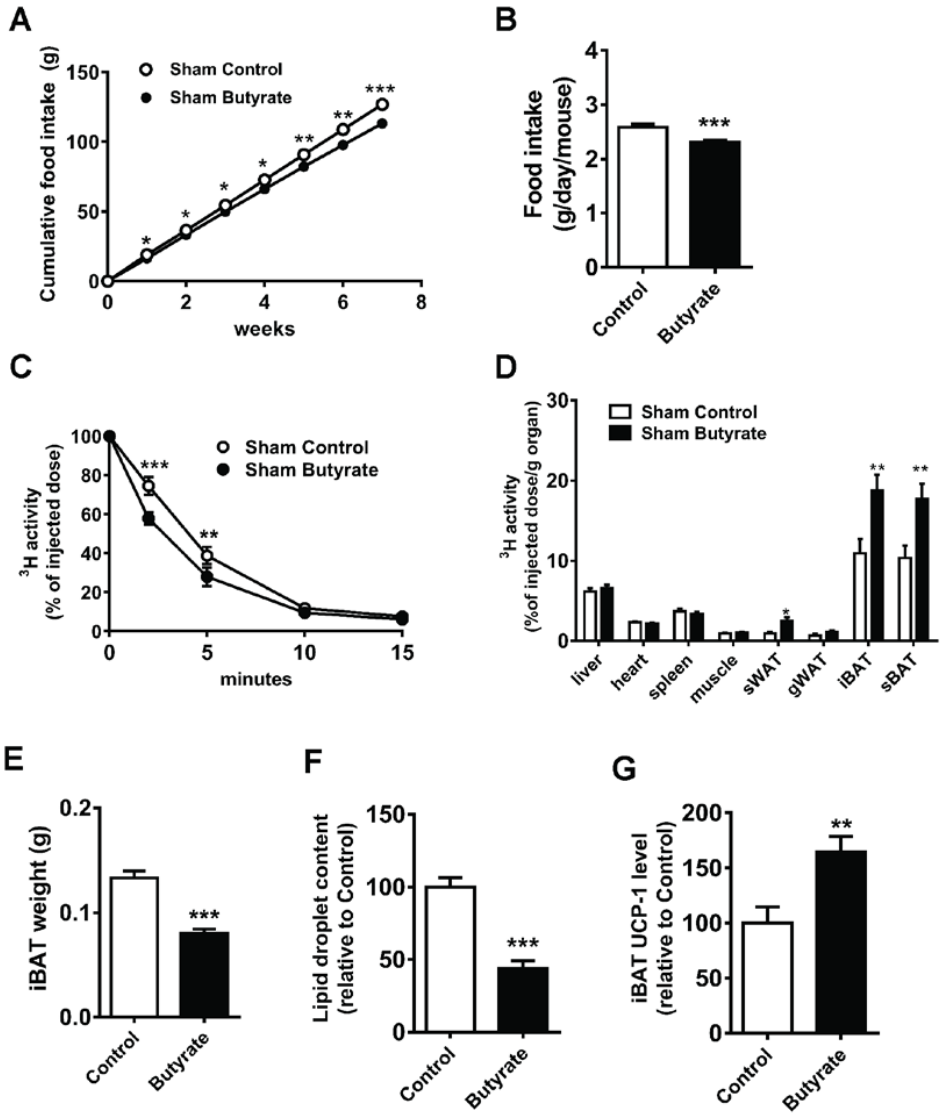

Figure S4. Butyrate decreases food intake and activates brown adipose tissue in mice received sham surgery (related to Figure 6). Mice were individually housed and received sham surgery. One week after the surgery, mice were fed a HFD without (Sham Control) or with 5% (w/w) sodium butyrate (Sham Butyrate) for 7 weeks. Food intake was measured weekly and cumulative food intake (A) and average food intake *per se* (B) was calculated. At the end of this study, a TG clearance test by i.v. injection of [^{3}H]TO-labeled TRL-like particles was performed. The clearance of [^{3}H]TO from the circulation (C) and uptake of ^{3}H by various tissue (D) was assessed. The weight of iBAT pad (E) was measured and the lipid content within the iBAT was quantified after the H&E staining (F). The protein expression of UCP-1 in iBAT was quantified after IHC of UCP-1 (G). Data are means ± SEM (n=8-9); *P<0.05, **P<0.01, ***P<0.001 compared to sham control.

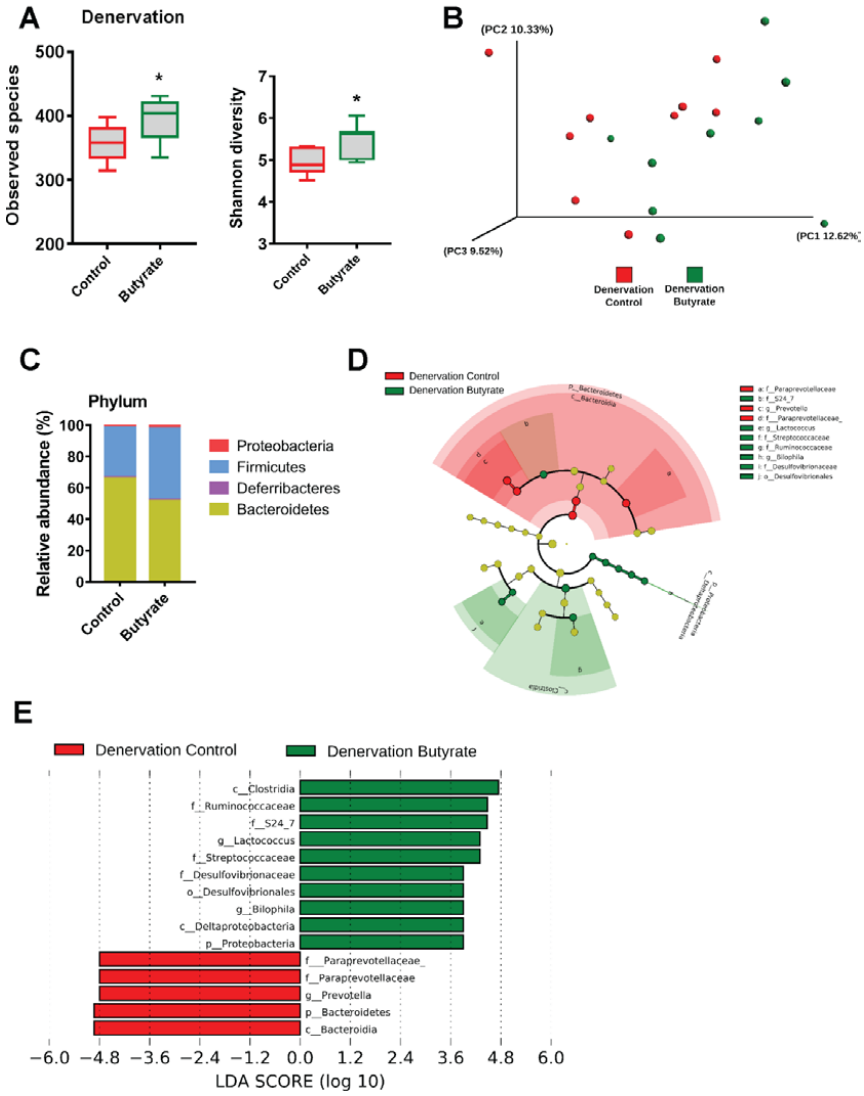

Figure S5. Butyrate consumption alters gut microbiota composition. After 7 weeks of intervention, total cecal bacterial DNA was isolated from the cecum content in mice received subdiaphragmatic vagotomy surgery and 16S rRNA genes were sequenced. (A) The α diversity including observed species and Shannon diversity of the gut microbiota. (B) Principal coordinates analysis plot of Unweighted Unifrac distances. Composition of abundant bacterial phyla (C), Cladogram generated from LEfSe analysis (D) and the LDA score (E) showing the most differentially significant abundant taxa enriched in microbiota from the denervation control (red) and denervation butyrate (green) group. For A, data was shown as Box& whiskers, Mann-Whitney test, *P<0.05 as compared to denervation control group.

Supplemental references

1. Tomcik, K., et al., *Isotopomer enrichment assay for very short chain fatty acids and its metabolic applications.* Anal Biochem, 2011. **410**(1): p. 110-7.
2. Bligh, E.G. and W.J. Dyer, *A rapid method of total lipid extraction and purification.* Can J Biochem Physiol, 1959. **37**(8): p. 911-7.
3. Wang, Y., et al., *Exendin-4 decreases liver inflammation and atherosclerosis development simultaneously by reducing macrophage infiltration.* Br J Pharmacol, 2014. **171**(3): p. 723-34.
4. Mather, K., *Surrogate measures of insulin resistance: of rats, mice, and men.* Am J Physiol Endocrinol Metab, 2009. **296**(2): p. E398-9.
5. Van Klinken, J.B., et al., *Estimation of activity related energy expenditure and resting metabolic rate in freely moving mice from indirect calorimetry data.* PLoS One, 2012. **7**(5): p. e36162.
6. Kooijman, S., et al., *Central GLP-1 receptor signalling accelerates plasma clearance of triacylglycerol and glucose by activating brown adipose tissue in mice.* Diabetologia, 2015. **58**(11): p. 2637-46.
7. Janssen, A.W.F., et al., *Modulation of the gut microbiota impacts nonalcoholic fatty liver disease: a potential role for bile acids.* J Lipid Res, 2017. **58**(7): p. 1399-1416.
8. Caporaso, J.G., et al., *QIIME allows analysis of high-throughput community sequencing data.* Nat Methods, 2010. **7**(5): p. 335-6.

CHAPTER 3

DIETARY BUTYRATE SELECTIVELY PROMOTES *LACHNOSPIRACEAE BACTERIUM 28-4* TO INDUCE SATIETY, ATTENUATE WEIGHT GAIN AND AMELIORATE METABOLIC HEALTH

Li Z, Zhou E, Liu C, Wicks H, Yildiz S, Razack F, Ying Z, Kooijman S, Koonen D, Heijink M, Giera M, Smits WK, Kuijper EJ, Groen AK, Willems van Dijk K, Rensen PCN, Wang Y

Submitted

Summary

The prevalence of obesity and associated cardiometabolic diseases reaches epidemic proportions. Recent studies revealed numerous beneficial cardiometabolic properties of short-chain fatty acids including butyrate. Here, we provide evidence for a crucial role of gut microbiota in the beneficial effects of dietary butyrate. Using high-fat diet (HFD)-fed APOE*3-Leiden.CETP mice, a well-established translational model for diet-induced cardiometabolic disease, we show that dietary butyrate reduces appetite and ameliorates weight gain, but only in the presence of gut microbiota. Fecal microbiota transplantation from butyrate-treated donor mice into lean gut microbiota-depleted mice attenuated HFD-induced weight gain by persistently reducing food intake, and improved insulin resistance, which was associated with a selective proliferation of *Lachnospiraceae bacterium 28-4* in the gut. In contrast, dietary butyrate did not ameliorate metabolic health or induced enrichment of *Lachnospiraceae bacterium 28-4* in obese mice. Collectively, these findings strongly suggest the therapeutic potential of *Lachnospiraceae bacterium 28-4* as a novel probiotic to improve cardiometabolic health.

Introduction

Obesity is related to cardiometabolic diseases including type 2 diabetes (T2D) and cardiovascular diseases [1] and is becoming a global health concern [2]. Although lifestyle intervention including calorie-restriction [3] and pharmacotherapy [4] has been shown to be effective in inducing weight loss, cessation of intervention generally leads to weight gain. Therefore, intervention strategies aimed at attaining persisted weight loss are still required.

Recently, a series of systematic reviews and meta-analyses revealed that increased fiber intake is associated with lower body weight, lower incidence of cardiometabolic diseases, and lower mortality from T2D and coronary heart disease [5]. As human cells cannot degrade dietary fiber, they are digested by gut microbiota into short-chain fatty acids (SCFAs) such as acetate, propionate and butyrate. These SCFAs are an energy source for intestinal cells, but in addition have many beneficial cardiometabolic properties [6]. Particularly, oral butyrate administration was previously found to prevent diet-induced obesity (DIO) [7], improve glucose homeostasis and alleviate insulin resistance in mice [8]. Consistently, we recently demonstrated that dietary butyrate prevents high-fat diet (HFD)-induced weight gain in mice mainly via reducing food intake, in addition to modestly increasing energy expenditure by activating brown adipose tissue (BAT) [9]. Given these beneficial metabolic effects of butyrate, further investigation of the precise molecular targets of butyrate could provide novel therapeutic handles to combat obesity and associated cardiometabolic diseases.

We previously revealed that oral butyrate changes the composition of gut microbiota [9], which may be related to butyrate-induced intracellular acidification of certain susceptible gut bacteria [10]. Thus, it is reasonable to speculate that oral butyrate induces metabolic benefits via modulation of gut microbiota. Notably, a ground-breaking human intervention study showed that adding fiber to a hypocaloric, isoenergetic diet beneficially alters the gut microbiota by promoting SCFAs-producing bacterial strains, which results in further alleviation of T2D as evident from the improvement of HbA1c [11]. Furthermore, another recent human study demonstrated that the overall gut microbiota shifts in parallel with glycemic status, the variation of which is strongly associated with insulin resistance of the host [12]. Collectively, these findings further infer that modulation of gut microbiota might be a novel therapeutic strategy to combat cardiometabolic diseases. Indeed, the metabolic benefits of bacterial modulation have been demonstrated by proof-of-concept bacterial transplantation studies in humans [13, 14]. However, the precise bacterial strains involved in the induction of the various metabolic benefits remain to be elucidated.

Here, we aimed to evaluate the causal role of gut microbiota in the induction of metabolic benefits of dietary butyrate, by using antibiotics-induced microbiota depletion (AIMD) of the gut [15] and fecal microbiota transplantation

(FMT) in APOE*3-Leiden.CETP (E3L.CETP) mice, a well-established translational model for developing human-like diet-induced cardiometabolic disease [16]. We reveal that the beneficial metabolic effects of dietary butyrate strictly occur in lean mice and are lost after AIMD, indicating the strict dependence of these effects on gut microbiota. In fact, dietary butyrate induces enrichment of *Lachnospiraceae bacterium 28-4*, which negatively correlated with body weight. Collectively, these findings will pave the way to assess *Lachnospiraceae bacterium 28-4* as a novel probiotic to prevent obesity and ameliorate metabolic health.

Materials and methods

Animals

Male APOE*3-Leiden.CETP (E3L.CETP) mice expressing the human APOE*3-Leiden and CETP genes were generated as previously described [17]. 12-16-weeks old mice were used, housed under standard conditions with a 12-h light/dark cycle (07:00-19:00) and with *ad libitum* access to regular chow and water unless indicated otherwise. For each experiment, mice were randomly divided into groups based on their body weight and plasma parameters (total cholesterol, triglycerides, glucose and free fatty acids). All animal experiments were performed under approval by the Ethics Committee on Animal Care and Experimentation of the Leiden University Medical Center and following the regulations of the Dutch law on animal welfare.

Gut microbiota depletion

For antibiotics-induced microbiota depletion (AIMD) of the gut, lean mice initially received 200 µl antibiotics cocktail (0.5 mg/ml ampicillin, 0.5 mg/ml neomycin, 0.5 mg/ml metronidazole (all Sigma-Aldrich, United States) and 0.25 mg/ml vancomycin (Xellia Pharmaceuticals, Denmark)) by oral gavage once a day for 1 week, which was followed by administration of these antibiotics in their drinking water (0.25 mg/ml ampicillin, 0.25 mg/ml neomycin, 0.25 mg/ml metronidazole and 0.125 mg/ml vancomycin) for the next 5 weeks. The control group received vehicle (saline) by oral gavage for 1 week followed by regular drinking water for 5 weeks. At the same time, mice were fed with a high-fat diet (HFD, 60% high fat and 0.25% cholesterol; Altromin, Germany) without or with 5% (w/w) sodium butyrate (Sigma-Aldrich, United States).

Diet-induced obese mice

For establishing diet-induced obese (DIO) mice to be used for subsequent experiments, lean mice were fed a HFD containing 60% high fat and 0.25% cholesterol (Altromin, Germany) for six weeks.

Fecal microbiota transplantation

Both lean and DIO mice received the HFD without or with 5% (w/w) sodium butyrate for 12 weeks. After 6 weeks, when a stable gut microbiota community has developed [18], fresh feces were collected weekly. Pellets of those feces were diluted in Ringer's solution supplemented with 0.05% L-cysteine hydrochloride (both Sigma Aldrich, United States). The fecal supernatant was centrifuged and filtered through a 100 µm cell strainer (Corning, United State) for subsequent fecal microbiota transplantation (FMT). In recipient mice, AIMD was first performed as detailed above, albeit 1 week by oral gavage followed by 1 week via drinking water. Subsequently, mice were subjected to FMT by oral gavage with 200 µl microbiota

from a specific donor group for 3 times a week during 6 weeks. The residual fecal supernatant was stored at -80°C until further analysis.

Dietary butyrate treatment

Mice were rendered obese by feeding a HFD for 6 weeks, and subsequently fed a HFD without or with 5% (w/w/) sodium butyrate for another 6 weeks.

Dietary butyrate prevention

Mice received a HFD without or with 5% (w/w) sodium butyrate for 6 weeks.

Body weight and body composition

Body weight was measured with a scale. Body composition was measured in conscious mice using an EchoMRI-100 (EchoMRI, United States).

Plasma parameters

At the end of each experiment, venous blood samples of approx. 100 µl were collected from the tail of 5 h-fasting mice (8:00-13:00) using heparin-coated capillary tubes. Plasma was isolated after centrifugation and stored at -80°C. Plasma glucose was measured using a commercially available enzymatic kit (Roche Diagnostics, Switzerland) and plasma insulin was determined with an ultra-sensitive mouse insulin ELISA kit (Crystal Chem, United States). Homeostatic model assessment of insulin resistance (HOMA-IR) was calculated with the equation for mice: IR_{HOMA} = [insulin] (unit) / ($22.5 \times e^{-\ln([\text{glucose}]\ (\text{unit}))}$) as described [19].

Indirect calorimetry

Energy expenditure of individually housed mice was measured by indirect calorimetry using automatic metabolic cages (Sable Systems, Germany) for five consecutive days. After 2 days of acclimatization, oxygen consumption (VO_2) and carbon dioxide production (VCO_2) were recorded. The average respiratory exchange ratio, fat oxidation rate and carbohydrate oxidation rate were calculated from day 3 to day 5, as described [20].

***In vivo* lipid clearance**

When indicated, mice were intravenously injected via the tail vein with 80 nm-sized glycerol tri[^{3}H]oleate-labeled triglyceride (TG)-rich lipoprotein (TRL)-like particles (1 mg TG in 200 µl) [21]. Blood samples were taken from the tail vein at 2, 5, 10 and 15 minutes to assess TG clearance by counting of ^{3}H-activity in 10 µl plasma. Subsequently, mice were sacrificed by CO_2 inhalation and were perfused via the heart with ice-cold saline for 5 min. Pieces of the collected organs (approx.

50 mg) were weighed and dissolved in tissue Solubilizer (Amersham Biosciences, United Kingdom) overnight at 56°C. ^{3}H-activity in both plasma and organ samples was determined using scintillation counting (TRI-CARB) after addition of liquid scintillation cocktail (Ultima Gold, both Perkin Elmer, United States).

Brown adipose tissue histology

Interscapular brown adipose tissue (iBAT) was isolated, fixed with formalin and embedded in paraffin. BAT sections (5 µm), prepared using a microtome, were stained with hematoxylin and eosin (H&E), and immunohistochemically stained for uncoupling protein-1 (UCP-1) (1/4000; Abcam, United Kingdom) and tyrosine hydroxylase (TH, 1/2000; Abcam, United Kingdom) as previously described [22]. Quantification of the intracellular lipid area, uncoupling protein-1 (UCP-1) protein, and tyrosine hydroxylase (TH) protein within BAT was performed using Image J software (Version 1.50i). Results were expressed as percentage of positive area versus total BAT area.

Genomic DNA extraction

At the end of the experiments, cecum contents were collected in sterile Eppendorf tubes. Genomic bacterial DNA was isolated from cecum samples with fast DNA stool mini kits (QIAamp, Germany) following the manufacturer's instructions.

16S rRNA sequence processing and data analysis

Once we collected the DNA samples, a quality test has been done first. Then all the qualified DNA is used to construct libraries. We used fusion primer with dual index and adapters for PCR. Fragments too short would be removed by Ampure beads. Only the qualified library can be used for sequencing. The paired-end reads were generated using the Illumina MiSeq (BGI Genomics, Hong Kong). Briefly, the reads with e.g., sequencing adapters, N base, poly base and low quality were filtered out with default parameters to generate clean reads. Overlapping paired-end reads were generated by Fast Length Adjustment of Short reads (FLASH, v1.2.11) [23] and merged to tags. Next, the tags were clustered to Operational Taxonomic Unit (OTU) by scripts of software USEARCH (v7.0.1090) at 97% sequence similarity [24]. OTU representative sequences were taxonomically classified using Ribosomal Database Project (RDP) Classifier v.2.2 trained on the SILVA database (Release 128), using 0.7 confidence values as cut-off. Alpha and beta diversity were analyzed based on OTU using the free online Majorbio I-Sanger Cloud Platform (www.i-sanger.com). In brief, alpha diversity metrics of observed richness was calculated using mothur (v1.30.1) and visualized with Prism GraphPad (v8.0, boxplot whiskers at min/max). Several beta diversity metrics were determined by QIIME and visualized with Prism GraphPad. Principal co-ordinates analysis based on bray-curtis was visualized using R. Significance of clustering was determined by Bray-Curtis distance matrices.

Metagenomic sequencing and processing

Once we collected the DNA samples, a quality test has been done first. Qualified bacterial DNA samples were first sheared into smaller fragments by nebulization. Then the overhangs resulting from fragmentation were converted into blunt ends by using T4 DNA polymerase, Klenow Fragment and T4 Polynucleotide Kinase. After adding an adenine (A) base to the 3' end of the blunt phosphorylated DNA fragments, adapters were ligated to the ends of the DNA fragments. Then short fragments were removed with Ampure beads. Agilent 2100 Bioanalyzer and ABI StepOnePlus Real-Time PCR System were used to qualify and quantify the sample libraries. Finally, the qualified libraries were sequenced using Illumina HiSeqTM4000 according to the workflow specified by the service provider (BGI Genomics, Hong Kong).

Reads smaller than 50 bp and gene contamination were further removed by mapping the reads against the host reference genome through the software Burrows-Wheeler Aligner (BWA) [25] and removed compare highly similar polluted reads. On average 4.8 Gbp clean data per sample was generated. Clean reads were then *de novo* assembled using Multiple–MEGAHIT [26]. MetaGeneMark (v2.10) [27] was then used to predict the bacterial open reading frames (ORFs) from assembled contigs of at least 500 bp. CD-HIT software (v4.5.8) was used to exclude the redundant genes from all predicted ORFs to construct a preliminary non-redundant gene catalog [28]. The predicted ORFs with lengths over 100 bp were translated into amino acid sequences via NCBI ORF finder and which were subsequently blasted against public databases including NCBI-NR and Kyoto Encyclopedia of Genes and Genomes (KEGG) [29] to obtain taxonomic and metabolic functional annotation.

Metagenomic data analysis

Based on the profiles abundance, analysis of differences in microbial taxonomy and functional enrichment were then performed using free online Majorbio I-Sanger Cloud Platform (www.i-sanger.com). Briefly, statistical significance on species level was determined with unpaired two-tailed student's t-test or LEfSe with standard parameters (LDA score 2.0). Relationships between abundance of gut microbe (top 30 based on relative abundance) and metabolic parameters were presented using spearman correlation heatmap in R package of heatmap.

Redundancy analysis (RDA) demonstrating the relationships between gut microbe distribution (top 10 based on relative abundance) and metabolic parameters was visualized using R with package of vegan. Statistical significance on bacterial functional contribution mapping with KEGG level 2 was determined using unpaired two-tail student's T-test and visualized with heatmap using R and Python with package of NetworkX. The butyrate kinase (2.7.2.7) and phosphate butyryltransferase (2.3.1.19) mapping with KEGG pathway (butanoate metabolism, map00650) were presented as partial pathway adapted from KEGG database, which

statistical significance was determined using unpaired two-tail student's T-test.

16S rRNA and Lachnospiraceae bacterium 28-4 PCR

PCR amplification targeting the V4 region of bacterial 16S rRNA was performed using the highly efficient and universal primers: (926F) 5'-AAACTCAAAKGAATTGACGG-3' and (1062R) 5'-CTCACRRCACGAGCTGAC-3'. The primers above were also used as control of the real-time PCR amplification identifying Lachnospiraceae bacterium 28-4 that using the primers: 5'-GGGTGTACAGAAGGGAAGATTACG-3' and 5'-AAACTCCGGTGGTACAGGATG-3'.

Statistics analysis

Data are expressed as mean ± SEM or boxplot whiskers at min/max unless indicated otherwise. Statistical significance between two groups was determined with two-tailed Student unpaired t-test. All statistical analyses were performed using Prism 8 (GraphPad Prism Software). $P < 0.05$ were considered to be significant.

Results

Dietary butyrate attenuates HFD-induced weight gain as dependent on gut microbiota

We first explored the role of gut microbiota in the metabolic benefits of dietary butyrate. To this end, lean male E3L.CETP mice underwent AIMD or received saline (Vehicle), and were simultaneously fed a HFD without or with sodium butyrate for 6 weeks (figure 1A). Compared to Vehicle, AIMD dramatically reduced the 16S rRNA expression (-95%, $P<0.01$) in fresh fecal samples collected after the intervention (figure 1B), indicating the depletion of gut microbiota. In the Vehicle group, butyrate administration attenuated HFD-induced fat mass gain (-49%, $P<0.05$) without affecting lean mass (figure 1C), as explained by reduced daily (-15%, $P<0.05$) and cumulative (-13%, $P<0.05$) food intake (figures 1D and 1E). In contrast, AIMD abolished the effects of butyrate on fat mass gain (figure 1F) and food intake (figures 1G and1H), indicating that the induction of the metabolic benefits by dietary butyrate is strictly dependent on the presence of gut microbiota.

Additionally, we examined the role of gut microbiota in the effects of dietary butyrate on energy expenditure, lipid metabolism and the activity of BAT, a key regulator in energy hemostasis [30]. In the Vehicle group, dietary butyrate decreased the respiratory exchange ratio during the night period (-5%, $P<0.05$; figure S1A), as a result of the increased fat oxidation (+14%, $P<0.05$; figure S1B) at the expense of carbohydrate oxidation (-28%, $P<0.01$; figure S1C). In addition, dietary butyrate also accelerated the clearance of glycerol tri[^{3}H]oleate ([^{3}H]TO)-labeled triglyceride-rich lipoprotein (TRL)-like particles from the circulation ($P<0.05$; figure S1D) and increased the uptake of [^{3}H]TO-derived radioactivity by BAT (+110%, $P<0.05$; figure S1E). Consistent with our previous findings [9], butyrate activated BAT and enhanced BAT thermogenic capacity, as evidenced by reducing intracellular lipid content (figure S1F and S1I), as well as increasing protein expression of both uncoupling protein-1 (UCP-1) (figure S1G and S1I) and tyrosine hydroxylase (TH), a marker of sympathetic nerve activity (figure S1H and S1I). On the contrary, in the AIMD group, butyrate neither affected the respiratory exchange ratio (figure S1J), fat oxidation and carbohydrate oxidation rate (figures S1K and S1L), nor influenced the [^{3}H]TO clearance from the circulation and the tissue uptake of [^{3}H]TO-derived radioactivity (figures S1M and S1N). In addition, AIMD abolished the effects of butyrate on BAT activation (figures S1O-S1R). These results together suggest that gut microbiota play an essential role in the beneficial effects of dietary butyrate on host energy metabolism.

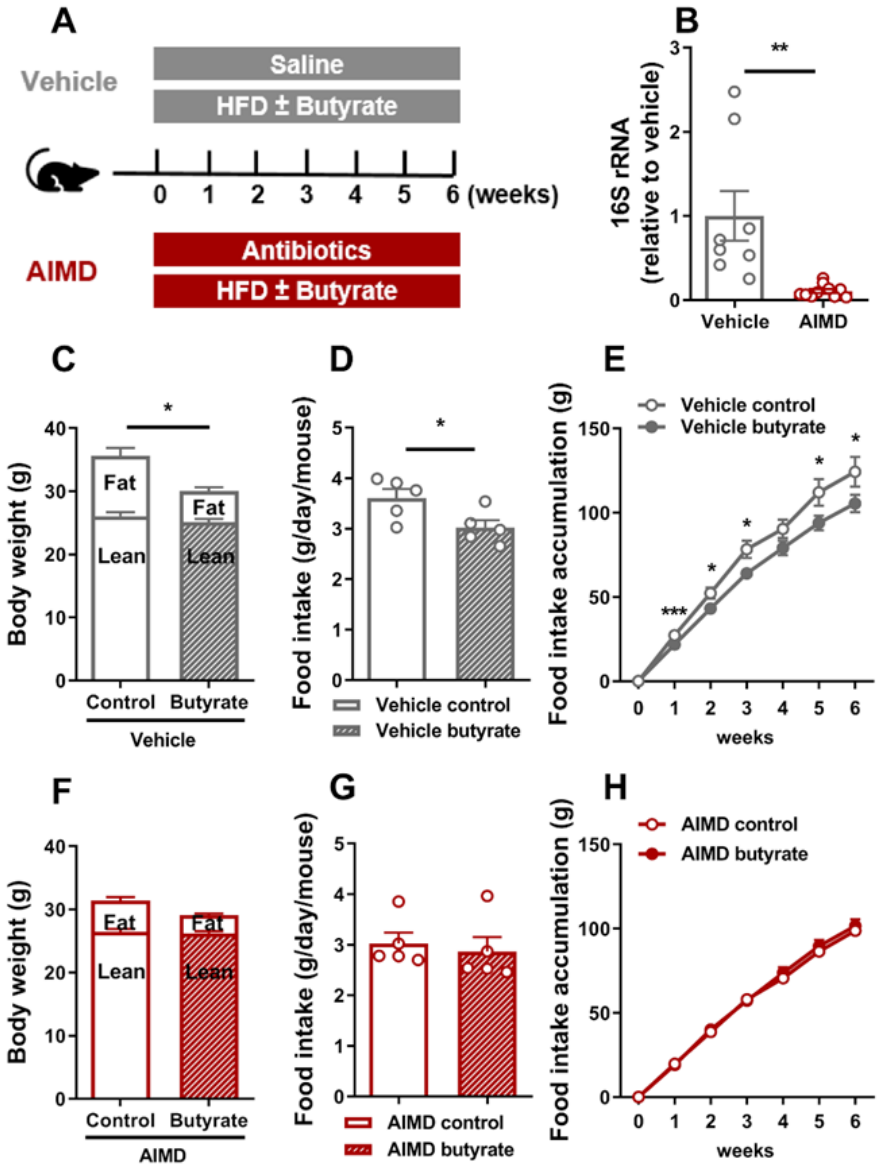

Figure 1. Dietary butyrate attenuates HFD-induced weight gain as dependent on gut microbiota. Mice underwent antibiotics-induced microbiota depletion (AIMD) or received saline (Vehicle) for six weeks while being fed a high fat diet (HFD) without or with 5% (w/w) sodium butyrate (A). At the end of the treatment, fresh feces were collected and bacterial DNA was quantified by 16S rRNA genes amplification by PCR (B, n=8-9). Body composition was measured by MRI (C, F, n=8). The average food intake per day throughout the whole intervention period (D, G, n=5) and the cumulative food intake were calculated (E, H, n=5). Data are shown as means ± SEM; *P<0.05, **P<0.01, ***P<0.001; AIMD vs Vehicle (B) or Butyrate vs Control (C-H).

Fecal microbiota transplantation from butyrate-treated lean donor mice attenuates HFD-induced weight gain and improves insulin resistance in lean recipient mice

To further confirm the causal relationship between the metabolic benefits of butyrate and gut microbiota, fresh fecal bacteria were isolated from lean donor mice fed a HFD without (Control) or with butyrate (Butyrate) between 6-12 weeks of treatment, and transplanted to lean recipient mice during HFD feeding for 6 weeks (figure 2A). Compared with mice receiving FMT from control-treated mice, FMT from butyrate-treated mice caused a persistent decrease in body weight gain (-54% at 6 weeks, $P<0.01$; figure 2B), accompanied by decreased fat mass (-26%, $P<0.05$; figure 2C), as well as a reduction in daily food intake (-15%, $P<0.05$; figure 2D). In addition, FMT from butyrate-treated mice tended to decrease fasting plasma levels of glucose (-11%, $P=0.07$; figure 2E) and insulin (-25%, $P=0.07$; figure 2F), and markedly reduced the homeostatic model assessment of insulin resistance (HOMA-IR) marker (-32%, $P<0.05$; figure 2G).

Compared with FMT from control-treated mice, FMT from butyrate-treated mice decreased respiratory exchange ratio (-3%, $P<0.05$; figure S2A), accompanied by a comparable fat oxidation rate (figure S2B) and decreased carbohydrate oxidation rate (-28%, $P<0.05$; figure S2C). The clearance of [^{3}H]TO from the circulation (figure S2D) and uptake of [^{3}H]TO-derived radioactivity by various organs including BAT were not altered (figure S2E). In line, BAT activity was comparable between both groups, as no differences were observed for intracellular lipid content (figures S2F and S2I), UCP-1 expression (figures S2G and S2I) and TH expression (figures S2H and S2I) within BAT. Collectively, these data confirm that butyrate alters the gut microbiota to cause satiety and attenuate HFD-induced weight gain and insulin resistance.

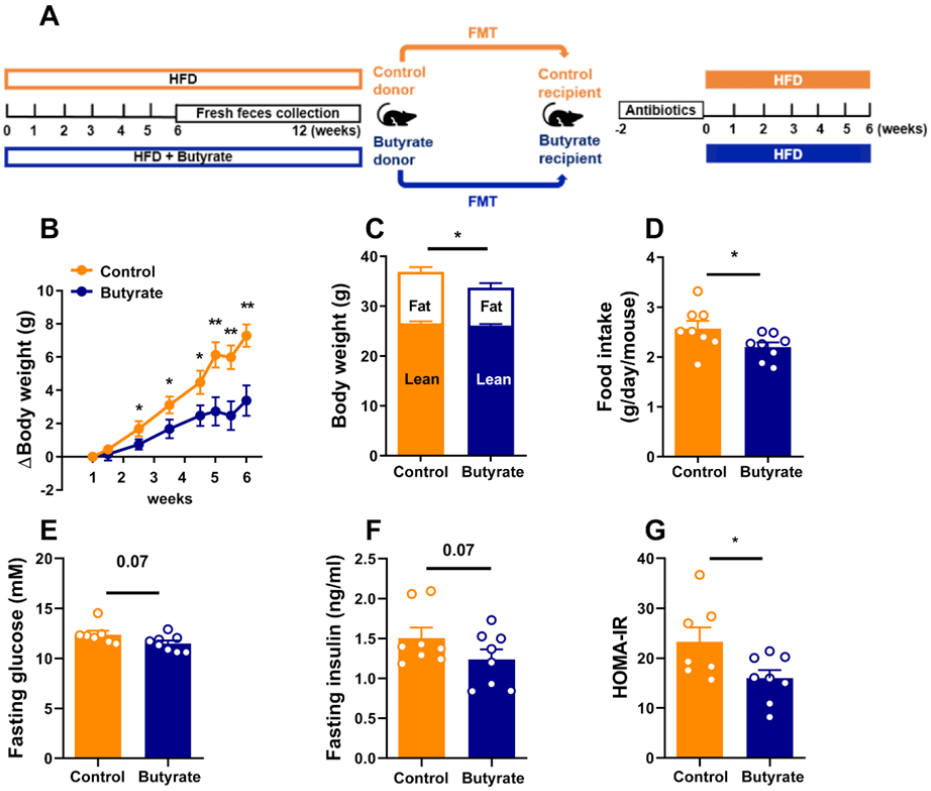

Figure 2. Fecal microbiota transplantation from butyrate-treated lean donor mice attenuates HFD-induced weight gain and improves insulin resistance in lean recipient mice. Mice were fed a high-fat diet (HFD) without or with 5% (w/w) sodium butyrate during 12 weeks. In the final 6 weeks, fresh feces were collected weekly, and used for fecal microbiota transplantation (FMT) to recipient lean mice that were fed a HFD (A). Body weight was measured weekly and body weight change was calculated (B, n=8). At the end of the experiment, body composition was measured by MRI (C, n=8). The average food intake per day throughout the intervention period was calculated (D, n=8). Fasting glucose (E, n=7-8) and insulin (F, n=8) plasma levels were measured, and used for calculation of homeostatic model assessment of insulin resistance (HOMA-IR; G, n=7-8). Data are shown as means ± SEM; *P<0.05, **P<0.01, ***P<0.001; Butyrate vs Control.

Fecal microbiota transplantation from butyrate-treated lean donor mice selectively enriches *Lachnospiraceae bacterium 28-4* within the gut of lean recipient mice

unravel the specific effects of butyrate on the gut microbiota in relation to its metabolic effects on the host, 16S rRNA sequencing as well as metagenomic sequencing were performed on caecal bacterial genomic DNA of all mice receiving FMT from control-treated or butyrate-treated mice. 16S rRNA sequence analysis revealed changes in gut microbial ecology in recipient mice. The observed richness (α-diversity) of the operational taxonomic unit (OTU) was not different between recipient groups (figure 3A). In favorable contrast, FMT from butyrate-treated mice induced an apparent difference in composition (β-diversity) of gut microbiota, as presented by an increase in abundance of Firmicutes (+28%, $P<0.05$; figure 3B), at the expense of predominantly Bacteroidetes, and induced different clustering in unweighted uniFrac principal coordinates analysis (PCoA) on OTU (β-diversity, figure 3C). Altogether, these data demonstrate a successful FMT, as evidenced by the change in microbiota composition with an increased abundance of Firmicutes.

Next, metagenomic analysis revealed more distinctive variations in the gut microbiome at the species level. We identified 6840 species in total, spanning 1851 genus and 104 phyla. Among those, 859 species were significantly regulated by FMT from butyrate-treated mice compared to control-treated mice. In particular, among the top 30 species based on relative abundance, FMT from butyrate-treated mice markedly increased the relative abundance of *Lachnospiraceae bacterium 28-4* (+2.9 fold, $P<0.01$), while it decreased the relative abundance of *Bacteroides sp. CAG:709*, *Bacteroides sp. CAG:770*, *Bacteroides sp. CAG:545*, *Alistipes sp. CAG:435*, *Flavonifractor plautii*, *Alistipes sp. CAG:514* and *Pseudoflavonifractor capillosus* (figure 3D). Enrichment with *Lachnospiraceae bacterium 28-4* was also shown by further analysis using linear discriminant analysis of effect size (LefSe, figure S3A) and real-time PCR with in house-designed primers (+6.6 fold, $P<0.01$; figure S3B), confirming that FMT from butyrate-treated mice selectively promotes the proliferation of *Lachnospiraceae bacterium 28-4*. Collectively, these data suggest that dietary butyrate may exert its metabolic benefits by inducing selective outgrowth of *Lachnospiraceae bacterium 28-4*.

The richness of *Lachnospiraceae bacterium 28-4* in the gut negatively correlates with host body weight

To elucidate whether the alteration of gut microbiota by FMT from butyrate-treated mice correlates to the metabolic health of the host, we analyzed the predicted functional contributions of the richest stains (top 30 based on relative abundance) using the Kyoto Encyclopedia of Genes and Genomes (KEGG) database (Pathway level 2, figure S4). Correlation heatmap analysis showed the involvement of *Lachnospiraceae bacterium 28-4*, *Eubacterium plexicaudatum*, *Lachnospiraceae bacterium COE1* and *Pseudoflavonifractor capillosus* with various aspects of host

metabolic health in mice receiving FMT from control and butyrate-treated mice. Particularly, the abundance of *Lachnospiraceae bacterium 28-4* is associated with carbohydrate metabolism (F1), energy metabolism (F8) and lipid metabolism (F13, figure S4). Consistent with this predictive analysis, functional correlation analysis using measured metabolic parameters, including body weight, food intake, glucose level and insulin level of FMT recipient mice revealed that the richness of *Lachnospiraceae bacterium 28-4* negatively correlates with host body weight (R^2=-0.541, P<0.01, figure 3D and figure S5). Furthermore, redundancy analysis (RDA) confirmed a negative correlation between *Lachnospiraceae bacterium 28-4* and metabolic health parameters including body weight, food intake, fasting plasma glucose level and insulin level (figure 3E). Collectively, these data provide further evidence for the involvement of *Lachnospiraceae bacterium 28-4* in the metabolic benefits induced by dietary butyrate.

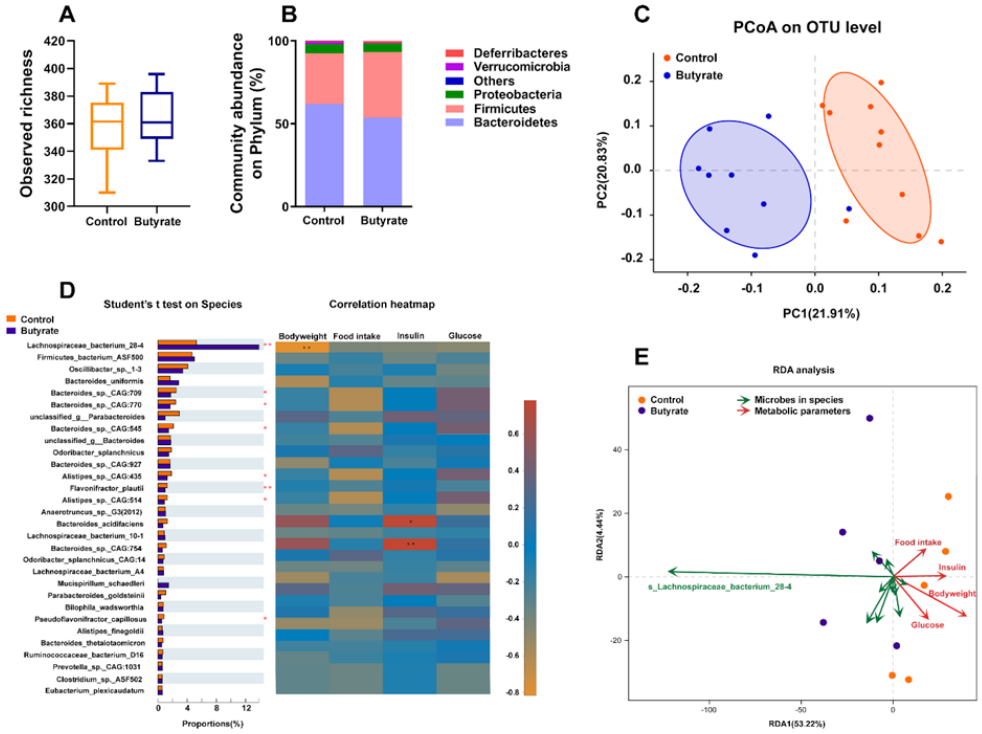

Figure 3. Fecal microbiota transplantation from butyrate-treated lean donor mice selectively enriches *Lachnospiraceae bacterium 28-4*, negatively correlating with host body weight. Mice were fed a high-fat diet (HFD) without or with 5% (w/w) sodium butyrate during 12 weeks. In the final 6 weeks, fresh feces were collected weekly, and used for weekly fecal microbiota transplantation (FMT) to recipient lean mice that were fed a HFD. At the end of the study, the recipients' bacterial genomic DNA was isolated from the caecum content and sequenced. The number of observed species (A, n=9-10) and the community abundance of gut microbiota on phylum level (B, n=9-10) were assessed. Principal coordinates analysis (PCoA) plot of unweighted UniFrac distances on operational taxonomic unites (OTU) level was calculated (C, n=9-10). The richness of gut microbiota (top 30 based on relative abundance) on species level was compared using student T-test and its correlation with metabolic outcomes (bodyweight, food intake, glucose and insulin) were presented in Spearman correlation heatmap (D, n=5). Correlations of abundance of *Lachnospiraceae bacterium 28-4* with metabolic outcomes (bodyweight, food intake, glucose and insulin) were analyzed using redundancy analysis (RDA) (E, n=5). Data are shown as boxplot whiskers at min/max (A) or means ± SEM, *P<0.05, **P<0.01, ***P<0.001; Butyrate vs Control (B and D).

Dietary butyrate is ineffective in inducing weight loss, ameliorating metabolic health, or promoting *Lachnospiraceae bacterium 28-4* in diet-induced obese mice

After having established that butyrate prevents DIO in HFD-fed lean mice [9], we next investigated the therapeutic potential of dietary butyrate in treating pre-existing DIO. To this end, mice were first rendered obese by HFD feeding, and were subsequently fed a HFD without or with butyrate supplementation for 6 weeks (figure 4A). Strikingly, butyrate did not cause any reduction in either body weight (figure 4B), fat mass (figure 4C), food intake (figure 4D), fasting plasma glucose (figure 4E), fasting plasma insulin (figure 4F), or HOMA-IR (figure 4G). Likewise, dietary butyrate failed to alter the gut microbiota in DIO mice with respect to observed OUT richness (α-diversity, figure 4H) and community abundance on phylum (β-diversity, figure 4I), resulting in overlapping clustering between control and butyrate-treated mice in unweighted uniFrac PcoA analysis (β-diversity, figure 4J). Of note, in DIO mice, butyrate also did not promote the proliferation of *Lachnospiraceae bacterium 28-4* (figure 4K). Taken together, these data show that butyrate does not improve metabolic health in the context of pre-existing obesity, probably related to the absence of effects on gut microbiota.

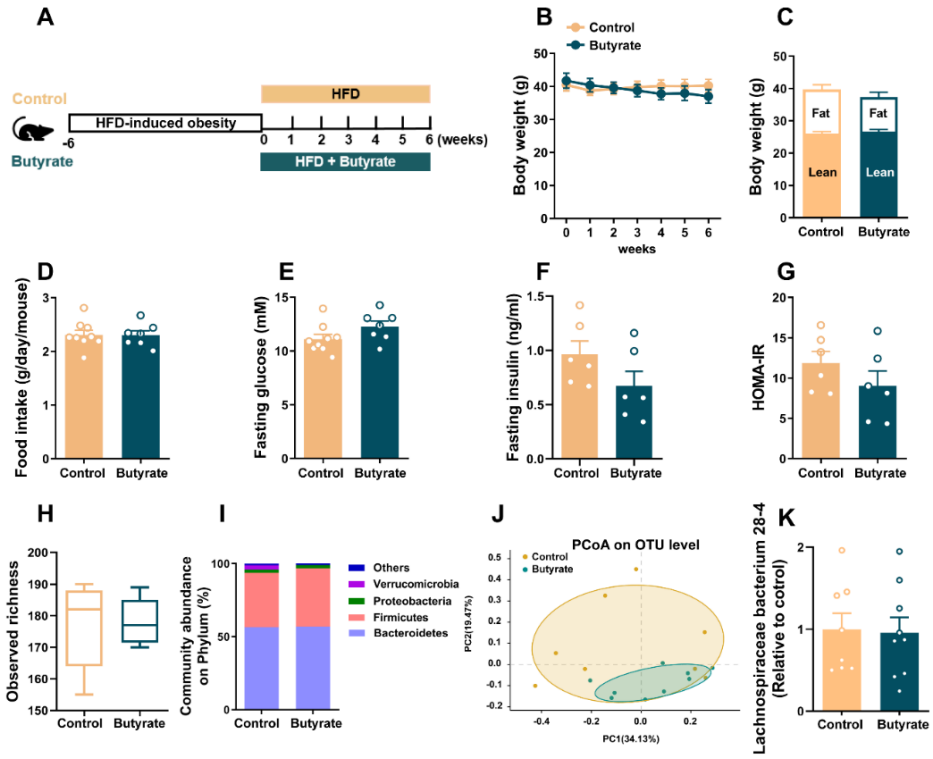

Figure 4. Dietary butyrate is ineffective in inducing weight loss, ameliorating metabolic health, or promoting *Lachnospiraceae bacterium 28-4* in diet-induced obese mice. Mice were rendered obese by feeding a high-fat diet (HFD) for 6 weeks, and subsequently fed a HFD without or with 5% (w/w/) butyrate for another 6 weeks (A). Bodyweight was measured weekly (B, n=7-9) and at the end of the treatment period body composition was measured by MRI (C, n=7-9). The average food intake per day was calculated (D, n=7- 9). Fasting plasma glucose (E, n=7-9) and insulin (F, n=6) were measured and used to calculate homeostatic model assessment of insulin resistance (HOMA-IR; G, n=6). Cecum bacterial DNA was collected, sequenced, and the observed richness of taxonomy (H, n=7-9) of gut microbiota was calculated. The composition of abundant bacteria on phylum (I, n=7-9) and principal coordinates analysis (PCoA) plot of unweighted UniFrac distances on operational taxonomic units (OTU) level (J, n=7-9) were calculated. The abundance of *Lachnospiraceae bacterium 28-4* was quantified by real-time PCR (K, n=8-9). Data are shown as means ± SEM (B-G, I and K) or boxplot whiskers at min/max (H).

Fecal microbiota transplantation from butyrate-treated diet-induced obese mice does not attenuate weight gain, ameliorate metabolic health, or enrich *Lachnospiraceae bacterium 28-4* in lean recipient mice

Finally, we assessed whether the failure of dietary butyrate to exert metabolic benefits in DIO mice is related to the gut microbiota. To this end, fecal microbiota was isolated from DIO donor mice that received HFD without or with butyrate, and was transplanted to recipient lean mice (figure 5A). In full support that butyrate does not ameliorate metabolic health in DIO mice (figure 4B-4G), FMT from butyrate-treated DIO mice as compared control-treated DIO mice did not affect body weight and fat mass (figure 5B), food intake (figure 5C), or markers related to insulin resistance including fasting plasma glucose, insulin and HOMA-IR (figure 5D-5F). Although some differences in the β-diversity of gut microbiota, rather than in α-diversity, was observed in the recipient mice from different groups (figure 5G-5I), FMT from butyrate-treated DIO mice did not manipulate the richness of *Lachnospiraceae bacterium 28-4* (figure 5J).

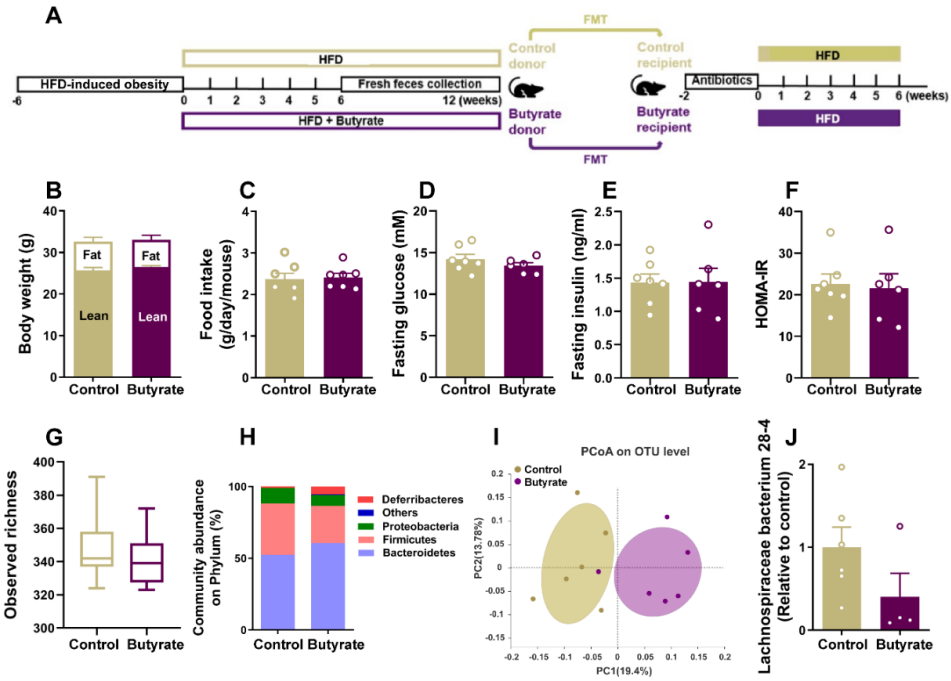

Figure 5. Fecal microbiota transplantation from butyrate-treated diet-induced obese mice does not attenuate weight gain, ameliorate metabolic health, or enrich *Lachnospiraceae bacterium 28-4* in lean recipient mice. Mice were rendered obese by feeding a high-fat diet (HFD) for 6 weeks, and subsequently fed a HFD without or with 5% (w/w/) butyrate for another 12 weeks. In the final 6 weeks, fresh feces were collected weekly, and used for fecal microbiota transplantation (FMT) to lean recipient mice that were fed a HFD (A). Body composition was calculated by MRI at the end of the study (B, n=6-7). The average food intake per day throughout the intervention period was calculated (C, n=6-7). Fasting plasma glucose (D, n=6-7) and insulin (E, n=6-7) were measured and used to calculate homeostatic model assessment of insulin resistance (HOMA-IR; F, n=6-7). Cecum bacterial DNA was collected, sequenced, and the observed richness of taxonomy (G, n=6) of gut microbiota was calculated. The composition of abundant bacteria on phylum (H, n=6) and principal coordinates analysis (PCoA) plot of unweighted UniFrac distances on operational taxonomic units (OTU) level (I, n=6) were calculated. The abundance of *Lachnospiraceae bacterium 28-4* was quantified by real-time PCR (J, n=5 or 6). Data are shown as means ± SEM (B-F, H and J) or boxplot whiskers at min/max (G).

Discussion

Gut microbiota have emerged as a critical regulator of host metabolic health [31, 32], with respect to regulating fat storage [33], influencing the thermogenesis of BAT [34] and contributing to host energy metabolism by harvesting energy from the diet by themselves [35]. However, the causal interactions between bacterial strains and host metabolic health are still under debate. Here, by performing AIMD and FMT, two widely used approaches to manipulate gut microbiota, we demonstrate that the beneficial effects of butyrate are crucially dependent on the presence of gut microbiota, and provide the first evidence of the specific involvement of *Lachnospiraceae bacterium 28-4* in the metabolic benefits induced by dietary butyrate, as evidence by a negative correlation between the richness of *Lachnospiraceae bacterium 28-4* and metabolic health parameters including body weight, food intake and insulin resistance.

We previously revealed that dietary butyrate prevents DIO, mainly by reducing appetite and to a lower extent by activating BAT, as related to a change in the gut microbiota composition [9]. Thus, in the current study, we first investigated the causal role of gut microbiota in these metabolic properties of dietary butyrate. By performing AIMD, we observed that eradication of gut microbiota (>95%) completely abolished the dietary butyrate-induced appetite reduction and BAT activation, implying these metabolic benefits of dietary butyrate are strictly dependent on the presence of gut microbiota. Therefore, it was crucial to investigate which specific changes in gut microbiota induced by butyrate are causal for these metabolic benefits. By performing FMT, we found that the predominant benefits of dietary butyrate to improve host energy metabolism, i.e., reducing appetite, ameliorating weight gain and improving insulin resistance were transferable by bacterial transplantation. However, FMT from butyrate-treated mice did not activate BAT, indicating dietary butyrate activates BAT independently of gut microbiota, although this is in seeming contrast to the observation that AIMD abolished the BAT-activating effects of dietary butyrate. Gut microbiota depletion has been demonstrated to promote browning of white adipose tissue and reduce obesity [36], indicating the depletion of gut microbiota *per se* might affect BAT activity. Indeed, we found that AIMD itself increases the uptake of TG-derived fatty acids by BAT and reduces the lipid content within brown adipocytes. Thus, based on the activated state of BAT resulting from AIMD, changes in gut microbiota induced by dietary butyrate were probably unable to promote BAT activation further.

Next, in search for the specific gut microbe change(s) that may contribute to the beneficial effects of dietary butyrate, we screened the gut microbiota of mice receiving FMT by metagenomic sequencing, and discovered more than 800 significantly regulated species. Among the top 30 species based on relative abundance, the richness of *Lachnospiraceae bacterium 28-4* was markedly increased by FMT from butyrate-treated mice. Of utmost interest is that the richness of *Lachnospiraceae bacterium 28-4* negatively correlated with the host metabolic

health parameters, including satiety, body weight, fasting glucose and insulin levels, indicating that the enrichment of *Lachnospiraceae bacterium 28-4* may be the key underlying the beneficial effects of dietary butyrate.

Lachnospiraceae bacterium 28-4 is a bacterial strain within the unclassified genus *Lachnospiraceae*; family *Lachnospiraceae*; order *Clostridiales*; class *Clostridia*; phylum *Firmicutes* that was previously found in murine cecum content by Duck et al. [37]. The presence of *Lachnospiraceae bacterium 28-4* in the murine gut was recently confirmed by a single-cell resolution genome analysis [38]. Furthermore, in a study of the evolution of mammals and their gut microbes, the genome of *Lachnospiraceae bacterium 28-4* was reported to be present in the fecal microbiota of Western lowland gorilla [39], indicating the possibility of the existence of this strain in the gut of humans. However, as yet there is still limited information about the potential functions of this strain.

Predictive analysis of microbiome using KEGG pathways previously demonstrated that *Lachnospiraceae bacterium 28-4* might be enriched in enzymes involved in the butyrate synthesis [40]. This is confirmed by the high expression of genes coding butyrate kinase (EC2.7.2.7) and phosphate butyryltransferase (EC2.3.1.19), both of which are the key enzymes involved in the butyrate synthesis (figure S6A-6C), strongly suggesting that *Lachnospiraceae bacterium 28-4* might exert its metabolic functions by increasing endogenous butyrate production. This is consistent with the well-reported function of genus *Lachnospiraceae* in producing butyrate [41]. We indeed observed higher level of butyrate in caecal content of mice receiving dietary butyrate than expected from the HFD content (control, figure S7A). Collectively, these findings lead us to speculate that dietary butyrate specifically promotes the proliferation of *Lachnospiraceae bacterium 28-4*, thereafter interactively increasing endogenous butyrate production and consequently inducing satiety and improving insulin sensitivity. Nevertheless, we did not observe increased caecal butyrate upon FMT from butyrate-treated lean mice (figure S7B). This may be attributed to the low production rate of endogenous butyrate when using the current diet without adding fiber for fermentation to produce butyrate [42], or due to the presence of other butyrate-producing strains in the gut to add to butyrate production, which conceals the amount of butyrate produced by *Lachnospiraceae bacterium 28-4*. Thus, isolation of *Lachnospiraceae bacterium 28-4* is needed for future studies to prove its causal role in endogenous butyrate production in relation to metabolic benefits.

In the current study, we observed that dietary butyrate did not restore metabolic health in pre-existing DIO mice. Likewise, a recent clinical study found that butyrate-improved insulin resistance is only observed in healthy individuals but not in metabolic syndrome individuals [23]. Of particular interest is why butyrate exerts different metabolic effects in lean versus DIO subjects. HFD has been shown to result in an imbalance in gut microbiota that leads to dysbiosis, which has been shown to dramatically affect metabolic health [43]. Thus, it is attempting

to speculate that the HFD-induced dysbiosis of gut microbiota in pre-existing DIO mice inhibits the outgrowth of *Lachnospiraceae bacterium 28-4* in the gut, thereby blocking the associated beneficial metabolic effects. Indeed, in contrast to the increased abundance of *Lachnospiraceae bacterium 28-4* by dietary butyrate in lean mice, dietary butyrate failed to increase the abundance of *Lachnospiraceae bacterium 28-4* in DIO mice (figure S8). In addition, FMT from butyrate-treated DIO mice also did not improve metabolic health in lean recipient mice. Altogether, these findings indicate that the richness of *Lachnospiraceae bacterium 28-4*, in relation to a favorable environment in the gut for its proliferation, may be the main explanation of the beneficial effects of dietary butyrate on metabolic health. Thus, strategies to specifically increase the richness of *Lachnospiraceae bacterium 28-4* might provide novel therapeutic handles to combat obesity.

Of interest, it has already been proven that some probiotics, such as *Lactobacillus Rhamnosus GG* and *VSL#3*, used alone or in symbiotic mixtures, are able to exert anti-obese effects in animal and human studies [44, 45], although the precise actions of those probiotics in combating obesity are still not elucidated. Interestingly, a recent proof-of-concept study demonstrated the feasibility of administered *Akkermansia muciniphila* to improve insulin resistance, providing a promising start for developing future clinical interventions with gut microbiota manipulation [13]. Most notably, *Pendulum Glucose Control*, a probiotics production containing *Akkermansia muciniphila*, *etc.*, was launched in 2020 as the first and only medical probiotic designed specifically for the dietary management of T2D, which has been demonstrated to lower blood glucose spikes by 33% and reduce HbA1C levels by 0.6 [46]. All these findings collectively pave the way of access to the therapeutic potential of *Lachnospiraceae bacterium 28-4* in inducing satiety and combating obesity and its associated cardiometabolic diseases in humans.

In summary, we revealed that gut microbiota play a crucial role in the beneficial metabolic effects of dietary butyrate, and found the involvement of *Lachnospiraceae bacterium 28-4* in the butyrate-induced decreasing in food intake, attenuation of DIO and improvement of insulin resistance, altogether strongly indicating the therapeutic potential of *Lachnospiraceae bacterium 28-4* in combating obesity and the associated metabolic diseases.

References

1. Must, A., et al., *The disease burden associated with overweight and obesity.* JAMA, 1999. **282**(16): p. 1523-9.
2. Collaborators, G.B.D.O., et al., *Health Effects of Overweight and Obesity in 195 Countries over 25 Years.* N Engl J Med, 2017. **377**(1): p. 13-27.
3. Most, J. and L.M. Redman, *Impact of calorie restriction on energy metabolism in humans.* Exp Gerontol, 2020. **133**: p. 110875.
4. Kumar, R.B. and L.J. Aronne, *Efficacy comparison of medications approved for chronic weight management.* Obesity (Silver Spring), 2015. **23 Suppl 1**: p. S4-7.
5. Reynolds, A., et al., *Carbohydrate quality and human health: a series of systematic reviews and meta-analyses.* Lancet, 2019. **393**(10170): p. 434-445.
6. Chambers, E.S., et al., *Role of Gut Microbiota-Generated Short-Chain Fatty Acids in Metabolic and Cardiovascular Health.* Curr Nutr Rep, 2018. **7**(4): p. 198-206.
7. Lin, H.V., et al., *Butyrate and propionate protect against diet-induced obesity and regulate gut hormones via free fatty acid receptor 3-independent mechanisms.* PLoS One, 2012. **7**(4): p. e35240.
8. Gao, Z., et al., *Butyrate improves insulin sensitivity and increases energy expenditure in mice.* Diabetes, 2009. **58**(7): p. 1509-17.
9. Li, Z., et al., *Butyrate reduces appetite and activates brown adipose tissue via the gut-brain neural circuit.* Gut, 2018. **67**(7): p. 1269-1279.
10. Sorbara, M.T., et al., *Inhibiting antibiotic-resistant Enterobacteriaceae by microbiota-mediated intracellular acidification.* J Exp Med, 2019. **216**(1): p. 84-98.
11. Zhao, L., et al., *Gut bacteria selectively promoted by dietary fibers alleviate type 2 diabetes.* Science, 2018. **359**(6380): p. 1151-1156.
12. Wu, H., et al., *The Gut Microbiota in Prediabetes and Diabetes: A Population-Based Cross-Sectional Study.* Cell Metab, 2020.
13. Depommier, C., et al., *Supplementation with Akkermansia muciniphila in overweight and obese human volunteers: a proof-of-concept exploratory study.* Nat Med, 2019. **25**(7): p. 1096-1103.
14. Vrieze, A., et al., *Transfer of intestinal microbiota from lean donors increases insulin sensitivity in individuals with metabolic syndrome.* Gastroenterology, 2012. **143**(4): p. 913-6 e7.
15. Kennedy, E.A., K.Y. King, and M.T. Baldridge, *Mouse Microbiota Models: Comparing Germ-Free Mice and Antibiotics Treatment as Tools for Modifying Gut Bacteria.* Front Physiol, 2018. **9**: p. 1534.
16. van den Hoek, A.M., et al., *APOE*3Leiden.CETP transgenic mice as model for pharmaceutical treatment of the metabolic syndrome.* Diabetes Obes Metab, 2014. **16**(6): p. 537-44.

17. Westerterp, M., et al., *Cholesteryl ester transfer protein decreases high-density lipoprotein and severely aggravates atherosclerosis in APOE*3-Leiden mice.* Arterioscler Thromb Vasc Biol, 2006. **26**(11): p. 2552-9.

18. Frost, F., et al., *A structured weight loss program increases gut microbiota phylogenetic diversity and reduces levels of Collinsella in obese type 2 diabetics: A pilot study.* PLoS One, 2019. **14**(7): p. e0219489.

19. Matthews, D.R., et al., *Homeostasis model assessment: insulin resistance and beta-cell function from fasting plasma glucose and insulin concentrations in man.* Diabetologia, 1985. **28**(7): p. 412-9.

20. Van Klinken, J.B., et al., *Estimation of activity related energy expenditure and resting metabolic rate in freely moving mice from indirect calorimetry data.* PLoS One, 2012. **7**(5): p. e36162.

21. Rensen, P.C., et al., *Particle size determines the specificity of apolipoprotein E-containing triglyceride-rich emulsions for the LDL receptor versus hepatic remnant receptor in vivo.* J Lipid Res, 1997. **38**(6): p. 1070-84.

22. Kooijman, S., et al., *Central GLP-1 receptor signalling accelerates plasma clearance of triacylglycerol and glucose by activating brown adipose tissue in mice.* Diabetologia, 2015. **58**(11): p. 2637-46.

23. Magoc, T. and S.L. Salzberg, *FLASH: fast length adjustment of short reads to improve genome assemblies.* Bioinformatics, 2011. **27**(21): p. 2957-63.

24. Edgar, R.C., *UPARSE: highly accurate OTU sequences from microbial amplicon reads.* Nat Methods, 2013. **10**(10): p. 996-8.

25. Li, H. and R. Durbin, *Fast and accurate short read alignment with Burrows-Wheeler transform.* Bioinformatics, 2009. **25**(14): p. 1754-60.

26. Li, D., et al., *MEGAHIT: an ultra-fast single-node solution for large and complex metagenomics assembly via succinct de Bruijn graph.* Bioinformatics, 2015. **31**(10): p. 1674-6.

27. Noguchi, H., J. Park, and T. Takagi, *MetaGene: prokaryotic gene finding from environmental genome shotgun sequences.* Nucleic Acids Res, 2006. **34**(19): p. 5623-30.

28. Fu, L., et al., *CD-HIT: accelerated for clustering the next-generation sequencing data.* Bioinformatics, 2012. **28**(23): p. 3150-2.

29. Kanehisa, M. and S. Goto, *KEGG: kyoto encyclopedia of genes and genomes.* Nucleic Acids Res, 2000. **28**(1): p. 27-30.

30. Cypess, A.M. and C.R. Kahn, *The role and importance of brown adipose tissue in energy homeostasis.* Curr Opin Pediatr, 2010. **22**(4): p. 478-84.

31. Nieuwdorp, M., et al., *Role of the microbiome in energy regulation and metabolism.* Gastroenterology, 2014. **146**(6): p. 1525-33.

32. Zmora, N., J. Suez, and E. Elinav, *You are what you eat: diet, health and the gut microbiota.* Nat Rev Gastroenterol Hepatol, 2019. **16**(1): p. 35-56.

33. Backhed, F., et al., *The gut microbiota as an environmental factor that regulates fat storage.* Proc Natl Acad Sci U S A, 2004. **101**(44): p. 15718-23.

34. Li, B., et al., *Microbiota Depletion Impairs Thermogenesis of Brown Adipose Tissue and Browning of White Adipose Tissue.* Cell Rep, 2019. **26**(10): p. 2720-2737 e5.

35. Turnbaugh, P.J., et al., *An obesity-associated gut microbiome with increased capacity for energy harvest.* Nature, 2006. **444**(7122): p. 1027-31.

36. Suarez-Zamorano, N., et al., *Microbiota depletion promotes browning of white adipose tissue and reduces obesity.* Nat Med, 2015. **21**(12): p. 1497-1501.

37. Duck, L.W., et al., *Isolation of flagellated bacteria implicated in Crohn's disease.* Inflamm Bowel Dis, 2007. **13**(10): p. 1191-201.

38. Chijiiwa, R., et al., *Single-cell genomics of uncultured bacteria reveals dietary fiber responders in the mouse gut microbiota.* Microbiome, 2020. **8**(1): p. 5.

39. Ley, R.E., et al., *Evolution of mammals and their gut microbes.* Science, 2008. **320**(5883): p. 1647-51.

40. Daniel, S.G., et al., *Functional Changes in the Gut Microbiome Contribute to Transforming Growth Factor beta-Deficient Colon Cancer.* mSystems, 2017. **2**(5).

41. Vital, M., A. Karch, and D.H. Pieper, *Colonic Butyrate-Producing Communities in Humans: an Overview Using Omics Data.* mSystems, 2017. **2**(6).

42. den Besten, G., et al., *The role of short-chain fatty acids in the interplay between diet, gut microbiota, and host energy metabolism.* J Lipid Res, 2013. **54**(9): p. 2325-40.

43. Janssen, A.W. and S. Kersten, *The role of the gut microbiota in metabolic health.* FASEB J, 2015. **29**(8): p. 3111-23.

44. Luoto, R., et al., *The impact of perinatal probiotic intervention on the development of overweight and obesity: follow-up study from birth to 10 years.* Int J Obes (Lond), 2010. **34**(10): p. 1531-7.

45. Alisi, A., et al., *Randomised clinical trial: The beneficial effects of VSL#3 in obese children with non-alcoholic steatohepatitis.* Aliment Pharmacol Ther, 2014. **39**(11): p. 1276-85.

46. Perraudeau, F., et al., *Improvements to postprandial glucose control in subjects with type 2 diabetes: a multicenter, double blind, randomized placebo-controlled trial of a novel probiotic formulation.* BMJ Open Diabetes Res Care, 2020. **8**(1).

Supplemental figures

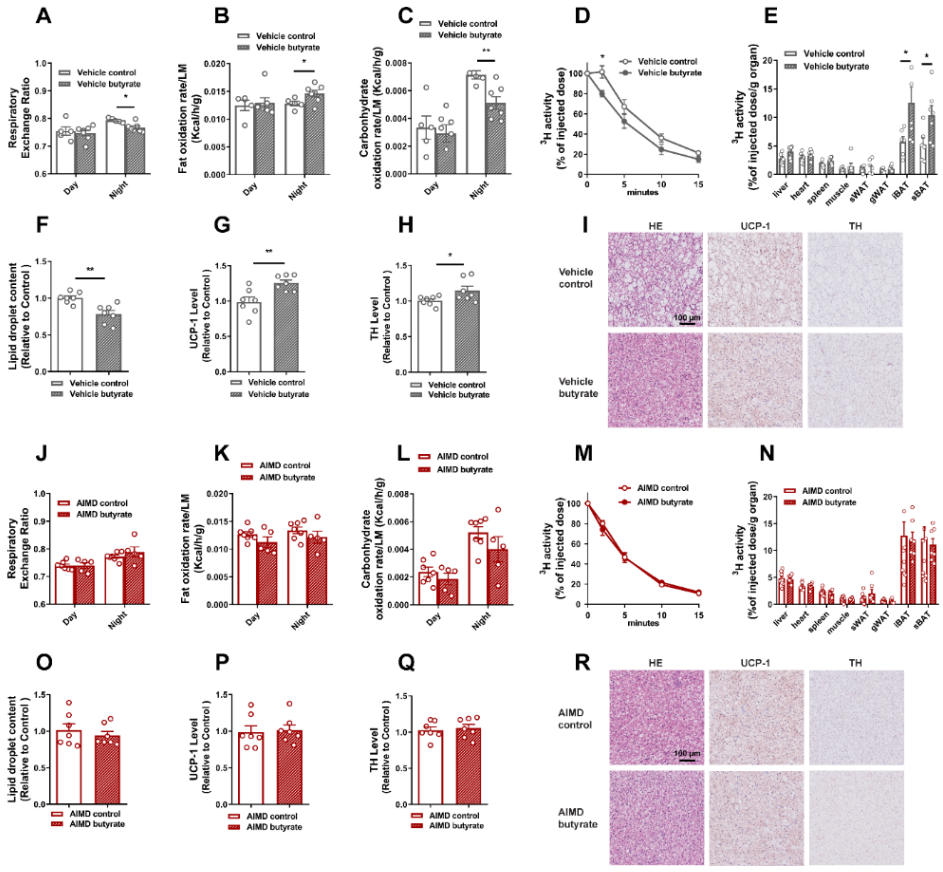

Figure S1. Dietary butyrate increases fat oxidation accompanied by parameters of BAT activation as dependent on gut microbiota. Mice received antibiotics-induced microbiota depletion (AIMD) or saline (Vehicle) for six weeks while being fed a high-fat diet (HFD) without or with 5% (w/w) sodium butyrate. In the second week, mice were individually housed in automatic metabolic cages to assess energy expenditure by indirect calorimetry. Respiratory exchange ratio (A, J, n=5-7), fat oxidation (B, K, n=5-7) and carbohydrate oxidation (C, L, n=5-7) were calculated from data obtained during 3 consecutive days. Just before termination, mice were intravenously injected with glycerol tri[^{3}H]oleate-labeled triglyceride-rich lipoprotein-like particles, and ^{3}H-activity was assessed in plasma (D, M, n=6) and various organs (E, N, n=6). Interscapular brown adipose tissue (iBAT) was isolated and used for immunohistochemistry staining (F-I, O-R, n=7). Lipid content (F, O), uncoupling protein-1 (UCP-1) protein content (G, P) and tyrosine hydroxylase (TH) protein content (H, Q) were quantified as representative pictures shown (I, R). Data are shown as means ± SEM; *P<0.05, **P<0.01, ***P<0.001; Butyrate vs Control. gWAT, gonadal white adipose tissue; HE, hematoxylin and eosin; LM, lean body mass; sBAT, subscapular brown adipose tissue; sWAT, subcutaneous white adipose tissue.

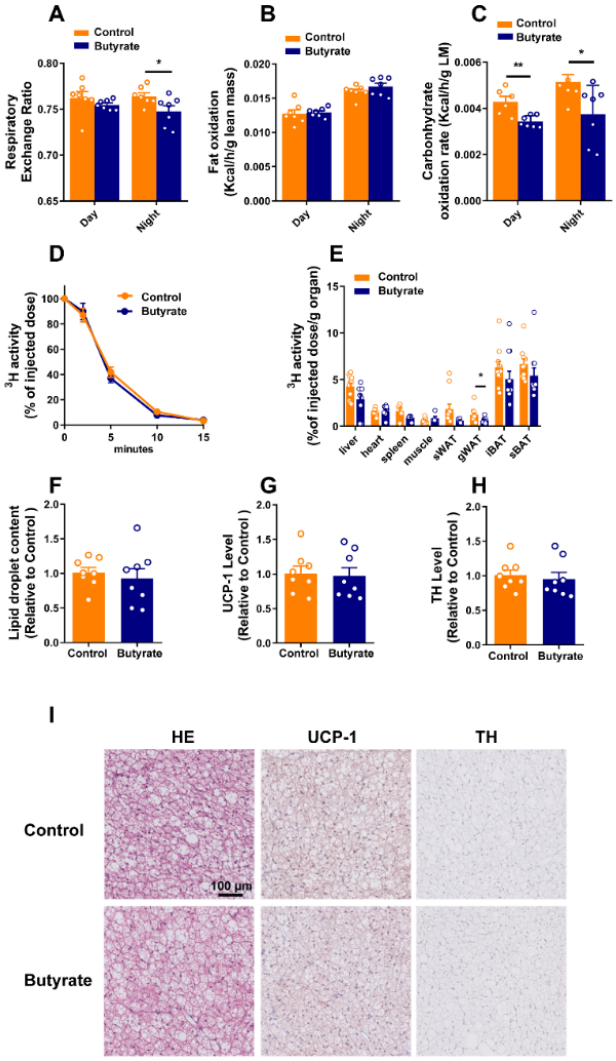

Figure S2. FMT from butyrate-treated lean mice does not affect fat oxidation and activate brown adipose tissue in lean recipient mice. Mice were fed a high-fat diet (HFD) without or with 5% (w/w) sodium butyrate during 12 weeks. In the final 6 weeks, fresh feces were collected weekly, and used for weekly fecal microbiota transplantation (FMT) to recipient lean mice that were fed a HFD. In the second week, mice were individually housed in automatic metabolic cages for 3 consecutive days to assess energy expenditure by indirect calorimetry measurement, and respiratory exchange ratio (A, n=7), fat oxidation (B, n=7) and carbohydrate oxidation (C, n=7) were calculated. Just before termination, mice we were intravenously injected with glycerol tri[^{3}H]oleate-labeled triglyceride-rich lipoprotein-like particles, and ^{3}H-activity was assessed in plasma (D, n=8) and various organs (E, n=8). iBAT was collected and used for immunohistochemistry staining, and lipid content (F, n=8), UCP-1 protein (G, n=8) and TH protein (H, n=8) was quantified as presentative pictures shown (I). Data are shown as means ± SEM. *P<0.05, **P<0.01, ***P<0.001; Butyrate vs Control.

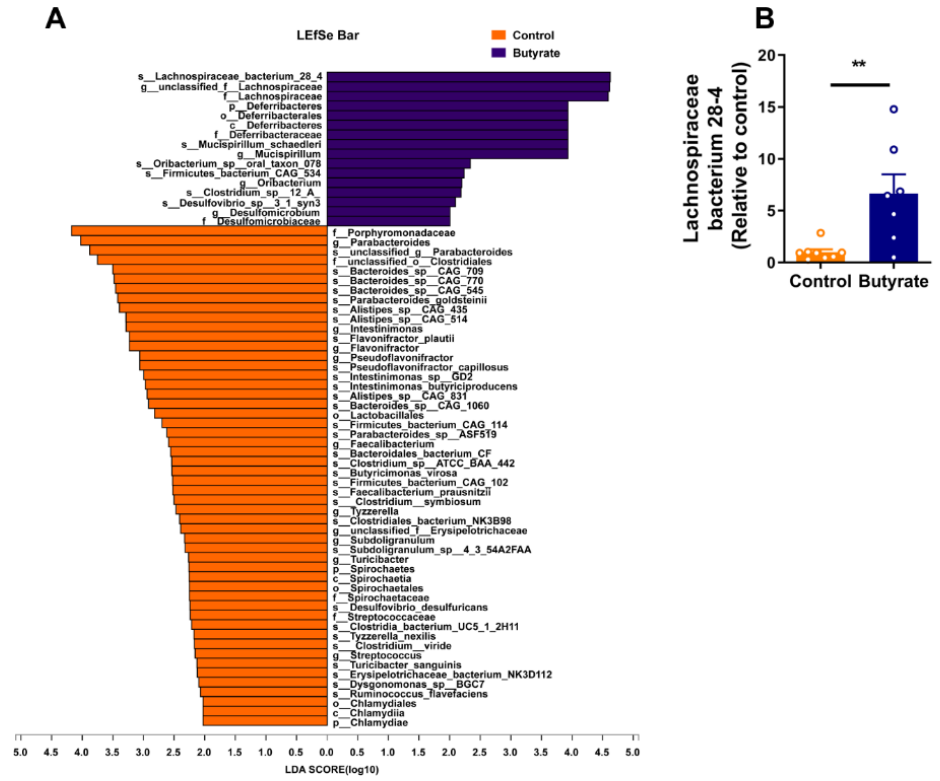

Figure S3. FMT from butyrate-treated lean mice selectively enriches *Lachnospiraceae bacterium 28-4*. Linear discriminant analysis (LDA) score of taxonomic cladogram was obtained from linear discriminant analysis effect size (LEfSe) analysis of gut microbiota (A, n=5). Gene of *Lachnospiraceae bacterium 28-4* was quantified by real-time PCR (B, n=7-8). Data are shown as means ± SEM; *P<0.05, **P<0.01, ***P<0.001; Butyrate vs Control.

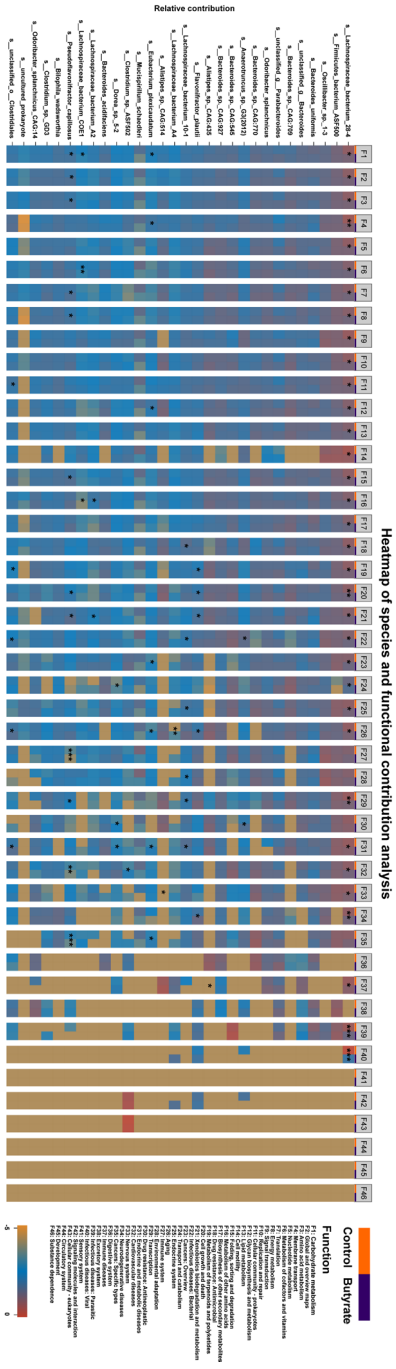

Figure S4. Gut microbiota functional contribution analysis. Functional contributions of the gut microbiota (top 30 based on relative abundance) were analyzed using the Kyoto Encyclopedia of Genes and Genomes (KEGG) database (Pathway level 2). Data are shown as means ± SEM; *P<0.05, **P<0.01, ***P<0.001; Butyrate vs Control.

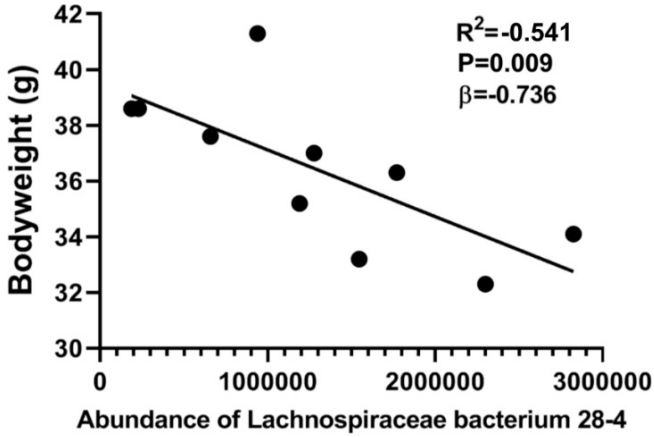

Figure S5. The richness of *Lachnospiraceae bacterium 28-4* in the gut negatively correlates with host body weight.

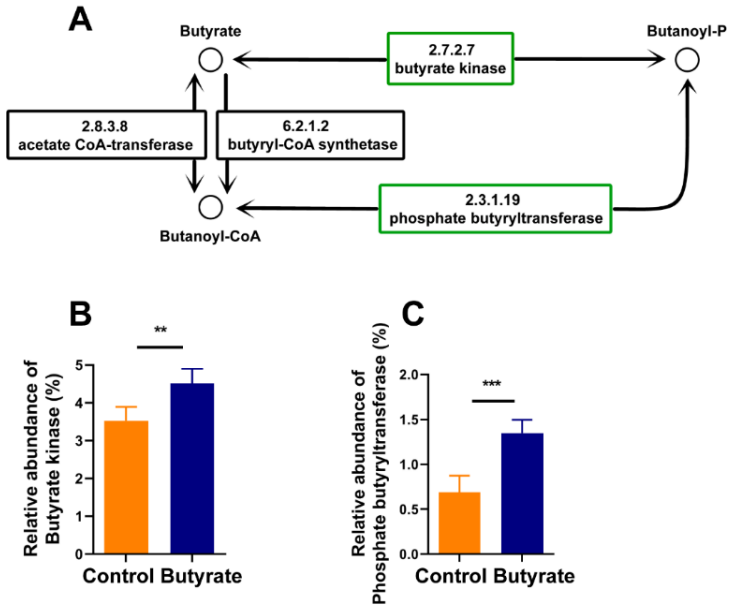

Figure S6. FMT from butyrate-treated lean mice increases the expression of genes coding key enzymes involved in the butyrate synthesis. Partial pathway of butyrate (butanoate) metabolism with a green box to highlight genes was adapted from Kyoto Encyclopedia of Genes and Genomes (KEGG) pathway database (A). The expression of genes coding butyrate kinase (B, n=5) and phosphate butyryltransferase (C, n=5) were quantified using KEGG pathway database. Data are shown as means ± SEM; *P<0.05, **P<0.01, ***P<0.001; Butyrate vs Control.

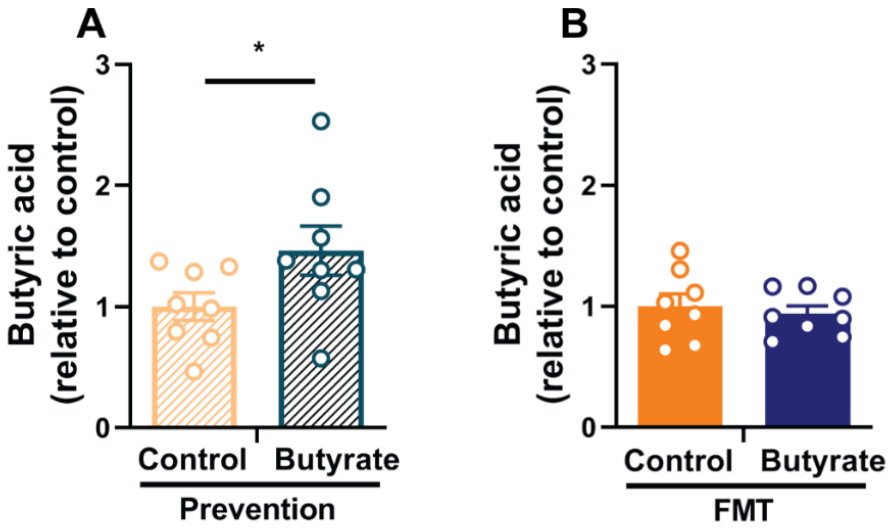

Figure S7. Caecal butyrate is increased by dietary butyrate, but not by FMT from butyrate-treated lean mice. The concentration of butyric acid within caecum samples from butyrate prevention study (A) and FMT study (B) were quantified by GC-MS (n=8). Data are shown as means ± SEM; *P<0.05, **P<0.01, ***P<0.001; Butyrate vs Control.

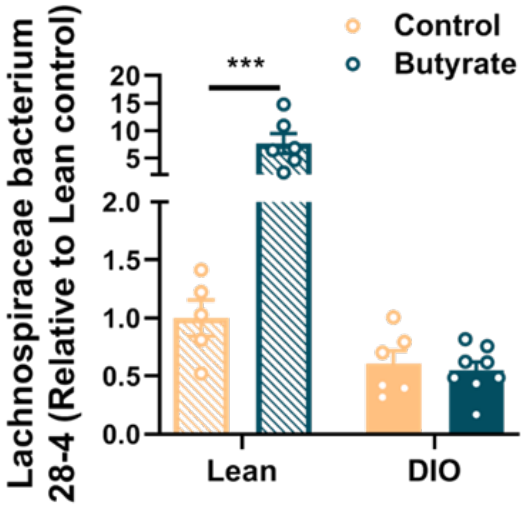

Figure S8. Dietary butyrate increases the abundance of *Lachnospiraceae bacterium 28-4* in lean mice, but not in DIO mice. The gene of *Lachnospiraceae bacterium 28-4* was quantified by real-time PCR (n=5-8). Data are shown as means ± SEM; *P<0.05, **P<0.01, ***P<0.001; Butyrate vs Control.

CHAPTER 4

DIETARY BUTYRATE PROMOTES INTESTINAL GLP-1 RELEASE, REDUCES APPETITE AND INDUCES FAT OXIDATION VIA CENTRAL GLP-1 RECEPTOR SIGNALING

Li Z, Zhou E, Razack F, Kooijman S, Willems van Dijk K, Rensen PCN, Wang Y

Submitted

Abstract

Introduction: The prevalence of obesity has been increasing steadily and requires efficient therapeutic strategies to reduce energy intake and/or increase energy expenditure. We recently showed that dietary butyrate reduces energy intake and increases energy expenditure by activating brown adipose tissue (BAT) as dependent on the gut-brain neural circuit. In the present study, we aimed to elucidate the involvement of central GLP-1 receptor signaling in the metabolic benefits induced by dietary butyrate.

Methods: Male APOE*3-Leiden.CETP mice, a well-established translational model for human-like cardiometabolic disease, received a high-fat diet (HFD; 60% of total calories derived from lard and 0.25% cholesterol) with or without 5% (w/w) sodium butyrate for 12 weeks, while receiving intracerebroventricular infusion of the GLP-1 receptor antagonist Exendin-(9-39) or vehicle during the final 4 weeks. Energy metabolism was assessed by indirect calorimetry and nutrient partitioning was assessed by intravenous injection of glycerol tri[^{3}H]oleate-labeled triglyceride-rich lipoprotein-like particles and [^{14}C]deoxyglucose.

Results: Dietary butyrate increased GLP-1-positive cells in the ileum (+33%), as well as active GLP-1 in plasma (+41%), accompanied by a reduction in food intake (-15%), body weight gain (-73%) and fat mass (-57%). Also, dietary butyrate increase fat oxidation (+~30%) at the expense of glucose oxidation (-~85%), and increased [^{3}H]oleate uptake, e.g., by BAT (+~50%). Intracerebroventricular infusion of Exendin-(9-39) abolished the effect of butyrate on food intake and largely attenuated the effects on nutrient oxidation, without affecting the effects on body weight gain, fat mass and nutrient partitioning.

Conclusions: Dietary butyrate stimulates the intestinal GLP-1 release and reduces appetite and increases fatty acid oxidation at the expense of carbohydrate oxidation via central GLP-1 receptor signaling, while butyrate improves nutrient partitioning and activates BAT independent of central GLP-1 receptor signaling.

Introduction

The prevalence of obesity and associated cardiometabolic diseases has been increasing steadily and obesity is becoming one of the most significant public health problems [1]. Obesity can be reversed by inducing a negative energy balance through lower energy intake and/or higher energy expenditure via increasing physical activity and activating brown adipose tissue (BAT), which is a metabolically active tissue that contributes to energy expenditure [2]. Although adapting lifestyle to reduce food intake and increase energy expenditure is effective, it is hard to adhere to in practice, and cessation of lifestyle adaptation generally leads to weight regain [3]. Therefore, novel strategies to attain persistent weight loss are warranted.

A recent clinical study demonstrated that dietary fiber intake predicts weight loss [4], indicating the therapeutic potential of dietary fiber in combating obesity. Indeed, a series of systemic reviews and meta-analyses revealed that higher fiber intake associates with lower body weight and decreased incidence of T2D [5]. As human cells cannot degrade fibers, they are digested in the gut by bacterial fermentation into short-chain fatty acids (SCFAs), including acetate, propionate, and butyrate, all of which have beneficial metabolic properties [6]. A recent ground-breaking human study showed that dietary fiber promotes butyrate-producing bacterial strains in the gut and increases the glucagon-like peptide-1 (GLP-1) response, which was accompanied by amelioration of T2D as evidenced by lowering hemoglobin A1c (HbA1c) [7]. These findings indicate the potential involvement of butyrate in enhanced GLP-1 signaling, which may underlie the beneficial metabolic effects of dietary fiber. Recently, we revealed that dietary butyrate improves metabolic health in mice, mainly by reducing appetite in addition to activating BAT [8]. We also showed the crucial involvement of the gut-brain axis in these effects, but the precise molecular targets remain to be determined.

The gastrointestinal tract is closely involved in maintaining whole-body energy homeostasis, not only by digestion of food for energy uptake but also by releasing hormones that are involved in nutrient handling after intestinal uptake. One of these gut hormones is GLP-1, which is mainly secreted by enteroendocrine L-cells after sensing nutrients, but also by neurons in the hindbrain [9]. GLP-1 regulates energy intake and expenditure via acting on its receptors that are located in peripheral organs, e.g., pancreas, and neural systems, e.g., vagal nerve and central neural system. Direct intracerebroventricular (ICV) administration of either GLP-1 and the GLP-1 receptor agonist Exendin-4 in rodents reduces appetite and induces weight loss [10, 11], which can be reversed by ICV administration of the GLP-1 receptor antagonist Exendin (9-39) (EX-(9-39)) [12]. Likewise, peripheral injection of the GLP-1 analogue liraglutide induced weight loss in mice, as it reaches the central GLP-1 receptor after crossing the blood-brain barrier [13, 14]. In line, various clinical trials have demonstrated that liraglutide also reduces body weight in humans [15, 16]. Activation of central GLP-1 receptor signaling not only decreases food intake but also stimulates sympathetic outflow to increase nutrient uptake by

BAT in mice [11, 17] as well as humans [18].

In addition to acting centrally, GLP-1 can also reduce appetite via the vagal nerve, as selective knockdown of GLP-1 receptors in the vagal nerve has been shown to increase meal size, accelerate gastric emptying and elevate postprandial glycemia in rats [19]. Since we previously showed through vagal nerve denervation that the vagal nerve plays a crucial role in the appetite-reducing effects of dietary butyrate [8], and since butyrate stimulates GLP-1 secretion by intestinal L-cells, at least *in vitro* [20], we hypothesized that dietary butyrate increases the endogenous production of GLP-1 to regulate energy metabolism. Therefore, the aim of this study was to explore the effects of dietary butyrate on intestinal GLP-1 release and to elucidate the involvement of central GLP-1 receptor signaling in the metabolic benefits induced by dietary butyrate. To this end, we evaluated the effects of dietary butyrate on energy metabolism in APOE*3-Leiden.CETP mice, a well-established translational model for human-like cardiometabolic disease [21], without or with antagonizing central GLP-1 receptor signaling.

Materials and methods

Animals

Hemizygous APOE*3-Leiden.CETP mice expressing the human APOE*3-Leiden and CETP genes were generated as previously described [22]. Male mice were group-housed in individually ventilated cages at room temperature with 40 ± 5% relative humidity and a 12-h light/dark cycle (07:00-19:00). Water and standard rodent chow were available *ad libitum*, and mice were used for experiments at the age of 14-16 weeks.

In a first experiment, mice were fed a high-fat diet (HFD, 60% of total calories derived from lard and 0.25% cholesterol, Altromin International, Germany) without or with 5% (w/w) sodium butyrate (Sigma-Aldrich, United States) for 8 weeks. In a second experiment, mice were fed the HFD without or with 5% (w/w) sodium butyrate for 12 weeks. After 8 weeks, mice received intracerebroventricular (ICV) surgery for subsequent infusion with EX-(9-39) (Bachem, Germany) or vehicle (artificial cerebrospinal fluid; aCSF, Harvard Apparatus, United States) during 4 weeks. In brief, mice were anesthetized by subcutaneous injection with Dex-Domitor (0.5 mg/kg, Orion Pharma, United Kingdom), Dormicum (5 mg/kg, Roche, Switzerland) and Fentanyl (0.05 mg/kg, Janssen, Belgium). Next, cannulas (Brain Infusion Kit 3, Alzet, United States) were stereotactically implanted into the left lateral ventricle of the brain as previously described [11]. Osmotic minipumps (Model 1004, Alzet, United States) connecting the cannula via a catheter filled with aCSF to delay drug delivery by 1 day were implanted subcutaneously on the back of the mouse. The minipumps assured continuous delivery of 0.72 nmol/kg/day EX-(9-39) or vehicle for 4 weeks. After the surgery, the anesthesia was antagonized using Antisedan (0.5 mg/kg, Pfizer, United States), Anexate (0.5 mg/kg, Roche, Switzerland) and Naloxon (1.2 mg/kg, Orpha, Austria) via subcutaneous injection. In addition, postoperative analgesia was provided by subcutaneous administration of 0.05 mg/kg buprenorphine (Temgesic; Schering-Plough, United States).

This study was approved by the Animal Ethical Committee of Leiden University Medical Center, Leiden, The Netherlands. All animal procedures were performed conform the guidelines from Directive 2010/63/EU of the European Parliament on the protection of animals used for scientific purposes, implementing guidelines on reporting research using animals (ARRIVE *etc.*).

Food intake, body weight and body composition

Food intake and body weight were measured with a scale and body composition was measured of conscious mice using an EchoMRI-100 (EchoMRI, United States) every week. The food intake, body weight, and body composition of mice that crumbled their diet a lot during the intervention were not taken into account for the final calculation, leading to a final sample size of 5-7.

Indirect calorimetry

In the second experiment, two weeks after starting ICV infusion of EX-(9-39), indirect calorimetry was performed using fully automatic metabolic cages (Sable Systems, Germany) for five consecutive days. After 2 days of acclimatization in the system, oxygen consumption (VO_2) and carbon dioxide production (VCO_2) were measured. The average respiratory exchange ratio, fat and carbohydrate oxidation rates were calculated as described [23]. Due to the limited number of automatic metabolic cages available, only part of the mice from each group (n=6-7) underwent this study.

Plasma glucose, lipid and GLP-1 assays

In the first experiment, 5-h (8:00-13:00) fasted blood samples were obtained via tail vein bleeding into heparin and dipeptidyl peptidase (DPP)-IV inhibitor (Sigma-Aldrich, United States)-coated capillaries. Plasma was collected after centrifugation and stored at -80°C until further measurements. Plasma was assayed for active GLP-1 using V-PLEX GLP-1 Active Kit (K1503OD-1, Meso Scale Discovery, United States) following the manufacturer's instructions. Plasma glucose, total cholesterol, triglycerides, and free fatty acids were assayed using commercial kits as described previously [24].

Histology

In the first experiment, after 8 weeks of dietary butyrate treatment, formalin-fixed and paraffin-embedded ileum sections (5 µm) were prepared (each group has one ileum sample that was not fixed well, resulting in the sample size of 7). Ileum sections were stained for GLP-1 (1/1000, ab22625, Abcam, United Kingdom). GLP-1 positive cell numbers were expressed versus total ileum area, as quantified using Image J software (National Institutes of Health, United States). In the second experiment, four weeks after starting ICV infusion of EX-(9-39) or vehicle, formalin-fixed and paraffin-embedded interscapular BAT (iBAT) sections (5 µm) were prepared. iBAT sections were stained with hematoxylin and eosin (H&E) and immunohistochemically stained for uncoupling protein-1 (UCP-1, 1/4000, ab10983, Abcam, United Kingdom) and tyrosine hydroxylase (TH, 1/2000, ab6211, Abcam, United Kingdom) as previously described [25]. Quantification of the intracellular lipid area, UCP-1 and TH protein content within BAT was performed using Image J software. Results were expressed as a percentage of positive area versus total BAT area.

***In vivo* lipid and glucose clearance and organ uptake**

Triglyceride (TG)-rich lipoprotein (TRL)-like particles (average size of 80 nm) labeled with glycerol tri[^{3}H]oleate ([^{3}H]TO) (3.7 MBq) were prepared [26] and mixed with 2-[1-^{14}C]deoxy-D-glucose ([^{14}C]DG) in a 4:1 ratio based on radioactive counts. Emulsions were stored at 4°C under argon and used for *in vivo* kinetic experiments.

At the end of the second experiment, mice were injected with 200 µL containing [^{3}H]TO-labeled TRL-like particles (1 mg TG) and [^{14}C]DG via the tail vein. Blood samples were taken from the tail vein at 2, 5, 10, and 15 min after injection to assess ^{3}H and ^{14}C-activities. Subsequently, mice were sacrificed by CO_2 and were perfused with ice-cold saline via the heart. Pieces of various organs were harvested, weighed, and dissolved in Tissue Solubilizer (Amersham Biosciences, United Kingdom) overnight at 56°C. ^{3}H- and ^{14}C-activities in plasma and organs were counted after adding liquid scintillation cocktail (Ultima Gold, Perkin Elmer, United States) using scintillation counting (TRI-CARB, Perkin Elmer, United States) and expressed as percentage of injected dose (plasma) and as percentage of injected dose per gram wet weight (tissues).

Statistics analysis

All data are expressed as means ± SEM. Differences between two groups were determined using two-tailed Student unpaired t-test, or differences among three groups were determined by Fisher's least significant difference (LSD) test following one-way analysis of variance (ANOVA). All statistical analyses were performed using Prism 8 (GraphPad Software, United States). $P<0.05$ was considered to be statistically significant.

Results

Dietary butyrate increases intestinal GLP-1 production

We first explored the effect of dietary butyrate on intestinal GLP-1 production by performing immunohistochemical staining for GLP-1 in the ileum. Eight weeks after butyrate administration, the number of GLP-1 positive cells in the ileum was significantly higher (+33%, P<0.05; Figure 1A, B) as compared to that of HFD controls. In addition, dietary butyrate markedly increased plasma levels of active GLP-1 (+41%, P<0.05; Figure 1C), suggesting that butyrate promotes intestinal GLP-1 synthesis and release into the systemic circulation.

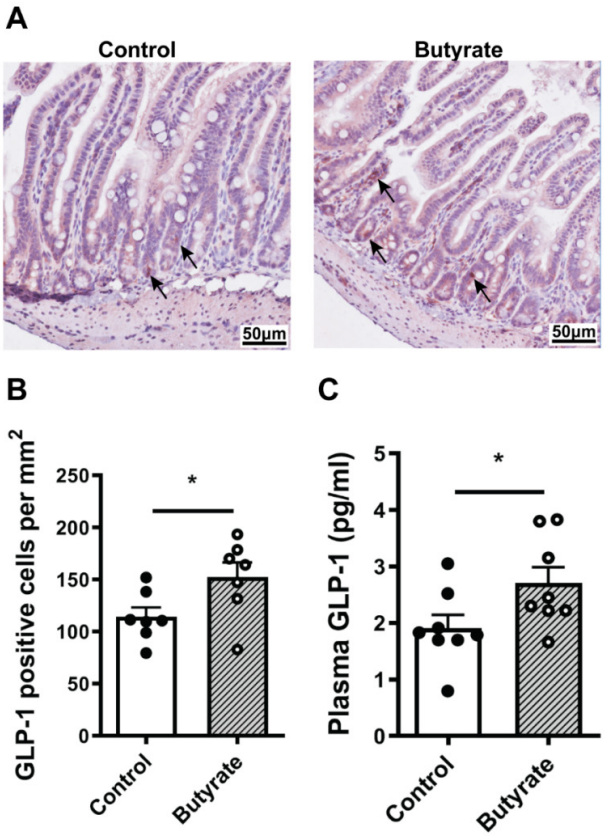

Figure 1. Dietary butyrate increases intestinal GLP-1 production. Mice received a high-fat diet without (Control) or with 5% (w/w) sodium butyrate (Butyrate) for 8 weeks. The ileum of each mouse was stained for GLP-1 (red; A, representative pictures shown for each group) and GLP-1-postive cells were quantified per area (B, n=7). Blood was collected for determining active GLP-1 levels in plasma (C, n=8). Differences between the groups were determined with a two-tailed Student unpaired t-test. Data are shown as means ± SEM; *P<0.05 as compared with the control group.

Blockage of central GLP-1 receptor signaling abolishes the dietary butyrate-induced reduction in food intake, but not body weight and fat mass

Next, we assessed the role of central GLP-1 receptor signaling in regulating the beneficial metabolic effects of dietary butyrate by antagonizing the central GLP-1 receptor using EX-(9-39). In line with our previous findings [8], dietary butyrate significantly reduced food intake (-15%, P<0.05; Figure 2A). This reduction of food intake by dietary butyrate was abolished by central EX-(9-39) infusion, indicating that butyrate reduces appetite as dependent on central GLP-1 receptor signaling. In addition, dietary butyrate ameliorated HFD-induced body weight gain (-73%, P<0.001; Figure 2C), accompanied by decreased fat mass (-57%, P<0.001; Figure 2B). However, blockage of central GLP-1 receptor signaling did not influence the dietary butyrate-induced amelioration of body weight gain and body composition, as body weight and body composition in mice received dietary butyrate without or with EX-(9-39) were not significantly different (Figure 2B, C).

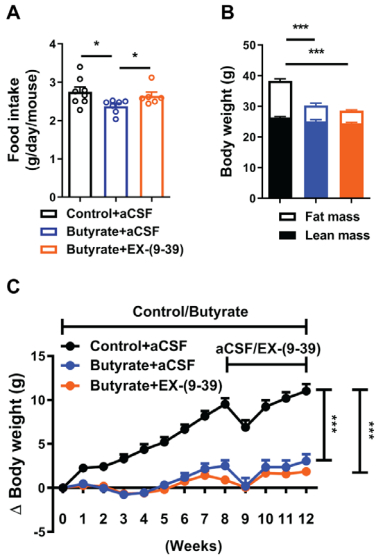

Figure 2. Blockage of central GLP-1 receptor signaling abolishes the dietary butyrate-induced reduction in food intake, but not body weight and fat mass. Mice received a high-fat diet without (Control) or with 5% (w/w) sodium butyrate (Butyrate) for 12 weeks. After 8 weeks of the diet intervention, mice additionally received the GLP-1 receptor antagonist Exendin-(9-39) (EX-(9-39)) or vehicle by intracerebroventricular (ICV) infusion for 4 weeks. The average food intake per day per mouse throughout the intervention period was calculated (A). At the end of the experiment, body composition was measured by MRI (B). Body weight was measured weekly, and body weight change throughout the whole study was calculated (C). Differences between each two groups were determined using the Fisher's least significant difference (LSD) test following one-way analysis of variance (ANOVA). Data are shown as means ± SEM (n=5-7); *P<0.05, **P<0.01, ***P<0.001 as compared with control+aCSF group. aCSF, artificial cerebrospinal fluid.

Blockage of central GLP-1 receptor signaling abolishes the dietary butyrate-induced increase in fat oxidation at the expense of carbohydrate oxidation

Next, indirect calorimetry was performed to determine whether central GLP-1 receptor signaling mediates the effects of dietary butyrate on nutrient oxidation. In the second week of intervention with EX-(9-39) versus vehicle, mice were housed in fully automated metabolic cages. Although dietary butyrate did not affect total energy expenditure (Figure 3A), butyrate significantly decreased the respiratory exchange ratio (RER) during both the day phase (-8%, $P<0.001$) and night phase (-10%, $P<0.001$; Figure 3B), which is explained by increased fat oxidation (day: +27%, $P<0.05$; night: +31%, $P<0.05$; Figure 3C) at the expense of carbohydrate oxidation (day: -93%, $P<0.001$; night: -79%, $P<0.001$; Figure 3D). Antagonism of central GLP-1 receptor largely attenuated the effects of butyrate on RER (Figure 3B), fat oxidation (Figure 3C), and carbohydrate oxidation (Figure 3D) during the day and night phases. Collectively, these results indicate that central GLP-1 receptor signaling also plays a crucial role in the effects of dietary butyrate on nutrient oxidation.

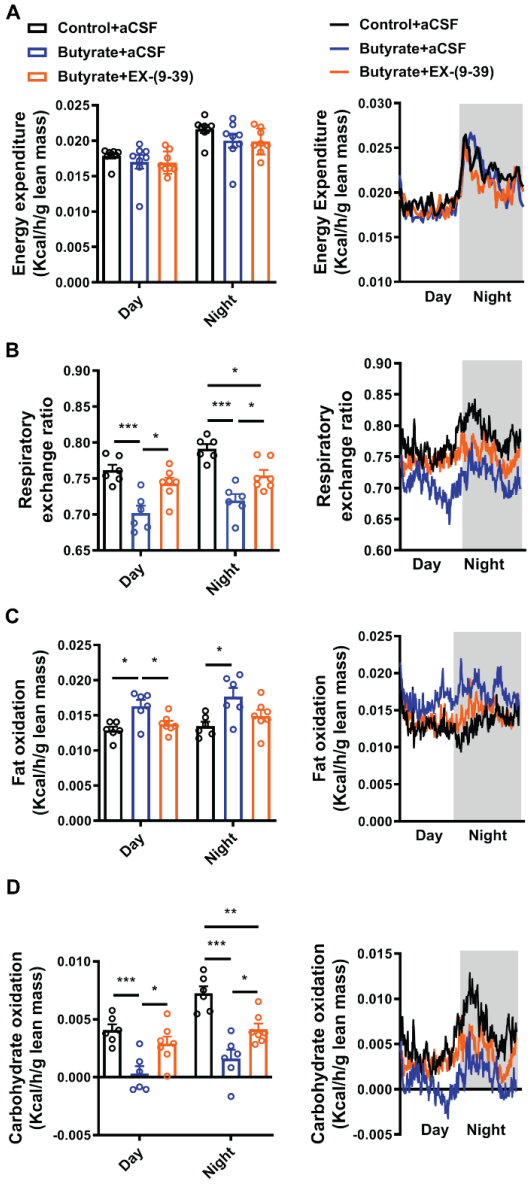

Figure 3. Blockage of central GLP-1 receptor signaling abolishes the dietary butyrate-induced increase in fat oxidation at the expense of carbohydrate oxidation. In the second week of intervention with EX-(9-39) versus vehicle, mice were housed in fully automated metabolic cages. Energy expenditure (A), respiratory exchange ratio (B), fat oxidation (C), and carbohydrate oxidation (D) were calculated from data obtained during 3 consecutive days. Differences between each two groups were determined using the LSD test following one-way ANOVA. For bar graphs, data are shown as means ± SEM (n=6-7); *P<0.05, **P<0.01, ***P<0.001 as compared with control+aCSF group. For line graphs, data are shown as the mean for each group during a 24-hour cycle (07:00-07:00).

Blockage of central GLP-1 receptor signaling does not affect the dietary butyrate-induced improvement of nutrient partitioning

To determine the effects of central GLP-1 receptor signaling on the butyrate-induced increased uptake of nutrients from the circulation, at the end of the treatment period with dietary butyrate without or with EX-(9-39) we injected mice with [^{3}H]TO-labeled TRL-like particles and [^{14}C]DG. In line with our previous study [24], dietary butyrate accelerated the plasma clearance of [^{3}H]TO (Figure 4A) and [^{14}C]DG (Figure 4B). For [^{3}H]TO, this was caused by a significantly increased uptake of ^{3}H-activity by liver (+25%, P<0.05), subcutaneous white adipose tissue (sWAT; +70%, P<0.05), gonadal WAT (gWAT; +65%, P<0.05) interscapular BAT (iBAT; +54%; P<0.05) and subscapular BAT (sBAT; +44%; P<0.05) (Figure 4C). For [^{14}C]DG, this was caused by a significantly increased uptake of ^{14}C-activity by heart (+88%, P<0.05), sWAT (+63%, P<0.05) and gWAT (+42%, P<0.05) (Figure 4D). Antagonism of the central GLP-1 receptor neither counteracted the butyrate-induced accelerated clearance rate of [^{3}H]TO (Figure 4A) and [^{14}C]DG (Figure 4B) nor reversed the butyrate-induced increased organ uptake of ^{3}H-activity (Figure 4C) and ^{14}C-activity (Figure 4D), showing that dietary butyrate improves nutrient partitioning independent of the central GLP-1 receptor signaling.

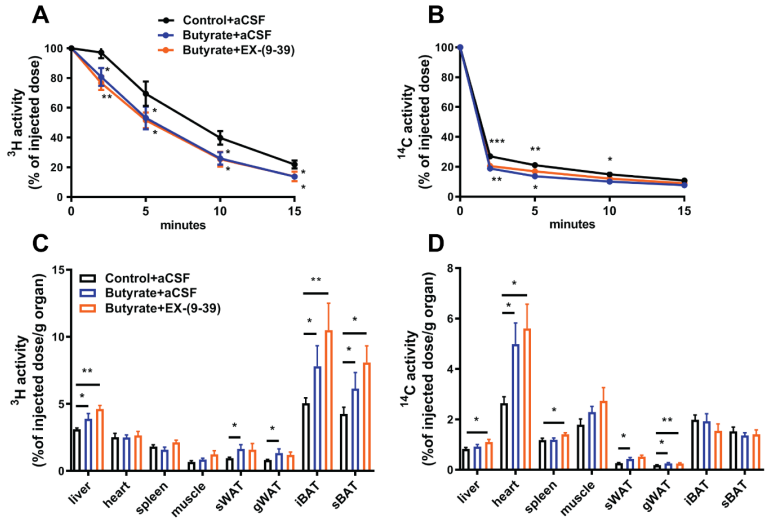

Figure 4. Blockage of central GLP-1 receptor signaling does not affect the dietary butyrate-induced improvement of nutrient partitioning. After receiving 4 weeks ICV infusion of EX-(9-39) or vehicle, mice were intravenously injected with glycerol tri[^{3}H]oleate ([^{3}H]TO)-labeled triglyceride-rich lipoprotein-like particles and 2-[1-^{14}C]deoxy-D-glucose ([^{14}C]DG). ^{3}H and ^{14}C derived-radioactivity were assessed in plasma (A and B) and various organs (C and D). Differences between each two groups were determined using the Fisher's LSD test following one-way ANOVA. Data are shown as means ± SEM (n=7-10); *P<0.05, **P<0.01, ***P<0.001 as compared with control+aCSF group. gWAT, gonadal white adipose tissue; iBAT, interscapular brown adipose tissue; sBAT, subscapular brown adipose tissue; sWAT, subcutaneous white adipose tissue.

Blockage of central GLP-1 receptor signaling does not affect the dietary butyrate-induced BAT activation

Since EX-(9-39) did not attenuate the dietary butyrate-induced increase in uptake of [^{3}H]TO-derived ^{3}H by BAT, we reasoned that histological changes in BAT induced by butyrate would also not be reversed by EX-(9-39). Dietary butyrate markedly decreased the intracellular lipid vacuole content in BAT (-27%, P<0.01; Figure 4A, D), concomitant with increased protein levels of UCP-1 (+37%, P<0.05; Figure 4B, D) and TH, a marker of sympathetic nerve activity (+23%, P<0.05; Figure 4C, D), confirming that dietary butyrate increases BAT thermogenic capacity and sympathetic outflow towards BAT. Indeed, GLP-1 antagonism did not reverse the effects of dietary butyrate on intracellular lipid content (Figure 4A, D), UCP-1 (Figure 4B, D) and TH (Figure 4C, D), showing that butyrate activates BAT independent of central GLP-1 receptor signaling.

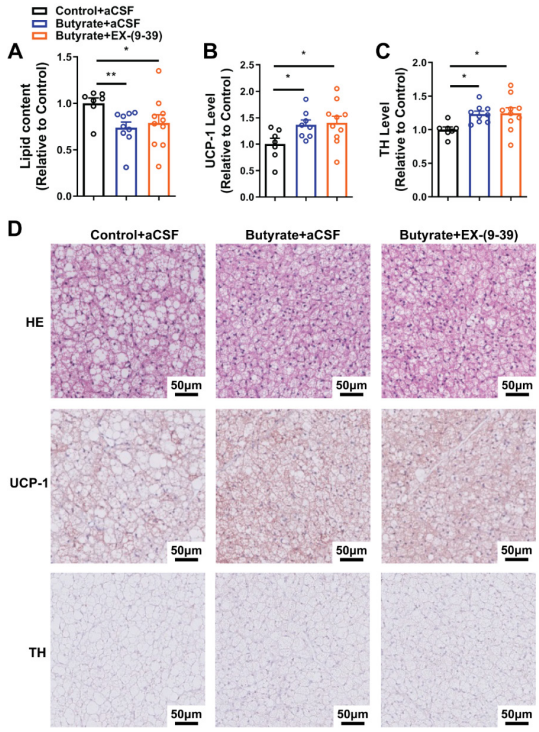

Figure 5. Blockage of central GLP-1 receptor signaling does not affect dietary butyrate-induced BAT activation. After receiving 4 weeks ICV infusion of EX-(9-39) or vehicle, mice were sacrificed and iBAT was collected and sectioned for immunohistochemistry staining. Lipid content (A), uncoupling protein-1 (UCP-1) protein content (B), and tyrosine hydroxylase (TH) protein content (C) were quantified and shown as representative pictures (D). Differences between each two groups were determined using the Fisher's LSD test following one-way ANOVA. Data are shown as means ± SEM (n=7-10); *P<0.05, **P<0.01, ***P<0.001 as compared with control+aCSF group. HE, hematoxylin and eosin.

Discussion

Dietary butyrate is known to prevent diet-induced obesity, improve glucose homeostasis, and alleviate insulin resistance in rodents [27, 28]. Previously, by performing mechanistic studies in APOE*3-Leiden.CETP mice, we showed that these effects could mainly be attributed to reduced appetite and to a lower extent by BAT activation [8]. In this study, we aimed to investigate the role of GLP-1 in these beneficial effects of dietary butyrate. Here, we found that dietary butyrate stimulates the intestinal GLP-1 release and reduces food intake and increases fatty acid oxidation at the expense of carbohydrate oxidation via central GLP-1 receptor signaling, while butyrate improves nutrient partitioning and activates BAT independent of central GLP-1 receptor signaling.

Dietary butyrate increases intestinal GLP-1 secretion since butyrate induced an increase in GLP-1-expressing cells in the ileum as well as active GLP-1 in plasma. This is in line with the previous observation that butyrate stimulates GLP-1 secretion by intestinal L-cells *in vitro* [20]. By blocking central GLP-1 receptor signaling, we were able to show that GLP-1 is crucially involved in the appetite-reducing effect of dietary butyrate. Although it is tempting to assume that GLP-1 travels from the intestine to the brain via the circulation to activate central GLP-1 receptors and as a consequence reduces appetite, we previously showed that the appetite-reducing effects of dietary butyrate were abrogated by subdiaphragmatic vagotomy. Collectively, these data suggest that GLP-1, produced by intestinal L-cells directly acts on GLP-1 receptors on the vagal nerve rather than on central GLP-1 receptors to reduce appetite. Indeed, a previous study in rats has demonstrated that the GLP-1 receptor in the vagal afferent plays a crucial role in the effect of endogenous GLP-1 on inhibiting food intake [29]. Likely, GLP-1-mediated activation of the vagal nerve is coupled to the central release of GLP-1 that subsequently acts on central GLP-1 receptors to reduce appetite. This hypothesis is supported by a clinical study demonstrating that the effect of GLP-1 on reducing food intake is lost in vagotomised males [30]. However, future studies using e.g., knock down of the GLP-1 receptor in the vagal afferent, are still needed to conclusively establish the involvement of GLP-1 receptor signaling in the vagal nerve in the effects of butyrate on appetite.

Interestingly, we previously demonstrated that the effects of dietary butyrate on reduction of appetite were abolished after antibiotics-induced gut microbiota depletion (see Chapter 3). This strongly suggests that dietary butyrate may not be sufficient to trigger GLP-1 secretion, but may crucially depend on the previously observed dietary butyrate-induced changes in the composition of gut microbiota [8]. Of note, by performing fecal microbiota transplantation studies, we indeed revealed that dietary butyrate changes the gut microbiota to reduce food intake (Chapter 3). In fact, by using metagenomics we revealed dietary butyrate selectively increases the abundance of a specific bacterial strain named *Lachnospiraceae bacterium 28-4*, of which the richness negatively correlates with food intake (Chapter 3). Since this bacterial strain is predicted to be a strong producer of butyrate, it is tempting to

speculate that dietary butyrate results in outgrowth of *Lachnospiraceae bacterium 28-4* to amplify local butyrate production in the intestine to levels that are sufficient to trigger an efficient GLP-1 response that reduces appetite.

Our findings that butyrate reduced appetite via increasing GLP-1 production are likely relevant to humans. In fact, human studies demonstrated that gut microbial fermentation of prebiotics, e.g., oligofructose and inulin, which is an effective approach to manipulate gut microbiota community [31], increased satiety and improved glucose homeostasis associated with increased GLP-1 [32, 33]. Likewise, another human study showed that dietary fiber promotes butyrate-producing bacterial strains in the gut accompanied by an increased GLP-1 response, which was accompanied by amelioration of T2D [7]. However, although these studies indicate a role of gut microbiota in the promotion of intestinal GLP-1 release in humans, the causal role of butyrate in the secretion of GLP-1 and reduction of appetite in humans still has to be conclusively demonstrated.

In addition to reducing food intake, central GLP-1 receptor signaling has also been demonstrated to accelerate the clearance of plasma lipids by activating BAT in mice [11]. In the current study, we confirmed the effect of butyrate on metabolic activity of BAT as evidenced by a lower lipid content of BAT in combination with increased triglyceride-derived fatty acid uptake by BAT, which seemed to result from increased sympathetic outflow evidence by higher TH staining of BAT. Counterintuitively, we found this effect to be independent of central GLP-1 receptor signaling, indicating the involvement of other central mechanisms in the BAT-activating effects of dietary butyrate. Butyrate binds to the SCFA receptor G protein-coupled receptor 43 (GPR43) [34], which is expressed during the late phase of brown adipocyte differentiation [35]. However, the possibility that butyrate directly activates BAT via GPR43 is unlikely since intravenous injection of butyrate did not affect BAT activity [8]. Of note, it has been shown that the SCFA propionate can induce sympathetic outflow directly via acting on the G protein-coupled receptor 41 (GPR41) expressed at the sympathetic ganglion and consequently increases oxygen consumption and energy expenditure [36]. Since butyrate can also bind to GPR41 [37], it is reasonable to speculate that butyrate might act on the sympathetic ganglion, thereafter increasing the sympathetic outflow to BAT. However, that would not explain our current observation why the dietary butyrate-induced increase in fat oxidation at the expense of carbohydrate oxidation is largely abolished by central GLP-1 receptor inhibition.

In conclusion, dietary butyrate stimulates the intestinal GLP-1 release and reduces appetite and increases fatty acid oxidation at the expense of carbohydrate oxidation via central GLP-1 receptor signaling, while butyrate improves nutrient partitioning and activates BAT independent of central GLP-1 receptor signaling. Although we speculate that GLP-1 acts on vagal afferents to mediate the effects of butyrate on appetite, the validity of such an underlying mechanism should still be revealed in future studies.

References

1. Collaborators, G.B.D.O., et al., *Health Effects of Overweight and Obesity in 195 Countries over 25 Years.* N Engl J Med, 2017. **377**(1): p. 13-27.
2. Virtanen, K.A., et al., *Functional brown adipose tissue in healthy adults.* N Engl J Med, 2009. **360**(15): p. 1518-25.
3. Hall, K.D. and S. Kahan, *Maintenance of Lost Weight and Long-Term Management of Obesity.* Med Clin North Am, 2018. **102**(1): p. 183-197.
4. Miketinas, D.C., et al., *Fiber Intake Predicts Weight Loss and Dietary Adherence in Adults Consuming Calorie-Restricted Diets: The POUNDS Lost (Preventing Overweight Using Novel Dietary Strategies) Study.* J Nutr, 2019. **149**(10): p. 1742-1748.
5. Reynolds, A., et al., *Carbohydrate quality and human health: a series of systematic reviews and meta-analyses.* Lancet, 2019. **393**(10170): p. 434-445.
6. Chambers, E.S., et al., *Role of Gut Microbiota-Generated Short-Chain Fatty Acids in Metabolic and Cardiovascular Health.* Curr Nutr Rep, 2018. **7**(4): p. 198-206.
7. Zhao, L., et al., *Gut bacteria selectively promoted by dietary fibers alleviate type 2 diabetes.* Science, 2018. **359**(6380): p. 1151-1156.
8. Li, Z., et al., *Butyrate reduces appetite and activates brown adipose tissue via the gut-brain neural circuit.* Gut, 2018. **67**(7): p. 1269-1279.
9. Jin, S.L., et al., *Distribution of glucagonlike peptide I (GLP-I), glucagon, and glicentin in the rat brain: an immunocytochemical study.* J Comp Neurol, 1988. **271**(4): p. 519-32.
10. Meeran, K., et al., *Repeated intracerebroventricular administration of glucagon-like peptide-1-(7-36) amide or exendin-(9-39) alters body weight in the rat.* Endocrinology, 1999. **140**(1): p. 244-50.
11. Kooijman, S., et al., *Central GLP-1 receptor signalling accelerates plasma clearance of triacylglycerol and glucose by activating brown adipose tissue in mice.* Diabetologia, 2015. **58**(11): p. 2637-46.
12. Turton, M.D., et al., *A role for glucagon-like peptide-1 in the central regulation of feeding.* Nature, 1996. **379**(6560): p. 69-72.
13. Secher, A., et al., *The arcuate nucleus mediates GLP-1 receptor agonist liraglutide-dependent weight loss.* J Clin Invest, 2014. **124**(10): p. 4473-88.
14. Sisley, S., et al., *Neuronal GLP1R mediates liraglutide's anorectic but not glucose-lowering effect.* J Clin Invest, 2014. **124**(6): p. 2456-63.
15. Pi-Sunyer, X., et al., *A Randomized, Controlled Trial of 3.0 mg of Liraglutide in Weight Management.* N Engl J Med, 2015. **373**(1): p. 11-22.
16. Kelly, A.S., et al., *A Randomized, Controlled Trial of Liraglutide for Adolescents with Obesity.* N Engl J Med, 2020. **382**(22): p. 2117-2128.

17. Beiroa, D., et al., *GLP-1 agonism stimulates brown adipose tissue thermogenesis and browning through hypothalamic AMPK.* Diabetes, 2014. **63**(10): p. 3346-58.

18. Janssen, L.G.M., et al., *Twelve weeks of exenatide treatment increases [(18)F] fluorodeoxyglucose uptake by brown adipose tissue without affecting oxidative resting energy expenditure in nondiabetic males.* Metabolism, 2020. **106**: p. 154167.

19. Krieger, J.P., et al., *Knockdown of GLP-1 Receptors in Vagal Afferents Affects Normal Food Intake and Glycemia.* Diabetes, 2016. **65**(1): p. 34-43.

20. Yadav, H., et al., *Beneficial metabolic effects of a probiotic via butyrate-induced GLP-1 hormone secretion.* J Biol Chem, 2013. **288**(35): p. 25088-97.

21. van den Hoek, A.M., et al., *APOE*3Leiden.CETP transgenic mice as model for pharmaceutical treatment of the metabolic syndrome.* Diabetes Obes Metab, 2014. **16**(6): p. 537-44.

22. Westerterp, M., et al., *Cholesteryl ester transfer protein decreases high-density lipoprotein and severely aggravates atherosclerosis in APOE*3-Leiden mice.* Arterioscler Thromb Vasc Biol, 2006. **26**(11): p. 2552-9.

23. Van Klinken, J.B., et al., *Estimation of activity related energy expenditure and resting metabolic rate in freely moving mice from indirect calorimetry data.* PLoS One, 2012. **7**(5): p. e36162.

24. Li, Z., et al., *Butyrate reduces appetite and activates brown adipose tissue via the gut-brain neural circuit.* Gut, 2018. **67**(7): p. 1269-1279.

25. Berbee, J.F., et al., *Brown fat activation reduces hypercholesterolaemia and protects from atherosclerosis development.* Nat Commun, 2015. **6**: p. 6356.

26. Rensen, P.C., et al., *Particle size determines the specificity of apolipoprotein E-containing triglyceride-rich emulsions for the LDL receptor versus hepatic remnant receptor in vivo.* J Lipid Res, 1997. **38**(6): p. 1070-84.

27. Gao, Z., et al., *Butyrate improves insulin sensitivity and increases energy expenditure in mice.* Diabetes, 2009. **58**(7): p. 1509-17.

28. Hong, J., et al., *Butyrate alleviates high fat diet-induced obesity through activation of adiponectin-mediated pathway and stimulation of mitochondrial function in the skeletal muscle of mice.* Oncotarget, 2016. **7**(35): p. 56071-56082.

29. Bucinskaite, V., et al., *Receptor-mediated activation of gastric vagal afferents by glucagon-like peptide-1 in the rat.* Neurogastroenterol Motil, 2009. **21**(9): p. 978-e78.

30. Plamboeck, A., et al., *The effect of exogenous GLP-1 on food intake is lost in male truncally vagotomized subjects with pyloroplasty.* Am J Physiol Gastrointest Liver Physiol, 2013. **304**(12): p. G1117-27.

31. Krupa-Kozak, U., N. Drabinska, and E. Jarocka-Cyrta, *The effect of oligofructose-enriched inulin supplementation on gut microbiota, nutritional status and gastrointestinal symptoms in paediatric coeliac disease patients on a gluten-free diet: study protocol for a pilot randomized controlled trial.* Nutr J, 2017. **16**(1): p. 47.

32. Cani, P.D., et al., *Oligofructose promotes satiety in healthy human: a pilot study.* Eur J Clin Nutr, 2006. **60**(5): p. 567-72.

33. Cani, P.D., et al., *Gut microbiota fermentation of prebiotics increases satietogenic and incretin gut peptide production with consequences for appetite sensation and glucose response after a meal.* Am J Clin Nutr, 2009. **90**(5): p. 1236-43.

34. Pirozzi, C., et al., *Butyrate Modulates Inflammation in Chondrocytes via GPR43 Receptor.* Cell Physiol Biochem, 2018. **51**(1): p. 228-243.

35. Hu, J., et al., *Expression of GPR43 in Brown Adipogenesis Is Enhanced by Rosiglitazone and Controlled by PPARgamma/RXR Heterodimerization.* PPAR Res, 2018. **2018**: p. 1051074.

36. Kimura, I., et al., *Short-chain fatty acids and ketones directly regulate sympathetic nervous system via G protein-coupled receptor 41 (GPR41).* Proc Natl Acad Sci U S A, 2011. **108**(19): p. 8030-5.

37. Chang, P.V., et al., *The microbial metabolite butyrate regulates intestinal macrophage function via histone deacetylase inhibition.* Proc Natl Acad Sci U S A, 2014. **111**(6): p. 2247-52.

CHAPTER 5

ELECTRICAL NEUROSTIMULATION PROMOTES BROWN ADIPOSE TISSUE THERMOGENESIS

Li Z, Jonge WJ, Wang Y, Rensen PCN, Kooijman S

***Front Endocrinol 2020**, 11: 567545*

Abstract

Background: Brown adipose tissue (BAT) is present in humans and rodents, and contributes to energy expenditure by converting energy stored in lipids and glucose into heat. Beta adrenergic receptor (β-AR) agonists have been proposed as pharmacological tools to activate BAT, but they lack selectivity for this tissue. This study aimed to investigate the possibility to apply electrical neurostimulation as a novel approach to activate BAT by promoting the sympathetic outflow towards BAT.

Methods: Male C57BL/6J mice were treated with either unilateral electrical neurostimulation of interscapular BAT or with the β3-AR agonist CL316,243. Thermogenesis, nutrient uptake by BAT and downstream signaling of adrenergic receptors in BAT were examined.

Results: Electrical neurostimulation and β3-AR agonism acutely increased heat production by BAT, as evidenced by an increase in local temperature in BAT, without influencing the core body temperature. Both treatments acutely increased tyrosine hydroxylase content in the nerve terminals thereby confirming enhanced sympathetic activity. In addition, we identified increased phosphorylation of hormone-sensitive lipase coinciding with reduced intracellular lipids in BAT, without affecting acute nutrient uptake from plasma. The increased BAT temperature as induced by electrical neurostimulation was reversed by β3-AR antagonism.

Conclusion: Electrical neurostimulation acutely promotes thermogenesis in BAT as dependent on β3-AR signaling. We anticipate that electrical neurostimulation may be further developed as a novel strategy to activate BAT and thereby combat cardiometabolic diseases.

Introduction

Brown adipose tissue (BAT) is a metabolically active tissue with a crucial role in thermogenesis in small rodents and infants, but is yet also present and active in human adults [1, 2]. Human studies identified a negative correlation between BAT activity and BMI/fasting glucose, suggesting that BAT is an important tissue for glucose homeostasis and a potential therapeutic target to combat cardiometabolic diseases [3, 4].

The physiological activator of BAT is cold exposure [5, 6]. Mechanistically, upon cold exposure, sympathetic outflow to BAT increases local norepinephrine production and release, which activates β-adrenergic receptors (β-AR) on the brown adipocyte to promote an intracellular signaling cascade. Via the production of cyclic AMP (cAMP) and activation of protein kinase A (PKA), β-AR signaling stimulates lipolysis as well as the transcription of genes involved in thermogenesis [7]. Fatty acids (FAs) that are released upon intracellular lipolysis allosterically activate uncoupling protein-1 (UCP1) and serve as fuel for non-shivering thermogenesis [8]. To replenish lipid stores, brown adipocytes take up large amounts of triglyceride (TG)-derived FAs and glucose [9]. In addition, accelerated TG-rich lipoprotein turnover stimulates reverse cholesterol transport [10]. The combined effect is attenuated dyslipidemia and atherosclerosis development .

The β3-adrenergic receptor (β3-AR) is the dominant adrenergic receptor in murine BAT, while the β2-adrenergic receptor is most likely responsible for promoting thermogenesis in human BAT [11]. Independent of the ongoing debate about the relative contributions of the various β-ARs in human BAT function, targeting any of the β-ARs with the goal to activate BAT will be challenging given their critical involvement in the cardiovascular and pulmonary systems. Thus, a different approach to selectively activate BAT to combat cardiometabolic diseases is highly warranted.

As an alternative for the use of sympathomimetics, one might think of promoting endogenous sympathetic outflow to BAT. Previous studies demonstrated that electrical stimulation of specific hypothalamic nuclei can promote sympathetic outflow and as a results BAT thermogenesis[12, 13]. In addition, electrical field stimulation of the dorsal surface of interscapular BAT was shown to cause an acute increase in BAT temperature [14]. Moreover, others have used local optogenetics to selectively promote activity of the tyrosine hydroxylase (TH)-expressing neurons innervating BAT, which suggested that stimulation of the sympathetic nerves is sufficient to elicit thermogenesis in BAT [15]. However, the main disadvantage of optogenetics is the hurdle to take such an approach to the clinic.

In the current study, we have taken a state of art approach by applying electrical neurostimulation to specifically promote outflow of the postganglionic sympathetic nerves that innervate BAT in mice. This is the first step toward the use of implantable devices that can very specifically promote BAT thermogenesis.

Materials and methods

Animals

Male C57Bl/6J mice at the age of 12 to 16 weeks were housed under standard conditions with a 12-h light/dark cycle (lights on 07.00h; lights off 19.00h) with *ad libitum* access to regular chow diet and water. At the beginning of the experiments, mice were randomly divided into the respective groups. Animal experiments were performed under approval by the Ethics Committee on Animal Care and Experimentation of the Leiden University Medical Center and following the regulations of the Dutch law on animal welfare.

Temperature recording

Mice were anesthetized by inhalation of isoflurane (4%, v/v air) for 3 min, and their backs were shaved. Because anesthesia affects thermoregulation, the mice were placed on a heating plate (HP-4M Small Animal Heating Plate, Physitemp) that was connected to a temperature controller (TCAT -2LV; Physitemp), while being kept under anesthesia by isoflurane (<2.5%, v/v air) during the whole subsequent intervention period. A rectal temperature probe (RET-3 Rectal Probe, Physitemp) connected to the temperature controller was inserted into the rectum of mice to measure their core body temperature. Their core body temperature was set to be stable at approx. 36.6°C by automatically switching the heating plate on and off. Approached from the back, both pads of interscapular BAT (left and right) were exposed by a midline incision in the skin and white fat along the upper dorsal surface. Flexible probes (IT-18 Flexible Implantable Microprobe, Physitemp) were plugged into both the left and right BAT pad to monitor the local temperature in BAT. The core body temperature and temperature in BAT were recorded per second during the whole intervention by a sensitive temperature data acquisition system (THERMES-USB; Physitemp) connecting to a laptop using Dasylab software (Version 12.0).

Pharmacological stimulation of BAT

10 min after starting temperature monitoring, mice received either the β3-adrenergic receptor (β3-AR) agonist CL316,243 (CL; Tocris Bioscience Bristol, United Kingdom; 20 μg/mouse) or vehicle (phosphate-buffered saline; PBS) by subcutaneous injection (100 μl/mouse).

Electrical neurostimulation of BAT

For unilateral electrical neurostimulation of interscapular BAT, the sympathetic nerves of the left BAT pad were connected to an electrical stimulator by using a homemade hook electrode. 10 min after the start of temperature monitoring, mice received continuous sympathetic neural stimulation with 4 V, 2 ms pulses at 6 Hz

for 60 min. The sympathetic nerves of the right BAT pad were just exposed by sham operation (control). The experimental procedure is depicted in Figure 1E. When indicated, mice received the β3-AR antagonist SR59230A (Sigma-Aldrich; 1 µM; 100 µl/mouse) by subcutaneous injection after 30 min of electrical stimulation.

***In vivo* triglyceride and glucose clearance**

TG-rich lipoprotein (TRL)-like particles (80 nm), radiolabeled with glycerol tri[^{3}H] oleate (3.7 MBq) were prepared as described before , and stored at 4°C under argon until use at the second day after preparation. TRL-like particles were mixed 2-[1-^{14}C]deoxy-D-glucose ([^{14}C]DG) in a 4:1 ratio (^{3}H:^{14}C). 15 min before the end of the pharmacological or electrical intervention, mice were intravenously injected via the tail vein with the combination of TRL-like particles (1 mg TG) and deoxyglucose (200 µl/mouse). After 15 min, mice were killed by CO_2 inhalation, perfused with ice-cold PBS, and both left and right interscapular BAT was collected and a piece of each BAT pad was dissolved in 500 µl of Solvable (Perkin Elmer) overnight at 56°C. The uptake of ^{3}H and ^{14}C activity by BAT was determined using scintillation counting (Ultima Gold XR, Perkin Elmer).

BAT histology

At the end of the pharmacological or electrical neurostimulation, both left and right interscapular BAT were harvested and another piece of each BAT pad was snap-frozen in liquid N_2 and subsequently stored at -80°C until histological analysis. BAT cryostat sections (10 µm) were cut and stained with hematoxylin and eosin (H&E) using a standard protocol, and stained for tyrosine hydroxylase (TH, 1/2000; Ab112; Abcam) and phospho-hormone sensitive lipase (HSL, Ser563, 1/2000; #4139; Cell Signaling). The areas occupied by intracellular lipid vacuoles, TH and HSL (positive area per total area) were quantified using Image J software.

Western Blotting

Pieces of BAT were lysed in RIPA buffer (25 mM Tris-HCl pH 7.6, 150 mM NaCl, 1% NP-40, 1% sodium deoxycholate and 1% SDS; Thermo Fisher Scientific) supplemented with Complete Protease and phosSTOP phosphatase inhibitors (Roche Diagnostics) with the Qiagen TissueLyser II (Qiagen). Protein concentrations were determined using a bicinchoninic acid (BCA) assay (Thermo Fisher Scientific). Western blots were carried out on the Wes system (ProteinSimple) following the manufacturer's instructions using the primary antibody of tyrosine hydroxylase (TH, 1/250; Ab112; Abcam) and phospho-hormone-sensitive lipase (HSL, Ser563, 1/500; #4139; Cell Signaling). Protein expression levels were normalized to GAPDH (1/1000; #25778; Santa Cruz) housekeeping protein expression. Western blot quantifications were done with Image J software.

Statistical analysis

Differences between the groups were determined with a two-tailed Student unpaired t-test. Data on temperature changes are shown as average curves, and average temperature changes per period are calculated and shown as mean ± SEM (n=4 mice per group). Statistical analysis was performed using GraphPad Prism 8. P-values <0.05 were considered significant.

Results

Electrical neurostimulation acutely increases the thermogenic activity of BAT

To test our experimental set-up, we first evaluated the effect of pharmacological activation on the thermogenic capacity of intrascapular BAT. Thereto, mice were sedated, connected to the temperature maintenance recording system and received a subcutaneous injection with either β3-AR agonist CL316243 (CL treatment) or PBS (vehicle). While the temperature of both BAT pads was not affected by vehicle treatment (Figures 1A, B), CL treatment acutely increased the temperature in the tissue (right BAT: +1.53°C, left BAT: +1.56°C, Figures 1C, D). Core body temperature was not affected by the treatment, which was expected as the mice were sedated and body temperature was kept stable using an automated heating plate combined with a rectal temperature probe (Figures S1A, B).

Next, to assess the effect of electrical neurostimulation (E-stimulation) on the thermogenic activity of BAT, a hook electrode was unilaterally connected to the sympathetic nerves innervating the left interscapular BAT as schematically shown in Figure 1E. During E-stimulation, the temperature of the stimulated left BAT pad was consistently increased by on average +0.42°C when compared to baseline recordings. In contrast, the temperature of the unstimulated right BAT pad was not increased during this period (Figures 1F, G). Similar to the pharmacological stimulation of BAT, E-stimulation did not influence core body temperature (Figure S1C).

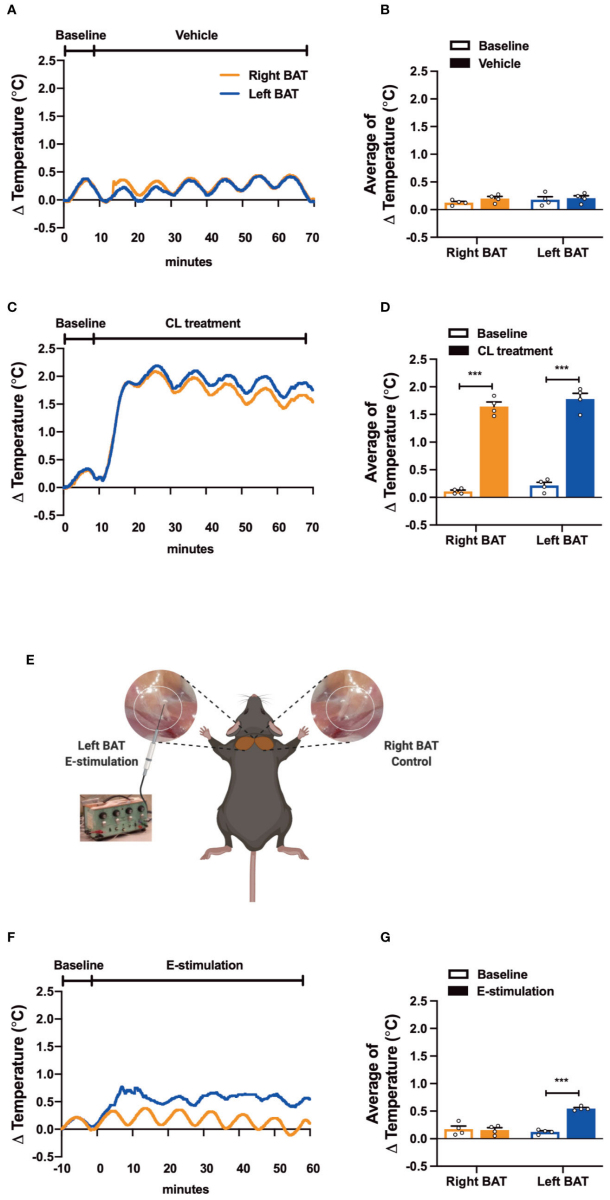

Figure 1. Electrical neurostimulation acutely increases the thermogenic activity of BAT. After recording local BAT temperature for 10 min (baseline), mice received vehicle (A, B), CL316243 (CL treatment) (C, D), or electrical sympathetic neural stimulation (E-stimulation) of the left BAT lobe with the right lobe as unstimulated control (schematically shown; E) for 60 minutes (F, G), during which BAT temperature was still recorded. The temperature changes (A, C, F) and average temperature changes within the intervention periods (B, D, G) were calculated. Differences between groups were determined with a two-tailed Student unpaired t-test. Data are shown as average curves (A, C, F) or mean ± SEM (B, D, G) (n=4 mice per group). ***P<0.001.

Electrical neurostimulation reduces intracellular lipid droplets in BAT

After 1 hour of pharmacological or electrical neurostimulation of BAT, the mice were injected with radiolabeled lipoprotein-like particles to determine TG-derived FA uptake by BAT and tissues were collected for further analysis. We observed a marked decrease of lipid droplet content in BAT of the mice receiving CL treatment as compared with the vehicle (-25%, Figures 2A, B). The BAT pad of mice that had received E-stimulation also showed a significant decrease in lipid droplet content (-13%, Figures 2C, D). Despite the decrease in lipid content, there was no effect on the uptake of [^{3}H]oleate or [^{14}C]deoxyglucose by BAT of the CL treated mice (Figures 2E, F), nor was there in the E-stimulated BAT depot (Figures 2G, H).

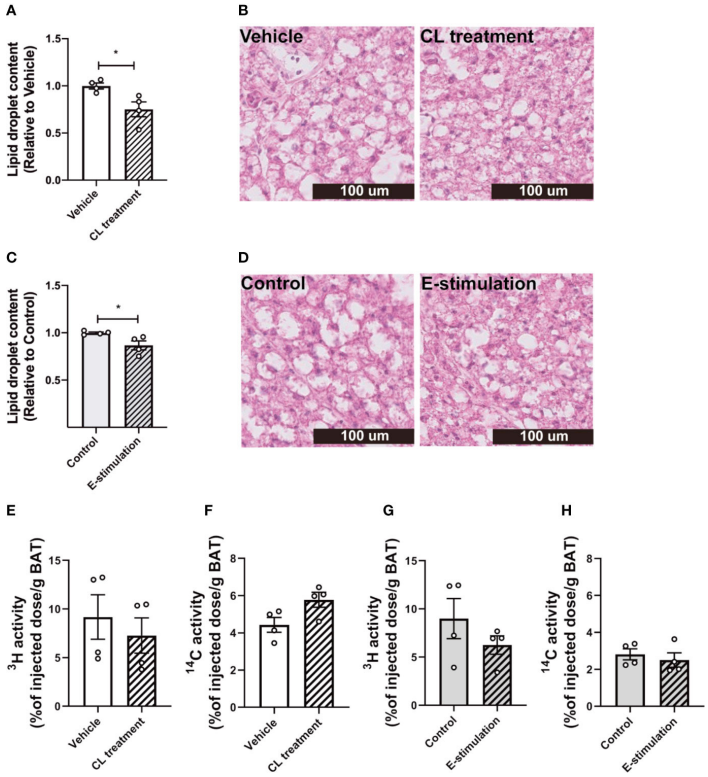

Figure 2. Electrical neurostimulation reduces intracellular lipid droplets in BAT. At 60 min of intervention with vehicle or CL316243 (A, B), or electrical neural sympathetic stimulation (E-stimulation) of the left BAT lobe (C, D), BAT was collected and sectioned for HE staining. The lipid content within BAT was quantified (A, C) with representative pictures shown (B, D). Lipid and glucose uptake by BAT was assessed by injection of glycerol tri[^{3}H]oleate-labeled triglyceride-rich lipoprotein-mimicking particles and [^{14}C]deoxyglucose injection, 15 min before termination. The uptake of ^{3}H and ^{14}C-activity by BAT were assessed in mice receiving vehicle versus CL316243 (E, F) and E-stimulation of the left lobe (G, H). Differences between groups were determined with a two-tailed Student unpaired t-test. Data are shown as mean ± SEM (n=4 mice per group). *P<0.05.

Electrical neurostimulation acutely increases tyrosine hydrolase and hormone-sensitive lipase phosphorylation in BAT

To investigate whether norepinephrine production and downstream signaling of adrenergic receptors were promoted by E-stimulation, we next quantified protein levels of tyrosine hydroxylase (TH), the rate-limiting enzyme in norepinephrine production and phosphorylation of hormone-sensitive lipase (HSL) Ser563, essential for the intracellular lipolysis of TG. CL treatment increased the TH content (Histology: 9 fold, Figures 3A, 3B; Western blot: 3.6 fold, Figure S3A, S3B), possibly as part of a positive feedback loop and explained by rapid axoplasmic transport from the cell bodies to the terminals. This effect was accompanied by a nonsignificant increase in phosphorylated HSL (Figures 3C, 3D, S3D and S3E). E-stimulation resulted in an increased TH level (Histology: 2.4 fold, Figures 3E, 3F; Western blot: 3.6 fold, S3A and S3C) and a significant increase in phosphorylated HSL (Histology: 1.7 fold, Figures 3G, 3H; Western blot: 3.1 fold, S3D and S3F).

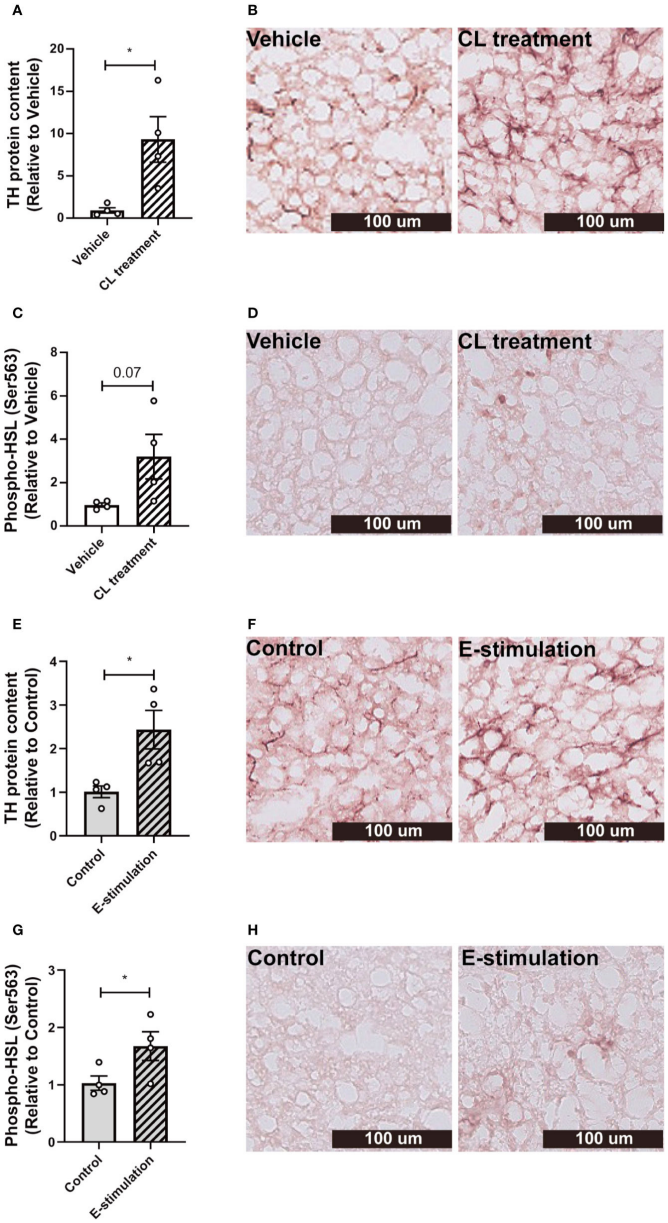

Figure 3. Electrical neurostimulation acutely increases tyrosine hydrolase and hormone-sensitive lipase phosphorylation in BAT. After intervention with vehicle or CL316243 (A-D), or electrical neural sympathetic stimulation (E-stimulation) of the left BAT lobe (E-H), BAT was collected and sectioned for immunohistochemical staining. The protein expression of tyrosine hydrolase (TH) (A, B, E, F) and phospho-hormone sensitive lipase (HSL) (C, D, G, H) were quantified (A, C, E, G) with representative pictures shown (B, D, F, H). Differences between the groups were determined with a two-tailed Student unpaired t-test. Data are shown as mean ± SEM (n=4 mice per group). *P<0.05.

The effect of electrical neurostimulation on the thermogenic activity of BAT is dependent on β3-adrenergic receptor signaling

To confirm that electrical neurostimulation indeed results in enhanced sympathetic outflow and thereby promotes thermogenesis, we repeated E-stimulation while concomitantly administering a specific β3-AR antagonist. The β3-AR antagonist SR59230A had no effect on BAT temperature in sham-operated mice (Figures 4A, B), but acutely reduced the increased temperature in the E-stimulated BAT pad (Figures 4C, D). There was no effect on core body temperature during E-stimulation or treatment with the β3-AR antagonist (Figure S2A, B).

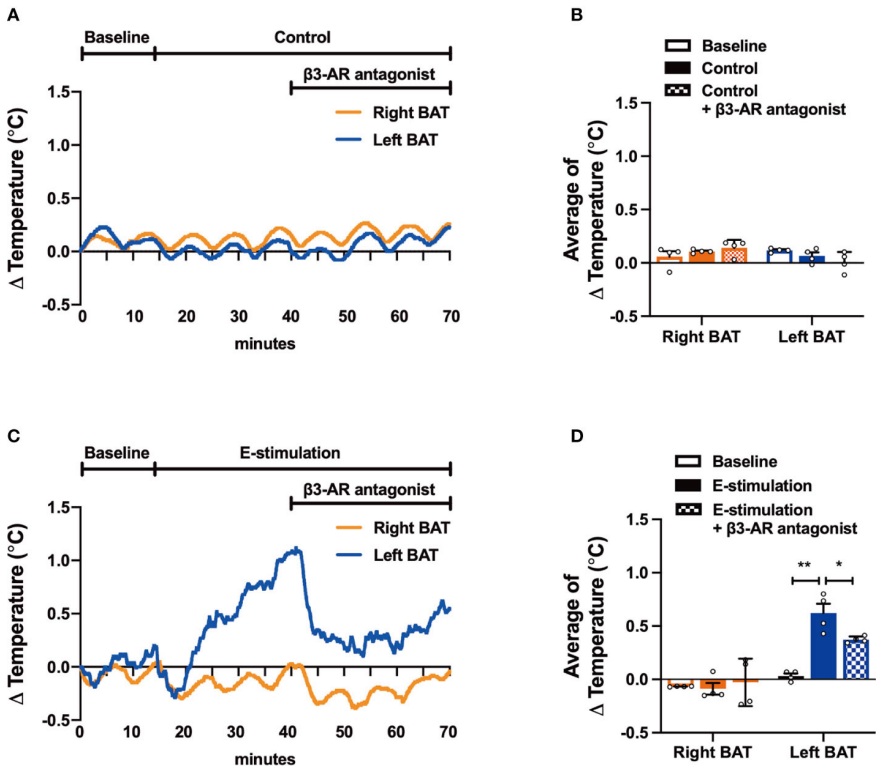

Figure 4. The effect of electrical neurostimulation on the thermogenic activity of BAT is dependent on β3-adrenergic receptor signaling. After recording local BAT temperature for 10 min (baseline), mice were sham-operated as control (A, B) or received electrical neural sympathetic stimulation (E-stimulation) of specifically the left BAT lobe for 60 minutes (E, F), during which BAT temperature was still recorded. After 30 min of intervention, all mice in addition received a β3-adrenergic (β3-AR) antagonist by subcutaneous injection. The temperature changes (A, C) and the average temperature changes in different intervention periods (B, D) were calculated in control mice (A, B) and in mice receiving E-stimulation (C, D). Differences between the groups were determined with a two-tailed Student unpaired t-test. Data are shown as mean ± SEM (n=4 mice per group). *P<0.05, **P<0.01.

Discussion

Here, we have described a novel method of applying electrical neurostimulation to selectively promote sympathetic outflow to BAT in mice. In this proof of concept study, by using C57BL/6J mice we demonstrated that electrical neurostimulation of BAT promotes thermogenesis dependent on β3-AR signaling. Although we are not the first to target BAT by electrical stimulation, previous studies used techniques that were nonspecific (i.e., electrical field stimulation of dorsal surface)) [14], very difficult to translate to the clinic (i.e., with the use of optogenetics) [15] or a combination of these two limitations (i.e., electrical stimulation of hypothalamic nuclei) [12, 13]. The method described in our manuscript involves electrodes that are directly positioned around the sympathetic nerves innervating BAT; this is the first step towards the use of implantable devices to selectively promote thermogenesis in BAT.

In contrast to other organs such as white adipose tissue and liver, BAT is densely innervated. Almost every single brown adipocyte is in close proximity to a sympathetic nerve ending , as also reflected by the abundant TH staining shown in the present study. This not only suggests that BAT is under stringent control of the nervous system, but is also consistent with the critical role of BAT in the acute response and tolerance to cold. Indeed, in line with the previous studies showing that the activation of BAT acutely increases intracellular lipolysis to release FA that serve as fuel for thermogenesis [8], in the current study we demonstrated that electrical neurostimulation of BAT acutely increases the thermogenic capacity of BAT. Although one hour of electrical stimulation was seemingly insufficient to already promote uptake of lipids and glucose from the circulation, given that both acute CL injection and electrical neurostimulation did lead to decreased lipid content in BAT, and chronic CL treatment does attenuate diet-induced adiposity, hyperlipidemia and atherosclerosis [10, 16], we anticipate that prolonged neurostimulation would be a feasible alternative to activate BAT and prevent cardiometabolic diseases as shown for the use of sympathomimetics [9]. More studies are needed to further explore the potential application of prolonged electrical neurostimulation of BAT preferably in free-living animals by using cuff electrodes connected to a swivel.

Electrical stimulation of peripheral nerves is already applied in a variety of conditions in humans [17, 18]. Evidently, the approach used in the current study, which involves surgery to expose the nerves innervating BAT and wired connections to a pulse generator, is not suitable for clinical application yet. In addition, important questions related to the similarities between BAT physiology of humans [19] and rodents [20], as well as the effects of prolonged and/or repeated neurostimulation have to be addressed first. Interestingly, a human study involving vagus nerve stimulation, used to treat refractory epilepsy, also demonstrated increased energy expenditure and weight loss in association with increased BAT activity [21], highlighting the potential of neurostimulation in the clinical treatment of cardiometabolic disorders.

In summary, we demonstrated that direct electrical stimulation of the sympathetic nerves innervating BAT potently induces heat production, which is dependent on β3-AR signaling. Future studies should show whether prolonged and/or repeated neurostimulation of BAT, preferentially using implantable devices, can protect from cardiometabolic diseases.

References

1. Labbe, S.M., et al., *In vivo measurement of energy substrate contribution to cold-induced brown adipose tissue thermogenesis.* FASEB J, 2015. **29**(5): p. 2046-58.
2. Ouellet, V., et al., *Brown adipose tissue oxidative metabolism contributes to energy expenditure during acute cold exposure in humans.* J Clin Invest, 2012. **122**(2): p. 545-52.
3. Cypess, A.M., et al., *Identification and importance of brown adipose tissue in adult humans.* N Engl J Med, 2009. **360**(15): p. 1509-17.
4. Saito, M., et al., *High incidence of metabolically active brown adipose tissue in healthy adult humans: effects of cold exposure and adiposity.* Diabetes, 2009. **58**(7): p. 1526-31.
5. Hanssen, M.J., et al., *Short-term cold acclimation improves insulin sensitivity in patients with type 2 diabetes mellitus.* Nat Med, 2015. **21**(8): p. 863-5.
6. Hanssen, M.J., et al., *Short-term Cold Acclimation Recruits Brown Adipose Tissue in Obese Humans.* Diabetes, 2016. **65**(5): p. 1179-89.
7. Townsend, K.L. and Y.H. Tseng, *Brown fat fuel utilization and thermogenesis.* Trends Endocrinol Metab, 2014. **25**(4): p. 168-77.
8. Cannon, B. and J. Nedergaard, *Brown adipose tissue: function and physiological significance.* Physiol Rev, 2004. **84**(1): p. 277-359.
9. Khedoe, P.P., et al., *Brown adipose tissue takes up plasma triglycerides mostly after lipolysis.* J Lipid Res, 2015. **56**(1): p. 51-9.
10. Bartelt, A., et al., *Thermogenic adipocytes promote HDL turnover and reverse cholesterol transport.* Nat Commun, 2017. **8**: p. 15010.
11. Blondin, D.P., et al., *Human Brown Adipocyte Thermogenesis Is Driven by beta2-AR Stimulation.* Cell Metab, 2020. **32**(2): p. 287-300 e7.
12. Halvorson, I., L. Gregor, and J.A. Thornhill, *Brown adipose tissue thermogenesis is activated by electrical and chemical (L-glutamate) stimulation of the ventromedial hypothalamic nucleus in cold-acclimated rats.* Brain Res, 1990. **522**(1): p. 76-82.
13. Freeman, P.H. and P.J. Wellman, *Brown adipose tissue thermogenesis induced by low level electrical stimulation of hypothalamus in rats.* Brain Res Bull, 1987. **18**(1): p. 7-11.
14. Iwami, M., et al., *Activation of brown adipose tissue thermogenesis by electrical stimulation to the dorsal surface of the tissue in rats.* Biomed Res, 2013. **34**(4): p. 173-8.
15. Lyons, C.E., et al., *Optogenetic-induced sympathetic neuromodulation of brown adipose tissue thermogenesis.* FASEB J, 2020. **34**(2): p. 2765-2773.
16. Berbee, J.F., et al., *Brown fat activation reduces hypercholesterolaemia and protects from atherosclerosis development.* Nat Commun, 2015. **6**: p. 6356.
17. Oddo, C.M., et al., *Intraneural stimulation elicits discrimination of textural features by artificial fingertip in intact and amputee humans.* Elife, 2016. **5**: p. e09148.

18. Ortiz-Catalan, M., B. Hakansson, and R. Branemark, *An osseointegrated human-machine gateway for long-term sensory feedback and motor control of artificial limbs.* Sci Transl Med, 2014. **6**(257): p. 257re6.

19. Nedergaard, J., T. Bengtsson, and B. Cannon, *Unexpected evidence for active brown adipose tissue in adult humans.* Am J Physiol Endocrinol Metab, 2007. **293**(2): p. E444-52.

20. Frontini, A. and S. Cinti, *Distribution and development of brown adipocytes in the murine and human adipose organ.* Cell Metab, 2010. **11**(4): p. 253-6.

21. Vijgen, G.H., et al., *Vagus nerve stimulation increases energy expenditure: relation to brown adipose tissue activity.* PLoS One, 2013. **8**(10): p. e77221.

Supplemental figures

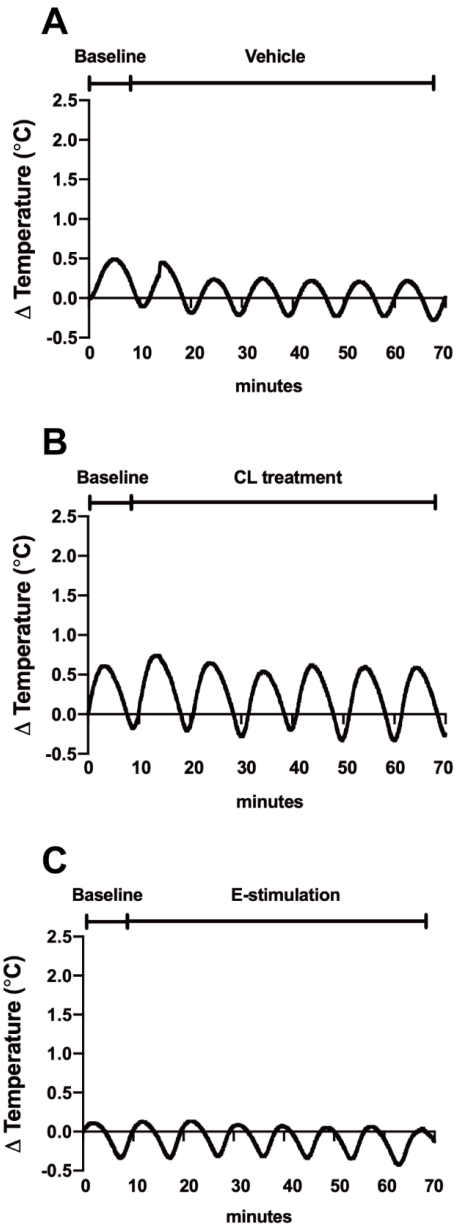

Figure S1. Electrical neurostimulation does not influence the core body temperature. After recording core body temperature for 10 min (baseline), mice received vehicle (A), CL316243 (CL treatment) (B), or electrical neurostimulation (E-stimulation) of the left BAT lobe for 60 minutes (C), during which core body temperature was still recorded. The temperature changes were calculated as average curves (n=4 mice per group).

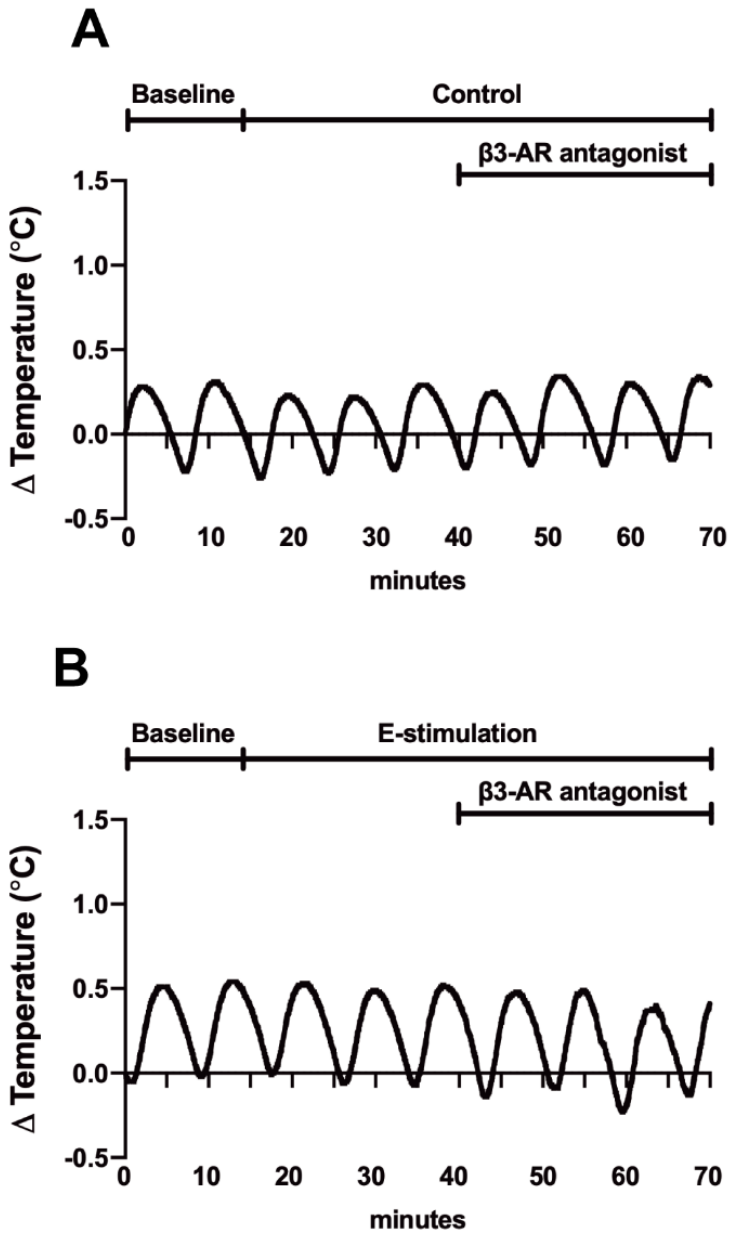

Figure S2. β3-adrenergic antagonism without and with electrical neurostimulation does not influence the core body temperature. After recording core body temperature for 10 min, mice were sham-operated (control, A) or received electrical neurostimulation (E-stimulation) of the left BAT lobe for 60 minutes (B), during which core body temperature was still recorded. After 30 min of intervention, all mice in addition received a β3-adrenergic (β3-AR) antagonist by subcutaneous injection. The temperature changes were calculated as average curves (n=4 mice per group).

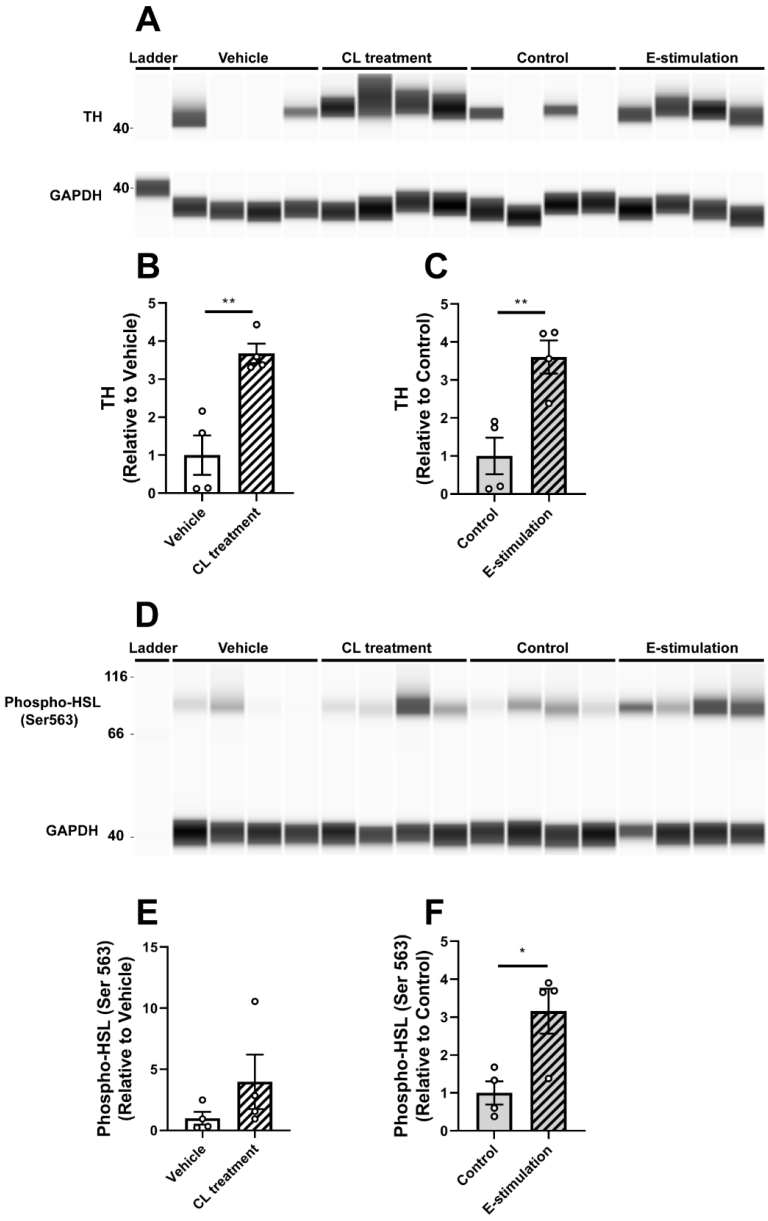

Figure S3. Electrical neurostimulation acutely increases tyrosine hydroxylase and phosphorylated hormone-sensitive lipase in BAT. After intervention with vehicle or CL316243, or electrical neural sympathetic stimulation (E-stimulation) of the left BAT lobe, BAT was collected and lysed for western blot. The protein level of tyrosine hydroxylase (TH) (A) and phospho-hormone-sensitive lipase (HSL) (D) were quantified (B, C, E, F). Differences between the groups were determined with a two-tailed Student unpaired t-test. Data are shown as mean ± SEM (n=4 mice per group). *P<0.05, **P<0.01.

CHAPTER 6

LIPOPOLYSACCHARIDE LOWERS CHOLESTERYL ESTER TRANSFER PROTEIN BY ACTIVATING F4/80^{+} CLEC4F^{+} VSIG4^{+} LY6C^{-} KUPFFER CELL SUBSETS

Van der Tuin SJ*, **Li Z***, Berbée JFP, Verkouter I, Ringnalda LE, Neele AE, Van Klinken JB, Rensen SS, Fu J, De Winther MPJ, Groen AK, Rensen PCN, Willems van Dijk K, Wang Y

*Authors contributed equally

***J Am Heart Assoc 2018**, 7: e008105*

Abstract

Background: Lipopolysaccharide (LPS) decreases hepatic cholesteryl ester transfer protein (CETP) expression albeit that the underlying mechanism is disputed. We recently showed that plasma CETP is mainly derived from Kupffer cells (KCs). In this study, we investigated the role of KC subsets in the mechanism by which LPS reduces CETP expression.

Methods and Results: In CETP-transgenic mice, LPS markedly decreased hepatic *CETP* expression and plasma CETP concentration without affecting hepatic macrophage number. This was paralleled by decreased expression of the resting KC markers *Clec4f* and *Vsig4*, while expression of the infiltrating monocyte marker *Ly6C* was increased. Simultaneously, the ratio of plasma HDL-cholesterol over nonHDL-cholesterol transiently increased. After ablation hepatic macrophages via injection with liposomal clodronate, the reappearance of hepatic gene and protein expression of CETP coincided with Clec4f and Vsig4, but not Ly6C. Double-immunofluorescence staining showed that CETP co-localized with Clec4f^{+} KCs and not Ly6C^{+} monocytes. In humans, microarray gene-expression analysis of liver biopsies revealed that hepatic expression and plasma level of CETP both correlated with hepatic *VSIG4* expression. LPS administration decreased the plasma CETP concentration in humans. *In vitro* experiments showed that LPS reduced LXR-mediated CETP expression.

Conclusions: Hepatic expression of CETP is exclusively confined to the resting KC subset (i.e., F4/80^{+}Clec4f^{+}Vsig4^{+}Ly6C^{-}). LPS activated resting KCs, leading to reduction of Clec4f and Vsig4 expression and reduction of hepatic CETP expression, consequently decreasing plasma CETP and raising HDL-cholesterol. This sequence of events is consistent with the anti-inflammatory role of HDL in the response to LPS and may be relevant as a defense mechanism against bacterial infections.

Introduction

Kupffer cells (KCs) are the resident tissue macrophages of the liver. KCs are characterized by specific surface proteins such as C-type lectin domain family 4, member f (Clec4f) and V-set and immunoglobulin domain containing 4 (Vsig4) [1-4]. These surface markers distinguish KCs from other hepatic macrophages, which may have lost or have yet to acquire these KC markers. KCs play an important role in the response to various harmful agents such as intestine-derived bacterial lipopolysaccharide (LPS) in the portal blood. LPS, a constituent of Gram-negative bacteria, is a potent endotoxin that induces a strong cytokine-mediated inflammatory response in the host [5]. LPS activates KCs via the Toll-like receptor 4 (TLR4) signaling pathway to release pro-inflammatory cytokines, such as tumor necrosis factor α (TNFα) [6] and interleukin-1β (IL-1β) [7]. Therefore, KCs are crucial to detect LPS and trigger an antibacterial response [8, 9].

We have recently shown that KCs are the main source of plasma cholesteryl ester transfer protein (CETP), and that plasma CETP concentration predicts hepatic macrophage content in humans [10]. In that study, we also found that CETP was expressed by only a subset of hepatic macrophages in livers of both humans and mice transgenic for human CETP. Plasma CETP plays a pivotal role in the metabolism of high-density lipoproteins (HDL) and (very-) low-density lipoproteins ((V)LDL) by mediating the exchange of cholesteryl ester for triglycerides (TG) between HDL and (V)LDL. Genetic deficiency for CETP increases plasma HDL-cholesterol (C) and decreases cardiovascular events [11]. This has led to the development of CETP inhibition as a potential strategy for the treatment of cardiovascular disease (CVD). Despite clearly favorable effects on the lipoprotein profile, pharmacological CETP inhibitors, such as torcetrapib [12], dalcetrapib [13] and evacetrapib [14], failed to show clinical benefit on CVD outcomes including atherosclerosis and vascular inflammation. While, very recently, the Merck Company announced that the REVEAL study, which studies the effects of Anacetrapib on CVD outcome met its primary endpoint, significantly reducing major coronary events defined as the composite of coronary death, myocardial infarction, and coronary revascularization [15]. These results illustrate that the role and underlying mechanism of CETP in CVD pathology is more complex than initially anticipated.

CETP not only has a role in lipid and lipoprotein metabolism, but also belongs to the family of lipid transfer/LPS-binding proteins (LT/LBP) [16]. A previous study has demonstrated that CETP expression increases the mouse survival rate after injection of a lethal dose of LPS [17]. In addition, LPS administration to CETP transgenic mice resulted in a rapid and marked decrease in plasma CETP concentration and hepatic CETP expression, accompanied by an increase in HDL-C level [18]. These data indicate that CETP may play a complex role in the response to LPS.

We previously observed that a subsets of F4/80-positive hepatic macrophages co-express CETP [10]. In the current study, we determined which subset of KCs is the

predominant cellular source to the plasma CETP pool. Also, we investigated the role of KC subsets in the mechanism by which LPS reduces CETP expression. To this end, we determined the regulation of CETP in relation to hepatic macrophage markers after injection of LPS in APOE*3-Leiden.CETP (E3L.CETP) mice, and followed the kinetics of reappearance of CETP in relation to macrophage markers after removal of hepatic macrophages by liposomal clodronate. Furthermore, liver biopsies and plasma samples from two clinical studies were used to evaluate the CETP expression in KC subsets and effects of LPS on plasma CETP in humans.

Materials and methods

The data, analytic methods, and study materials will not be made available to other researchers for purposes of reproducing the results or replicating the procedure.

Animals and experimental procedure

Female APOE*3-Leiden.CETP (E3L.CETP) transgenic mice [19] were housed under standard conditions with a 12 h light-dark cycle and had free access to food and water during the experiment. At the age of 10-15 weeks, mice were fed a semi-synthetic cholesterol-rich diet, containing 15% (w/w) cacao butter, 1% (w/w) corn oil and 0.1% cholesterol (w/w, Western-type diet; AB-Diets, Woerden, The Netherlands) for a run-in period of 6 weeks, followed by LPS injection or liposomal clodronate injection. Body weight and food intake were monitored during this study. The Institutional Ethics Committee for Animal Procedures from the Leiden University Medical Centre, Leiden, The Netherlands, approved the following studies.

LPS injection

After randomization according to plasma levels of triglycerides, total cholesterol, HDL-C, body weight and age, mice received an intraperitoneal injection of LPS (25 µg per mouse; *E. coli* serotype 055:B5, Sigma-Aldrich) or vehicle (LPS-free phosphate-buffered saline, Control group), and blood samples were drawn before and 8, 24 and 48 hours after the injection. In a second study, mice were terminated 4, 8 and 48 hours after the injection of LPS.

Liposomal clodronate injection

After randomization according to plasma total cholesterol (TC), HDL-C, triglycerides, body weight and age, ensuring that all mice were equally old when they were sacrificed, mice received two intraperitoneal injections of liposomal clodronate (20 mg/kg bodyweight; purchased from Dr. N. van Rooijen, Amsterdam) at a 3-day interval to deplete macrophages from the liver [10]. Blood samples were drawn before and after the second injection weekly up to 9 weeks. In a second study, mice were terminated 3 days (0 week), or 3, 6 or 9 weeks after the second injection. Control mice received no liposomal clodronate treatment.

Blood sampling, plasma lipid and lipoprotein profiles

Blood was obtained via tail vein bleeding into heparin-coated capillary tubes. The tubes were placed on ice and centrifuged, and obtained plasma was snap-frozen in liquid nitrogen and stored at -80°C until further measurements. Plasma was assayed for triglycerides and cholesterol using the commercially available enzymatic kits 11488872 and 236691 (Roche Molecular Biochemicals, Indianapolis, IN, USA), respectively. To measure plasma HDL-C, apoB-containing lipoproteins were

precipitated from plasma with 20% polyethylene glycol 6000 (Sigma Aldrich) in 200 mM glycine buffer (pH 10) and HDL-C was measured in the supernatant. Plasma non-HDL-C was calculated by subtracting HDL-C from plasma total cholesterol.

Plasma CETP concentration

Plasma CETP concentration was measured using the DAIICHI CETP ELISA kit according to manufacturer's instructions (Daiichi, Tokyo, Japan).

Hepatic gene expression

Liver pieces were isolated and total RNA was extracted using the Nucleospin RNAII kit (Macherey-Nagel) according to manufacturer's protocol. RNA concentration was determined by Nanodrop technology (Thermo Scientific). Total RNA was reverse-transcribed with the iScript cDNA synthesis kit (Bio-Rad) and qPCR was performed using a CFX96 (Bio-Rad). Gene expression was normalized to Beta-2 microglobulin (β2m), hypoxanthine ribosyltransferase (*Hprt*) and Beta-actin (βactin). Relative expression was calculated and normalized to control group using Bio-Rad CFX ManagerTM software 3.0 (Bio-Rad). Primer sequences can be found in the Supplemental Table 1.

Liver histology

Paraffin-embedded sections of mouse liver (5 µm) were stained for F4/80 and human CETP (ab51771; 1/1000, Abcam) as described previously [10], Clec4f (MAB2784; 1/1000, R&D Systems), Vsig4 (AF4674; 1/1000, R&D Systems) and Ly6C (ab15627; 1/400, Abcam). For immunofluorescence staining, the secondary antibodies donkey anti-rabbit Alexa488 (A21206; Invitrogen) and goat anti-rat Alexa555 (A21434; Invitrogen) were used. Finally, tissue sections were mounted with VECTASHIELD® Mounting Medium with DAPI (Vector Laboratories). Positive cells were counted using a LeicaCTR5500 fluorescence microscope (Leica Microsystems GmbH). Representative pictures of immunostaining for CETP in liver sections of non-CETP transgenic mice (APOE*3-Leiden mice), APOE*3-Leiden.CETP transgenic mice, and a healthy human donor are shown in Supplemental Fig I.

Design of human studies

93 severely obese subjects (BMI 30-74) underwent elective bariatric surgery from 2006 to 2009 at the Dept. of General Surgery, Maastricht University Medical Center, Maastricht, The Netherlands, as described [20]. Subjects using anti-inflammatory drugs or having acute or chronic inflammatory diseases, degenerative diseases, and subjects reporting alcoholic intake >10 g/day, were excluded. During surgery, liver biopsies were taken for mRNA isolation and in situ analyses. Venous blood samples were obtained after overnight fasting (approx. 8 h) on the morning of surgery for analysis of the plasma CETP concentration. This study was approved by the Medical

Ethics Board of Maastricht University Medical Centre, in line with the Declaration of Helsinki. All participants provided informed written consent.

The second study (i.e., HEAVEN study) consisted of 20 healthy male subjects as described [21]. Subjects with known genetic causes for low HDL-cholesterol, secondary dyslipidemias such as familial combined hyperlipidemia, metabolic syndrome or secondary to hypertriglyceridemia, were excluded. On the morning of the study day at 7:30 am after an overnight fast, study participants were admitted to the research unit. At 7.45 am a catheter was inserted in an antecubital vein of each arm. At 8.00 am (time [t]=0), blood was drawn for baseline measurements. Subsequently, subjects received a bolus infusion of 1 ng/kg body weight of endotoxin (*E. coli* LPS, catalog number 1235503, lot G2B274; United States Pharmacopeial Convention Inc, Rockville, Md) in the antecubital vein of the contralateral arm. The next morning at 8.00 am, 24 hours after endotoxin infusion, study participants returned after an overnight fast for the blood withdrawal. The study protocol was approved by the institutional review board at the Academic Medical Center in Amsterdam. Written informed consent was obtained from all subjects.

In vitro LPS simulation in human monocyte- derived macrophages

Peripheral blood mononuclear cells were isolated from a buffycoat (Sanquin blood supply, Amsterdam, the Netherlands) through density centrifugation using Lymphoprep™ (Axis-Shield, Dundee, Scotland). Monocytes were then purified using human CD14 magnetic beads and MACS® cell separation columns (Miltenyi Biotec, Bergisch Gladbach, Germany). Monocytes were plated in 24-well tissue culture plates at a density of $1*10^6$ cells/mL (500 µL per well) and differentiated to macrophages for 6 days in Iscove's Modified Dulbecco's Medium (IMDM, Sigma-Aldrich) supplemented with 2mM l-glutamine, penicillin (100 U/mL), Streptomycin (100 µg/mL) and 10% fetal calf serum (FCS; All Gibco, Waltham, MA) in the presence of 50 ng/mL MCSF (Miltenyi Biotec, Bergisch Gladbach, Germany). On day 3, the medium was removed and substituted by fresh IMDM with 10% FCS and 50 ng/mL MCSF. On day 6, all medium was removed and replaced by IMDM with 10% FCS without MCSF and cells were activated for 18 hour with vehicle (DMSO), LPS (10 ng/mL, Sigma-Aldrich), a liver X receptor (LXR) agonist (TO-901317, 10 µmol/L, Sigma-Aldrich), and LPS+LXR agonist. Total RNA was extracted from the cell lysate.

Statistical analysis

Data were analyzed by Graphpad Prism software, version 7, unless indicated otherwise. Significance of differences between the groups was calculated non-parametrically using a Mann-Whitney U-test for independent samples. All groups were compared to the control group. Bonferroni's method was used to determine significance in case of multiple comparisons. For the human LPS exposure study, the Student paired *t* test was used. To analyze the *in vitro* LPS exposure study, One-way ANOVA was used, followed by the Fisher's Least Significant Difference (LSD)

test to identify the differing groups. Spearman correlation was used to determine the correlations between parameters in both mouse and human studies. Linear regression analysis was performed on the associations between hepatic expression of CETP and macrophage markers and the coefficients of determination (R^2) were reported. For linear regression analysis of human liver microarray data, unadjusted Crude models (Model 1) and a Model adjusted for age and sex (Model 2) were applied using STATA Statistical Software, version 12.0. For experiments involving repeated measures of plasma lipids and CETP levels in the same animal (Fig 2 and Fig 3A), we used a linear mixed-effects model with a heterogeneous first-order autoregressive covariance matrix structure to model subject-specific deviances from the group mean using IBM SPSS Statistical Software, version 23. Values are presented as means ± SEM. P values of less than 0.05 were considered statistically significant for single comparison.

Results

LPS reduces hepatic CETP expression, paralleled by decreased expression of resting Kupffer cell markers and increased expression of macrophage activation markers

To investigate the role of hepatic macrophages in the mechanism by which LPS reduces CETP expression, we determined the regulation of CETP in relation to macrophage markers after injection of LPS in E3L.CETP mice. As expected, LPS injection caused a massive upregulation of hepatic mRNA expression of tumor necrosis factor α (*Tnf*α; 21-fold), interleukin-1β (*Il-1β*; 19-fold), and monocyte chemotactic protein-1 (*Mcp-1*; 28-fold) at 4 h after injection (all P<0.001, Fig 1A), indicating LPS-induced KC activation [6, 7, 22]. LPS also increased the expression of lipopolysaccharide-binding protein (*Lbp*, Supplemental Fig IIA). These effects were transient as gene expression returned to baseline at 48 h after injection. LPS markedly decreased mRNA expression of phospholipid transfer protein (*Pltp*) (Supplemental Fig IIB) and ATP binding cassette subfamily G member 1 *(Abcg1)* (Supplemental Fig IIC) in liver, up to 48 hours after LPS injection. Simultaneously, LPS injection rapidly and markedly decreased hepatic mRNA expression of *CETP* (-75% at 8 h after injection; P<0.001, Fig 1B) in E3L.CETP mice. At 48 h after LPS injection, *CETP* expression was still reduced. In parallel, LPS markedly decreased the hepatic expression of resting KC markers *Clec4f* and *Vsig4* to a similar extent (-75% and -83% at 8 h after injection; P<0.01, Fig 1B). In contrast, LPS increased hepatic mRNA expression of lymphocyte antigen 6 complex locus C (*Ly6C*), a marker of infiltrating monocytes/ macrophages [23] (+48% at 8 h after injection; P<0.001, Fig 1D). Correlation analyses using data of all time points (Fig 1D) showed that hepatic *CETP* expression strongly positively correlated with the expression of *Clec4f* (r=0.735; P<0.001) and *Vsig4* (r=0.904; P<0.001), whereas hepatic expression of *CETP* inversely correlated with *Ly6C* (r=-0.493; P<0.05).

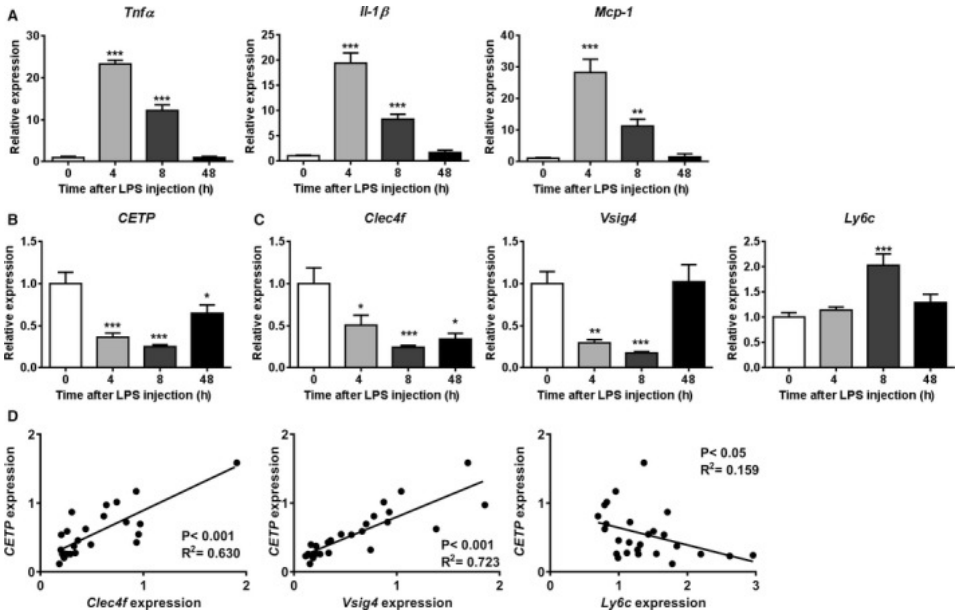

Figure 1. LPS reduces hepatic CETP expression, paralleled by decreased expression of resting Kupffer cell markers and increased expression of macrophage activation markers. Female APOE*3-Leiden.CETP mice fed a Western-type diet were intraperitoneally injected with 25 µg LPS, after which mice were sacrificed at the indicated time points. Livers were assayed for mRNA of (A) *Tnfa*, *Il-1ß*, *Mcp-1*; (B) *CETP* and (C) *Clec4f*, *Vsig4*, *Ly6C*. The correlations between hepatic mRNA expression of *CETP* with *Clec4f*, *Vsig4* and *Ly6C* were performed, and the goodness of fit R^2 from linear regression analyses were shown (D). For A, B and C, data are presented as means ± SEM (0, 4 and 48 h group: n=7; 8 h group: n=8); *P<0.05, **P<0.01, ***P<0.001 as compared to the 0 h group.

LPS acutely changes Kupffer cell subsets but not the hepatic F4/80$^+$ cell number

We next performed immunohistochemistry (IHC) on liver sections and the numbers of F4/80$^+$, Ly6C$^+$, Clec4f$^+$and CETP$^+$ cells were quantified. LPS administration did not affect the hepatic total macrophage/monocyte content as evidenced by the number of F4/80$^+$ cells (Supplemental Fig IIIA). In line with the observation that LPS markedly increased the gene expression of *Ly6C*, LPS significantly increased the number of Ly6C$^+$ monocytes after 4 h (2.6-fold) and 8 h (3.4-fold) (Supplemental Fig IIIB). LPS decreased the number of Clec4f$^+$ KC only after 48 h (-28%; P<0.01, Supplemental Fig IIIC), which coincided with a tendency of a decreased number of CETP$^+$ cells at 48 h after injection (-20%; P=0.06, Supplemental Fig IIID). The numbers of Clec4f$^+$ cells and CETP$^+$ cells were not affected at 4 and 8 h after LPS injection, which may be explained by a relatively slow turnover of CETP protein as compared to mRNA. Collectively, these data indicate that LPS acutely decreases hepatic CETP expression accompanied by changes in KC subsets.

LPS reduces plasma CETP and transiently increases plasma HDL-C level and HDL-C/non-HDL-C ratio

Plasma CETP, lipid and lipoprotein concentrations were assayed at baseline and 8, 24, 48 h after LPS or vehicle injection in E3L.CETP mice. LPS rapidly reduced plasma CETP concentration already at 8 h as compared to the control group (-51%; P<0.01, Fig 2A), and this reduction in plasma CETP concentration persisted until 48 h after injection, consistent with the reduced hepatic *CETP* mRNA expression. As compared to the control group, LPS significantly decreased plasma TG level after 24 and 48 h (Fig 2B), and total cholesterol level throughout the 48 h (Fig 2C). To investigate the effect of LPS on the distribution of cholesterol over plasma lipoproteins, HDL-C and non-HDL-C levels were determined. LPS transiently tended to increase HDL-C level 8 h after injection (+81%; Fig 2D), while persistently decreasing non-HDL-C level throughout the 48 h (Fig 2E). As a result, the HDL-C/non-HDL-C ratio transiently increased at 8 h after LPS injection (Fig 2F), suggesting that LPS induced a rapid and transient shift of cholesterol from non-HDL lipoproteins to HDL.

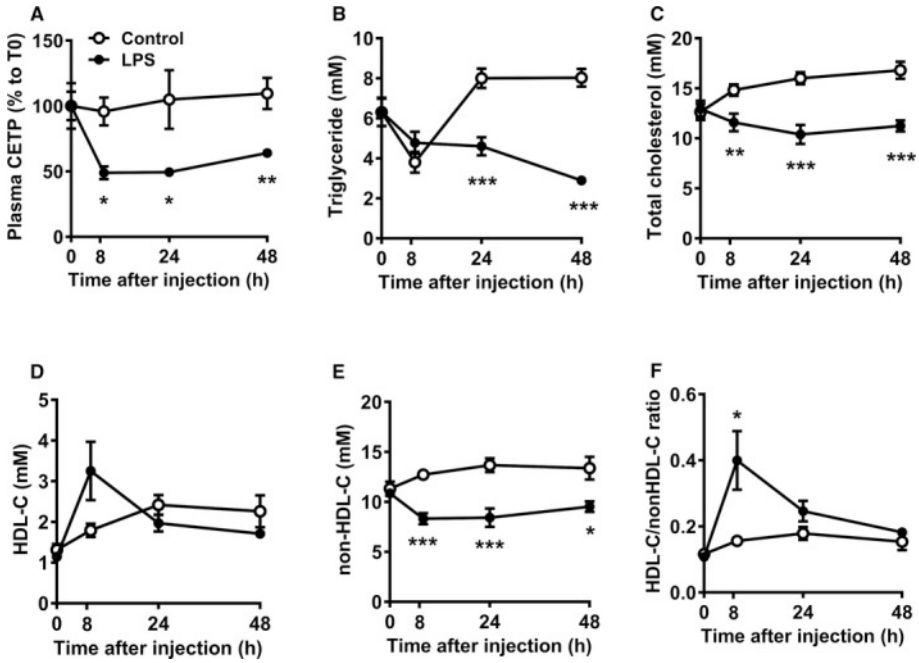

Figure 2. LPS reduces plasma CETP, and transiently increases plasma HDL-cholesterol level and HDL-C/non-HDL-C ratio. Female APOE*3-Leiden.CETP mice fed a Western-type diet were intraperitoneally injected with 25 µg LPS or vehicle (control), after which blood samples were collected at the indicated time points. Plasma was assayed for CETP concentration and data are expressed relative to t=0 (A). Plasma levels of triglyceride (B), total cholesterol (C), HDL-cholesterol (HDL-C, D), non-HDL-C (E) were determined, and the ratio between HDL-C and non-HDL-C (F) was calculated. Data are presented as means ± SEM (Control and LPS group: n=7); *P<0.05, **P<0.01, ***P<0.001 as compared to the Control group.

Reappearance of hepatic CETP expression after elimination of hepatic macrophages coincides with reappearance of hepatic Clec4f and Vsig4 expression

Since LPS administration has similar time-dependent effects on *CETP* expression and expression of the KC markers *Clec4f* and *Vsig4*, we reasoned that CETP, Clec4f and Vsig4 may be co-expressed by a similar subset of macrophages. This would imply that, following elimination of hepatic macrophages, reappearance of hepatic CETP expression due to monocyte infiltration would coincide with reappearance of *Clec4f* and *Vsig4*. Therefore, in a next experiment we eliminated hepatic macrophages from E3L.CETP mice by clodronate injection, without induction of inflammation [24, 25], and followed the reappearance of CETP and macrophage markers in the liver.

In line with our previous study [10], liposomal clodronate rapidly and markedly decreased plasma CETP concentration compared to vehicle (-75%; Fig 3A). The plasma CETP concentration was only gradually restored to levels observed in the control group at 8 weeks after injection. Similarly, liposomal clodronate virtually depleted the liver from *CETP* mRNA (-92%), which slowly returned to baseline levels (control group) only 9 weeks after the injection. In contrast, liposomal clodronate induced an immediate decrease in *F4/80* mRNA (-82%), which was restored already 3 weeks after injection (Fig 3B). Notably, the immediate effect of liposomal clodronate treatment on mRNA expression of *Clec4f* and *Vsig4* paralleled the CETP *mRNA* expression, while liposomal clodronate had virtually no effect on *Ly6C* mRNA (Fig 3B). Furthermore, data on protein expression of the macrophage subset markers are in line with data on mRNA expression (Fig 3C and Fig 4).

Correlation analyses between hepatic expression of *CETP* and macrophage marker genes (Figs 5A-C), or the number of $CETP^+$ cells and $Clec4f^+$ cells, $Vsig4^+$ cells, as well as $Ly6C^+$ cells (Figs 5D-E), again showed strong positive correlations between CETP and Clec4f (Fig 5A and 5D) or Vsig4 (Fig 5B and 5E), and less clear correlation between CETP and Ly6C (Fig 5C and 5F).

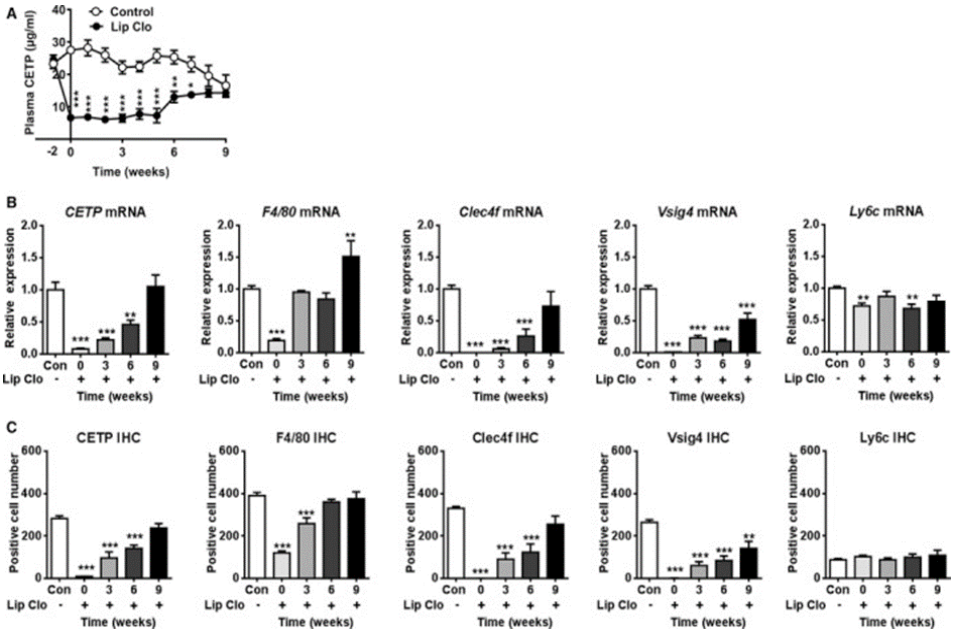

Figure 3. Reappearance of hepatic CETP expression after removal of hepatic macrophages coincides with reappearance of hepatic Clec4f and Vsig4 but not Ly6C. Female APOE*3-Leiden.CETP mice fed a Western-type diet were intraperitoneally injected with liposomal clodronate (Lip Clo) and sacrificed 3 days (0), 3, 6 and 9 weeks after injection. Untreated mice were taken along as control. Blood samples were collected at the indicated time points and plasma was assayed for plasma CETP (A). Livers were assayed for mRNA (B) and protein (C) of CETP, F4/80, Clec4f, Vsig4 and Ly6C. Data are presented as means ± SEM (Control and 0 week group: n=9; 3, 6 and 9 weeks group: n=7). *P<0.05, **P<0.01, ***P<0.001 compared to the Control group.

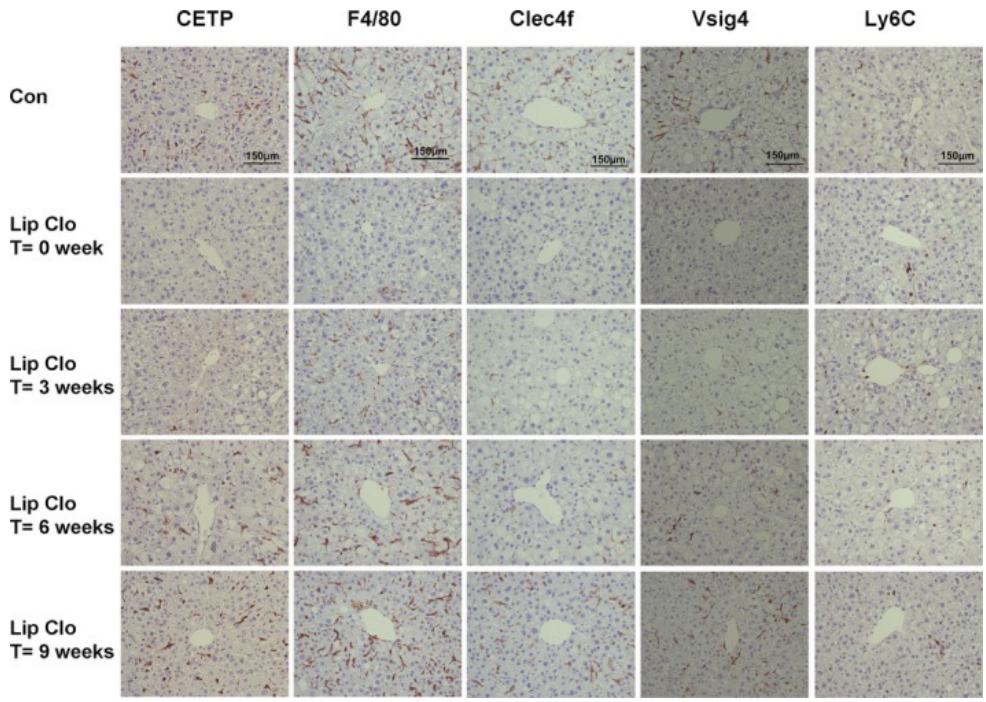

Figure 4. Reappearance of hepatic CETP protein and hepatic macrophage subsets after liposomal clodronate injection. Female APOE*3-Leiden.CETP mice fed a Western-type diet were intraperitoneally injected with liposomal clodronate (Lip Clo) and sacrificed 3 days (0), 3, 6 and 9 weeks after injection. Untreated mice were taken along as control (Con). Representative pictures of IHC staining of CETP, F4/80, Clec4f, Vsig4 and Ly6C in liver sections from each group are shown.

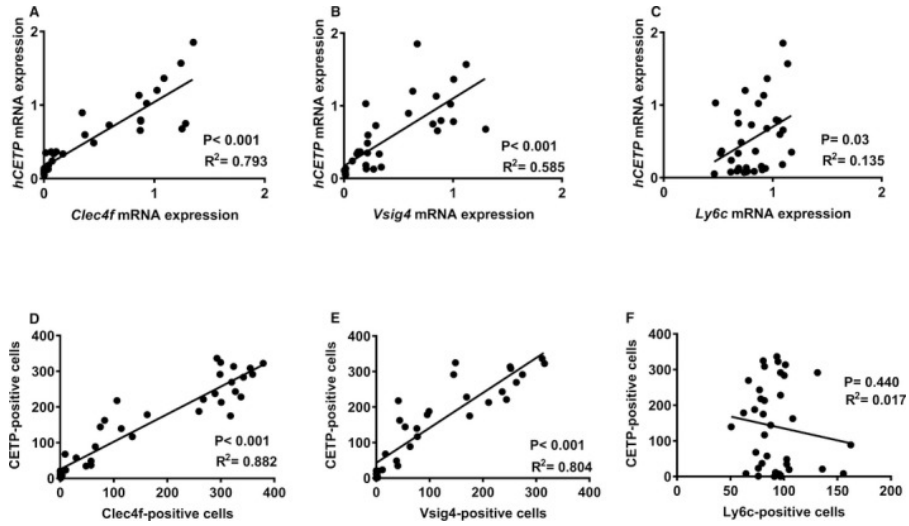

Figure 5. Hepatic CETP mRNA and positive cells strongly correlate with those of Clec4f and Vsig4, but not Ly6C. The correlations between hepatic CETP mRNA (A, B, C) or protein (D, E, F) with Clec4f (A, D), Vsig4 (B, E) and Ly6c (C, F) were performed, and the goodness of fit R^2 from linear regression analyses are shown.

CETP is exclusively expressed by Clec4f$^+$ Kupffer cells

To assess whether the strong correlations observed between hepatic CETP and Clec4f/Vsig4 (both mRNA expression and number of positive cells) are due to co-expression, we next performed double immunofluorescence staining of CETP and F4/80, Clec4f, or Ly6C on liver sections. Hepatic CETP co-localized in cells that also express F4/80, albeit that only a subset of F4/80$^+$ cells (65.4±9.9%) were CETP positive (Fig 6A), which is in agreement with our previous findings [10]. While Ly6C$^+$ cells did not stain for CETP protein (only 4.4±3.9% Ly6C$^+$ cells were CETP positive, Fig 6B), 94.9±8.7% Clec4f$^+$ cells stained positive for CETP protein (Fig 6C).

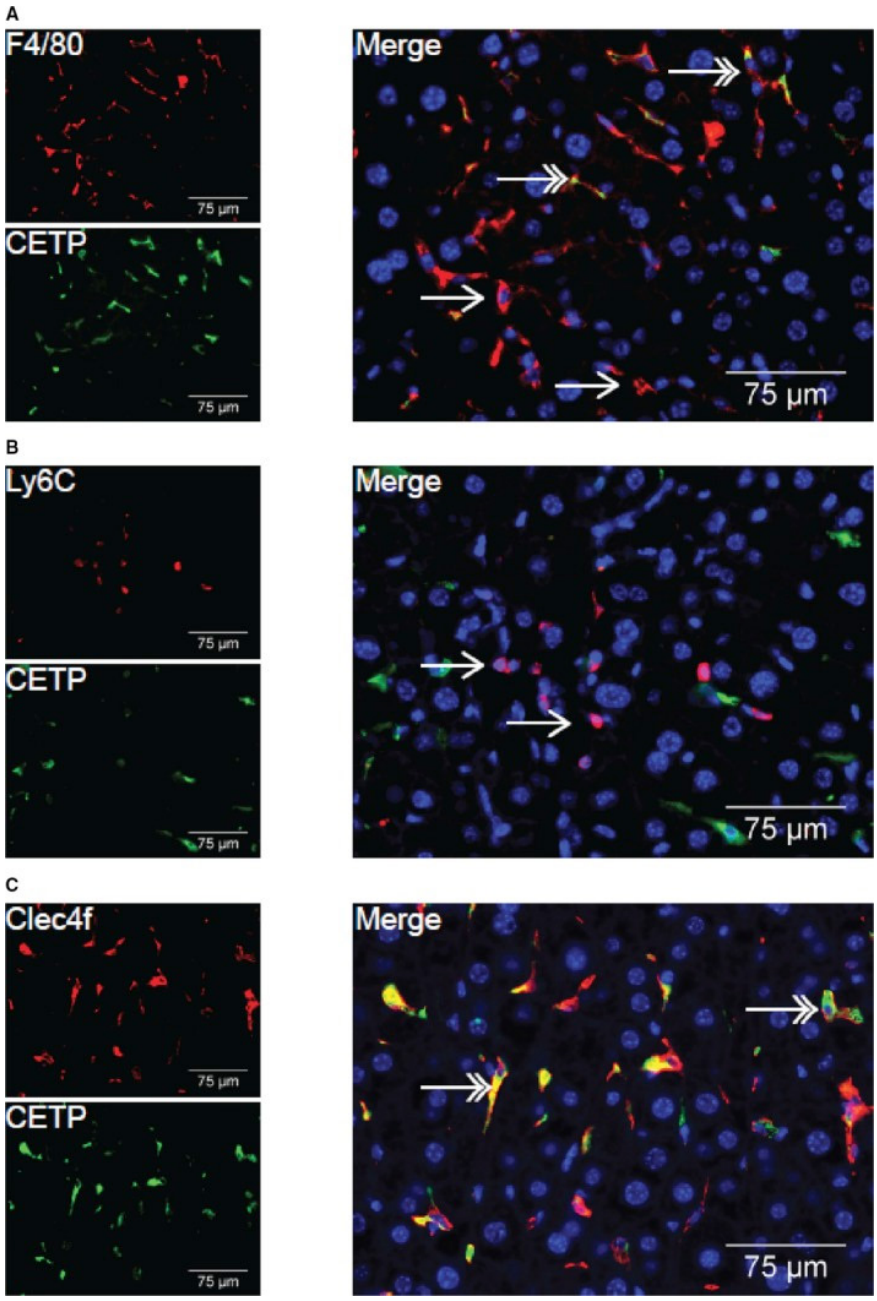

Figure 6. CETP protein is not co-localized with Ly6C protein, but does co-localize with Clec4f protein. Livers of non-injected female APOE*3-Leiden-CETP mice were assayed for co-localization of CETP and F4/80 (A), Ly6C (B) and Clec4f (C). Red; F4/80, Ly6C or Clec4f, Green; CETP, Blue; DAPI. Double headed arrows indicate co-localization, single headed arrows indicate no co-localization.

In humans, plasma CETP concentration correlates with hepatic VSIG4 expression and is reduced by LPS injection

By using previously generated microarray gene expression data from liver biopsies of 93 subjects who underwent elective bariatric surgery [20], we evaluated the correlation between hepatic expressions of CETP with markers for macrophage subsets in humans. In line with findings from E3L.CETP mice, hepatic expression of *CETP* in humans correlated with *VSIG4* (r=0.441; P<0.001, Fig 7A), but not *CD14* (Fig 7B), a marker for human monocytes [26]. Importantly, hepatic *VSIG4* expression significantly correlated with plasma CETP concentration in these subjects (r=0.303; P<0.05, Fig 7C). Adjustment for age and sex did not change these findings (not shown). Also, from a publicly available large data set of subjects undergoing bariatric surgery [27], we previously observed a high correlation between hepatic expression of CETP and the general macrophage marker MARCO (r=0.62, P=1.74x10-71) [10]. Using data from the same database, we now observed an even better correlation between the hepatic expression of *CETP* and *VSIG*4 (r=0.67, P=5.27x10-86) (Supplemental Fig IV), which suggests that, in humans, CETP is also expressed by KCs.

To evaluate whether LPS lowers plasma CETP levels in humans similarly as in E3L.CETP mice, we determined CETP levels in 20 healthy male individuals just before and 24 h after administration of LPS (HEAVEN study) [21]. Indeed, we observed that LPS also decreases plasma CETP concentration in humans (-10%; P<0.001, Fig 7D).

LPS stimulation decreases the LXR-mediated upregulation of CETP and VSIG4

In search for the underlying mechanism why KCs show decreased CETP expression in response to LPS, we performed an *in vitro* experiment using human peripheral blood monocyte-derived macrophages. As expected, treatment with the liver X receptor (LXR) agonist TO-901317 strongly increased mRNA expression of the target genes *ABCG1* (15-fold, Fig 7E) and *CETP* (6-fold, Fig 7F). Interestingly, stimulation with LPS decreased the LXR-mediated upregulation of *ABCG1* (Fig 7E) and *CETP* (Fig 7F), while LPS alone had no effect. Notably, the LXR agonist also increased the expression of *VSIG4* (+39%; P<0.05), which was similarly counteracted by LPS stimulation (Fig 7G). Collectively, these data suggest that LPS decreases the LXR-mediated upregulation of CETP and VSIG4 in KCs.

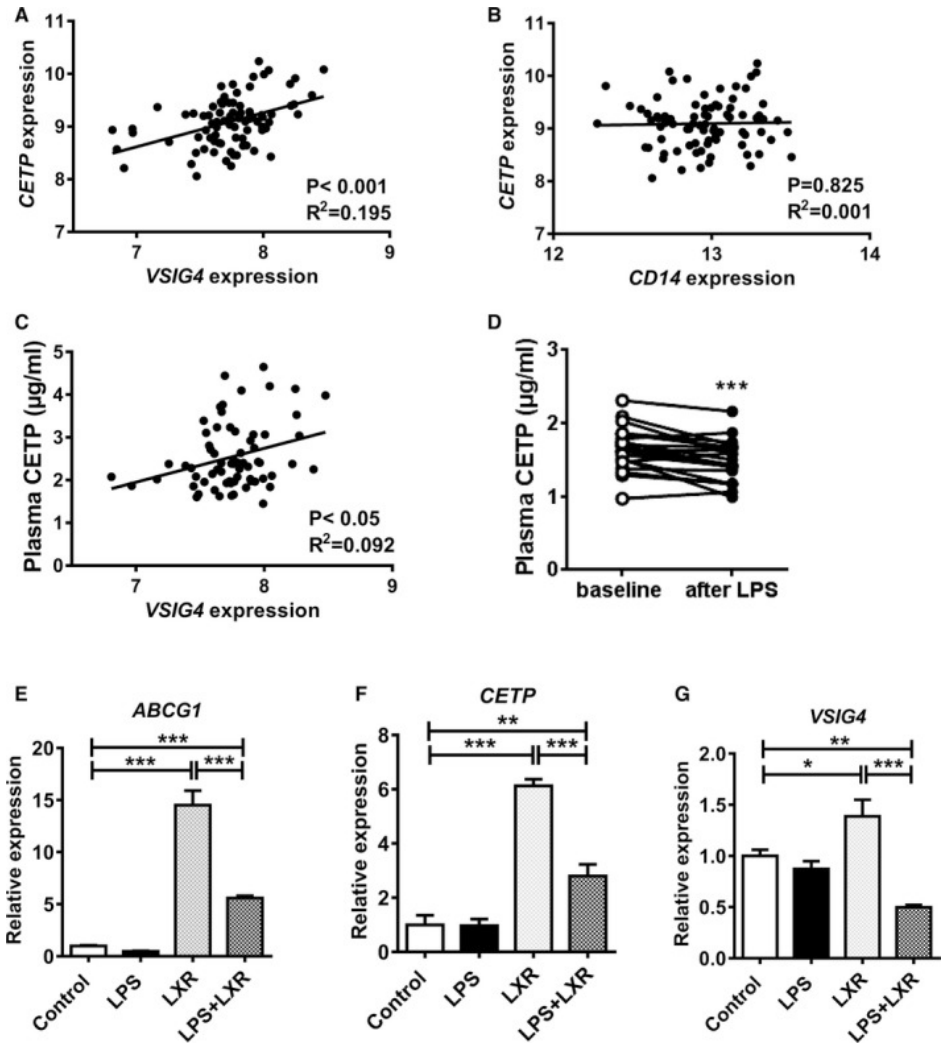

Figure 7. LPS reduces plasma CETP concentration that correlates with hepatic VSIG4 expression in humans. 93 liver biopsies were taken during bariatric surgery, and assayed for gene expression by microarray analysis. The correlation between the expression of *CETP* and *VSIG4* (A) and *CD14* (B), and plasma CETP concentration and *VSIG4* expression (C) were determined, and the goodness of fit R^2 from linear regression analyses was shown. (D) 20 healthy male subjects received a bolus infusion of 1 ng/kg body weight of LPS via the antecubital vein. After an overnight fast, blood samples were collected before (baseline) and 24 hours after LPS infusion, and plasma CETP concentration was determined. ***P<0.001 as compared to the baseline. (E-G) Human monocyte-derived macrophages were treated with vehicle (Control group), LPS (LPS group), TO-901317 (LXR group) and LPS+TO-901317 (LPS+LXR group). The mRNA expression of *ABCG1*, *CETP* and *VSIG4* was normalized to the Control group. Data are presented as means ± SEM (n=4).*P<0.05, **P<0.01, ***P<0.001.

Discussion

In the present study, we investigated the role of KC subsets in the mechanism by which LPS reduces hepatic CETP expression and plasma CETP concentration. Our data showed that LPS rapidly and markedly reduces hepatic expression of CETP in parallel with KC activation and reduced expression of resting KC markers, without affecting the hepatic macrophage content. The reduction in hepatic CETP expression caused a decrease in plasma CETP concentration, and consequently a shift of plasma cholesterol from non-HDL lipoproteins to HDL. We next confirmed that hepatic CETP is exclusively confined to the resting KC subset (i.e., F4/80^{+}Ly6C^{-}Clec4f^{+}Vsig4^{+}), while being absent from immature monocytes and/or activated KCs in the liver (i.e., F4/80^{+}Ly6C^{+}Clec4f^{-}Vsig4^{-}). Our data indicated that LPS regulates CETP expression and plasma lipoprotein composition via activating the resting KC subset.

We have previously demonstrated that the liver is the main source of plasma CETP, and that hepatic macrophages are responsible for the expression of CETP in humans and CETP transgenic (E3L.CETP) mice [10]. Furthermore, a recent study in which hepatectomized mice were repopulated with human primary hepatocytes showed that these liver-humanized mice did not express CETP in the liver and completely lacked CETP in serum [28], confirming that human hepatocytes do not express CETP. In addition, we observed that not all hepatic macrophages produce CETP, as supported by the fact that in the liver only 57% of F4/80+ macrophages co-express CETP in E3L.CETP mice and 39% of CD68+ macrophages co-express CETP in humans [10]. In the current study, double immunofluorescence staining of liver sections of E3L.CETP mice demonstrated that the CETP protein is confined to F4/80+Ly6C-Clec4f+ hepatic macrophages, and absent from F4/80+Ly6C+Clec4f- macrophages. Additionally, the kinetics of the restoration of plasma CETP concentration and hepatic macrophage subsets upon liposomal clodronate injection indicated that F4/80+Ly6C-Clec4f+ macrophages in the liver are the predominant cellular source of the plasma CETP pool. It should be noted that F4/80 is a general marker for monocytes and macrophages including, but not restricted to, KCs [3, 29]. Clec4f, also known as Kupffer cell receptor, has been identified as an exclusive marker for the resting KC [3, 30]. The reappearance of the different macrophage subsets indicated that Clec4f^{+} KCs take longer to reappear in the liver than F4/80^{+} macrophages (9 weeks versus 3-6 weeks), confirming that F4/80^{+}Clec4f^{+} KCs are more mature KCs than F4/80^{+}Clec4f^{-} macrophages. In contrast to mice, in humans *CLEC4F* expression is not confined to liver macrophages, while *VSIG4* is exclusively expressed by resting mature KCs [2, 31]. Here, we showed in mice that *Vsig4* mRNA and protein expression paralleled the reappearance of Clec4f and CETP expression. Gene expression analysis using microarrays of 93 liver biopsies obtained from bariatric surgery revealed a strong correlation between hepatic *CETP* expression and *VSIG4* expression in humans. Also, plasma CETP concentration correlates with *VSIG4* expression in human livers. Therefore, we conclude that hepatic CETP expression in humans is also confined to resting KCs, which is thus the predominant pool of plasma CETP.

We showed that a bolus injection of LPS into E3L.CETP mice rapidly reduces hepatic *CETP* expression, without affecting total hepatic macrophage content as shown by the number of $F4/80^+$ cells, indicating that LPS reduced CETP expression in hepatic macrophages *per se*. This finding is in concordance with previous *in vitro* data showing that LPS, and other inflammatory stimuli, such as TNFα and INFγ reduced *CETP* mRNA expression in bone marrow-derived macrophages from CETP transgenic mice and in human monocyte-derived macrophages [32]. In fact, LPS strongly reduced *Clec4f* expression in KCs *in vitro* [33]. Also, we now showed that upon LPS administration, hepatic *CETP* expression markedly positively correlates with the *Clec4f* expression, while it inversely correlates with the expression of *Ly6C* and macrophage activation markers, i.e., *Tnf*α, *Il-1*β and *Mcp-1*. This acute-phase rise in *Lbp* expression is probably mediated by pro-inflammatory cytokines, such as interleukin-1 [34], which has been shown to protect against LPS induced systemic inflammation [35]. We further observed that in healthy subjects, LPS also rapidly decreases plasma CETP concentration. Given the fact that hepatic CETP expression is confined to $F4/80^+Ly6C^-Clec4f^+Vsig4^+$ resting mature KCs, our data indicate that LPS rapidly activates resting KCs to become $Clec4f^-$ macrophages in mice, or $VSIG4^-$ macrophages in human livers, simultaneously reducing hepatic CETP expression and decreasing plasma CETP concentration. The pro-inflammatory signals derived from activated KCs, such as TNFα, IL-1β and MCP-1, may drive a vicious cycle activating $F4/80^+Ly6C^-VSIG4^+$ KCs to lose the expression of VSIG4. Indeed, a previous study [2] has demonstrated that VSIG4 expression is restricted to resting macrophages and that expression was completely lost in inflamed macrophages.

The CETP gene promoter contains LXR binding elements [36], and LXR activation strongly increases CETP gene expression and plasma CETP levels [37]. In addition, LXR signaling plays a crucial role in driving the specialization of macrophage subsets [38]. In pursuit of the underlying mechanism why KCs show decreased CETP expression in response to LPS, we treated human blood monocyte-derived macrophages with an LXR agonist, LPS or both. Our data are consistent with a mechanism in which LPS reduces the LXR-induced expression of CETP in macrophages. Interestingly, we observed that LXR activation also increased the expression of *VSIG4*, which was counteracted by LPS stimulation. Since the promoter of *VSIG4* contains no classical LXR-responsive element [39], the exact mechanism underlying this upregulation is currently unknown, but may involve a distal or non-classical LXR-responsive element. Nevertheless, it is thus likely that downregulation of CETP and VSIG4 by LPS in the macrophage are parallel events. Notably, LPS administration to mice also largely decreased the mRNA expression of the LXR-target gene *Abcg1* in liver. Since *Abcg1* mRNA expression levels in KCs is 70-fold higher than in parenchymal hepatocytes [40], our *in vivo* data confirm that LPS stimulation decreases LXR activation in KCs.

CETP is a member of the LPS binding protein (LBP) family, which includes phospholipid transfer protein (PLTP), bactericidal permeability increasing protein (BPI) and LBP itself. While LPS decreased *CETP* expression, it increased *Lbp* expression.

Interestingly, the reduction in *Pltp* mRNA expression, which is in line with previous findings [41], coincided with the reduction in *CETP* mRNA expression. CETP has a very low binding affinity to LPS (Kd>25 mM), as compared to LBP (Kd=0.8 nM) and BPI (Kd=0.5 nM) [42]. Therefore, CETP likely only plays a role in LPS binding in the acute phase of LPS exposure, when circulating LPS concentration is high. This may explain the observation that CETP expression markedly improves the mouse survival rate after injection of a lethal dose of LPS [17]. In addition, CETP plays an important role in lipoprotein metabolism in humans. After secretion into the circulation, the CETP protein binds mainly to HDL, and promotes bidirectional transfer of CE, TG, and to lesser extent phospholipid between plasma lipoproteins. Upon LPS administration, reduced plasma CETP concentration results in increased HDL, which has well-documented anti-inflammatory properties [43, 44]. A recent study showed that increasing HDL via CETP inhibition inhibited neointimal hyperplasia in balloon-injured rabbits, that the benefit was attributed to the anti-inflammatory properties of HDL [45]. In fact, it has previously been demonstrated that low HDL-C in healthy subjects was associated with an increased inflammatory response to an LPS challenge [21], further supporting the anti-inflammatory role of endogenous HDL. It is thus tempting to speculate that CETP-expressing species have increased flexibility to respond to invading Gram-negative organisms that release endotoxin/LPS. The rapid conversion of KC subsets to lose CETP expression and subsequently increase HDL may be of importance in the defense against Gram-negative bacterial infections.

It should be mentioned that the E3L.CETP mice express the human CETP minigene under the control of its natural flanking regions [36]. Although it cannot be excluded that some regulatory elements may be missing from this construct, this human CETP transgenic mice were shown to respond in a human-like fashion to LXR agonism [37] and FXR agonism [46]. Notably, in E3L.CETP mice, the markedly increased HDL-C/nonHDL-C ratio was already normalized at 48 hours after LPS injection, whereas plasma CETP level and hepatic CETP mRNA expression were still lower at this time point. Moreover, in healthy subjects, 24 hours after LPS injection, they had decreased plasma TG [21] and CETP concentration as shown in the present study, while plasma HDL-C was not changed [21]. Together, this indicates that LPS exposure not only affects CETP expression but also other pathways involved in lipoprotein metabolism [47].

In conclusion, our findings show that hepatic CETP is exclusively expressed by resting KCs (i.e., F4/80^{+}Ly6CClec4f^{+}) but not by activated macrophages or monocytes in the liver. In response to inflammatory stimuli, i.e., LPS exposure, resting KCs become activated and lose CETP expression. As a consequence, plasma CETP concentration is also rapidly decreased and HDL-C is raised. This sequence of events may play a role in the host defense via the anti-inflammatory effects of HDL. The strong association between the expression of CETP and activation markers by KCs implies that modulating HDL metabolism via CETP inhibition may affect the inflammatory status of the liver.

References

1. Helmy, K.Y., et al., *CRIg: a macrophage complement receptor required for phagocytosis of circulating pathogens.* Cell, 2006. **124**(5): p. 915-27.
2. Vogt, L., et al., *VSIG4, a B7 family-related protein, is a negative regulator of T cell activation.* J Clin Invest, 2006. **116**(10): p. 2817-26.
3. Yang, C.Y., et al., *CLEC4F is an inducible C-type lectin in F4/80-positive cells and is involved in alpha-galactosylceramide presentation in liver.* PLoS One, 2013. **8**(6): p. e65070.
4. Lavin, Y., et al., *Tissue-resident macrophage enhancer landscapes are shaped by the local microenvironment.* Cell, 2014. **159**(6): p. 1312-26.
5. Harris, R.L., et al., *Manifestations of sepsis.* Arch Intern Med, 1987. **147**(11): p. 1895-906.
6. Lichtman, S.N., J. Wang, and J.J. Lemasters, *Lipopolysaccharide-stimulated TNF-alpha release from cultured rat Kupffer cells: sequence of intracellular signaling pathways.* J Leukoc Biol, 1998. **64**(3): p. 368-72.
7. Chensue, S.W., et al., *In vivo biologic and immunohistochemical analysis of interleukin-1 alpha, beta and tumor necrosis factor during experimental endotoxemia. Kinetics, Kupffer cell expression, and glucocorticoid effects.* Am J Pathol, 1991. **138**(2): p. 395-402.
8. McCuskey, R.S., et al., *Kupffer cell function in host defense.* Rev Infect Dis, 1987. **9 Suppl 5**: p. S616-9.
9. Bilzer, M., F. Roggel, and A.L. Gerbes, *Role of Kupffer cells in host defense and liver disease.* Liver Int, 2006. **26**(10): p. 1175-86.
10. Wang, Y., et al., *Plasma cholesteryl ester transfer protein is predominantly derived from Kupffer cells.* Hepatology, 2015. **62**(6): p. 1710-22.
11. Thompson, A., et al., *Association of cholesteryl ester transfer protein genotypes with CETP mass and activity, lipid levels, and coronary risk.* JAMA, 2008. **299**(23): p. 2777-88.
12. Barter, P.J., et al., *Effects of torcetrapib in patients at high risk for coronary events.* N Engl J Med, 2007. **357**(21): p. 2109-22.
13. Schwartz, G.G., et al., *Effects of dalcetrapib in patients with a recent acute coronary syndrome.* N Engl J Med, 2012. **367**(22): p. 2089-99.
14. Eyvazian, V.A. and W.H. Frishman, *Evacetrapib: Another CETP Inhibitor for Dyslipidemia With No Clinical Benefit.* Cardiol Rev, 2017. **25**(2): p. 43-52.
15. *Kenilworth NJ*. June 27, 2017]; Available from: http://www.businesswire.com/news/home/20170627005544/en/Merck-Update-REVEAL-Outcomes-Study-Anacetrapib.
16. Bingle, C.D. and C.J. Craven, *Meet the relatives: a family of BPI- and LBP-related proteins.* Trends Immunol, 2004. **25**(2): p. 53-5.

17. Cazita, P.M., et al., *Human cholesteryl ester transfer protein expression enhances the mouse survival rate in an experimental systemic inflammation model: a novel role for CETP.* Shock, 2008. **30**(5): p. 590-5.

18. Masucci-Magoulas, L., et al., *Decreased cholesteryl ester transfer protein (CETP) mRNA and protein and increased high density lipoprotein following lipopolysaccharide administration in human CETP transgenic mice.* J Clin Invest, 1995. **95**(4): p. 1587-94.

19. Westerterp, M., et al., *Cholesteryl ester transfer protein decreases high-density lipoprotein and severely aggravates atherosclerosis in APOE*3-Leiden mice.* Arterioscler Thromb Vasc Biol, 2006. **26**(11): p. 2552-9.

20. Wolfs, M.G., et al., *Co-expressed immune and metabolic genes in visceral and subcutaneous adipose tissue from severely obese individuals are associated with plasma HDL and glucose levels: a microarray study.* BMC Med Genomics, 2010. **3**: p. 34.

21. Birjmohun, R.S., et al., *High-density lipoprotein attenuates inflammation and coagulation response on endotoxin challenge in humans.* Arterioscler Thromb Vasc Biol, 2007. **27**(5): p. 1153-8.

22. Mandrekar, P., et al., *An essential role for monocyte chemoattractant protein-1 in alcoholic liver injury: regulation of proinflammatory cytokines and hepatic steatosis in mice.* Hepatology, 2011. **54**(6): p. 2185-97.

23. Murray, P.J. and T.A. Wynn, *Protective and pathogenic functions of macrophage subsets.* Nat Rev Immunol, 2011. **11**(11): p. 723-37.

24. Inokuchi, S., et al., *Disruption of TAK1 in hepatocytes causes hepatic injury, inflammation, fibrosis, and carcinogenesis.* Proc Natl Acad Sci U S A, 2010. **107**(2): p. 844-9.

25. van Rooijen, N. and A. Sanders, *Elimination, blocking, and activation of macrophages: three of a kind?* J Leukoc Biol, 1997. **62**(6): p. 702-9.

26. Yang, J., et al., *Monocyte and macrophage differentiation: circulation inflammatory monocyte as biomarker for inflammatory diseases.* Biomark Res, 2014. **2**(1): p. 1.

27. Greenawalt, D.M., et al., *A survey of the genetics of stomach, liver, and adipose gene expression from a morbidly obese cohort.* Genome Res, 2011. **21**(7): p. 1008-16.

28. Minniti, M.E., et al., *Liver-Humanized Mice Exhibit Lipoprotein-Specific Phenotypes When Grafted with Human Hepatocytes from Different Donors.* Atherosclerosis, 2017. **263**: p. E7-E7.

29. Klein, I., et al., *Kupffer cell heterogeneity: functional properties of bone marrow derived and sessile hepatic macrophages.* Blood, 2007. **110**(12): p. 4077-85.

30. Haltiwanger, R.S., et al., *The distribution and localization of the fucose-binding lectin in rat tissues and the identification of a high affinity form of the mannose/N-acetylglucosamine-binding lectin in rat liver.* J Biol Chem, 1986. **261**(16): p. 7433-9.

31. Jung, K., et al., *Protective role of V-set and immunoglobulin domain-containing 4 expressed on kupffer cells during immune-mediated liver injury by inducing tolerance of liver T- and natural killer T-cells.* Hepatology, 2012. **56**(5): p. 1838-48.

32. Lakomy, D., et al., *Liver X receptor-mediated induction of cholesteryl ester transfer protein expression is selectively impaired in inflammatory macrophages.* Arterioscler Thromb Vasc Biol, 2009. **29**(11): p. 1923-9.

33. Beattie, L., et al., *Bone marrow-derived and resident liver macrophages display unique transcriptomic signatures but similar biological functions.* J Hepatol, 2016. **65**(4): p. 758-768.

34. Kirschning, C., et al., *Control of transcriptional activation of the lipopolysaccharide binding protein (LBP) gene by proinflammatory cytokines.* Cytokines Cell Mol Ther, 1997. **3**(1): p. 59-62.

35. Lamping, N., et al., *LPS-binding protein protects mice from septic shock caused by LPS or gram-negative bacteria.* J Clin Invest, 1998. **101**(10): p. 2065-71.

36. Agellon, L.B., et al., *Reduced high density lipoprotein cholesterol in human cholesteryl ester transfer protein transgenic mice.* J Biol Chem, 1991. **266**(17): p. 10796-801.

37. Luo, Y. and A.R. Tall, *Sterol upregulation of human CETP expression in vitro and in transgenic mice by an LXR element.* J Clin Invest, 2000. **105**(4): p. 513-20.

38. N, A.G., et al., *The nuclear receptor LXRalpha controls the functional specialization of splenic macrophages.* Nat Immunol, 2013. **14**(8): p. 831-9.

39. Boergesen, M., et al., *Genome-wide profiling of liver X receptor, retinoid X receptor, and peroxisome proliferator-activated receptor alpha in mouse liver reveals extensive sharing of binding sites.* Mol Cell Biol, 2012. **32**(4): p. 852-67.

40. Hoekstra, M., et al., *Specific gene expression of ATP-binding cassette transporters and nuclear hormone receptors in rat liver parenchymal, endothelial, and Kupffer cells.* J Biol Chem, 2003. **278**(28): p. 25448-53.

41. Jiang, X.C. and C. Bruce, *Regulation of murine plasma phospholipid transfer protein activity and mRNA levels by lipopolysaccharide and high cholesterol diet.* J Biol Chem, 1995. **270**(29): p. 17133-8.

42. Clark, R.W., et al., *Assessment of cholesteryl ester transfer protein inhibitors for interaction with proteins involved in the immune response to infection.* J Lipid Res, 2010. **51**(5): p. 967-74.

43. Barter, P.J., et al., *Antiinflammatory properties of HDL.* Circ Res, 2004. **95**(8): p. 764-72.

44. Morin, E.E., et al., *HDL in sepsis - risk factor and therapeutic approach.* Front Pharmacol, 2015. **6**: p. 244.

45. Wu, B.J., et al., *Reduction of In-Stent Restenosis by Cholesteryl Ester Transfer Protein Inhibition.* Arterioscler Thromb Vasc Biol, 2017. **37**(12): p. 2333-2341.

46. Gautier, T., et al., *Farnesoid X receptor activation increases cholesteryl ester transfer protein expression in humans and transgenic mice.* J Lipid Res, 2013. **54**(8): p. 2195-205.

47. Konig, V., et al., *The significance of high-density lipoproteins (HDL) in the clearance of intravenously administered bacterial lipopolysaccharides (LPS) in mice.* Hepatogastroenterology, 1988. **35**(3): p. 111-5.

Supplemental tables and figures

Gene	Forward primer	Reverse primer
	CAGGAAGATTAGACACTGTGG	GAAAGGGGAATGGAGAGAAGA
βactin	AACCGTGAAAAGATGACCCAGAT	CACAGCCTGGATGGCTACGTA
β-2m	*TGACCGGCTTGTATGCTATC*	*CAGTGTGAGCCAGGATATAG*
CETP	CATGTCTCGGCTCGAGGTAG	TTCTGCTACAAGCCCCATCC
Clec4f	ACTGAAGTACCAAATGGACAATGTTAGT	GTCAGCATTCACATCCTCCAGA
F4/80	CTTTGGCTATGGGCTTCCAGTC	GCAAGGAGGACAGAGTTTATCGTG
Hprt	TTGCTCGAGATGTCATGAAGGA	AGCAGGTCAGCAAAGAACTTATAG
Il-1β	GCAACTGTTCCTGAACTCAACT	ATCTTTTGGGGTCCGTCAACT
Ly6c	CTGCAACCTTGTCTGAGAGGA	GTCCCTGAGCTCTTTCTGCAC
Mcp-1	GCATCTGCCCTAAGGTCTTCA	TTCACTGTCACACTGGTCACTCCTA
Tnfα	AGCCCACGTCGTAGCAAACCAC	TCGGGGCAGCCTTGTCCCTT
Vsig4	TCACCTATGGCCACCCCACC	AGGCGGCCTCTGTACTTTGCCT
VSIG4	CACTGACATGGATGGCTACCT	AAGACAGGCAGGCTCTTTCC

Supplemental Table 1. Primers sequences use for RT-qPCR.

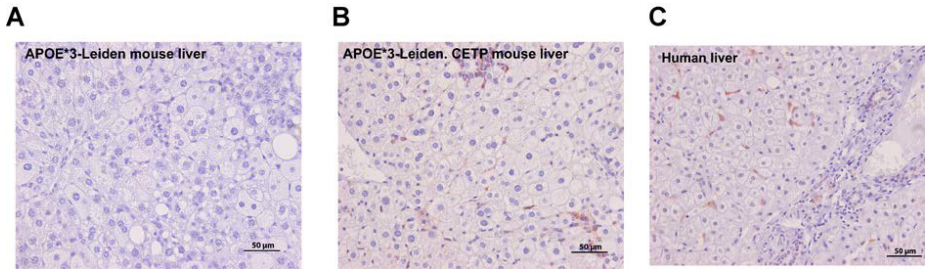

Figure S1. CETP staining in mouse and human livers. Representative picures of IHC staining of CETP protein in liver sections of (A) non-CETP transgenic mice (APOE*3-Leiden mice), (B) APOE*3-Leiden.CETP transgenic mice, and (C) a healthy human donor.

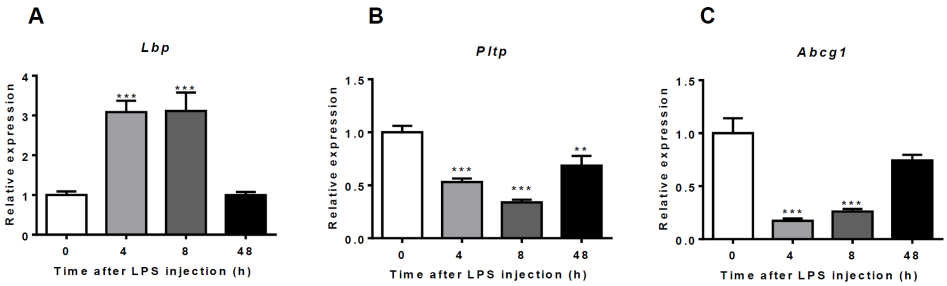

Figure S2. LPS acutely increases hepatic *Lbp* expression and decreases *Pltp* and *Abcg1* expression. Female APOE*3-Leiden.CETP mice fed a Western-type diet were intraperitoneally injected with 25 µg LPS, after which mice were sacrificed at the indicated time points. Livers were assayed for mRNA of (**A**) *Lbp*, (**B**) *Pltp* and (**C**) *Abcg1*. Data are presented as means ± SEM (n=7-8); **P<0.01, ***P<0.001 as compared to the 0 h group.

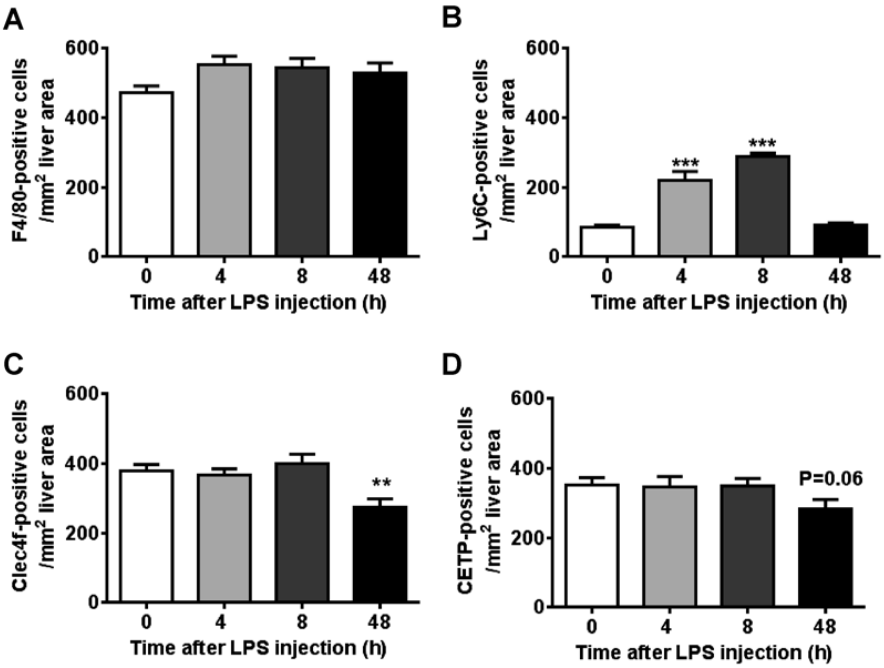

Figure S3. LPS acutely changes hepatic macrophage subsets rather than macrophage number. Female APOE*3-Leiden.CETP mice fed a Western-type diet were intraperitoneally injected with 25 µg LPS, after which mice were sacrificed at the indicated time points. Livers were assayed for F4/80-positive macrophages (**A**), Ly6C-positive monocytes (**B**), Clec4f-positive Kupffer cells (**C**) and CETP-positive cells (**D**). Data are presented as means ± SEM (n=7-8); **P<0.01, ***P<0.001 as compared to the 0 h group.

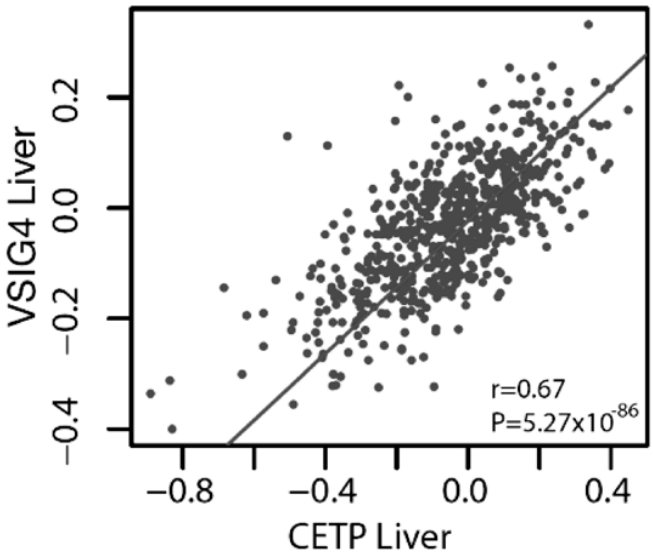

Figure S4. Hepatic *CETP* expression correlates with *VSIG4* expression in humans. Scatter plots of the correlation between the expression of *CETP* and *VSIG4* in liver was determined by using a publicly available dataset consisting of 651 subjects [1].

Supplemental Reference

1. Greenawalt, D.M., et al., *A survey of the genetics of stomach, liver, and adipose gene expression from a morbidly obese cohort.* Genome Res, 2011. **21**(7): p. 1008-16.

CHAPTER 7

GENERAL DISCUSSION AND FUTURE PERSPECTIVES

Obesity, an ever-growing health problem all over the world, is one of the leading causes of cardiometabolic diseases including type 2 diabetes (T2D), non-alcoholic fatty liver disease and cardiovascular diseases (CVD), with increasing morbidity and mortality. A systemic review from 16 cohort studies from the USA and Europe demonstrated that the risk of cardiometabolic multimorbidity increases as body mass index (BMI) increases: from 2-fold in overweight people (BMI between 25 and 30 kg/m^2) to more than 10-fold in severely obese people (BMI ≥ 35 kg/m^2) compared with individuals with a healthy BMI (between 18.5 and 25 kg/m^2) [1]. Thus, maintaining a healthy weight is essential for cardiometabolic health. The most direct way to lose weight is keeping a lower energy intake and/or higher energy expenditure. Thus, restriction of energy intake by adapting lifestyle or pharmacotherapy, and increasing energy expenditure by exercising more or activating brown adipose tissue (BAT), are drawing increasing attention in combating obesity. However, most current interventions are hard to adhere to in practice. Therefore, research into the development of novel strategies to combat obesity and associated cardiometabolic diseases should be of utmost scientific priority in our obesogenic society.

This thesis has investigated the bidirectional involvement of the gut-brain axis in cardiometabolic health: dietary administration of the short chain fatty acid (SCFA) butyrate appeared to both decrease food intake and increase energy expenditure via vagal stimulation, and electric stimulation of sympathetic outflow towards BAT appeared to increase energy expenditure. The promise and future of these therapeutic strategies to regulate energy metabolism will be discussed in this chapter.

Novel strategies based on gut-brain interaction to reduce appetite and combat obesity

The gut harbors an enormous diversity of microbes that have emerged as critical regulators of host energy homeostasis [2], particularly energy intake [3]. That is because gut microbiota interact with each other and/or the host, which can modulate cardiometabolic health in various ways, including through the metabolites they produce [4]. Among the gut microbial metabolites that impact on host health, SCFAs including acetate, propionate, and butyrate are perhaps the most extensively studied. SCFAs are the main products of gut microbiota-mediated fermentation of dietary fiber, of which high consumption has been widely accepted to be associated with lower body weight, lower incidence of metabolic diseases, and lower mortality from CVD [5, 6].

In mammals, the most abundant SCFA in both the gut and systemic circulation is acetate [7], showing a concentration up to approx. 69 mmol/L in the caecum [8] and approx. 125 μmol/L in blood plasma [9]. The fact that the concentration of acetate in the gut is approx. 1000-fold higher than in plasma suggests that acetate likely acts locally in the gut, probably by binding to the SCFAs receptors G-protein

coupled receptors 41 (GPR41) and 43 (GPR43). Besides in the intestine [10, 11], both receptors are also expressed in adipose tissue [12], pancreatic beta cells [13], skeletal muscle and liver [14], indicating that acetate may also directly act on these metabolic organs after absorption from the gut into the circulation. Convincing evidence indicates that administration of acetate to mice through intragastric injection [15] or dietary supplementation [16] protects against high fat diet (HFD)-induced body weight gain. However, evidence for such an effect of acetate in humans is still limited. Nevertheless, in humans, distal colonic infusion of acetate has been demonstrated to promote fat oxidation and improve metabolic health in obese subjects [17]. Altogether these findings suggest that acetate could exert beneficial metabolic effects by various ways of administration. Acetate has been shown to control appetite, although the way of administration seems important in that respect. Although evidence in humans is still lacking, rodent studies revealed that intragastric [18], intravenous or colonic administration of acetate [19] induce a significant reduction in food intake, but chronic dietary supplementation of acetate is ineffective [20]. Given that continuous oral acetate administration might affect the pH value of the stomach, thereby influencing gastral functions such as gastric emptying, food release and digestion, the differences in administration routes likely explain the different effects of oral acetate on controlling appetite. On the other hand, differences in results can also be attributed to differences in dosages, treatment durations, and animal models. Therefore, future comprehensive studies are still needed to compare the effects of different administration ways of acetate on energy intake, using comparable doses and treatment duration, and within a same experimental model.

Propionate is another SCFA, of which the abundance in humans is almost one-third of acetate [21]. Despite its lower concentration and being less frequently studied compared to acetate, propionate has also been demonstrated to act on GPR41 and GPR43 [14], and also protects against diet-induced obesity (DIO) and insulin resistance [20] in mice studies. Being one of the major gluconeogenic substrates in ruminants [22], propionate plays a particularly important role in regulating energy intake in these animals [23], but it also has certain effects on energy intake in non-ruminants. In fact, in contrast to acetate, chronic oral administration of propionate reduces cumulative food intake in mice [20]. Although the currently available evidence obtained from animal studies suggests the potential of propionate in combating obesity by reducing appetite, application of propionate in humans is hampered because of its poor organoleptic properties. To deal with this issue, propionate has been esterified to inulin. Interestingly, a study using inulin-propionate ester has been performed in the clinic, which confirmed that propionate is in fact able to reduce food intake and prevent weight gain in overweight humans, at least on short term [24]. However, in line with the findings showing that oral acetate does not affect food intake chronically in mice [20], supplementation of this inulin-propionate ester is also ineffective in regulating food intake in humans in the long term [24]. Since this ester liberates propionate directly in the colon, thereby bypassing the stomach and small intestine, it is unlikely that long-term treatment

with either acetate or propionate fails to reduce food intake by e.g., effects of pH in the stomach [25]. Alternatively, the SCFAs receptors GPR41 and GPR43 may be desensitized upon chronic SCFA administration, but this possibility still needs to be further investigated.

Although butyrate is the least abundant SCFA, with the abundance of butyrate in humans only around one-fourth of acetate [26], it has received much attention because it being one of the major energy sources for colonocytes [27]. In addition, butyrate has been described as an anticarcinogenic agent that prevents the growth of colon epithelial cells [28] by inhibiting histone deacetylase (HDAC) [29] and binding to GPR109A, a third SCFA receptor [30]. Therefore, butyrate has been emerging in the clinic as an agent for the treatment of colorectal cancer [31] and inflammatory bowel disease [32]. In addition to these beneficial anti-tumor and anti-inflammatory effects, accumulating evidence suggests similar beneficial properties of butyrate on cardiometabolic health as that of acetate and propionate. Butyrate appeared to also act on GPR41 [33] and GPR43 [14], and was previously found to acutely reduce food intake in mice when administered by mixing into the diet [20], and to prevent DIO [20], improve glucose homeostasis and alleviate insulin resistance [34]. Although at that time there was still limited understanding of the long-term effects of butyrate on appetite, all of the above findings collectively suggest the potential of applying butyrate in the clinic to combat obesity and improve cardiometabolic health. To compare the effects of different administration ways of butyrate on cardiometabolic health and investigate whether there is desensitization of the response of SCFA receptors to butyrate with respect to regulating food intake on the long term, we performed a comprehensive study in APOE*3-Leiden.CETP mice, a well-established translational model for human-like cardiometabolic diseases, that received butyrate by intragastric gavage, intravenous injection, or by chronic (i.e., 9-weeks) dietary supplementation. We found that intragastric butyrate, but not intravenous butyrate, acutely reduced food intake (**Chapter 2**), suggesting that the effect of butyrate on energy intake is indeed dependent on the way of administration, and hints to potential pathways underlying the butyrate-induced reduction in appetite as will be discussed later. In addition, long-term treatment with dietary butyrate showed a persistent reduction in food intake, strongly indicating that desensitization of the response of SCFA receptors to butyrate does not occur (**Chapter 2**). Furthermore, by performing a pair-feeding study in which a group of mice received the same amount of diet as that consumed by butyrate group, we elucidated that dietary butyrate mainly (i.e., 60-70%) prevents DIO and improves insulin sensitivity by reducing energy intake (**Chapter 2**). Collectively, our findings propose dietary administration of butyrate rather than acetate or propionate as a promising strategy to reduce appetite and combat obesity and associated cardiometabolic diseases.

Although certain beneficial anti-tumor [31] and anti-inflammatory [32] effects of butyrate have been confirmed in the clinic, the metabolic effects of butyrate in humans still remain controversial. A recent, and actually the only clinical

study to investigate the beneficial effects of dietary butyrate on cardiometabolic health showed that oral butyrate treatment improves glucose metabolism in lean individuals, but not in individuals with the metabolic syndrome [35]. One of the underlying reasons may be the differences in age, since in that study individuals with metabolic syndrome were significantly older than lean controls. Another plausible reason is that the dose used for both lean and obese subjects (i.e., 4 g/day) might result in a subtherapeutic dose of butyrate in the more obese subjects, especially as dosing is usually adjusted to body weight or surface area. Thus, future studies designed to include subjects with the same age, and with adjustment of the dose of butyrate to BMI are still needed. In fact, we performed such a study in lean and DIO APOE*3-Leiden.CETP mice of the same age, who received butyrate mixed in the diet. Interestingly, similar to the findings from the human study, while dietary butyrate effectively reduced food intake and prevented body weight gain in lean mice, butyrate was ineffective in reducing food intake and inducing weight loss in DIO mice (**Chapter 3**). Our study thus strongly suggests that the differential metabolic effects of dietary butyrate in lean versus obese human subjects is caused by metabolic state rather than age. Although the precise underlying reason is still unclear, this may well be related to differences in gut microbiome composition between lean and obese subjects, as will be elaborated on later in this Chapter. Additional human studies aimed at revealing beneficial effects of butyrate on cardiometabolic health might provide valuable information and clues to help us understand and unravel mechanisms further.

Studies on physiological concentrations of SCFAs in the brain are still scarce. However, in addition to being present in the gut and circulation, acetate, propionate and butyrate are also detectable in the human cerebrospinal fluid [36]. Since SCFAs are not produced in the brain, this indicates that SCFAs may travel from the intestine through the circulation to directly regulate energy intake within the brain. Indeed, a mouse study using *in vivo* ^{11}C-acetate and PET-CT scanning has shown that colonic acetate is able to cross the blood-brain barrier [19]. To our knowledge, whether propionate and butyrate can also cross the blood brain barrier is currently unknown. Interestingly, instead of via the circulation, propionate has been reported to reduce appetite in ruminants via acting in the gut on the vagal nerve [37]. It is known that central terminals of the vagal nerve innervate the brainstem, where vagal nerve transmission, such as energy status signals from the gut, projects onto the hypothalamus, thereby forming a circuit to regulate energy intake [38]. However, whether butyrate would attenuate energy intake by directly acting on the brain via traveling through the circulation (as shown for acetate) or indirectly acting on the brain via the vagal nerve (as shown for propionate) was still unclear. Thus, in **Chapter 2**, we investigated the involvement of these two pathways in the regulation of appetite in APOE*3-Leiden.CETP mice by increasing circulating butyrate via intravenous injection, or increasing butyrate in the gut via oral administration. Our findings that only dietary butyrate reduces food intake, coinciding with reduced activity of orexigenic NPY neurons, which control appetite in the hypothalamus, and decreased neuron activity within the NTS, where terminals of the vagal nerve

innervate the brainstem (**Chapter 2**), collectively indicate that the effect of butyrate on reducing energy intake is likely mediated via vagal inputs to NPY neurons. In fact, we confirmed this by showing that subdiaphragmatic vagotomy, which blocks vagal signaling, abolished the dietary butyrate-induced reduction in appetite (**Chapter 2**). In addition, our findings that a specific increase of butyrate within the circulation is ineffective in reducing energy intake (**Chapter 2**), in fact suggest that hypothalamic neuronal sensing of peripheral energy status via the vagal nerve is likely the only pathway underlying the dietary butyrate-induced reduction in appetite. Thus, although there is still no evidence to support the role of the vagal nerve in the effect of acetate to regulate energy intake, we speculate that probably all SCFAs that are produced within the gut can act on the vagal nerve as the main pathway by which they indirectly regulate energy intake. However, in addition to the neural circuit, and in contrast to propionate and butyrate, acetate seems to also act on the brain directly through the circulation, which may be related to its higher abundance within the circulation and its smaller molecular weight, by which it passes the blood-brain barrier more readily. However, the exact mechanisms underlying potential actions of acetate within the brain are yet to be elucidated. Likewise, how SCFAs activate the vagal nerve was yet to be fully elucidated.

Incretins such as GLP-1 are likely involved in the effects of SCFAs on activation of the vagal nerve to regulate energy intake centrally. Firstly, it was demonstrated that SCFAs can increase intestinal GLP-1 secretion in humans, as both rectal and intravenous administration of acetate increase plasma GLP-1 [39]. Although the relevance for humans still has to be shown, propionate was also observed to stimulate intestinal GLP-1 secretion in rodents [40]. We now added to these finding by demonstrating that dietary butyrate increases intestinal GLP-1 secretion and plasma GLP-1 in mice (**Chapter 4**). Although the increase in plasma GLP-1 could mediate the effects of dietary SCFAs by binding to central GLP-1 receptors (GLP-1R), such a pathway explaining the effects of SCFAs on energy intake is unlikely, again given that dietary butyrate is ineffective after vagotomy. Rather, GLP-1 that is released from intestinal L-cells can regulate food intake by directly acting on GLP-1R located on the vagal nerve [41]. In fact, this mechanism is strongly supported by a rodent study showing that peripherally administered GLP-1 activates vagal afferents [42] as well as by a clinical study demonstrating that the effect of GLP-1 on reducing food intake is lost in vagotomised males [43]. Future studies using e.g., knockdown of the GLP-1R in the vagal afferent, are still needed to conclusively establish the involvement of GLP-1R signaling in the vagal nerve in the effects of butyrate on regulating energy intake. Nevertheless, it is likely that GLP-1-mediated activation of the vagal nerve is coupled to the central release of GLP-1 that subsequently acts on central GLP-1R to reduce appetite. In fact, although GLP-1 is mainly secreted by intestinal L-cells, it is also produced to a modest extent by neurons in the hindbrain [44] to bind to GLP-1R expressed in the central neural system [45]. This hypothesis is supported by rodent studies demonstrating that direct intracerebroventricular (ICV) administration of either GLP-1 or the GLP-1R agonist Exendin-4 reduce appetite and induce weight loss [46, 47], which can be reversed by ICV administration of

the GLP-1R antagonist Exendin (9-39) [48]. Indeed, in **Chapter 4** we revealed the involvement of central GLP-1R signaling in the dietary butyrate-induced reduction in appetite, as ICV administration of GLP-1R antagonist Exendin (9-39) completely abolished the effect of dietary butyrate on reducing food intake in mice. It would be of interest to further study the contribution of central GLP-1R signaling to the role of dietary SCFAs in the regulation of energy intake using brain/neuron-specific GLP-1R knockout mice. Taken all these findings together, it is reasonable to speculate that dietary butyrate, and probably also acetate and propionate, stimulates L-cells in the gut to promote secretion of GLP-1, which binds to GLP-1R in the vagal nerve and subsequently reduces energy intake via secondarily activating central GLP-1R signaling. In addition to GLP-1, other gut hormones including peptide YY (PYY) and glucose-dependent insulinotropic polypeptide (GIP) may also contribute to the effects of gut SCFAs on regulating food intake. At least PYY is increased by acetate [39], propionate [40] and butyrate [49] administrated to experimental models and humans. However, whether PYY is causative to the SCFAs-regulated energy intake, and whether GIP may play an additional role, remains to be further elucidated.

Mice that lack GPR41 or GPR43 exhibit reduced SCFA-triggered GLP-1 secretion [50] indicating that acetate, propionate and butyrate increase GLP-1 secretion by acting on these receptors. Interestingly, in **Chapter 3**, we demonstrated that the effects of dietary butyrate on the reduction of appetite were completely abolished after antibiotics-induced gut microbiota depletion, strongly suggesting that dietary butyrate *per se* is not likely to trigger GLP-1 secretion via binding to GPR41 or GPR43. Rather, dietary butyrate stimulates GLP-1 via acting on gut microbiota, the composition of which we showed to be changed by dietary butyrate (**Chapter 2**). In fact, fecal microbiota transplantation studies proved the causality of gut microbiota in the dietary butyrate-induced reduction in appetite (**Chapter 3**). Such a mechanism is likely relevant to humans as well, since gut microbial fermentation of prebiotics, e.g., oligofructose and inulin, which is an effective approach to produce SCFAs, increases satiety and improves glucose homeostasis associated with increased plasma GLP-1 [51, 52]. Likewise, a seminal human study showed that dietary fiber promotes butyrate-producing bacterial strains in the gut accompanied by an increased GLP-1 response and amelioration of T2D [53]. However, although these studies collectively indicate a role of gut microbiota in promoting intestinal GLP-1 release by SCFAs, the specific strain(s) involved in the beneficial effects of SCFAs on stimulating GLP-1 production still had to be conclusively demonstrated. By performing metagenomics in **Chapter 3**, we revealed that dietary butyrate in lean mice, but not in DIO mice, rather specifically increases the abundance of the bacterial strain *Lachnospiraceae bacterium 28-4*. Furthermore, we demonstrated that the richness of this specific strain negatively correlates with energy intake, indicating that dietary butyrate probably triggers the GLP-1 pathway to regulate food intake via promoting the amplification of this specific strain. As such, the richness of *Lachnospiraceae bacterium 28-4*, in relation to a favorable environment in the gut for its proliferation, may be the main explanation underlying the observation that dietary butyrate has beneficial metabolic effects in lean but not obese subjects.

However, the causality of *Lachnospiraceae bacterium 28-4* in the beneficial effects of dietary butyrate on regulating GLP-1 secretion and food intake should still be clarified. To answer these questions, isolation and amplification of *Lachnospiraceae bacterium 28-4 in vitro* would be essential to perform future intervention studies and show causality. Nevertheless, our findings collectively indicate the potential of *Lachnospiraceae bacterium 28-4* as a novel therapeutic handle to reduce appetite and combat obesity and related cardiometabolic diseases. Of note, a recent concept study demonstrated the feasibility of administering *Akkermansia muciniphila*, which is another gut bacterial strain, to improve insulin resistance, providing a promising start for developing future clinical interventions with gut microbiota manipulation [54]. Most notably, *Pendulum Glucose Control* ™, a combination of probiotics containing *Akkermansia muciniphila*, was launched in 2020 as the first and only medical probiotic designed specifically for the dietary management of T2D [55]. All these findings collectively pave the way for assessing the therapeutic potential of *Lachnospiraceae bacterium 28-4* in reducing energy intake and combating obesity and its associated cardiometabolic diseases in humans. However, we still have some obvious hurdles to take to achieve this goal in the clinic.

Based on our studies and literature to date, as depicted in **Figure 1**, our working hypothesis is that dietary butyrate attenuates DIO and ameliorates cardiometabolic health, mainly by reducing appetite, via selectively promoting the growth of *Lachnospiraceae bacterium 28-4* within the gut to stimulate intestinal L-cells to secrete GLP-1*,* which targets the GLP-1R in the vagal nerve to activate an afferent neural circuit and secondarily activates central GLP-1R signaling to reduce the activity of NPY neurons in the hypothalamus.

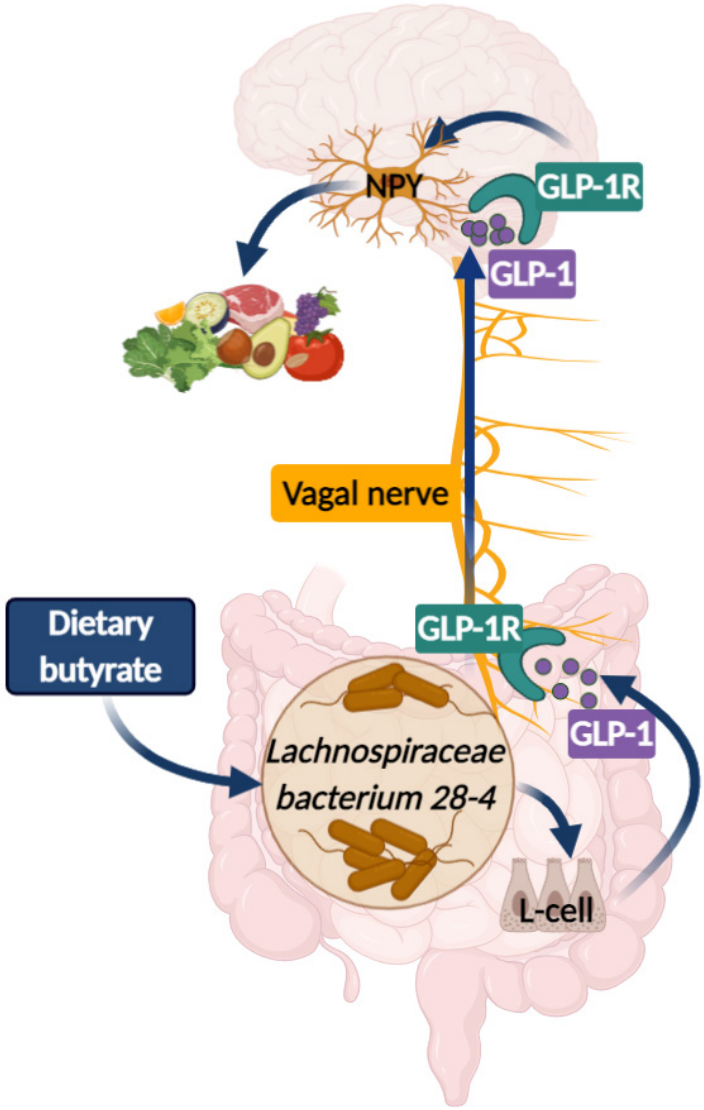

Figure 1. Working hypothesis explaining the effect of dietary butyrate on reducing appetite. We hypothesize that dietary butyrate selectively promotes *Lachnospiraceae bacterium 28-4* within the gut to stimulate intestinal L-cells to secrete GLP-1, which activates GLP-1R on the vagal nerve that subsequently projects to the hypothalamus to activate central GLP-1R signaling to reduce the activity of NPY neurons and reduce appetite. GLP-1, glucagon-like peptide-1; GLP-1 receptors, GLP-1R; NPY, neuropeptide Y.

Undoubtedly, energy intake restricting strategies are among the most effective interventions for treating obesity and related cardiometabolic diseases. Although the most prominent effects on reducing obesity in the clinic are probably achieved with bariatric surgery, this procedure is only available to morbidly obese individuals, is highly invasive, and suffers from several adverse events including surgical complications, perioperative technical adverse outcomes and mortality [56, 57]. In addition, several anti-obesity agents have been developed and are clinically applied to regulate energy intake. For example, subcutaneous administration of GLP-1 analogues such as liraglutide has been widely demonstrated to induce weight loss in mice and humans by downregulating energy intake [58, 59], and less invasive GLP-1R agonists are being developed including semaglutide that is effective after oral administration [60]. An even more promising pharmacological treatment strategy for obesity and T2D being developed is dual GIP and GLP-1R agonism, showing even better efficacy with regard to glucose control and weight loss than stimulation of GLP-1R alone [61]. However, a high probability of developing adverse effects, e.g., nausea and vomiting, is still the main concern of these pharmacotherapies, particularly in their application for long-term weight management [62].

As previously outlined in this chapter, SCFAs are the main intermediates in the beneficial effects of dietary fiber, and have shown various metabolic properties in improving cardiometabolic health [63], particularly by reducing energy intake [64] and inducing weight loss [65]. Among the SCFAs, butyrate has already been widely emerging as a nutritional supplementary in the clinic for the treatment of cancer, inflammatory bowel disease, inherited disorders and neurodegeneration [66]. Our collective data as described in this thesis show that dietary butyrate reduces energy intake, thereby preventing DIO and improving insulin resistance, without inducing any apparent unfavorable effects, at least in mice (**Chapters 2, 3 and 4**). Since non-invasive treatment with dietary butyrate would be more practical and acceptable to attain persistent weight loss compared to other pharmacotherapies, e.g., using subcutaneous GLP-1 agonists [59], dietary butyrate has great therapeutic potential as a novel and feasible strategy to regulate energy intake and combat obesity in humans.

Novel strategies to sympathetically activate brown adipose tissue in the context of obesity

BAT has long been known as a metabolic tissue contributing to energy expenditure in small rodents and infants. Only twelve years ago, BAT has been revealed to be present in human adults as well [67], and to contribute to metabolic health [68]. In fact, chronic cold exposure to activate BAT results in modest weight loss [69]. Collectively, these findings indicate the theoretic therapeutic potential of activation of BAT in combating obesity and associated cardiometabolic diseases. However, given the relatively low abundance of BAT in humans, especially as compared to mice in which BAT activation very efficiently induces weight loss, effective strategies

to activate BAT thereby combating obesity clinically are still needed.

Cold exposure is one of the most effective physiological activators of BAT by inducing adrenergic stimulation through the sympathetic nervous system. Previous studies have already shown that short-term cold exposure activates BAT with respect to increased uptake of the glucose analogue [^{18}F]fluorodeoxyglucose ([^{18}F]FDG) in healthy men [70] as well as obese men [71], and only 10 days of cold exposure even increases peripheral insulin sensitivity in patients with T2D [72]. Collectively, these studies indicate that cold acclimation is a feasible strategy to activate BAT and improve metabolic health in the clinic. Indeed, cold bathing, a general method to induce cold acclimation, has been claimed to have multiple beneficial effects on metabolic health, such as improving cardiovascular circulation and vitality [73]. However, for many individuals long-term cold exposure does not seem suitable as it is uncomfortable and, therefore, hard to adhere to. Hence, innovative strategies aimed to chronically activate BAT in the context of obesity are still warranted.

Agonism of beta-adrenergic receptors (β-ARs, including β1-AR, β2-AR and β3-AR) has been proposed as an effective pharmacological strategy to increase sympathetic nervous system activity resulting in activating BAT. For example, the β3-AR agonist *CL-316243* was initially found to increase energy expenditure in rats [74] and our group has demonstrated that *CL-316243* also reduces hypercholesterolemia and protects from atherosclerosis development by activating BAT, at least in APOE*3-Leiden.CETP mice with an intact ApoE-LDL receptor clearance pathway for triglyceride-rich lipoprotein remnants [75]. In addition, *L-796568* was among the first β3-AR agonists to increase energy expenditure in humans [76], and caused an acute increase in energy expenditure by +8% in obese subjects [77]. However, *L-796568* did not show beneficial effects on the long term, as evidenced by lack of significant lipolytic or thermogenic effects on BAT after 4 weeks administration [78]. Another well-investigated β3-AR agonist in the clinic is mirabegron, which has been approved for the treatment of overactive bladder. In 2015, mirabegron (200 mg) was shown to acutely increase [^{18}F]FDG uptake by human BAT and increase energy expenditure [79], and intervention for 4 weeks with mirabegron was recently demonstrated to increase human BAT activity in addition to enhancing HDL cholesterol levels and insulin sensitivity [80]. These data initially suggested that mirabegron is a promising pharmacological entity to activate BAT and improve cardiometabolic health on the long term. However, mirabegron was also shown to elevate heart rate, systolic blood pressure and myocardial oxygen consumption [80]. This may at least partly contribute to its energy expenditure-increasing effect [79], and likely results from cross-reaction with β1-AR on the heart [81]. In fact, the dose of mirabegron used to activate BAT (i.e., 200 mg) is higher than the pharmacological dose to treat hyperactive bladder (i.e., 50 mg), and 50 mg mirabegron does not activate BAT or increase energy expenditure [82]. This suggests that the β3-AR is not responsible for human BAT activation. In full agreement with that notion, in collaboration with researchers from Vancouver and Copenhagen our group recently identified the β3-AR to be even absent in human BAT. In fact, the effects of both mirabegron as

well as norepinephrine on activating human brown fat cells *in vitro* were completely blocked by a selective β2-AR inhibitor, leading to the conclusion that in contrast to mouse BAT that is activated by β3-AR, human BAT is in fact activated by β2-AR [82]. Future proof-of-concept studies should thus be conducted to show that selective β2-AR agonism, for example with salbutamol, increases [^{18}F]FDG uptake by human BAT, hopefully with less off-target effects on the heart.

Given the general issues of cold exposure (i.e., discomfort) and β-AR agonism (i.e., receptor specificity), nutritional supplementation is gaining interest in chronic activation of BAT without inducing discomfort and side effects. Numerous dietary components, including capsaicin, resveratrol, curcumin, green tea, menthol and fish-derived omega 3 fatty acids, have been demonstrated to activate BAT and/or induce white adipose tissue (WAT) browning [83]. In **Chapter 2**, we discovered that dietary supplementation with the SCFA butyrate can also activate BAT resulting from increased sympathetic outflow to BAT. Although this was accompanied by ameliorated DIO and improved glucose and fat metabolism, these effect probably mainly resulted from reduced food intake as elaborated on in the previous section of this chapter. As for the effects of butyrate on activating BAT, mechanistically we revealed that dietary butyrate activates BAT as dependent on the vagal nerve (**Chapter 2**) and the presence of gut microbiota (**Chapter 3**), while this effect is independent of central GLP-1R signaling (**Chapter 4**). Collectively, although dietary butyrate has therapeutic potential to activate BAT, this would probably just be an advantageous side effect besides reducing energy intake, in combating obesity and associated cardiometabolic disorders.

All of these physiological, pharmacological and nutritional strategies discussed above aimed to activate BAT are based on broad activation of the sympathetic nervous system. Such general systemic sympathetic stimulation is likely an effective and promising route to activate overall energy expenditure. However, given the widespread distribution of β-ARs in various organs, e.g., heart, liver, skeletal muscle and WAT, such broad sympathetic stimulation will simultaneously induce effects additional to BAT activation, including increased heart rate and cardiac output, lipolysis in WAT and vasodilatation in skeletal muscles [84]. Thus, alternatives for sympathomimetics that broadly stimulate the sympathetic system should be developed to specifically activate BAT. Of note, electrical stimulation to activate specific peripheral nerves has already been applied in various conditions in the clinic [85, 86], indicating the feasibility of electrical stimulation to promote sympathetic outflow specifically towards BAT. In fact, previous studies have tried to achieve this by electrically stimulating hypothalamic nuclei to specifically promote sympathetic outflow to BAT, which indeed was shown to induce BAT thermogenesis in rats [87, 88]. In addition, others have used local optogenetics to selectively promote the activity of the tyrosine hydroxylase-expressing neurons that innervate BAT in mice [89]. However, the main disadvantage of these methods is the hurdle to take such an approach to the clinic. Interestingly, implantable spiral nerve cuff electrodes have been found to be effective to innervate peripheral nerves

in humans even after 2 to 11 years after implantation [90], indicating that such implantable electrodes are suitable for long-term clinical application to stimulate neural systems. Thus, an implantable device to specifically innervate BAT may be a promising strategy to activate BAT chronically in humans.

As a first step towards such a clinical development, in **Chapter 5** we described an innovative method to connect electrodes directly around the sympathetic nerve innervating BAT in mice, and indeed found acute specific effects on BAT thermogenesis upon electrical stimulation. Although such acute BAT stimulation was still insufficient to promote uptake of lipids and glucose from the circulation, this is probably just due to the short-term stimulation of BAT, as we did already observed decreased lipid content within BAT. Taken these findings from this pilot study together, we anticipate that prolonged electrical neurostimulation, preferentially using implantable electrodes, may be a feasible strategy to chronically activate BAT on demand in humans. However, further studies with such implantable electrodes should be performed in preclinical models including APOE*3-Leiden. CETP mice, also focusing on cardiometabolic benefits such as adiposity, glucose and lipid metabolism, and atherosclerosis development. Interestingly, vagal nerve stimulation in humans to treat refractory epilepsy has been demonstrated to increase energy expenditure and induce weight loss associated with increased BAT activity [91]. Besides further supporting our findings that the vagal nerve is involved in the BAT-activating effects of dietary butyrate, these findings also highlight the potential of neurostimulation in the activation of BAT to combat obesity and associated cardiometabolic disorders in the clinic (**Chapter 2**).

Overall, BAT activation has now been widely demonstrated to improve glucose metabolism and insulin sensitivity in humans [68, 72, 92], and to ameliorate cardiometabolic health in mice with respect to increasing triglyceride clearance [93], reducing hypercholesterolemia and protecting from atherosclerosis development [75, 94]. Notably, cold exposure to activate BAT was also demonstrated to induce modest weight loss in humans [69]. Collectively, these findings indicate the therapeutic potential of activation of BAT in combating obesity and associated cardiometabolic diseases. Very recently, this was further supported by an analysis of > 130,000 [^{18}F]FDG PET-CT scans, showing that individuals with detectable BAT had lower prevalence of cardiometabolic diseases, and that the presence of BAT was independently correlated with lower odds of T2D, dyslipidemia, coronary artery disease, cerebrovascular disease, congestive heart failure and hypertension [95]. Nevertheless, we have to realize that full activation of human BAT probably results in only a small increase in total energy expenditure of approx. 100 kcal/day, which is probably insufficient to induce significant weight loss [96]. Even if a 203 kcal/day increase in energy expenditure can be achieved, as shown by the maximum allowable dosage of mirabegron (200 mg) [79], this could lead to a calculated maximum weight loss of approx. 5 kg in one year [97]. However, this is still less than the weight loss induced by reduction of energy intake, since as much as approx. 11 kg weight reduction can be attained in 26 weeks treatment by dual GLP-1/GIP

receptor agonism [61]. Thus, activating BAT to increase energy expenditure, at least with the currently available tools, is likely less effective to combat obesity when compared to the reduction of energy intake, given the overwhelming contribution of restricting energy intake to total energy metabolism. Nonetheless, BAT activation to increase energy expenditure is still a potential and realistic contributor to weight loss maintenance as induced by restriction of energy intake. Interestingly, in **Chapter 2**, we demonstrated that the beneficial effects of dietary butyrate on attenuating DIO and improving insulin resistance are mainly explained by the reduction of food intake, and to a lower extent assisted by the activation of BAT, which again points butyrate as a strong candidate as a novel effective therapeutic strategy to combat obesity and associated cardiometabolic diseases.

Concluding remarks

Our increasing obesogenic and aging society has resulted in a steeply increasing prevalence of cardiometabolic diseases. The main underlying reason is our modern lifestyle with respect to a higher availability and intake of food, that often appears unhealthy, and lower energy expenditure related to a sedentary lifestyle. Although the most efficient ways to slow this high prevalence of obesity are just eating less and more healthy, and moving more, to reduce energy intake and increase energy expenditure, respectively, current strategies to achieve this in the long-term are still both insufficient and ineffective, and novel strategies are still eagerly warranted.

Energy intake restricting strategies are among the most effective interventions for combating obesity and related cardiometabolic diseases, while strategies to activate BAT to increase energy expenditure show additional modest contributing effects. Physiological strategies, e.g., bariatric surgery and cold exposure, and pharmacological strategies, e.g., GLP-1R agonism and dual GIP and GLP-1R agonism, indeed show significant improvement of cardiometabolic health in the clinic. However, in general, these strategies are either highly invasive or suffer from several adverse effects during long-term treatment. Thus, nutritional supplements without inducing discomfort and side effects are gaining increased interest. In this thesis, we found in experimental studies using a well-established translational humanized mouse model dietary butyrate ameliorates DIO and improves insulin resistance mainly by reducing appetite but also by activating BAT. In a series of subsequent mechanistic studies, we elucidated the mechanisms underlying these metabolic properties systematically from gut to brain, showing the involvement of *Lachnospiraceae bacterium 28-4* outgrowth, intestinal GLP-1 secretion, vagal nerve activation and finally central GLP-1R signaling to inhibit NPY neuronal activation. Although the causal involvement of *Lachnospiraceae bacterium 28-4* and central GLP-1R signaling in the effects of dietary butyrate should still be deciphered in mice, and translational studies should still confirm beneficial effects of dietary butyrate on reducing energy intake and activating BAT in a clinical setting, our collective findings revealed dietary butyrate as a promising and feasible

therapeutic strategy to treat obesity and related cardiometabolic diseases with respect to reducing appetite and activating BAT. In addition, our investigations on mechanisms underlying the beneficial effects of dietary butyrate provided valuable information on the development of therapeutic strategies for combating obesity and associated cardiometabolic diseases, which besides butyrate may include specific pre- and probiotics.

References

1. Kivimaki, M., et al., *Overweight, obesity, and risk of cardiometabolic multimorbidity: pooled analysis of individual-level data for 120 813 adults from 16 cohort studies from the USA and Europe.* Lancet Public Health, 2017. **2**(6): p. e277-e285.
2. Marchesi, J.R., et al., *The gut microbiota and host health: a new clinical frontier.* Gut, 2016. **65**(2): p. 330-9.
3. Fetissov, S.O., *Role of the gut microbiota in host appetite control: bacterial growth to animal feeding behaviour.* Nat Rev Endocrinol, 2017. **13**(1): p. 11-25.
4. Sharon, G., et al., *Specialized metabolites from the microbiome in health and disease.* Cell Metab, 2014. **20**(5): p. 719-730.
5. Reynolds, A., et al., *Carbohydrate quality and human health: a series of systematic reviews and meta-analyses.* Lancet, 2019. **393**(10170): p. 434-445.
6. Burkitt, D.P., A.R. Walker, and N.S. Painter, *Dietary fiber and disease.* JAMA, 1974. **229**(8): p. 1068-74.
7. Canfora, E.E., J.W. Jocken, and E.E. Blaak, *Short-chain fatty acids in control of body weight and insulin sensitivity.* Nat Rev Endocrinol, 2015. **11**(10): p. 577-91.
8. Cummings, J.H., et al., *Short chain fatty acids in human large intestine, portal, hepatic and venous blood.* Gut, 1987. **28**(10): p. 1221-7.
9. Pomare, E.W., W.J. Branch, and J.H. Cummings, *Carbohydrate fermentation in the human colon and its relation to acetate concentrations in venous blood.* J Clin Invest, 1985. **75**(5): p. 1448-54.
10. Karaki, S., et al., *Expression of the short-chain fatty acid receptor, GPR43, in the human colon.* J Mol Histol, 2008. **39**(2): p. 135-42.
11. Nohr, M.K., et al., *GPR41/FFAR3 and GPR43/FFAR2 as cosensors for short-chain fatty acids in enteroendocrine cells vs FFAR3 in enteric neurons and FFAR2 in enteric leukocytes.* Endocrinology, 2013. **154**(10): p. 3552-64.
12. Le Poul, E., et al., *Functional characterization of human receptors for short chain fatty acids and their role in polymorphonuclear cell activation.* J Biol Chem, 2003. **278**(28): p. 25481-9.
13. Tang, C., et al., *Loss of FFA2 and FFA3 increases insulin secretion and improves glucose tolerance in type 2 diabetes.* Nat Med, 2015. **21**(2): p. 173-7.
14. Brown, A.J., et al., *The Orphan G protein-coupled receptors GPR41 and GPR43 are activated by propionate and other short chain carboxylic acids.* J Biol Chem, 2003. **278**(13): p. 11312-9.
15. Yamashita, H., et al., *Improvement of obesity and glucose tolerance by acetate in Type 2 diabetic Otsuka Long-Evans Tokushima Fatty (OLETF) rats.* Biosci Biotechnol Biochem, 2007. **71**(5): p. 1236-43.
16. Lu, Y., et al., *Short Chain Fatty Acids Prevent High-fat-diet-induced Obesity in Mice by Regulating G Protein-coupled Receptors and Gut Microbiota.* Sci Rep, 2016. **6**: p. 37589.

17. van der Beek, C.M., et al., *Distal, not proximal, colonic acetate infusions promote fat oxidation and improve metabolic markers in overweight/obese men.* Clin Sci (Lond), 2016. **130**(22): p. 2073-2082.

18. Perry, R.J., et al., *Acetate mediates a microbiome-brain-beta-cell axis to promote metabolic syndrome.* Nature, 2016. **534**(7606): p. 213-7.

19. Frost, G., et al., *The short-chain fatty acid acetate reduces appetite via a central homeostatic mechanism.* Nat Commun, 2014. **5**: p. 3611.

20. Lin, H.V., et al., *Butyrate and propionate protect against diet-induced obesity and regulate gut hormones via free fatty acid receptor 3-independent mechanisms.* PLoS One, 2012. **7**(4): p. e35240.

21. Kim, K.N., Y. Yao, and S.Y. Ju, *Short Chain Fatty Acids and Fecal Microbiota Abundance in Humans with Obesity: A Systematic Review and Meta-Analysis.* Nutrients, 2019. **11**(10).

22. Bergman, E.N., *Energy contributions of volatile fatty acids from the gastrointestinal tract in various species.* Physiol Rev, 1990. **70**(2): p. 567-90.

23. Farningham, D.A. and C.C. Whyte, *The role of propionate and acetate in the control of food intake in sheep.* Br J Nutr, 1993. **70**(1): p. 37-46.

24. Chambers, E.S., et al., *Effects of targeted delivery of propionate to the human colon on appetite regulation, body weight maintenance and adiposity in overweight adults.* Gut, 2015. **64**(11): p. 1744-54.

25. Polyviou, T., et al., *Randomised clinical study: inulin short-chain fatty acid esters for targeted delivery of short-chain fatty acids to the human colon.* Aliment Pharmacol Ther, 2016. **44**(7): p. 662-72.

26. Spiller, G.A., et al., *Effect of purified cellulose, pectin, and a low-residue diet on fecal volatile fatty acids, transit time, and fecal weight in humans.* Am J Clin Nutr, 1980. **33**(4): p. 754-9.

27. Roediger, W.E., *Role of anaerobic bacteria in the metabolic welfare of the colonic mucosa in man.* Gut, 1980. **21**(9): p. 793-8.

28. Milovic, V., et al., *Effect of structural analogues of propionate and butyrate on colon cancer cell growth.* Int J Colorectal Dis, 2000. **15**(5-6): p. 264-70.

29. Steliou, K., et al., *Butyrate histone deacetylase inhibitors.* Biores Open Access, 2012. **1**(4): p. 192-8.

30. Thangaraju, M., et al., *GPR109A is a G-protein-coupled receptor for the bacterial fermentation product butyrate and functions as a tumor suppressor in colon.* Cancer Res, 2009. **69**(7): p. 2826-32.

31. Reid, T., et al., *Phase II trial of the histone deacetylase inhibitor pivaloyloxymethyl butyrate (Pivanex, AN-9) in advanced non-small cell lung cancer.* Lung Cancer, 2004. **45**(3): p. 381-6.

32. Vernia, P., et al., *Topical butyrate improves efficacy of 5-ASA in refractory distal ulcerative colitis: results of a multicentre trial.* Eur J Clin Invest, 2003. **33**(3): p. 244-8.

33. Kimura, I., et al., *Short-chain fatty acids and ketones directly regulate sympathetic nervous system via G protein-coupled receptor 41 (GPR41).* Proc Natl Acad Sci U S A, 2011. **108**(19): p. 8030-5.

34. Gao, Z., et al., *Butyrate improves insulin sensitivity and increases energy expenditure in mice.* Diabetes, 2009. **58**(7): p. 1509-17.

35. Bouter, K., et al., *Differential metabolic effects of oral butyrate treatment in lean versus metabolic syndrome subjects.* Clin Transl Gastroenterol, 2018. **9**(5): p. 155.

36. *Human Metabolome Database*. Available from: http://www.hmdb.ca/.

37. Anil, M.H. and J.M. Forbes, *The roles of hepatic nerves in the reduction of food intake as a consequence of intraportal sodium propionate administration in sheep.* Q J Exp Physiol, 1988. **73**(4): p. 539-46.

38. Schneeberger, M., R. Gomis, and M. Claret, *Hypothalamic and brainstem neuronal circuits controlling homeostatic energy balance.* J Endocrinol, 2014. **220**(2): p. T25-46.

39. Freeland, K.R. and T.M. Wolever, *Acute effects of intravenous and rectal acetate on glucagon-like peptide-1, peptide YY, ghrelin, adiponectin and tumour necrosis factor-alpha.* Br J Nutr, 2010. **103**(3): p. 460-6.

40. Psichas, A., et al., *The short chain fatty acid propionate stimulates GLP-1 and PYY secretion via free fatty acid receptor 2 in rodents.* Int J Obes (Lond), 2015. **39**(3): p. 424-9.

41. Nakagawa, A., et al., *Receptor gene expression of glucagon-like peptide-1, but not glucose-dependent insulinotropic polypeptide, in rat nodose ganglion cells.* Auton Neurosci, 2004. **110**(1): p. 36-43.

42. Bucinskaite, V., et al., *Receptor-mediated activation of gastric vagal afferents by glucagon-like peptide-1 in the rat.* Neurogastroenterol Motil, 2009. **21**(9): p. 978-e78.

43. Plamboeck, A., et al., *The effect of exogenous GLP-1 on food intake is lost in male truncally vagotomized subjects with pyloroplasty.* Am J Physiol Gastrointest Liver Physiol, 2013. **304**(12): p. G1117-27.

44. Jin, S.L., et al., *Distribution of glucagonlike peptide I (GLP-I), glucagon, and glicentin in the rat brain: an immunocytochemical study.* J Comp Neurol, 1988. **271**(4): p. 519-32.

45. Goke, R., et al., *Distribution of GLP-1 binding sites in the rat brain: evidence that exendin-4 is a ligand of brain GLP-1 binding sites.* Eur J Neurosci, 1995. **7**(11): p. 2294-300.

46. Meeran, K., et al., *Repeated intracerebroventricular administration of glucagon-like peptide-1-(7-36) amide or exendin-(9-39) alters body weight in the rat.* Endocrinology, 1999. **140**(1): p. 244-50.

47. Kooijman, S., et al., *Central GLP-1 receptor signalling accelerates plasma clearance of triacylglycerol and glucose by activating brown adipose tissue in mice.* Diabetologia, 2015. **58**(11): p. 2637-46.

48. Turton, M.D., et al., *A role for glucagon-like peptide-1 in the central regulation of feeding.* Nature, 1996. **379**(6560): p. 69-72.

49. Christiansen, C.B., et al., *The impact of short-chain fatty acids on GLP-1 and PYY secretion from the isolated perfused rat colon.* Am J Physiol Gastrointest Liver Physiol, 2018. **315**(1): p. G53-G65.

50. Tolhurst, G., et al., *Short-chain fatty acids stimulate glucagon-like peptide-1 secretion via the G-protein-coupled receptor FFAR2.* Diabetes, 2012. **61**(2): p. 364-71.

51. Cani, P.D., et al., *Oligofructose promotes satiety in healthy human: a pilot study.* Eur J Clin Nutr, 2006. **60**(5): p. 567-72.

52. Cani, P.D., et al., *Gut microbiota fermentation of prebiotics increases satietogenic and incretin gut peptide production with consequences for appetite sensation and glucose response after a meal.* Am J Clin Nutr, 2009. **90**(5): p. 1236-43.

53. Zhao, L., et al., *Gut bacteria selectively promoted by dietary fibers alleviate type 2 diabetes.* Science, 2018. **359**(6380): p. 1151-1156.

54. Depommier, C., et al., *Supplementation with Akkermansia muciniphila in overweight and obese human volunteers: a proof-of-concept exploratory study.* Nat Med, 2019. **25**(7): p. 1096-1103.

55. Perraudeau, F., et al., *Improvements to postprandial glucose control in subjects with type 2 diabetes: a multicenter, double blind, randomized placebo-controlled trial of a novel probiotic formulation.* BMJ Open Diabetes Res Care, 2020. **8**(1).

56. Maggard-Gibbons, M., et al., *Bariatric surgery for weight loss and glycemic control in nonmorbidly obese adults with diabetes: a systematic review.* JAMA, 2013. **309**(21): p. 2250-61.

57. Hopkins, J.C., et al., *Outcome reporting in bariatric surgery: an in-depth analysis to inform the development of a core outcome set, the BARIACT Study.* Obes Rev, 2015. **16**(1): p. 88-106.

58. Secher, A., et al., *The arcuate nucleus mediates GLP-1 receptor agonist liraglutide-dependent weight loss.* J Clin Invest, 2014. **124**(10): p. 4473-88.

59. Pi-Sunyer, X., et al., *A Randomized, Controlled Trial of 3.0 mg of Liraglutide in Weight Management.* N Engl J Med, 2015. **373**(1): p. 11-22.

60. Bucheit, J.D., et al., *Oral Semaglutide: A Review of the First Oral Glucagon-Like Peptide 1 Receptor Agonist.* Diabetes Technol Ther, 2020. **22**(1): p. 10-18.

61. Frias, J.P., et al., *Efficacy and safety of LY3298176, a novel dual GIP and GLP-1 receptor agonist, in patients with type 2 diabetes: a randomised, placebo-controlled and active comparator-controlled phase 2 trial.* Lancet, 2018. **392**(10160): p. 2180-2193.

62. Apovian, C.M., W.T. Garvey, and D.H. Ryan, *Challenging obesity: Patient, provider, and expert perspectives on the roles of available and emerging nonsurgical therapies.* Obesity (Silver Spring), 2015. **23 Suppl 2**: p. S1-S26.

63. Chambers, E.S., et al., *Role of Gut Microbiota-Generated Short-Chain Fatty Acids in Metabolic and Cardiovascular Health.* Curr Nutr Rep, 2018. **7**(4): p. 198-206.

64. Byrne, C.S., et al., *The role of short chain fatty acids in appetite regulation and energy homeostasis.* Int J Obes (Lond), 2015. **39**(9): p. 1331-8.

65. Sowah, S.A., et al., *Effects of Weight-Loss Interventions on Short-Chain Fatty Acid Concentrations in Blood and Feces of Adults: A Systematic Review.* Adv Nutr, 2019. **10**(4): p. 673-684.

66. Berni Canani, R., M. Di Costanzo, and L. Leone, *The epigenetic effects of butyrate: potential therapeutic implications for clinical practice.* Clin Epigenetics, 2012. **4**(1): p. 4.

67. Cypess, A.M., et al., *Identification and importance of brown adipose tissue in adult humans.* N Engl J Med, 2009. **360**(15): p. 1509-17.

68. Virtanen, K.A., et al., *Functional brown adipose tissue in healthy adults.* N Engl J Med, 2009. **360**(15): p. 1518-25.

69. Yoneshiro, T., et al., *Recruited brown adipose tissue as an antiobesity agent in humans.* J Clin Invest, 2013. **123**(8): p. 3404-8.

70. van Marken Lichtenbelt, W.D., et al., *Cold-activated brown adipose tissue in healthy men.* N Engl J Med, 2009. **360**(15): p. 1500-8.

71. Hanssen, M.J., et al., *Short-term Cold Acclimation Recruits Brown Adipose Tissue in Obese Humans.* Diabetes, 2016. **65**(5): p. 1179-89.

72. Hanssen, M.J., et al., *Short-term cold acclimation improves insulin sensitivity in patients with type 2 diabetes mellitus.* Nat Med, 2015. **21**(8): p. 863-5.

73. *Cold Showers. The definitive guide to cold water therapy.*; Available from: http://www.cold-showers.com/.

74. Atgie, C., et al., *Effects of chronic treatment with noradrenaline or a specific beta3-adrenergic agonist, CL 316 243, on energy expenditure and epididymal adipocyte lipolytic activity in rat.* Comp Biochem Physiol A Mol Integr Physiol, 1998. **119**(2): p. 629-36.

75. Berbee, J.F., et al., *Brown fat activation reduces hypercholesterolaemia and protects from atherosclerosis development.* Nat Commun, 2015. **6**: p. 6356.

76. Mathvink, R.J., et al., *Discovery of a potent, orally bioavailable beta(3) adrenergic receptor agonist, (R)-N-[4-[2-[[2-hydroxy-2-(3-pyridinyl)ethyl]amino]ethyl] phenyl]-4-[4 -[4-(trifluoromethyl)phenyl]thiazol-2-yl]benzenesulfonamide.* J Med Chem, 2000. **43**(21): p. 3832-6.

77. van Baak, M.A., et al., *Acute effect of L-796568, a novel beta 3-adrenergic receptor agonist, on energy expenditure in obese men.* Clin Pharmacol Ther, 2002. **71**(4): p. 272-9.

78. Larsen, T.M., et al., *Effect of a 28-d treatment with L-796568, a novel beta(3)-adrenergic receptor agonist, on energy expenditure and body composition in obese men.* Am J Clin Nutr, 2002. **76**(4): p. 780-8.

79. Cypess, A.M., et al., *Activation of human brown adipose tissue by a beta3-adrenergic receptor agonist.* Cell Metab, 2015. **21**(1): p. 33-8.

80. O'Mara, A.E., et al., *Chronic mirabegron treatment increases human brown fat, HDL cholesterol, and insulin sensitivity.* J Clin Invest, 2020. **130**(5): p. 2209-2219.

81. Madamanchi, A., *Beta-adrenergic receptor signaling in cardiac function and heart failure.* Mcgill J Med, 2007. **10**(2): p. 99-104.

82. Blondin, D.P., et al., *Human Brown Adipocyte Thermogenesis Is Driven by beta2-AR Stimulation.* Cell Metab, 2020. **32**(2): p. 287-300 e7.

83. El Hadi, H., et al., *Food Ingredients Involved in White-to-Brown Adipose Tissue Conversion and in Calorie Burning.* Front Physiol, 2018. **9**: p. 1954.

84. Zhang, D.Y. and A.S. Anderson, *The sympathetic nervous system and heart failure.* Cardiol Clin, 2014. **32**(1): p. 33-45, vii.

85. Oddo, C.M., et al., *Intraneural stimulation elicits discrimination of textural features by artificial fingertip in intact and amputee humans.* Elife, 2016. **5**: p. e09148.

86. Ortiz-Catalan, M., B. Hakansson, and R. Branemark, *An osseointegrated human-machine gateway for long-term sensory feedback and motor control of artificial limbs.* Sci Transl Med, 2014. **6**(257): p. 257re6.

87. Halvorson, I., L. Gregor, and J.A. Thornhill, *Brown adipose tissue thermogenesis is activated by electrical and chemical (L-glutamate) stimulation of the ventromedial hypothalamic nucleus in cold-acclimated rats.* Brain Res, 1990. **522**(1): p. 76-82.

88. Freeman, P.H. and P.J. Wellman, *Brown adipose tissue thermogenesis induced by low level electrical stimulation of hypothalamus in rats.* Brain Res Bull, 1987. **18**(1): p. 7-11.

89. Lyons, C.E., et al., *Optogenetic-induced sympathetic neuromodulation of brown adipose tissue thermogenesis.* FASEB J, 2020. **34**(2): p. 2765-2773.

90. Christie, B.P., et al., *"Long-term stability of stimulating spiral nerve cuff electrodes on human peripheral nerves".* J Neuroeng Rehabil, 2017. **14**(1): p. 70.

91. Vijgen, G.H., et al., *Vagus nerve stimulation increases energy expenditure: relation to brown adipose tissue activity.* PLoS One, 2013. **8**(10): p. e77221.

92. Chondronikola, M., et al., *Brown adipose tissue improves whole-body glucose homeostasis and insulin sensitivity in humans.* Diabetes, 2014. **63**(12): p. 4089-99.

93. Bartelt, A., et al., *Brown adipose tissue activity controls triglyceride clearance.* Nat Med, 2011. **17**(2): p. 200-5.

94. Hoeke, G., et al., *Role of Brown Fat in Lipoprotein Metabolism and Atherosclerosis.* Circ Res, 2016. **118**(1): p. 173-82.

95. Becher, T., et al., *Brown adipose tissue is associated with cardiometabolic health.* Nat Med, 2021.

96. Marlatt, K.L. and E. Ravussin, *Brown Adipose Tissue: an Update on Recent Findings.* Curr Obes Rep, 2017. **6**(4): p. 389-396.

97. Hall, K.D., et al., *Quantification of the effect of energy imbalance on bodyweight.* Lancet, 2011. **378**(9793): p. 826-37.

CHAPTER 8

SUMMARY
SAMENVATTING
LIST OF PUBLICATIONS
CURRICULUM VITAE
ACKNOWLEDGEMENTS

SUMMARY

The prevalence of obesity and its related cardiometabolic diseases, including type 2 diabetes (T2D) and cardiovascular diseases, have been increasing steadily in the past decades. The main reason for the development of obesity is the modern lifestyle with respect to a higher intake of energy contained less healthy nutrition combined with a lower energy expenditure due to the more sedentary behavior. This combination results in extra energy storage of nutrients within white adipocytes, but also within parenchymal cells of metabolic organs that as a consequence become insulin resistant, leading to hyperglycemia as well as atherosclerotic hyperlipidemia. Therefore, to understand how to modulate energy expenditure to outweigh energy intake is of great importance and useful for developing innovative strategies to combat obesity and associated cardiometabolic diseases. **Chapter 1** gives a general introduction of energy metabolism and obesity-associated cardiometabolic diseases that result from the imbalance of energy metabolism, as well as of current and promising strategies to improve energy metabolism and combat obesity-associated cardiometabolic diseases.

Current physiological and pharmacological therapeutic strategies aimed to combat obesity can effectively ameliorate weight gain and improve cardiometabolic health. However, in general, these therapeutic strategies are hard to adhere to and/or suffer from adverse effects. Therefore, nutritional strategies are gaining increasing interest in combating obesity and thereby improving cardiometabolic health. Based on previously discovered beneficial effects of butyrate on metabolic health, in **chapter 2**, we investigated the contribution of lower energy intake versus increased energy expenditure to the beneficial effects of dietary butyrate using male APOE*3-Leiden.CETP (E3L.CETP) mice, a well-established humanized model for diet-induced cardiometabolic disorders. First, we found that acute oral, but not intravenous, butyrate administration decreased food intake, suppressed the activity of orexigenic neurons that express neuropeptide Y in the hypothalamus, and decreased neuronal activity within the nucleus tractus solitarius and dorsal vagal complex in the brainstem, revealing that butyrate exerts its effect on appetite involving the gut-brain neural circuit. Next, to study the contribution of satiety to the metabolic benefits of butyrate, mice were fed a high-fat diet (HFD) without and with butyrate, and an additional group of mice was included that was pair-fed to the butyrate-treated group. Chronic butyrate supplementation prevented diet-induced obesity, hyperinsulinemia, hypertriglyceridemia and hepatic steatosis, all of which were largely attributed to the butyrate-induced reduction in food intake. Butyrate also modestly promoted fat oxidation by activating brown adipose tissue (BAT), as evidenced from increased utilization of plasma triglyceride-derived fatty acids, which was explained by an increased sympathetic outflow towards BAT. Subdiaphragmatic vagotomy, to disrupt neural signaling from gut to brain, abolished the effects of butyrate on both food intake and metabolic BAT activity. Finally, we showed that the beneficial metabolic effects of butyrate were accompanied by changes in

the composition of the gut microbiota. From these studies, we concluded that dietary butyrate acts on the gut-brain neural circuit to improve energy metabolism via reducing energy intake and enhancing fat oxidation by activating BAT, which is probably related to the observed change(s) in gut microbiota composition, indicating dietary butyrate could be a promising and innovative therapeutic strategy to combat obesity and associated cardiometabolic diseases.

Next, to investigate the role of gut microbiota in the beneficial effects of dietary butyrate on cardiometabolic health, in **Chapter 3**, male E3L.CETP mice underwent antibiotics-induced microbiota depletion or received saline as controls, and were simultaneously fed a HFD without or with butyrate for 6 weeks. This study revealed that dietary butyrate reduces appetite and ameliorates weight gain only in the presence of gut microbiota, indicating the crucial role of gut microbiota in the induction of beneficial effects of dietary butyrate. To further elucidate the causality between gut microbiota and the metabolic benefits of dietary butyrate, fresh fecal bacteria were isolated from donor mice fed a HFD without or with butyrate between 6-12 weeks of treatment, and transplanted to recipient mice that were fed a HFD simultaneously for 6 weeks. Subsequent 16S sequencing analysis revealed that fecal microbiota transplantation (FMT) from dietary butyrate-treated donors alters the gut microbiota composition in recipients, accompanied with attenuated HFD-induced weight gain by persistently reducing food intake, and improved insulin sensitivity. These effects were associated with a selective proliferation of *Lachnospiraceae bacterium 28-4* within the gut, indicating that dietary butyrate may exert its metabolic benefits by inducing selective outgrowth of *Lachnospiraceae bacterium 28-4*. Interestingly, in diet-induced obese mice, dietary butyrate was ineffective in inducing weight loss, ameliorating metabolic health or promoting *Lachnospiraceae bacterium 28-4* proliferation, showed that dietary butyrate does not improve metabolic health in the context of pre-existing obesity, probably related to the absence of effects of dietary butyrate on gut microbiota. Altogether, these findings reveal a causal role of gut microbiota in the beneficial metabolic effects of dietary butyrate with respect to reduction of food intake and improvement of insulin resistance, and hint towards the therapeutic potential of *Lachnospiraceae bacterium 28-4* as a novel probiotic to combat obesity and improve cardiometabolic health.

A recent ground-breaking human study showed that dietary fiber promotes butyrate-producing bacterial strains in the gut and increases the glucagon-like peptide-1 (GLP-1) response, which was accompanied by amelioration of T2D, indicating that dietary butyrate improves cardiometabolic health not only via modulating gut microbiota (Chapter 3), but probably also by affecting the production of GLP-1. Therefore, in **Chapter 4**, we aimed to elucidate the involvement of GLP-1 receptor (GLP-1R) signaling in the metabolic benefits induced by dietary butyrate. To achieve this end, male E3L.CETP mice received a HFD with or without butyrate for 12 weeks, while receiving an intracerebroventricular infusion of the GLP-1R antagonist Exendin-(9-39) or vehicle during the final 4 weeks. We indeed found

that dietary butyrate increases the number of GLP-1-positive cells in the ileum, as well as active GLP-1 levels in plasma, accompanied by a reduction in food intake, body weight gain and fat mass. Also, in line with results obtained in Chapter 2, we showed that dietary butyrate increases fat oxidation at the expense of glucose oxidation and increased plasma triglyceride-derived fatty acid uptake by BAT. Intracerebroventricular infusion of Exendin-(9-39) abolished the effect of butyrate on food intake and largely attenuated the effects on nutrient oxidation, however, without affecting the effects on body weight gain, fat mass and nutrient partitioning. We concluded that dietary butyrate stimulates the intestinal release of GLP-1 to reduce appetite and increase fatty acid oxidation at the expense of carbohydrate oxidation via central GLP-1R signaling, while butyrate improves nutrient partitioning and activates BAT independent of central GLP-1R signaling.

In addition to the strategies focusing on restricting energy intake, specific stimulation of the sympathetic outflow towards BAT would be an innovative approach to increase energy expenditure. To this end, we evaluated the possibility of applying electrical neurostimulation aimed at specifically activating BAT in male wild-type mice in **Chapter 5**. We found that electrical neurostimulation acutely increases heat production by BAT, similarly to beta 3-adrenergic receptor (β3-AR) agonism, as evidenced by an increase in local temperature in BAT, without influencing the core body temperature. Both electrical neurostimulation and β3-AR agonism acutely increased tyrosine hydroxylase content in the nerve terminals within BAT thereby confirming the enhanced sympathetic activity. In addition, we identified increased phosphorylation of hormone-sensitive lipase in BAT, coinciding with reduced intracellular lipids in BAT, without affecting acute nutrient uptake from plasma. The increased BAT temperature as induced by electrical neurostimulation was reversed by β3-AR antagonism. Altogether, these findings indicate that electrical neurostimulation is an effective strategy to acutely and specifically promote thermogenesis in BAT as dependent on β3-AR signaling, and suggest that electrical neurostimulation may be further developed as a novel strategy to activate BAT and thereby combating cardiometabolic diseases.

Lipopolysaccharide (LPS) derived from the surface of Gram-negative bacteria is considered to be an important mediator in the effects of gut microbiota on host lipid metabolism, since it has been demonstrated to decrease hepatic cholesteryl ester transfer protein (CETP) expression, which plays a pivotal role in the metabolism of high-density lipoproteins (HDL) and (very-) low-density lipoproteins [(V)LDL] by mediating the exchange of cholesteryl ester for triglycerides between HDL and (V) LDL. However, how LPS decreases hepatic CETP expression was still disputed. Since our previous study showed that plasma CETP is mainly derived from Kupffer cells (KCs), in **Chapter 6**, we investigated the role of KC subsets in the mechanism by which LPS reduces hepatic CETP expression. In male E3L.CETP mice, LPS markedly decreased hepatic *CETP* mRNA expression and plasma CETP concentration without affecting hepatic macrophage number. This was paralleled by decreased expression of the resting KC markers C-type lectin domain family, member f (*Clec4f*) and V-set

and immunoglobulin domain containing 4 (*Vsig4*), while expression of the infiltrating monocyte marker lymphocyte antigen 6 complex locus C (*Ly6C*) was increased. Simultaneously, the ratio of plasma HDL-cholesterol over non-HDL-cholesterol transiently increased. After ablation of hepatic macrophages via injection with liposomal clodronate, the reappearance of hepatic gene and protein expression of CETP coincided with Clec4f and Vsig4, but not Ly6C. Double-immunofluorescence staining showed that CETP co-localized with Clec4f^{+} KCs and not Ly6C^{+} monocytes. In humans, microarray gene-expression analysis of liver biopsies revealed that hepatic expression and plasma level of CETP both correlated with hepatic *VSIG4* expression. LPS administration decreased the plasma CETP concentration in humans. *In vitro* experiments showed that LPS reduced liver X receptor-mediated CETP expression. Taken all these findings together, we concluded that hepatic expression of CETP is exclusively confined to the resting KC subset (e.g., F4/80^{+}Clec4f^{+}Vsig4^{+}Ly6C^{-}). LPS activates resting KCs, leading to the reduction of Clec4f and Vsig4 expression and reduces hepatic CETP expression, consequently decreasing plasma CETP and raising HDL-cholesterol. This sequence of events is consistent with the anti-inflammatory role of HDL in response to LPS and may be relevant as a defense mechanism against bacterial infections.

In conclusion, in **Chapter 7**, the findings of this thesis were placed in the context of the current scientific literature, and promising novel therapeutic strategies and the associated underlying mechanisms to reduce energy intake and/or increase energy expenditure to consequently treat obesity and associated cardiometabolic diseases were discussed. Collectively, the results described in this thesis emphasize dietary butyrate as a promising and feasible therapeutic strategy to combat obesity and related cardiometabolic diseases with respect to not only reducing appetite but also activating BAT. In addition, our investigations on mechanisms underlying the beneficial effects of dietary butyrate provide valuable information on development of additional novel therapeutic targets for treating obesity and associated cardiometabolic diseases, which besides butyrate may include specific pre- and probiotics.

SAMENVATTING

In de afgelopen decennia is de prevalentie van obesitas en geassocieerde cardiometabole ziekten zoals type 2 diabetes en hart- en vaatziekten aanzienlijk toegenomen. Onze moderne leefstijl, waarin we steeds meer en ongezonder eten en ook minder bewegen, is de voornaamste reden voor de ontwikkeling van obesitas. Meer eten en minder bewegen leidt tot een zogenaamde positieve energiebalans. Het teveel aan calorieën wordt niet alleen opgeslagen in cellen van het wit vetweefsel, die bedoeld zijn voor dergelijke opslag, maar ook in cellen van organen die betrokken zijn bij de energiestofwisseling, zoals de lever, het hart en skeletspieren. Deze organen worden vervolgens resistent voor de werking van insuline, wat de concentratie van suiker en vetten in het bloed doet stijgen en leidt tot type 2 diabetes en hart- en vaatziekten. Daarom is het van groot belang beter te begrijpen hoe we een positieve energiebalans zodanig kunnen aanpakken dat het calorisch verbruik groter wordt dan de calorische inname, om zo innovatieve strategieën te ontwerpen om obesitas en geassocieerde cardiometabole ziekten tegen te gaan. **Hoofdstuk 1** bevat een algemene introductie over de energiestofwisseling en obesitas-geassocieerde cardiometabole ziekten die ontstaan als de energiestofwisseling uit balans is, en beschrijft huidige en veelbelovende strategieën om de energiestofwisseling te verbeteren en op die manier cardiometabole ziekten te bestrijden.

De huidige fysiologische en farmacologische therapeutische strategieën om obesitas tegen te gaan zijn op zich effectief om gewichtsafname te bewerkstelligen en de cardiometabole gezondheid te verbeteren. In het algemeen is verandering van leefstijl echter moeilijk vol te houden, en de huidige medicijnen zijn niet zonder ongewenste bijeffecten zoals misselijkheid. Omdat eerder is aangetoond dat het korte-keten vetzuur butyraat gunstige effecten heeft op de metabole gezondheid, hebben we in **Hoofdstuk 2** onderzocht welk precieze effecten butyraat op de energiestofwisseling heeft door gebruik te maken van de zogenaamde APOE*3-Leiden.CETP muis, een uniek model voor dieet-geïnduceerde cardiometabole ziekten. Aanvankelijk toonden we aan dat butyraat effectief de voedselinname remt als het oraal wordt toegediend, terwijl intraveneuze toediening van butyraat geen effect had op de voedselinname. Oraal toegediend butyraat bleek in de hypothalamus van de hersenen de activiteit te remmen van zenuwcellen die betrokken zijn bij het hongergevoel, wat suggereert dat butyraat de voedselinname remt door een zenuwsignaal tussen darmen en hersenen te activeren. Vervolgens hebben we de muizen een vetrijk dieet gegeven met en zonder butyraat waarmee we konden aantonen dat langdurige behandeling met butyraat in staat was om gewichtstoename tegen te gaan. Behandeling met butyraat voorkwam ook de toename van insuline en vetten in het bloed en zelfs leververvetting, en deze effecten konden geheel worden toegeschreven aan de vermindering in voedselinname. Tegelijkertijd stimuleerde butyraat ook de vetverbranding door het bruine vetweefsel, wat we konden verklaren door stimulatie van een zogenaamd sympathisch zenuwsignaal vanuit de hypothalamus naar het bruine vet. Tenslotte konden we aantonen dat de

effecten van behandeling met butyraat in het voedsel leidde tot een verandering van de samenstelling van de darmflora, en dat het doorknippen van de zenuwbaan die de darm met de hersenen verbindt, ook wel vagotomie genoemd, de effecten van butyraat op zowel voedselinname als activatie van bruin vet teniet deed. Vanuit deze studies concludeerden wij dat behandeling met butyraat in het voedsel de zenuwbaan die de darmen met de hersenen verbindt activeert en op die manier de energiestofwisseling gunstig beïnvloedt door enerzijds de voedselinname te remmen en anderzijds de vetverbranding door bruin vet te stimuleren. Butyraat lijkt dus een innovatieve en veelbelovende strategie om obesitas en daarmee geassocieerde cardiometabole ziekten tegen te gaan.

Aangezien we in hoofdstuk 2 aantoonden dat de gunstige metabole effecten van butyraat gepaard gingen met een veranderde samenstelling van de darmflora, achtten we het waarschijnlijk dat darmbacteriën een rol spelen bij deze gunstige effecten van butyraat. Om de rol van de darmbacteriën in de gunstige cardiometabole effecten van butyraat verder in kaart te brengen, hebben we in **Hoofdstuk 3** APOE*3-Leiden.CETP muizen eerst behandeld met antibiotica om de darmbacteriën te doden, en hen vervolgens weer een vetrijk dieet gevoerd met en zonder butyraat. Deze studie toonde aan dat butyraat alleen een remmend effect heeft op de eetlust en gewichtstoename in aanwezigheid van darmbacteriën, wat suggereert dat bepaalde darmbacteriën blijkbaar cruciaal zijn. Om de betrokkenheid van de darmflora verder uit te zoeken hebben we vervolgens gebruik gemaakt van fecale transplantaties waarbij de darmflora vanuit verse feces van donormuizen de darmflora van ontvangende muizen vervangt. Hiertoe werden feces verzameld van muizen die behandeld werden met en zonder butyraat in het voer, en de aanwezige darmflora werd getransplanteerd naar muizen die gevoerd werden met een vetrijk dieet zonder butyraat. Genetische analyse van de feces van de ontvangende muizen toonde inderdaad aan dat de darmflora anders was na behandeling met darmflora van muizen die met butyraat waren gevoerd. Bovendien bleken de muizen die behandeld werden met darmflora van butyraat-gevoerde muizen minder te eten en daardoor in gewicht aan te komen, en daardoor bleven ze meer gevoelig voor insuline. Nadere analyse van de samenstelling van de darmbacteriën toonde aan dat deze gunstige metabole effecten gepaard gingen met een selectieve verhoging van de aanwezigheid van de bacterie *Lachnospiraceae bacterium 28-4* in de darm, wat suggereert dat butyraat gunstige metabole effecten sorteert door de groei van deze specifieke bacterie in de darmen te stimuleren. Interessant was dat butyraat geen gunstige effecten bleek te hebben op het gewicht en de metabole gezondheid van muizen die vooraf dik waren gevoerd, en dat butyraat in deze dikke muizen ook niet de aanwezigheid van deze specifieke darmbacterie wist te verhogen. Samengevat tonen de studies die beschreven staan in dit hoofdstuk aan dat darmbacteriën een sleutelrol hebben in de gunstige effecten van butyraat als het gaat om verlaging van de voedselinname en verbetering van de insulinegevoeligheid. Tevens suggereren deze studies dat *Lachnospiraceae bacterium 28-4* mogelijk toegepast kan worden als een nieuw probioticum om de ontwikkeling van obesitas tegen te gaan en cardiometabole ziekten te voorkomen.

Voedingsvezels die voorkomen in plantaardig voedsel kunnen niet worden verteerd door menselijke cellen, maar worden door darmbacteriën omgezet in korte-keten vetzuren waaronder butyraat. Een recente baanbrekende studie in mensen toonde aan dat verrijking van voedsel met voedingsvezels niet alleen leidt tot de meerdering van darmbacteriën die butyraat produceren, maar ook tot verhoging in het bloed van het verzadigingshormoon *glucagon-like protein-1* (GLP-1) dat vooral wordt aangemaakt in de darm, en tot verbetering van type 2 diabetes. Deze studie suggereert dat verrijking van voedsel met butyraat de cardiometabole gezondheid niet alléén verbetert via het moduleren van darmbacteriën, zoals aangetoond in Hoofdstuk 3, maar waarschijnlijk óók door de aanmaak van GLP-1 door de darm te stimuleren. Daarom was het doel van de studies beschreven in **Hoofdstuk 4** om de rol van GLP-1 te onderzoeken in de metabool gunstige effecten van butyraat. Hiertoe werden APOE*3-Leiden.CETP muizen weer gevoerd met een vetrijk dieet met en zonder butyraat, waarna we inderdaad aantoonden dat butyraat het aantal GLP-1-producerende cellen in het ileum van de darm en de hoeveelheid actief GLP-1 in het bloed verhoogde, wat samenging met de eerder geobserveerde gunstige metabole effecten zoals verhoging van de vetverbranding en metabole activiteit van het bruin vet. Vervolgens onderzochten we de bijdrage van GLP-1 receptoren in de hersenen aan deze gunstige effecten door deze te blokkeren met intracerebroventriculaire toediening van een zogenaamde GLP-1 receptorantagonist. Het blokkeren van deze receptoren bleek het gunstige effect van butyraat op de voedselinname en de vetverbranding sterk te verlagen, zonder de gunstige effecten op gewichtstoename, vetmassa en opname van voedingsstoffen uit het bloed te remmen. Wij concludeerden dan ook dat verrijken van de voeding met butyraat de productie van GLP-1 in de darm verhoogt en daarmee de eetlust remt en de vetverbranding stimuleert via GLP-1 receptoren in de hersenen, terwijl GLP-1 receptoren in de hersenen niet betrokken zijn bij de verhoogde opname van voedingsstoffen uit het bloed en activatie van de metabole activiteit van het bruin vet.

Naast therapeutische strategieën die gericht zijn op het beperken van de voedselinname, zou specifieke stimulatie van de sympathische zenuwbanen die vanuit de hersenen het bruin vet aansturen een innovatieve aanpak zijn om energieverbruik te verhogen. Om die reden hebben we in **Hoofdstuk 5** de mogelijkheid onderzocht om elektrische neurostimulatie toe te passen gericht op het specifiek activeren van bruin vet. In muizen konden we inderdaad aantonen dat elektrische neurostimulatie acuut de warmteproductie door bruin vet doet toenemen, vergelijkbaar met een agonist voor de beta-3 adrenerge receptor, aangezien de lokale temperatuur in bruin vet werd verhoogd zonder de kerntemperatuur te veranderen. Zowel elektrische neurostimulatie als de agonist bleken de sympathische activiteit te verhogen omdat het enzym dat in de zenuwuiteinden verantwoordelijk is voor de aanmaak van noradrenaline in hogere mate aanwezig was in bruin vet. Daarnaast toonden we activatie aan van eiwitten die in bruin vetcellen verantwoordelijk zijn voor het vrijmaken van vetzuren voor verbranding. Dit ging samen met een verlaging van vet in de bruin vetcellen, nog zonder de opname van voedingsstoffen vanuit het bloed

te verhogen. Tenslotte bleek het effect van elektrische neurostimulatie op verhoging van de temperatuur in bruin vet geheel afhankelijk van de beta-3-adrenerge receptor. Samengevat tonen deze studies aan dat elektrische neurostimulatie een effectieve strategie is om acuut, specifiek en afhankelijk van de beta-3-adrenerge receptor de warmteproductie in bruin vet te verhogen. Daarom postuleren wij dat elektrische neurostimulatie verder ontwikkeld zou kunnen worden als een nieuwe strategie om bruin vet te activeren en ook daarmee cardiometabole aandoeningen tegen te gaan.

Lipopolysaccharide (LPS) is een bestanddeel dat zich op het oppervlak bevindt van zogenaamde Gram-negatieve bacteriën, en wordt gezien als een belangrijke mediator in de effecten die darmbacteriën hebben op de vetstofwisseling van de gastheer. Eerder is namelijk aangetoond dat LPS een remmend effect heeft op de aanmaak van het *cholesteryl ester transfer protein* (CETP) in lever remt, dat betrokken is bij de uitwisseling van cholesterol en vetten tussen lipoproteïnen, d.w.z. de deeltjes die in bloed verantwoordelijk zijn voor het cholesterol- en vettransport. Echter, hoe LPS de aanmaak van CETP door de lever beïnvloedt was nog niet opgehelderd. Een eerdere studie uit onze groep had al aangetoond dat CETP vooral wordt aangemaakt door macrofagen in de lever, de zogenaamde Kupffercellen. Daarom hebben we in **Hoofdstuk 6** de rol van de diverse subsets van Kupffercellen onderzocht in het mechanisme waarmee LPS de expressie van CETP in de lever remt, wederom door aanvankelijk gebruik te maken van APOE*3-Leiden.CETP muizen. Toediening van LPS aan deze muizen leidde tot een aanzienlijk verlaging van de CETP expressie in de lever en verlaging van de concentratie van CETP in het bloed, echter zonder enig effect op het aantal macrofagen in de lever. Deze effecten gingen gepaard met verlaagde expressie van markers van niet-geactiveerde Kupffercellen, en een verhoogde expressie van markers van infiltrerende macrofagen. Tegelijkertijd nam de hoeveelheid cholesterol in het hoge-dichtheidslipoproteïne (HDL) ten opzichte van het totaal aanwezige cholesterol in het bloed tijdelijk toe. Vervolgens voerden we een experiment uit waarin alle macrofagen in de lever met een bepaalde techniek verwijderden, waarna we de toename van CETP expressie in de lever in de tijd vergeleken met die van de diverse macrofaagmarkers. Uit deze studie bleek dat de toename van CETP expressie sterk samenging met de toename in expressie van niet-geactiveerde Kupffercellen. Door vervolgens gebruik te maken van menselijke leverbiopten konden we vaststellen dat ook de CETP expressie in levers van mensen samenging met de expressie van markers van niet-geactiveerde Kupffercellen. Ook bleek injectie van LPS in mensen de concentratie van CETP in het bloed te verlagen. Tenslotte toonden met geïsoleerde macrofagen aan dat LPS via de lever X receptor de expressie van CETP verlaagt. Vanuit deze studies concludeerden wij dat CETP door de lever van zowel muis and mens exclusief tot expressie wordt gebracht door niet-geactiveerde Kupffercellen, en dat bacteriën via hun bestanddeel LPS in staat zijn om Kupffercellen te activeren waarbij de expressie van CETP wordt geremd en het HDL-cholesterol in het bloed wordt verhoogd. Deze opvolging van gebeurtenissen is consistent met een rol van HDL in respons op de verschijning van schadelijk LPS in de bloedsomloop en kan daarmee een relevante afweerreactie vormen tegen

bacteriële infecties.

Tenslotte werden in **Hoofdstuk 7** alle bevindingen vanuit de studies die beschreven zijn in dit proefschrift in de context van de beschikbare wetenschappelijke literatuur geplaatst en werden veelbelovende nieuwe therapeutische strategieën besproken die mogelijk kunnen worden ingezet om obesitas te bestrijden en daarmee cardiometabole ziekten zoals type 2 diabetes en hart- en vaatziekten te voorkomen. Samengevat tonen de studies beschreven in dit proefschrift aan dat verrijking van het dieet met butyraat een veelbelovende en haalbare therapeutische strategie is om de eetlust te verlagen en bruin vet te activeren, om zo de ontwikkeling van obesitas tegen te gaan en cardiometabole ziekten te voorkomen. Tevens hebben onze mechanistische studies waardevolle informatie opgeleverd voor de ontwikkeling van additionele strategieën voor het voorkomen van obesitas, waaronder specifieke pre- en probiotica.

LIST OF PUBLICATIONS

1. Li Z, Zhou E, Liu C, Wicks H, Yildiz S, Razack F, Ying Z, Kooijman S, Koonen D, Heijink M, Giera M, Smits WK, Kuijper EJ, Groen AK, Willems van Dijk K, Rensen PCN, Wang Y. Dietary butyrate selectively promotes *Lachnospiraceae bacterium 28-4* to induce satiety, attenuate weight gain and ameliorate metabolic health. *Submitted for publication.*

2. Li Z, Zhou E, Razack F, Kooijman S, Willems van Dijk K, Rensen PCN, Wang Y. Dietary butyrate promotes intestinal GLP-1 release to reduce appetite and induce fat oxidation via central GLP-1 receptor signaling. *Submitted for publication*.

3. Zhou E, Nakashima H, Li R, van der Zande HJP, Liu C, Li Z, Müller C, Bracher F, Mohammed Y, de Boer JF, Kuipers F, Guigas B, Rensen PCN, Giera M, Wang Y. Inhibition of DHCR24 ameliorates hepatic steatosis and inflammation through LXRα without inducing hyperlipidemia in mice. *Submitted for publication*.

4. Zhou E, Li Z, Nakashima H, Choukoud A, Kooijman S, Berbée JFP, Rensen PCN, Wang Y. Beneficial effects of brown fat activation on top of PCSK9 inhibition on dyslipidemia and atherosclerosis development in APOE*3-Leiden.CETP mice. **Pharmacol Res 2021**; *In press.*

5. Liu C, Schönke M, Zhou E, Li Z, Kooijman S, Boon MR, Larsson M, Wallenius K, Dekker N, Barlind L, Peng X, Wang Y, Rensen PCN. Pharmacological treatment with FGF21 strongly improves plasma cholesterol metabolism to reduce atherosclerosis. **Cardiovasc Res 2021**; *In press*.

6. Zhou E, Li Z, Nakashima H, Liu C, Ying Z, Foks AC, Berbée, Willems van Dijk K, Rensen PCN, Wang Y. Hepatic SRB1 (Scavenger Receptor Class B Type 1) knockdown reduces atherosclerosis and enhances the antiatherosclerotic effect of brown fat activation in APOE*3-Leiden.CETP Mice. **Arterioscler Thromb Vasc Biol 2021**; *In press*.

7. Li Z, de Jonge WJ, Wang Y, Rensen PCN, Kooijman S. Electrical neurostimulation promotes brown adipose tissue thermogenesis. **Front Endocrinol 2020**; 11: 567545.

8. Zhou E, Hoeke G, Li Z, Eibergen AC, Schonk AW, Koehorst M, Boverhof R, Havinga R, Kuipers F, Coskun T, Boon MR, Groen AK, Rensen PCN, Berbée JFP, Wang Y. Colesevelam enhances the beneficial effects of brown fat activation on hyperlipidaemia and atherosclerosis development. **Cardiovasc Res 2020**; 116(10): 1710-1720.

9. Li Z, Yi C, Katiraei S, Kooijman S, Zhou E, Chung CK, Gao Y, van den Heuvel JK, Meijer OC, Berbée JFP, Heijink, Giera M, Willems van Dijk K, Groen AK, Rensen PCN, Wang Y. Butyrate reduces appetite and activates brown adipose tissue via the gut-brain neural circuit. **Gut 2018**; 67(7): 1269-1279.

10. van der Tuin SJL*, Li Z*, Berbée JFP, Verkouter I, Ringnalda LE, Neele AE, van Klinken JB, Rensen SS, Fu J, de Winther MPJ, Groen AK, Rensen PCN, Willems van Dijk K, Wang Y. Lipopolysaccharide lowers cholesteryl ester transfer protein by activating F4/80^{+} Clec4f^{+} Vsig4^{+} Ly6C^{-} Kupffer cell subsets. **J Am Heart Assoc 2018**; 7(6): e008105.

11. Blauw LL, Li Z, Rensen SS, Greve JWM, Verhoeven A, Derks RJ, Giera M, Wang Y, Rensen PCN. Metabolic liver inflammation in obesity does not robustly decrease hepatic and circulating CETP. **Atherosclerosis 2018**; 275: 149-155.

12. Rozendaal YJW, Wang Y, Paalvast Y, Tambyrajah LL, Li Z, Willems van Dijk K, Rensen PCN, Kuivenhoven JA, Groen AK, Hilbers PAJ, van Riel NAW. In vivo and in silico dynamics of the development of metabolic syndrome. **PLoS Comput Biol 2018**; 14(6): e1006145.

13. Liu X, Pang D, Yuan T, Li Z, Li Z, Zhang M, Ren W, Ouyang H, Tang X. N-3 polyunsaturated fatty acids attenuates triglyceride and inflammatory factors level in hfat-1 transgenic pigs. **Lipids Health Dis 2016**; 15: 89.

14. Tang X, Wang G, Liu X, Han X, Li Z, Ran G, Li Z, Song Q, Ji Y, Wang H, Wang Y, Ouyang H, Pang D. Overexpression of porcine lipoprotein-associated phospholipase A2 in swine. **Biochem Biophys Res Commun 2015**; 465(3): 507-11.

15. Ran G, Ren L, Han X, Liu X, Li Z, Pang D, Ouyang H, Tang X. Development of a rapid method for the visible detection of pork DNA in halal products by loop-mediated isothermal amplification. **Food Anal Method 2015**; 9: 565–570.

16. Li Z, Ren W, Han X, Liu X, Wang G, Zhang M, Pang D, Ouyang H, Tang X. ω3-polyunsaturated fatty acids suppress lipoprotein-associated phospholipase A2 expression in macrophages and animal models. **Mol Nutr Food Res 2015**; 59(9): 1771-9.

17. Han X, Wang T, Zhang J, Liu X, Li Z, Wang G, Song Q, Pang D, Ouyang H, Tang X. Apolipoprotein CIII regulates lipoprotein-associated phospholipase A2 expression via the MAPK and NFκB pathways. **Biol Open 2015**; 4(5): 661-5.

18. Wang H, Ouyang H, Tian Y, Li Z, Han X, Liu X, Ran G, Wang G, Pang D, Tang X. Nitro-oleic acid decreases transcription of the angiotensin II type I receptor gene in aortic smooth muscle cells. **Biotechnol Bioproc E 2014**; 19: 740–746.

19. Wang G, Ji Y, Li Z, Han X, Guo N, Song Q, Quan L, Wang T, Han W, Pang D, Ouyang H, Tang X. Nitro-oleic acid downregulates lipoprotein-associated phospholipase A2 expression via the p42/p44 MAPK and NFκB pathways. **Sci Rep 2014**; 4: 4905.

CURRICULUM VITAE

Zhuang Li was born on 26 October 1988 in Changchun, Jilin Province, China. After graduating from the Jilin Provincial Experimental High School in Changchun, he was enrolled in Jilin University in 2008, with a major in Animal Biotechnology. In 2012, after obtaining his BSc degree, he continued his master study 'Biochemistry and Molecular Biology' at the same university. He worked on a 3-year research program entitled 'ω3-polyunsaturated fatty acids suppress lipoprotein-associated phospholipase A2 expression in macrophages and animal models' under the supervision of Prof. dr. Xiaochun Tang and Prof. dr. Ouyang Hongsheng, and received his MSc degree in 2015.

Sponsored by a prestigious personal fellowship by the Chinese Scholarship Council, he started his PhD project in October 2015 under the supervision of Prof. dr. Patrick C.N. Rensen and Prof. dr. Yanan Wang, at the Division of Endocrinology of the Department of Medicine, at Leiden University Medical Center, Leiden, The Netherlands. His research mainly focused on identifying novel gut-based therapeutic strategies to combat obesity and associated cardiometabolic disorders, as well as on elucidating underlying mechanisms. In particular, he demonstrated that dietary butyrate, via acting on the gut-brain neural circuit, reduces appetite and activates brown adipose tissue, hence improving energy metabolism (Li, Gut 2018, highly cited paper according to Web of Science). For this work he was awarded the Best Publication Award for best Dutch original research paper on obesity at the Netherlands Association for the Study of Obesity (NASO) Spring Meeting in 2018, as well as a Rexinchang Scholarship for best gut-related research at the China 1st GUT Festival in 2019.

From October 2019 till present, he continues to work in the same research group as a postdoctoral researcher, exploring the role of the gut microbiome in the beneficial effects of dietary butyrate on host metabolic health. He is currently supported by a personal international fellowship for Endocrinology research by the IBSA Foundation obtained in 2019 and by a Prof. dr. J. Terpstra Award for best diabetes research proposal by the Dutch Association for Diabetes Research (NVDO) in 2019.

ACKNOWLEDGMENTS

Without the support and understanding of many, I could not have overcome the language barrier and cope with cultural misunderstandings at the beginning of my PhD training abroad, and finally go through five years of research life that culminated in this thesis. Therefore, I wish to express my appreciation to everyone who stood behind me.

Throughout my PhD studies, the most irreplaceable persons were my promotors and supervisors, Prof. dr. Patrick Rensen and Prof. dr. Yanan Wang, who introduced me to this unknown but wonderful scientific world. You not only guided me how to become an independent scientist but also inspired me how to enjoy a colorful life. What I learnt from you is the most precious gift of my PhD training.

In addition, thanks to my fantastic and warmhearted colleagues from the big family of ENDO and HG for extending their compassion and providing flexibility when needed. Ko, Onno, Jimmy, Mariëtte, Sander, Lisanne, Milena, Borja, Jan, Andrea, Eline, Laura, Maaike Schilperoort, Maaike Straat, Robin, Wietse, Rob, Chris, Trea, Hetty, Amanda, Isabel, and others, with your unlimited support and help I never felt alone when I met difficult scientific questions. I am happy and lucky to still work as a team member with all of you.

Besides, I would like to show my gratitude to the collaborators who helped me completing this thesis. Many thanks Chunxia and Yuanqing for guiding me to investigate the gut-brain neural axis; Wiep Klaas and Ingrid for their great assistance in isolating and amplifying gut microbiota; and Martin and Marieke for their great expertise in measuring short-chain fatty acids.

Furthermore, I am incredibly grateful to my Chinese colleagues Enchen, Cong, Zhixiong, Xiaoke, Jinlan, who are also true friends. I very much enjoyed, and still enjoy, the relaxing Chinese lunchtimes with you, which allow to refresh myself in between full days of hard work. To all my Chinese friends in the Netherlands, thank you for enriching my life. I enjoyed the time we were playing and laughing together, which colored my life a lot.

Last but not least, there are no words that can express my thanks to my beloved family. My parents, thank you for constantly supporting me, forgiving me, loving me, and making me. My wife Jiaxin and my son Aiden, you are the light of my life, brightening my world with the warmth of your love.

Zhuang

April 2021